PROCESS MEASUREMENTS IN FLOTATION COLUMNS USING ELECTRICAL CONDUCTIVITY

Alejandro Uribe-Salas

Department of Mining and Metallurgical Engineering
McGill University, Montreal
August 1991

A Thesis submitted to the
Faculty of Graduate Studies and Research
in partial fulfillment of the requirements for
the degree of
Doctor of Philosophy

To my wife María Eugenia

and my daugthers Marysol and Edurné

ABSTRACT

Techniques based on electrical conductivity to estimate interface level, gas holdup and bias rate in flotation columns were developed.

A conductivity probe and associated data acquisition system for locating the froth/collection zone interface in flotation columns were developed and tested. The level detection technique is based on the collection of a conductance profile around the interface and on the location of the position at which a sharp change in conductance occurs. Such a change in conductance across the interface is caused by the difference in the effective conductivity of the froth and collection zone, primarily due to their difference in gas holdup.

A conductivity cell to measure the effective conduct vity of water-air, water-mineral, and water-mineral-air systems was developed. The cell consisted of two grid-electrodes covering the entire cross-sectional area of the cylinder containing the two or three phase system. Such an arrangement allowed the free movement of the phases and provided conditions for uniform potential and current (electrical) fields. It was found that Maxwell's model (1892) predicted the holdups of the non-conductive material reasonably well from the conductivity measurements.

Conditions encountered in industrial flotation columns allowed the use of conductivity to trace the flows of feed water and wash water across the interface, and therefore, to determine the bias rate. Alternative parameters to bias rate as measures of metallurgy such as fraction of feed water in the overflow water (called here feed water entrainment), feed water recovery, and conductance profiles, were explored.

MESURES DE VARIABLES DE PROCESS
BASÉES SUR LA CONDUCTIVITÉ ÉLECTRIQUE
DANS LES COLONNES DE FLOTTATION

RÉSUMÉ

Des techniques basées sur la conductivité électrique ont été développées afin d'estimer le niveau de l'interface, la teneur en gaz (holdup) et le biais dans les colonnes de flottation.

Une sonde mesurant la conductivité ainsi que son système d'acquisition de données ont été mis au point et testés. La technique utilisée pour localiser le niveau repose sur l'établissement d'un profil de conductance de part et d'autre du niveau de l'interface et sur l'identification de la région où l'on observe une différence significative de conductance. Une telle variation de part et d'autre de l'interface est due à la différence de conductivité effective entre la zone de mousse et celle de récupération. Cet écart est principalement dû à la différence de teneur en gaz des deux zones.

Une cellule pouvant mesurer la conductivité effective des systèmes eau-air, eau-minéral et eau-minéral-air a été mise au point. La cellule est composée de deux électrodes à structure grillagée couvrant entièrement une section transversale du cylindre contenant le système à deux ou trois phases. Un tel dispositif permet la circulation libre des phases et remplit les conditions d'uniformité des champs de potentiel et de courant (électrique). A partir des valeurs de conductivité mesurées il apparaît que le modèle de Maxwell (1892) prévoit raisonnablement bien les teneurs en substance non-conductrice.

Les conditions rencontrées dans des colonnes de flottation industrielles ont permis l'utilisation de la conductivité pour suivre les échanges au niveau de l'interface entre

l'eau d'alimentation et l'eau de lavage et la détermination du biais. L'utilisation de paramètres autres que le biais pour évaluer la métallurgie de système, tels que la fraction d'eau d'alimentation dans l'eau du concentré, la récupération de l'eau d'alimentation et les profils de conductance ont aussi été étudiés.

MEDICIONES DE PROCESO EN COLUMNAS DE FLOTACION
USANDO CONDUCTIVIDAD ELECTRICA

RESUMEN

Se desarrollaron técnicas basadas en conductividad eléctrica para la medición del nivel de la interface, del contenido de gas y de la velocidad de intercambio de liquido (bias) en columnas de flotación.

Se desarrolló un sensor de nivel para la medición de la interface espuma/pulpa en columnas de flotación. La técnica de detección de nivel se basa en la obtención de perfiles de conductancia a través de la interface, y en la localización de la posición en que se observa un cambio significativo en el valor de conductancia. Dicho cambio se debe a la diferencia en conductividad efectiva de las dos zonas, que depende, en primera instancia, de la diferencia en contenido de gas.

Se desarrolló una celda de conductividad para la medición de conductividades efectivas de systemas agua-aire, agua-mineral y agua-mineral-aire. La celda consiste de dos electrodos tipo rejilla cubriendo completamente el área transversal del cilindro conteniendo el sistema. Dicha celda permite el movimiento libre de las fases y el establecimiento de campos de potencial y de corriente electrica uniformes. Se observó que el modelo de Maxwell (1892) fué capaz de predecir con rasonable precisión la fracción volumétrica de las fases no conductoras.

Las condiciones encontradas en columnas de flotación industriales permitieron el uso de técnicas basadas en conductividad para detectar el flujo relativo de agua de lavado y de alimentación a través de la interface, y en consecuencia, para estimar la razón de intercambio de liquido. Parámetros alternativos igualmente relacionados con la metalurgia

del proceso tales como la fracción de agua de alimentación en el concentrado, la recuperación de agua de alimentación, y perfiles de conductancia, fueron también estudiados.

ACKNOWLEDGEMENTS

TABLE OF CONTENTS

NOMENCLATURE

A General term used for area, cm^2

A_c Cross-sectional area of the column, cm^2

C, F Conductance of the collection and froth zone (Fig. 4.31), mS

C_x Coefficient of variation (or relative standard deviation) of variable x (Eq. (A.1.4))

d_b Bubble diameter, cm

d_p Solid particle diameter, cm

g Acceleration due to gravity, 980 cm/s^2

H, h General terms used for height, cm

H_c Length of the collection zone, cm

H_f Interface level or froth depth, cm

H_{fP} Interface level obtained from pressure (Eq.(2.2)), cm

H_{fT} Interface level obtained from temperature (Eq. (2.10)), cm

I General term used for electrical current, A

i Electrical current density (Eq. (3.1)), A/cm^2

J_j Rate of the j (f, c, t, w) stream, cm/s

J_k Rate of the k (l, g) phase, cm/s

J_B Bias rate defined by Equation (2.25), cm/s

J_{t-f} Bias rate defined by Equation (2.24), cm/s

J_{cs} Rate of solids reporting to the concentrate (Eq. (2.26)), cm/s

K General term used for electrical conductance, mS

K_l Conductance of the liquid alone, mS

K_i Conductance of the i (froth, collection) zone, mS

K_j Conductance measured with the j (level, froth zone, collection zone) electrodes (Eq. (4.1)), mS

K_{jw} Conductance measured with the j (level, froth zone, collection zone)

electrodes in water alone (Eq. (4.1)), mS

$K_{l\text{-}g}$	Conductance of the liquid-gas dispersion, mS
$k_{c\text{-}d}$	Thermal conductivity of the continuous-dispersed phase (Eq. (3.18)), cal/cm·s·°C
k_c	Thermal conductivity of the continuous phase (Eq. (3.18)), cal/cm·s·°C
L, l	General terms used for distance, cm
l_e	Effective length (Eq. (3.24)), cm
m	Exponent in Equations (2.10) and (3.22)
n	Conductivity ratio (bubbling/froth zone) (Eq. (4.5))
P	General term used for hydrostatic pressure head, Pa (m of water)
Q_j	Volumetric flowrate of the j (f, c, t, w) stream, cm³/s
Q_{jw}	Volumetric flowrate of water in the j (f, c, t, w) stream, cm³/s
Q_{fj}	Volumetric flowrate of feed water reporting to the j (c, t) stream, cm³/s
Q_{wj}	Volumetric flowrate of wash water reporting to the j (c, t) stream, cm³/s
Q_{fwc}	Flowrate of feed water recovered in the overflow (Eq. (2.30)), cm³/s
R	General term used for resistance, ohm
R_i	Resistance of the i (froth, bubbling) zone (Eq. (4.3)), ohm
R_{fw}	Feed water recovery defined by Equation (2.30)
r	General term used for radius, cm
S	Fraction of bubble surface covered by particles (Eq. (2.5))
S_x^2	Variance of variable x
S_x	Covariance ($\approx$ standard deviation) of variable x
T	Time constant (Eq. (4.2)), s
T_i	Temperature measurement at position i, °C
T_j	Temperature of the j (f, c, t, w) stream, °C
t	Time, s
U_s	Bubble slip velocity, cm/s
U_T	Bubble terminal velocity, cm/s
V	General term used for voltage, V

x_j Mass fraction of solids in the j (f, c, t, w) stream

Greek Symbols

α, β Parameters in Maxwell's equation (Eq. (3.17))

$\alpha_{25°C}$ Coefficient of variation of temperature (Eq. (5.1)), °C^{-1}

γ Relative conductance defined by Equation (3.24)

Δh Length of the expanded bed (Eq. (2.13)), cm

ΔP Pressure differential, Pa (m of water)

ε_k Fractional holdup (sometimes expressed as percentage) of the k (l, s, g) phase

ε_d Fractional holdup of the dispersed phase

ε_{gc} Fractional gas holdup in the collection zone

ε_{gf} Fractional gas holdup in the froth zone

κ Electrical conductivity, mS/cm

κ_i Conductivity of the i (froth, bubbling) zone (Eq. (4.4)), mS/cm

κ_j Conductivity of the j (f, c, t, w) stream, mS/cm

κ_d Conductivity of the dispersed phase, mS/cm

κ_c Conductivity of the continuous phase (Eq. (3.18)), mS/cm

κ_{c-d} Effective conductivity of the continuous-dispersed phase (Eq. (3.18)), mS/cm

κ_{l-d} Effective conductivity of the liquid-dispersed phase, mS/cm

κ_{l-g} Effective conductivity of the liquid-gas system, mS/cm

κ_{l-s} Effective conductivity of the liquid-solids slurry, mS/cm

κ_{l-s-g} Effective conductivity of the liquid-solids-gas system, mS/cm

ν_{sj} Volumetric fraction of solids in the j (f, c, t, w) stream

ν_A, ν_B Volumetric fraction of A and B in an A-B mixture (Eq. (6.1))

ρ_{cs} Density of solids in the concentrate stream, gr/cm^3

ρ_i Density of the i (froth, collection) zone, gr/cm^3

ρ_j Density of the j (f, c, t, w) stream, gr/cm^3

ρ_k Density of the k (l, s, g) phase, gr/cm^3

ρ_{sl} Density of the slurry, gr/cm^3

ρ_{sf} Density of the slurry in the froth zone, gr/cm^3

ρ_b Density of the bubble-particle aggregate (Eq. (2.5)), gr/cm^3

ρ_w Density of water, gr/cm^3

φ_i' Gradient of temperature (Eq. (2.11)), cm^{-1}

φ_i Normalized temperature (Eq. (2.12))

ϕ Flux (electrical) function (Appendix 2)

ψ Potential (electrical) function (Appendix 2)

LIST OF FIGURES

LIST OF TABLES

LIST OF APPENDICES

CHAPTER 1

INTRODUCTION

The flotation column studied in the present thesis, now often referred to as the "conventional" column, was invented in Canada in the early 1960s by Boutin and Tremblay. Descriptions of the column and initial testwork were given by Wheeler (1966) and Boutin and Wheeler (1967). No substantial progress regarding industrial applications and fundamental studies was achieved in the 1970s; however, in the early 1980s the column started to attract the attention of researchers in Universities and mineral processors in industry. Since then, the number of new applications and studies has been increasing rapidly. As a measure of this activity, there have recently been two international conferences (Sastry, 1988; Agar et al., 1991) and a book (Finch and Dobby, 1990a).

1.1 Description of the Flotation Column

A flotation column is illustrated schematically in Figure 1.1. Commercial units are typically 9-15 m high and 0.5-3.0 m diameter. The cross-section of the column may be square or circular. The side of the square column or the diameter of the circular column is used to designate column size.

The column consists of two distinct zones: the collection zone (also termed slurry, pulp or recovery zone) and the froth zone (also known as cleaning zone). These two zones are separated by an interface which defines the interface level or froth depth. The mineral slurry is fed to the column in the collection zone below the interface. Solid particles settling downwards due to gravity are contacted countercurrently with a bubble swarm generated by blowing gas through a bubble generator (sparger) located near the
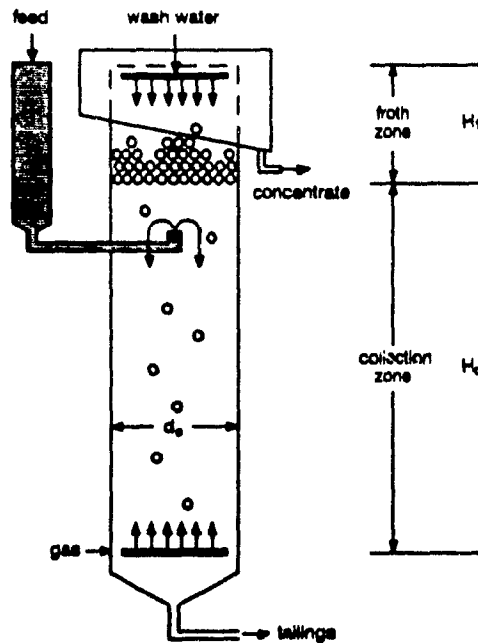
Figure 1.1   Schematic illustration of a flotation column

bottom of the column. Hydrophobic particles collide with and attach to the bubbles and are transported to the froth zone. Hydrophillic and less hydrophobic particles settle and are eventually removed from the bottom of the column through the tailings port. In the froth zone, wash water is added near the top of the froth to reduce the recovery by hydraulic entrainment of hydrophillic fine particles into the concentrate. Normally, a net downward flow of water through the froth, called a positive bias, is maintained.

1.2   Objectives of the Present Work

The optimization of the operation of a flotation column relies mostly on the identification of the key control variables, their accurate measurement and their dynamic interaction. Since the target output variables *grade* and *recovery* are often not measured on-line, secondary objectives such as interface level, gas holdup and bias rate have been suggested.

Conventional techniques to measure these control variables are based on the sensing of extensive properties of the system such as hydrostatic head and mass flowrate. It has been shown that such measurements are subject to error (Moys and Finch, 1988a and 1988b; Gomez et al., 1990; Finch and Dobby, 1990a). Techniques based on the measurement of intensive properties, e.g. temperature and conductivity, have been proposed to locate level and to estimate gas holdup and bias rate (Yianatos et al., 1985; Moys and Finch, 1988a and 1988b).

The objective of the thesis is to explore the use of techniques based on electrical conductivity to locate the interface level, and to estimate gas holdup and bias rate.

1.3   Structure of the Thesis

The thesis consists of eight chapters. In Chapter 1 the column is introduced along with a description of its operating characteristics. The objectives of the thesis and the structure of the thesis are also presented.

Chapter 2 introduces the process variables involved with the operation of the column. The available techniques to measure interface level, gas holdup and bias rate are presented and discussed.

Chapter 3 introduces the theory of electrical conductivity and the basis of conductivity measurements. Some of the available models in the literature to characterize the effective conductivity of two and three phase systems are presented.

In Chapter 4, the experimental techniques and results obtained in the detection of interface level using conductivity based techniques are presented. Results obtained both at the laboratory and industrial scale are presented. A conductivity probe developed for industrial application is described.

Chapter 5 addresses the measurement of gas holdup at the laboratory and industrial scale. Techniques developed for gas holdup estimation in two and three phase systems are presented. The role of non-conductive (silica) and conductive (sulphides) solids is explored.

Chapter 6 presents the experimental techniques and results obtained in the estimation of bias rate using conductivity. Alternative parameters, feed water recovery and feed water entrainment (as defined here), are also experimentally explored.

In Chapter 7 the significance of the techniques developed in this work and the feasibility and requirements for their implementation at the industrial scale is discussed.

Finally, in Chapter 8 the conclusions of the work, claims for original research, and recommendations for future work are presented.

CHAPTER 2

PROCESS MEASUREMENTS IN FLOTATION COLUMNS

In this Chapter, the process variables of specific interest for this Thesis are presented together with a number of ways they are measured.

2.1   Definition of Variables

Process variables in flotation columns are all those variables (gas rate, gas holdup, recovery, etc.) associated with the process of column flotation. These variables are divided in two groups (Stephanopoulos, 1984; Tsai et al., 1986): (1) *Input* variables, which denote the effect of the surroundings on the process, and (2) *Output* variables, which denotes the effect of the process on the surroundings.

The *input* variables can be further classified into *Manipulated* (or *Adjustable*) variables, if their value can be adjusted freely by the human operator or a control mechanism, and *Disturbances*, if their values are not the result of adjustment by an operator or a control system (according to their direct measurability, these are further classified into *measured* and *unmeasured*). In column flotation, tailings, feed, washwater and gas rates are typical input variables.

The *output* variables are also classified into *Measured* output variables, if their values are known by directly measuring them, and *Unmeasured* output variables, if they are not or cannot be measured directly.

In flotation columns, froth depth (or interface, or pulp level), gas holdup and bias rate are output variables that have an effect on the metallurgical performance of the

column. This Thesis addresses these three variables.

Froth Depth or Interface Level is usually classified as a measured output variable. This output variable can affect the *unmeasured output* variables grade and recovery (unmeasured because in most flotation columns, on-stream analysis is not available). Small froth depths may result in a reduction of grade since particle entrainment is not completely avoided (Yianatos et al., 1987). Excessive froth depths generally reduce recoveries because of the reduction in material transfer from the froth into the concentrate.

Gas Holdup is an output variable that is usually classified as an unmeasured since no reliable measurement technique exists to measure gas holdup on-line in slurry-gas reactors. Gas holdup is related to metallurgy because of its effect on flotation kinetics and residence time (Dobby et al., 1988).

Bias Rate may be classified as an *unmeasured* output variable since it cannot be measured directly (usually the bias is inferred from other measurements). A positive bias (net downward flow of liquid) is required to reduce gangue entrainment into the froth product, but a positive bias does mean decreased retention time in the collection zone; thus, bias rate is related to grade and recovery.

2.2   Techniques to Measure Interface Level, Gas Holdup and Bias rate

2.2.1 Interface level measurement

a).-   Introduction

Interface level (or froth depth) is defined here as the distance from the column lip to the location of the froth/slurry interface. Interface levels encountered in flotation

columns range from about 0.5 to 2 m.

Measuring interface level is not a trivial problem. Two zones, the froth and the collection zone, are involved; thus, techniques that exploit the differences in certain physical-chemical properties of these zones are commonly used.

b).- Techniques to measure interface level

Techniques based on the density gradient: The float

The float is probably the simplest device that has been used to measure the interface level in flotation cells. The float is a sensor which responds to the density gradient near the froth/slurry interface.

The simplest version of such a sensor is an arrangement whereby the position of the float, which is of a density intermediate between that of the slurry and the froth, is measured (Figure 2.1(a)). In flotation column this technique is difficult to apply because of the relatively large froth depths used (compared to conventional cells), and because the density gradient near the interface is not as marked as in conventional cells; froth density in conventional cells can sometimes approach or even exceed the density of water. It is thus difficult to select the density of the float which will apply to all possible conditions (Moys and Finch, 1988a). Nevertheless, floats are frequently selected (Hoffert, 1987; Redfearn, 1989; Konigsmann, 1990).

Devices combining the float principle with ultrasonic location systems have been reported. Hoffert (1987) developed a device consisting of a float with a target plate mounted on the shaft (Figure 2.1(b)). An ultrasonic beam is reflected from the target plate, allowing the distance between the source and the plate, and hence the position of the float, to be gauged.
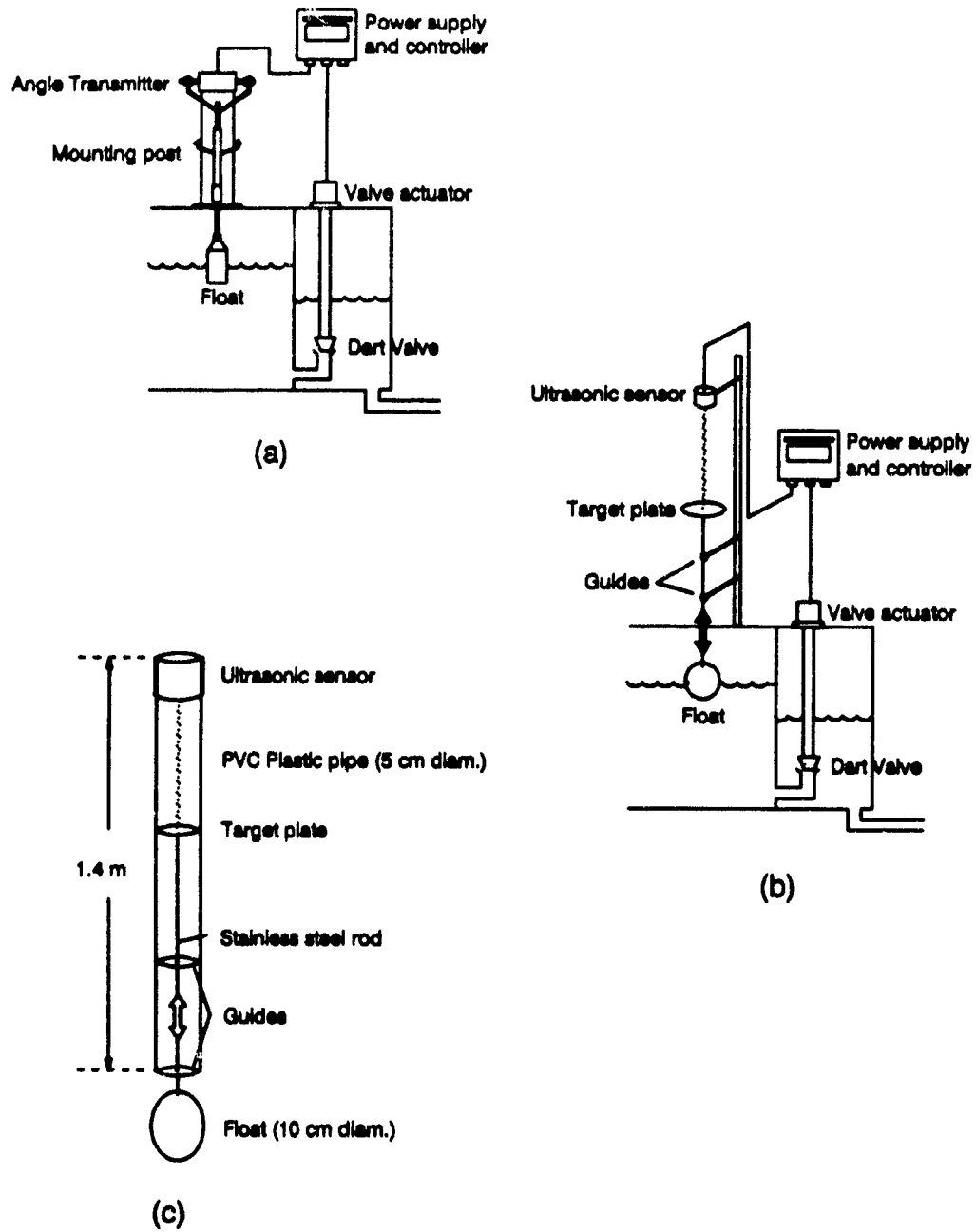
Figure 2.1 Level detection devices based on the response of a float: (a) Outokumpu; (b) Hoffert (1987); and (c) Konigsmann (1990)

In the device recently reported by Konigsmann (1990), the sensor (Figure 2.1(c)) consists of a 5 cm diameter tube fitted with two guides and a steel shaft with a target plate which rides up and down along the guides in the tube. The float, threaded onto the other end of the shaft, sinks through the froth to rest directly on the pulp itself The wave reflection time is directly related to the float position. In the situation described by Konigsmann this time signal was translated into an analog output for a pneumatic controller which regulated a dart valve.

Techniques based on hydrostatic pressure measurements

These methods, perhaps the most widely used currently, are based upon measurements of hydrostatic pressure at one, two or three strategic points along the column. Pressure transducers, differential pressure cells, water manometers and bubble tubes are commonly used to perform these measurements. (Another device dependent on pressure is the Metritape; this will be described latter as it utilises pressure in a different way).

The use of hydrostatic pressure measurements in flotation columns has been well described in the literature (Finch and Dobby, 1990a; Huls et al., 1990). Assuming static pressure is sensed at some point below the interface and all other variables remain constant, then gauge pressure P is linearly dependent on the interface height above the sensor L, or froth depth H_f (Figure 2.2(a)). This linear signal is ideal for control purposes.

It has been established, however, that methods based on a single measurement of the hydrostatic pressure below the interface suffer from errors that can exceed 0.5 m (Moys and Finch, 1988a; Gomez et al., 1990).

Hydrostatic pressure is not an accurate indicator of interface level because it is
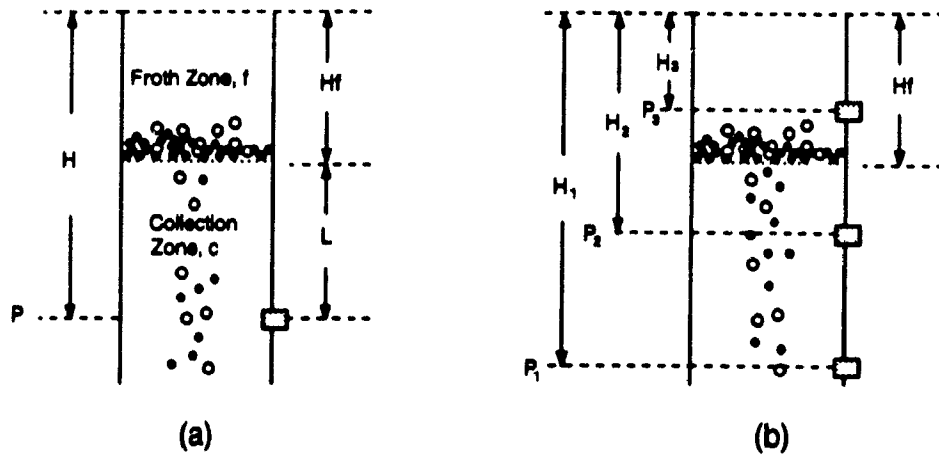
Figure 2.2   Arrangement for measuring level using: (a) single pressure sensor; and
(b) three pressure sensors (after Finch and Dobby, 1990a)
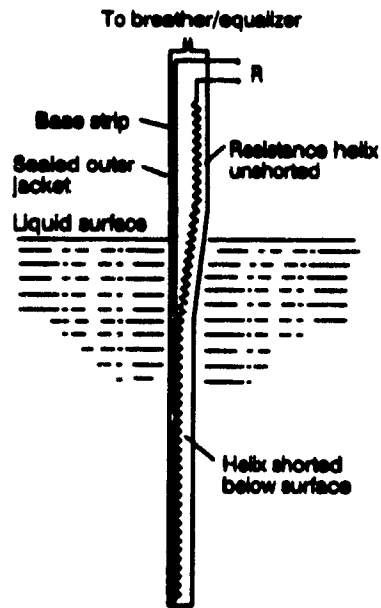
Figure 2.3   Schematic diagram of the Metritape

a strong function of the bulk densities of the froth (ρ_f) and collection (ρ_c) zones as they both depend on such unmeasured disturbance variables as slurry density, gas holdup and bubble loading. Potential for error can be illustrated by considering the basic equation for pressure:

The pressure gauge at point P (Figure 2.2(a)) is related to H_f by

$$P - (H - H_f)\rho_c g + H_f \rho_f g \tag{2.1}$$

Therefore

$$H_{fP} - \frac{H\rho_c g - P}{(\rho_c - \rho_f)g} \tag{2.2}$$

(H_{fP} is the froth depth obtained from pressure head measurements to distinguish from the true H_f) where ρ_c and ρ_f are the bulk densities of the collection zone (above the pressure sensor) and froth zone, respectively:

$$\rho_c - \rho_{sl}(1 - \varepsilon_{gc}) + \rho_b \varepsilon_{gc} \tag{2.3}$$

$$\rho_f - \rho_{sf}(1 - \varepsilon_{gf}) + \rho_b \varepsilon_{gf} \tag{2.4}$$

where ρ_{sl} and ρ_{sf} are the slurry density in the collection and froth zones, respectively; ε_{gc} and ε_{gf} are the gas holdup in the collection and froth zones, respectively; and ρ_b is the density of the bubble-particle aggregate (Finch and Dobby, 1990a; Yianatos et al., 1988):

$$\rho_b - \frac{S\pi d_p \rho_s}{d_b + S\pi d_p} \tag{2.5}$$

where S is the fraction of bubble surface covered by a monolayer of particles; ρ_s and d_p are the solids density and particle diameter; and d_b is the bubble diameter.

Most of these variables are unknown: Finch and Dobby (1990a) have shown that realistic changes in d_p, ρ_{sl} and S can lead to level estimates with errors in the order of those reported by Moys and Finch (1988a) and Gomez et al. (1990).

The problem of level measurement with a single pressure sensor is the dependence on ρ_c and ρ_f both of which vary with operating conditions in a manner that is difficult to predict. By using an array of three pressure sensors, ρ_c and ρ_f can be estimated continuously and hence H_f estimated with more accuracy (Dirsus, 1988; Huls et al.,1990; Finch and Dobby, 1990a). Figure 2.2(b) shows an arrangement of three pressure sensors two of which are in the collection zone. The pressure at each sensor is

$$P_1 - (H_1 - H_f)\rho_c g + H_f\rho_f g \qquad (2.6)$$

$$P_2 - (H_2 - H_f)\rho_c g + H_f\rho_f g \qquad (2.8)$$

$$P_3 - H_3\, \rho_f\, g \qquad (2.9)$$

Rearranging Equations (2.6) to (2.9), H_f is given by

$$H_{f\,P(3)} - \frac{H_3[H_1(P_1 - P_2) - P_1(H_1 - H_2)]}{H_3(P_1 - P_2) - P_3(H_1 - H_2)} \qquad (2.9)$$

Thus the pressure signals from the three sensor arrangement can be combined to give froth depth estimates independent of variations in ρ_c and ρ_f. This strategy has been recently adopted by some industrial operations with satisfactory results (Huls et al., 1990; Kosick and Dobby, 1990).

Metritape sensor

The Metritape sensor is an instrument sensitive to hydrostatic pressure and therefore can be regarded as a device to measure pressure head. This sensor (Figure 2.3) is a device which consists of a wire coil wound round a contact strip and insulated from the surrounding media by a flexible, corrosion-resistant sheath. The strip of Metritape is inserted in the vessel from the top. The design is such that the wire does not make contact with the contact strip until the pressure in the fluid outside the tape exceeds 100 mm water (Anon., 1987). This is sufficient to collapse the sheath and wire coil so that contact is made. The resistance of the wire which is not in contact with the contact strip is measured and provides an accurate ($\pm$ 1 cm) measure of the level at which the first contact is made. While Metritape is widely used for the measurement of fluid level in tanks, its use in column flotation has been limited. It suffers from the same problems of all single pressure sensors, plus this added restriction of needing a 100 mm of water pressure to actuate (Moys, 1989).

Techniques based on conductivity measurements

Kitzinger et al. (1979) report a conductivity sensor developed and used to continuously monitor and control froth depth in conventional mechanical flotation cells. The sensor has been used in zinc flotation circuits with satisfactory results (Miettunen, 1982; Koivistoinen and Miettunen, 1985).

(a)   (b)
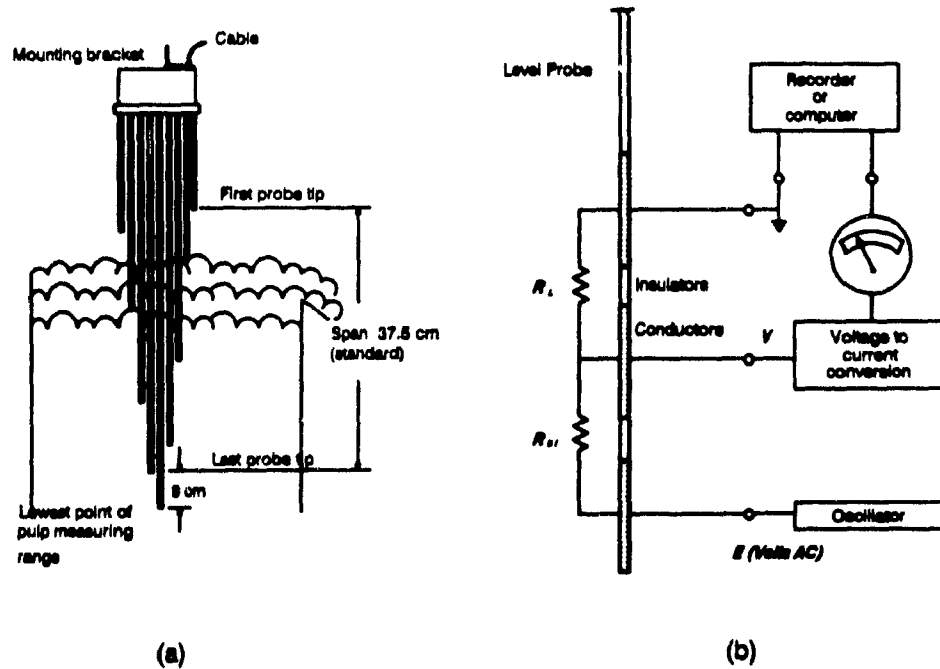
Figure 2.4   Devices based on electrical conductivity for measuring level: (a) the Pulp
height-Froth depth monitor (after Kitzinger et al., 1979); and (b) probe
reported by Moys (1989)

The sensor, the Pulp height-Froth depth monitor (Mineral Control Inst.), consists
of a series of probes plus a central electrode (Figure 2.4(a)). The central electrode is
much longer than the probes, and is designed always to be immersed in the pulp. The
probes have their tips aligned in a vertical spiral with equal vertical spacings (2.5 and 10
cm are typical values).

The central electrode is powered with a positive voltage, controlled so that the
current flowing from the central electrode to the deepest probe is held at a constant
value. The remaining probes sense current which is proportional to the conductivity of
the medium between each probe and the central electrode. If a particular probe is in
pulp, the conductivity will be relatively high, whereas if the probe is in froth, the

conductivity will be much less, and the current flowing will also be less. If a probe is in air, the current flowing through it will be negligible. The ratio of electric current flowing in pulp and froth is approximately 10:1, allowing very clear discrimination between the two phases. The current flowing through each probe is sensed by the appropriate electronic circuitry which decides whether each probe is in pulp, froth or air. Stepwise signals proportional to the froth depth (interface level) and froth height are generated.

The sensor has been used at the experimental level to measure froth depth in a flotation column processing coal (Nicol et al., 1988; Nicol, 1988). However, its use at the industrial level is limited because of fouling problems (Moys and Finch, 1988a).

Moys and Finch (1988a and 1988b) have extensively explored the use of electrical conductivity for measurement and control of interface level in flotation columns at the laboratory scale. For example, detection of level from measurements of conductivity between long, vertical electrodes facing each other and between two electrodes, one above and one below the interface, were examined. The method is based on the fact that gas holdup in the froth zone is larger than that in the collection zone and the measured conductivity accordingly becomes a function of the relative conductivity and volume of the two zones. Two factors which further promote a difference in the conductivity of the two phases are: 1, if the wash water is cooler than the feed water, which causes the froth temperature to fall and reduce conductivity; and 2, if the wash water contains fewer dissolved salts than the feed water. Both these may realised if fresh water is used as wash water. Moys and Finch (1988b) suggest that an advantage of the technique is its simplicity combined with the fact that conductivity exhibits a smooth variation with the interface level. However, the method as described requires that the conductivity of the two zones does not alter substantially, which is not realistic. Also, fouling, especially by non-conductive scale deposits is expected to be a problem (Moys and Finch, 1988a).

Recently, Moys (1989) described a device that consists of a probe and a tailor-made conductivity meter (Figure 2.4(b)). the probe is a rod-shaped structure supporting three 0.6 cm diam. x ~ 10 cm height electrodes separated ~ 3 cm from each other. The level is measured between the central electrode and the one at the top. A process signal proportional to level is obtained. The conductivity of the pulp is measured between the central electrode and the bottom one. The circuitry of the meter is such that this measurement is used to calibrate the apparatus, thus providing an on-line compensation for any change in conductivity of the flotation liquor. The major drawback of the apparatus appears to be the limited span of the probe which is ~ 15 cm in the laboratory unit described.

Techniques based on temperature measurements

Moys and Finch (1988a and 1988b) report a method for measuring level based on measurements of the temperature profile around the froth/collection zone interface. The method is based on the assumption that the wash water will be significantly cooler than the feed (which has passed through grinding mills and perhaps a bank of mechanically agitated flotation cells). Several measurements made on plants in Canada revealed temperature differences of 2-10°C in the spring and summer months (these differences are expected to increase in winter). When this temperature difference exists, the temperature distribution in the cleaning zone will be a function of the relative flowrates through it.

With current temperature transducers cheap and reliable ($\pm$ 0.05°C) temperature measurements can be made; thus a 2% resolution within the temperature range will be ensured if temperature differences between feed and wash water exceed 4°C (and there is a net downward flow of wash water through the froth phase, or a substantial proportion of the water in the froth is from wash water).

Particularly for a positive bias (i.e., with a net wash water flow downwards through the froth phase, so that the froth phase temperature is close to the wash water temperature), there is a sharp change in temperature at the base of the cleaning zone. H_{fT} was estimated from the following weighted average of the levels h_i at which measurements of φ_i were made:

$$H_{fT} = \frac{\sum \varphi_i' \varphi_i^m h_i}{\sum \varphi_i' \varphi_i^m} \tag{2.10}$$

where

$$\varphi_i' = \frac{\varphi_{i+1} - \varphi_i}{h_{i+1} - h_i} \tag{2.11}$$

and

$$\varphi_i = \frac{T_i - T_w}{T_f - T_w} \tag{2.12}$$

Equation (2.10) gives weight to levels associated with large numerical derivatives φ_i' and relatively large temperatures φ_i (this is required because fairly sharp changes in the derivatives can occur in the froth; these make little contribution to H_{fT} because they are associated with smaller values of φ_i that occur at the interface where $\varphi_i \approx 1$). m is a user selected constant. Figure 2.5 shows a typical temperature profile (Finch and Dobby, 1990a); accuracy of level detection depends on separation of temperature sensors.

The major disadvantage of the technique is that a substantial difference in temperature between the wash water and the feed streams and positive bias are required. Moreover, it is essential that the sensors respond rapidly to changes in temperature. Therefore, the sensors must be small so that they have a low heat capacity; this implies delicate probes which may also be subject to a large change in their response time if they
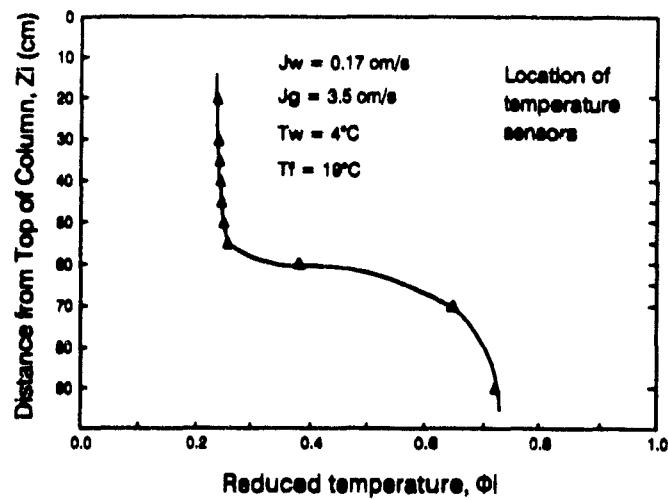
Figure 2.5   Example of temperature profile across the interface in a 0.76 m square column.
The profile was measured by a series of thermistors mounted on a probe.
Reduced temperature Φi is given by Equation (2.12)(after Finch and Dobby,
1990a)
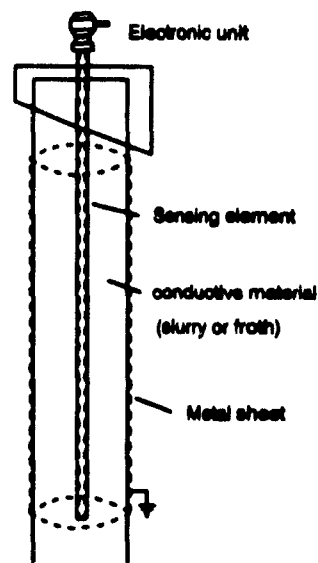
Figure 2.6   Schematic diagram of the capacitance probe for measuring interface level in
a laboratory column (after Barber, 1990)

become heavily fouled by scale deposits.

Other techniques

A *Capacitance system* has been suggested for level detection in laboratory flotation columns (Barber, 1990). The system consists of a probe, or sensing element, and of an electronic unit (Figure 2.6). the probe is an insulated (polypropylene or teflon) metal rod which is located in the top part of the column, concentric to it. A sheet of metal needs to be attached to the wall if the column is non-metallic. The system measures the dielectric constant of the material between the probe's insulated rod and the tank wall (Anon., 1978). It is expected that the capacitance of the system will be a linear function of the interface level since the dielectric constant of the froth and slurry phases are substantially different. No experimental results are available yet on the performance of such a system.

A *Microwave level transmitter* is being tested for level detection in large mechanical cells (Macnamara, 1990). The transmitter is mounted at the top of the cell and sends a low-level microwave beam down to the process material. The electronics (microprocessor-based) calculate the time of flight of the reflected return signal to gauge the distance from the transmitter to the surface of the vessel contents. It is claimed by the manufacturer that the system is able to discriminate between the froth surface and the actual froth/slurry interface. The major difference with conventional ultrasonic devices relies on the fact that microwaves are not dependent on air molecule collisions for signal transmission. Instead, microwaves are electromagnetic, high frequency waves which travel at the speed of light. Frequencies above 10 billion Hertz are used (ultrasonic frequencies are ~50 kHz)(Anon., 1989).

2.2.2 Gas holdup measurement

a).-   Introduction

Gas holdup ε_g, is defined as the volumetric fraction of gas in the system. It is common practice to express gas holdup as a volume percentage. Typical holdup values encountered in flotation columns range from 10 to 25% (Dobby et al., 1988). The complement $(1-\varepsilon_g)$ is the liquid (or slurry) holdup.

Although air is used in most cases, the generic term *gas* is also used throughout this Thesis to include other gases (for example, the use of nitrogen in Cu/Mo separation).

Gas holdup is an important process variable since the rate of particle collection in a flotation column is a function of gas rate and bubble diameter, both of which affect gas holdup. Thus, gas holdup appears to be a primary process control parameter (Dobby et al., 1988). In addition to this, gas holdup defines the volumetric fraction of the phases in the column and hence their residence time. Thus, gas holdup is related to metallurgy because of its effect on both kinetics and residence time.

b).-   Techniques to measure gas holdup

Gas holdup measurement methods have been described by Finch and Dobby (1990a). The methods can be divided in two groups: Methods which allow "overall" measurements such as the *Bed Expansion* and the *Pressure Difference Methods* (Figure 2.7(a) and 2.7(b)) and methods which allow "local" measurements such as the *Conductivity* and γ-*Ray* Methods (Figure 2.7(c)).
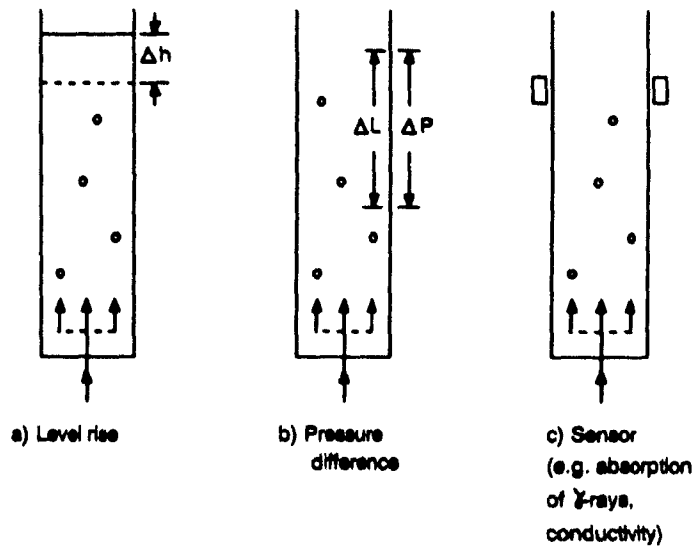
Figure 2.7 Methods of measuring gas holdup (after Finch and Dobby, 1990a)
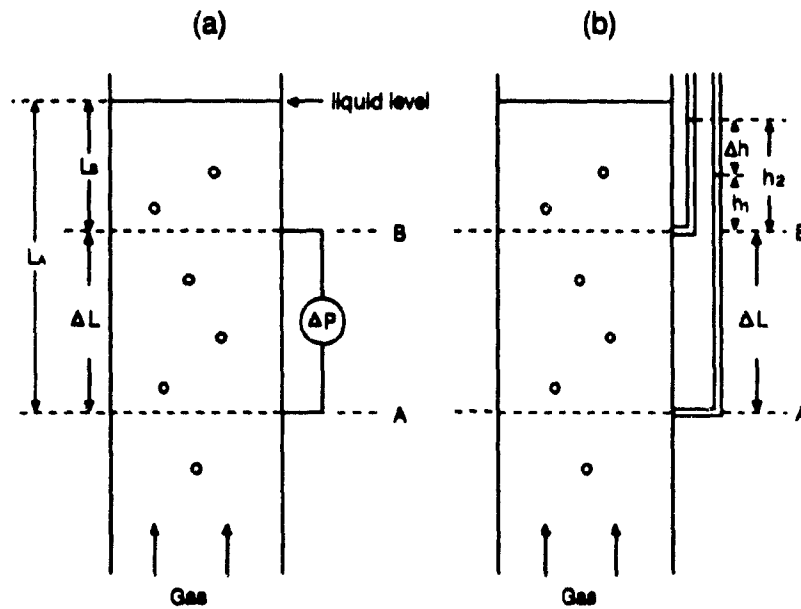
Figure 2.8 Measurement of gas holdup by pressure difference: (a) general; (b) using water manometers (after Finch and Dobby, 1990a)

The Bed Expansion Method

The Bed Expansion Method gives the overall gas holdup in the column by measuring the length of the expanded bed (Δh) of the aerated column of liquid (or slurry) and the clear (non-aerated) liquid (h):

$$\varepsilon_g = \frac{\Delta h}{\Delta h + h} \qquad (2.13)$$

This method is impractical when a layer of froth (of different gas content with respect to the aerated liquid) is present because the interface is not clearly defined; therefore, its application to column flotation is restricted to basic laboratory studies.

The pressure difference method

The pressure difference method gives the overall gas holdup in the section defined by the distance between the pressure tapping points. The practical case of the three-phase (slurry-gas) system is considered first. Assuming that the dynamic component of the pressure is negligible, the pressure above atmospheric at A and B (Figure 2.8) is given by

$$P_A = [\rho_{sl} (1 - \varepsilon_{gA}) + \rho_b \varepsilon_{gA}] \, g \, L_A \qquad (2.14)$$

and

$$P_B = [\rho_{sl} (1 - \varepsilon_{gB}) + \rho_b \varepsilon_{gB}] \, g \, L_B \qquad (2.15)$$

where ρ_{sl} is the slurry density; ε_{gA} and ε_{gB} are the gas holdup above A and B, respectively; and ρ_b is the bubble-particle aggregate density (given by Equation (2.5)). Equations (2.14) and (2.15) assume ρ_{sl} and ρ_b do not substantially change between A and B.

Defining $\Delta P = P_A - P_B$, and upon rearranging, the gas holdup between A and B is given by

$$\varepsilon_g = \frac{\rho_{sl}\, g\, \Delta L\, -\, \Delta P}{(\rho_{sl}\, -\, \rho_b)\, g\, \Delta L} \qquad (2.16)$$

Thus, knowledge of ρ_b and ρ_{sl} is required to obtain gas holdup from pressure readings. Common practice assumes $\rho_b \approx 0$ (bubbles lightly loaded) and ρ_{sl} as the average of the feed and tails densities. Since no independent and reliable technique exists to test these assumptions, no categorical evaluation has been reported so far.

Conditions where $\rho_b \approx 0$ are probably encountered close to the bottom of the column where bubbles are unlikely to be extensively loaded. Under this condition the slurry density, ρ_{sl}, is well represented by the density of the tails stream (Finch and Dobby, 1990a). However, this requires the measurements to be made as close as possible to the bottom of the column, thus becoming closer to a "local" measurement.

For two-phase (water-gas) systems, replacing ρ_{sl} with ρ_w and where $\rho_b = 0$ (no solids present) in Equation (2.16), the gas holdup is simply given by

$$\varepsilon_g = 1 - \frac{\Delta P}{\rho_w\, g\, \Delta L} \qquad (2.17)$$

(ΔP given in pascals (Pa), $\rho_w = 10^3$ kg/m^3, $g = 9.8$ m/s^2 and ΔL in meters (m)). When ΔP is given in meters of water (m H$_2$O) and ΔL in meters, Equation (2.17) is simplified to

$$\varepsilon_g = 1 - \frac{\Delta P}{\Delta L} \qquad (2.18)$$

If water-filled manometers are used to measure the pressure head instead of pressure transducers or bubble tubes (Figure 2.8(b)), the equations are as follows

$$P_A = \rho_w g (\Delta L + h_1) \qquad (2.19)$$

and

$$P_B = \rho_w g h_2 \qquad (2.20)$$

Therefore

$$\Delta P = \rho_w g (\Delta L - \Delta h) \qquad (2.21)$$

where Δh is positive when the upper manometer level is higher than the lower manometer level (the bulk density of the collection zone is less than that of water (ρ_w); Δh is negative when the bulk density is greater than that of water).

Substituting Equation (2.21) into Equation (2.16), ε_g is given by

$$\varepsilon_g = \frac{\rho_{sl} - \rho_w}{\rho_{sl} - \rho_b} + \frac{\rho_w}{\rho_{sl} - \rho_b} \frac{\Delta h}{\Delta L} \qquad (2.22)$$

As discussed above, in three phase systems (slurry-gas) knowledge of ρ_{sl} and ρ_b is required. In two phase systems (water-gas), since $\rho_{sl} = \rho_w$ and $\rho_b = 0$, Equation (2.22) reduces to

$$\varepsilon_g = \frac{\Delta h}{\Delta L} \qquad (2.23)$$

which is an expression extensively used in laboratory studies.

Methods to measure "local" gas holdup

These methods measure gas holdup in the section of the column defined by the signal path between probes. Methods based on electrical conductivity are among the most commonly used in two and three-phase systems (Serizawa, et al., 1975; Fan, 1989). Some of these methods and the theory behind them are described in Section (3.3). Punctual electrical resistivity probes are of common use in measuring local holdup (and bubble size and velocity, in some cases) in liquid-gas dispersions (Nassos, 1963; Serizawa et al., 1975; Burgess and Calderbank, 1975; Castillejos, 1986; Fukuma et al., 1987). These probes are intended to be used for large bubbles (>5 mm) compared to those encountered in flotation columns (0.5 to 2 mm (Yianatos and Levy, 1989)).

Methods based on the attenuation of β-rays (Nassos, 1963) and γ-rays (Lockett and Kirkpatrick, 1975) have been used for two-phase (liquid-gas) systems. These techniques employ a radioactive source and a detector. The strength of the attenuated beam passing through the dispersion (liquid-gas) is a function of the system density and, therefore, related to the volumetric fraction of gas (Nassos, 1963).

Isokinetic sampling methods have been used for local holdup measurements (Serizawa et al., 1975). In this technique a sample of the dispersion is collected to obtain the holdup value at the point of sampling (Chen et al., 1983).

An optical fibre probe method for holdup measurement in liquid-gas system is reported by Wachi et al. (1987). The principle is that phase detection using light is possible since the refractive index of gas and liquid differs considerably. Phase detection occurs at the surface of the probe tip. This surface is shaped to reflect incoming light

internally if gas surrounds it and to refract light if liquid surrounds it. The time fraction of the reflected light will then yield the local holdup (Vince et al., 1982).

Other methods based on light and ultrasonic pulse transmission (Stravs and Von Stockar, 1985) and scattering of a laser beam (Soto, 1989) are used in liquid-gas systems to estimate interfacial surface area which in conjunction with bubble diameter gives the holdup.

2.2.3 Bias rate measurement

a).-   Introduction

The bias rate is conventionally defined as the net water flow rate across the froth zone/collection zone interface. By convention the bias is positive when the direction of the flow is downwards and negative when it is upwards. From common use, cgs units (cm/s) have been adopted as well as the symbol J_b.

It has been traditionally accepted that a positive bias is required to achieve efficient washing of the froth: the concept is that a downward flow of water through the froth phase washes back particles of gangue material entrained in the water layer surrounding the gas bubbles, or prevents their crossing into the froth in the first place; this results in an increase of concentrate grade. Recent work has confirmed the hypothesis that fine non-hydrophobic particle recovery is proportional to the feed water recovered to the concentrate (Moys and Finch, 1989; Maachar et al., 1990).

Adding wash water into the column allows tailings water flow to exceed feed water flow, thus achieving a net downward flow of water through the froth. Espinosa-Gomez and Johnson (1991), for example, confirm that the position of the grade-recovery curve in plant columns (copper retreatment columns (Mount Isa Concentrator), and zinc

columns (Hilton Concentrator)) deteriorated by operating with a negative bias; work by Furey (1990)(flotation of gold telluride), however, suggests operation can be sustained into negative bias. Certainly, the bias rate should not be too large otherwise unnecessary dilution of the collection zone occurs with the correspondence loss of capacity; Yianatos et al.(1986) recommend $J_B < 0.4$ cm/s. Bias determination in flotation columns has been addressed by Moys and Finch (1988b 1989) and Finch and Dobby (1990a).

Conventionally, the bias flowrate has been "controlled" by measuring the feed flowrate (Q_f) while manipulating the tails flowrate (Q_t), at a value larger that Q_f to ensure that a positive bias exists. This assumes that the "bias rate", defined by

$$J_{t-f} - J_t - J_f \qquad (2.24)$$

where J_t and J_f are *slurry* rates, is a good estimate for the bias rate J_B. This is true only for dilute slurries.

For the slurry-gas system, a volumetric balance for the whole column gives

$$J_B - J_{t-f} + J_{cs} \qquad (2.25)$$

where J_{cs}, the rate of solids reporting to the concentrate per unit cross-sectional area of the column, is given by

$$J_{cs} - J_c \, x_c \, \frac{\rho_c}{\rho_{cs}} \qquad (2.26)$$

where x_c is the mass fraction of solids in the concentrate; ρ_c is the concentrate stream density (g/cm^3); and ρ_{cs} is the density of solids in the concentrate (g/cm^3).

Finch and Dobby (1990a) have shown that in cases where large amounts of

concentrate particles are removed (in cleaning circuits, for example), positive bias rates J_B are possible even if J_{t-f} is negative. Thus, control strategies relying on a positive Q_{t-f} will result in excess water being added to the system (Moys and Finch, 1988b), which may create undue demand for water and loss of capacity in the collection zone (Finch and Dobby, 1990a).

Compared with J_{t-f}, the bias rate J_B is the preferred variable to measure and control.

b).-   Techniques to measure bias rate

Bias rate from mass balancing

In principle the bias rate can be estimated by measuring the flowrates and pulp densities around the column, followed by mass balancing. The bias rate is expressed in terms of the operating variables as follows

$$J_B = \frac{(Q_{tw} - Q_{fw})}{A_c} - \frac{(Q_{ww} - Q_{cw})}{A_c} \qquad (2.27)$$

where Q_{tw}, Q_{fw}, and Q_{cw}, are the volumetric flowrates of water in the tails, feed and concentrate streams, respectively, cm³/s; Q_{ww} is the volumetric flowrate of wash water, cm³/s; and A_c is the column cross-sectional area, cm².

Since the concentrate flowrate and density are virtually impossible to obtain, as pointed out by Finch and Dobby (1990a), the approach adopted relies on measurements of feed and tailings streams. Thus, the bias rate is given by

$$J_B = \frac{Q_t \, \rho_t \, (1-x_t) - Q_f \, \rho_f \, (1-x_f)}{A_c} \qquad (2.28)$$

where Q_t and Q_f are the volumetric flowrate of the tails and feed streams, respectively, cm^3/s; x_t and x_f are the mass fraction of solids (%Solids/100) in the tails and feed streams, respectively; and ρ_t and ρ_f are the densities of the tails and feed streams, g/cm^3.

Q_t and Q_f are conventionally measured with *magnetic flow meters*; ρ_t and ρ_f are measured with *nuclear density meters or gamma gauges*. The mass fraction of solids (x_t and x_f) can be extracted from ρ_t and ρ_f provided the solids density is known. This is commonly achieved by considering statistical data on solids density in both streams.

This approach faces two major drawbacks: first, instrumentation is expensive, and second, it is subject to error propagation since several measurements and computations are required. For the bias rate expressed by

$$J_b = \frac{Q_t \, (1-v_{st}) - Q_f \, (1-v_{sf})}{A_c} \tag{2.29}$$

where v_{st} and v_{sf} are the volume fraction of solids in tails and feed slurries, Finch and Dobby (1990a) have shown that a relative standard deviation of 3% for each of the four process measurements gives rise to a relative standard deviation of J_b as high as 74%. (the theory of error propagation and application to bias determination is discussed in Appendix 1). A further problem is that the system is dynamic and estimates from mass balance calculations assume steady state.

The large error associated with the computation of bias has been also pointed out by Moys and Finch (1988b). The authors state that "the present methods used for bias rate estimation are inherently inaccurate since they involve the difference between the (inaccurate) measurement of two large and nearly equal flowrates, e.g. if the flowrate measurements are subject to 1% error and the bias difference Q_b is 5% of Q_f, the Q_b is subject to a 40% error." (Moys and Finch, 1988b).

Techniques based on temperature

The difference in wash water and feed pulp temperature exploited to detect level was also considered for bias detection (Moys and Finch, 1988b). The authors report that the temperature profile in the froth zone depended on operating variables including J_B. The use of the technique was extended to an industrial application, and though it does not measure J_B but a profile which is dependent on J_B, there is good evidence that shows the behaviour of the profile is related to metallurgical performance (Finch and Dobby, 1990a).

Similar temperature based techniques have been implemented to explore alternative approaches to bias measurement (froth washing efficiency (Moys and Finch, 1989) and feed water recovery (Maachar et al., 1990)). These measures are related to bias and are described below.

Moys and Finch (1989) reported data supporting the hypothesis that the recovery of fine hydrophillic particles is proportional to the recovery of feed water in the concentrate. By measuring the temperature in the streams around the column and performing an energy balance the authors obtained

$$\frac{Q_{fwc}}{Q_{cw}} = \frac{T_c - T_w}{T_f - T_w} \tag{2.30}$$

where Q_{fwc} is the flowrate of feed water recovered in the concentrate (cm^3/s); Q_{cw} is the flowrate of water in the concentrate (cm^3/s); and T_c, T_w, and T_f are the temperatures of the concentrate, wash water and feed streams (°C).

The authors found that the normalized temperature of the concentrate (2nd term in Equation (2.30)) is highly correlated with the recovery of hydrophillic particles (Figure 2.9).

The same temperature based technique and a similar approach is being investigated at the University of Toronto (Lin, 1988; Maachar et al., 1990). One of the objectives of the work is to evaluate feed water recovery and solids entrainment at the laboratory scale in liquid-gas and liquid-gas-solids systems. Feed water recovery is computed using the expression

$$R_{fw} = \frac{Q_c}{Q_f} \left(\frac{T_c - T_w}{T_f - T_w} \right)$$

(2.31)

where R_{fw} is the feed water recovery defined as the volumetric fraction of feed water that reports to the concentrate; Q_f and Q_c are the flowrates of the feed and concentrate (cm^3/s), respectively; T_c, T_w and T_f are the temperatures of the concentrate, wash water and feed streams (°C).

Maachar et al.(1990) report that the ratio *feed water recovery/hydrophillic solids recovery* depends on the solids particle size (Figure 2.10).

2.3   Summary

The process variables involved in the operation of flotation columns were introduced. The available methods to estimate interface level (or froth depth), gas holdup and bias rate were discussed. A number of devices and techniques in current use were described.

It was shown that methods based on the measurement of intensive properties of the system such as temperature and electrical conductivity appear to offer advantages over those relying on the measurement of extensive properties such as hydrostatic pressure head and volumetric or mass flowrates.
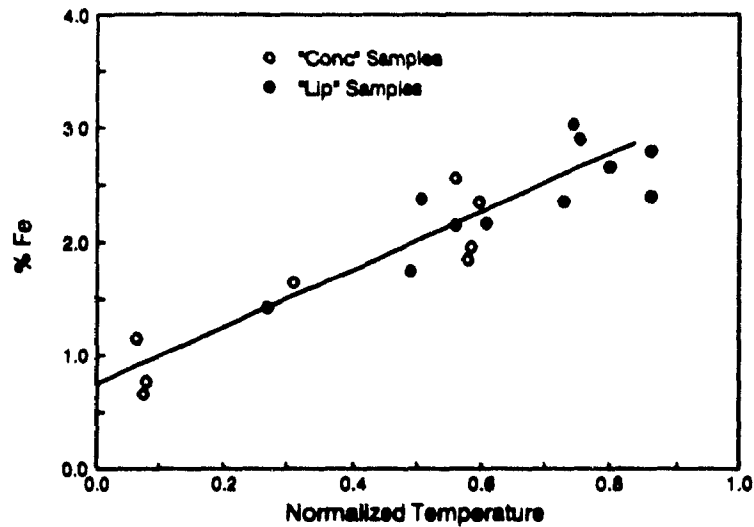
Figure 2.9   Correlation between grade of Fe (a gangue component) in the concentrate and normalized concentrate temperature (after Moys and Finch, 1989)
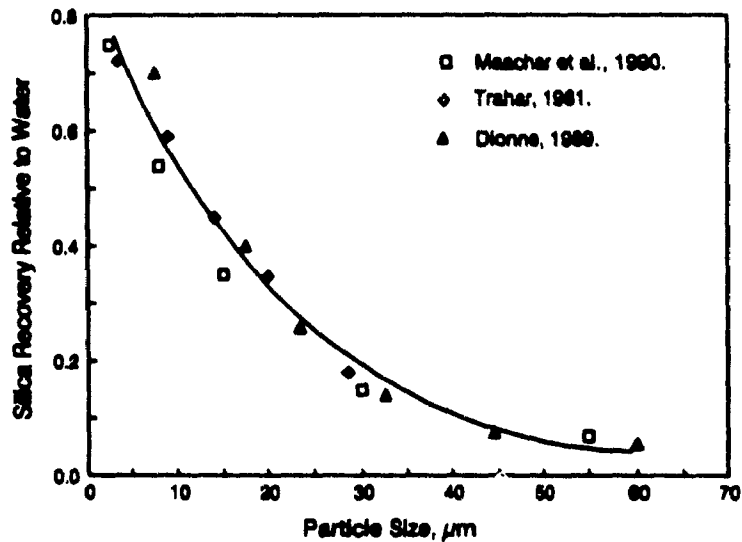
Figure 2.10   Effect of particle size on the ratio (slope) of solids recovery to feed water recovery for hydrophillic silica (after Maachar et al., 1990)

CHAPTER 3

ELECTRICAL CONDUCTIVITY, AN INTENSIVE PROPERTY

3.1 Basic Concepts

The electrical conductivity of a material is an intensive property, i.e. it does not depend on quantity or shape of the system. Chemical elements and compounds have well defined and tabulated electrical conductivities. Materials such as metal alloys, minerals and electrolytes are electrically more complex and have conductivities that depend on the chemical composition and the physical microstructure. Table 3.1 presents a sample of conductivity values reported for a variety of materials.

3.1.1 Definition of electrical conductivity

Electrical conductivity is the proportionality constant in Ohm's law. This law states, in its general form, that the current flow in any part of a given system is proportional to the potential gradient, that is

$$i = -\kappa \, \nabla V \qquad\qquad (3.1)$$

where i is the current density (A/cm^2), ∇V is the potential gradient (Volt/cm), and κ is the electrical conductivity (Ω^{-1}/cm). The sign indicates the current flows in the direction of the decreasing potential.

Electrical conductivity (or specific conductance) is an intensive property that may be thought of as the conductance (reciprocal of resistance) of a cube of 1 cm edge, assuming the current to be perpendicular to opposite faces of the cube (Braunstein and

Robbins, 1971).

Electrical conductivity has several equivalent terms: conductivity (Atkins, 1982; Levine, 1988; Braunstein and Robbins, 1971; Gilmont and Walton, 1956; Lord Rayleigh, 1892; Meredith and Tobias, 1962; Wagner, 1962), specific conductance (Condon, 1967; Andrews, 1970; Barrow, 1973), and specific conductivity (Adamson, 1979; Kasper, 1940). In the present Thesis, the term conductivity and the Greek letter kappa, κ, (the correct SI symbol) will be used.

Table 3.1   Representative values of electrical conductivity.

Substance	Type of conductor	Electrical Conductivity		Reference
		S/cm	t°C	
Copper	Metallic	6.4×10^5	0	Condon, 1967
Copper	Metallic	5.8×10^5	20	Shuey, 1975
Lead	Metallic	4.9×10^5	0	Condon, 1967
Iron	Metallic	1.1×10^5	0	Condon, 1967
Chalcopyrite, Galena and Pyrite	Mineral	~10	N.A.[a]	Shuey, 1975
Sodium fluoride, molten	Electrolytic	5.09	1000	Condon, 1967
4 molar H_2SO_4	Electrolytic	7.5×10^1	18	Condon, 1967
Process water in flotation circuits[b]	Electrolytic	0.01-0.04 0.001-0.007	N.A.[a] ~10°C	Hemmings, 1981 This work
0.1 molar KCl	Electrolytic	1.28×10^{-2}	25	Condon, 1967
0.01 molar KCl	Electrolytic	1.41×10^{-3}	25	Condon, 1967
Water	Nonelectrolyte[c]	4×10^{-8}	18	Condon, 1967
Xylene	Nonelectrolyte[c]	1×10^{-19}	25	Condon, 1967

a Not Available

b Range of conductivity of aqueous phase encountered in plant tests regarding flotation froths (Hemmings, 1981)

c Electrolytic in nature but showing such a small conductivity that may be called nonelectrolytes or perhaps nonconductors (Condon, 1967)

3.1.2 Units of conductivity

The units of the conductivity follow from Equation (3.1): If the current density is given in A/cm^2 and the voltage gradient in V/cm, the conductivity has units Ω^{-1}/cm.

The unit Ω^{-1} is sometimes written as mho (i.e. ohm spelled backwards); however, the correct SI name for the reciprocal ohm is the *siemens* (S): 1 S $\equiv$ 1 Ω^{-1}. Thus the SI units of conductivity are S m^{-1}. For convenience, the cgs unit S/cm (or the submultiple mS/cm) will be used throughout this Thesis.

3.1.3 Measurement of conductivity

The resistance R of an electrolyte solution cannot be reliably measured using direct current, because changes in concentration of the electrolyte and buildup of electrolysis products at the electrodes change the resistance of the solution. To eliminate these effects, an alternating current is used instead. By using the cell and the electric circuit shown in Figure 3.1, the resistance of the electrolyte is computed by simply applying Ohm's law $(I=(V_A-V_B)/R)$. Once R is known, the conductivity can be calculated from

$$\kappa - \frac{l}{A\,R} \tag{3.2}$$

where A and l are the area of and the separation between the electrodes (A complete derivation of this equation will be given in detail in Section 3.2.1).

Some of the more important phenomena associated with the application of a voltage between electrodes immersed in a liquid electrolyte are briefly discussed here with reference to Figure 3.2 (Braunstein and Robbins, 1971; Sawyer and Roberts, 1974).
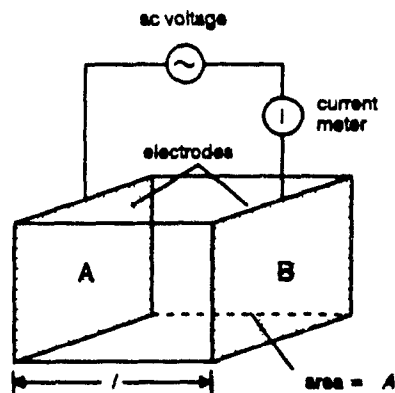
Figure 3.1 Conductivity cell and electric circuit to measure conductivity of electrolytes
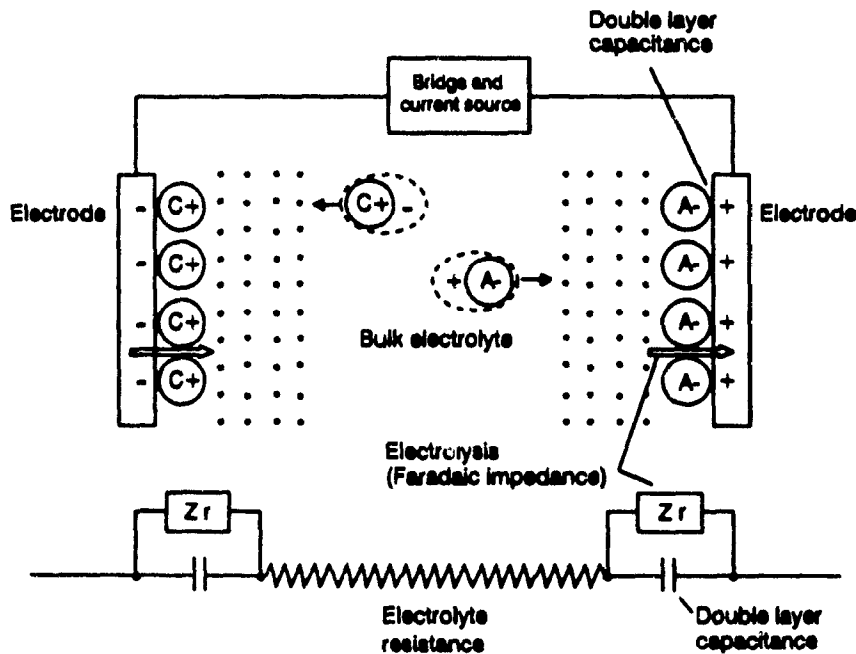
Figure 3.2 Electrolytic conductance cell and simplified schematic representation of the double-layer at the electrodes, Faradaic processes, and migration of ions through bulk electrolyte (after Braunstein and Robbins, 1971)

Double-layer capacitance. A positively charged electrode will preferentially attract a layer of negative ions (and a negative electrode a layer of positive ions). The double-layer, consisting of charges on the electrode and oppositely charged ions adjacent to it in solution (or separated from it by a layer of solvent molecules), constitutes an electrical capacitor, capable of storing charge. If a sufficiently low steady voltage is applied to the electrodes, virtually no current will flow beyond that required initially to charge the double-layer.

Electrolysis. As the voltage applied to the electrodes is increased, the charge accumulated in the double-layer increases until a decomposition voltage, analogous to the break-down voltage of a capacitor, is exceeded; current then flows across the electrode-solution interface, accompanied by oxidation at the positive electrode and reduction at the negative electrode. This Faradaic (electrolytic) process partially short circuits the double layer, behaving electrically akin to a resistor (although a voltage dependent one) shunting a capacitor.

Ohmic resistance. The current is carried through the bulk electrolyte by cations moving toward the cathode, anions toward the anode. Current flow is accompanied by dissipation of energy as heat, since the ions must overcome frictional forces in their motion through the medium.

Concentration polarization. On further increase of voltage, Faradaic removal of electroactive ions (i.e., ions reducible or oxidizable in the range of voltages applied to the electrodes) near the electrode may proceed faster than diffusion from the bulk electrolyte can replenish their supply. This can establish a concentration gradient between bulk electrolyte and the electrode surface, such that the current may reach a diffusion-limited value.

Calculation of the ohmic resistance of the electrolyte requires not only a measure

of the current (easily obtained) but also the voltage accelerating the ions. This is only part of the voltage applied to the electrodes, which also supplies the driving force for the electrical work needed for the Faradaic processes, double-layer charging and concentration polarization. The problem of resolving electrolytic conductance is that of eliminating the effect of these processes, and is generally accomplished by measurements with alternating current.

Alternating current effects. Reversal of the sign of the applied voltage reverses the direction of motion of the ions. With an alternating (ac) rather than a steady (dc) voltage applied to the electrodes, the above processes reverse themselves with the period of the alternating voltage. As the frequency is increased, concentration polarization can be greatly reduced or eliminated. The Faradaic effect can be eliminated by sufficiently reducing the applied voltage. Frequencies of 1 kHz and voltages less than 1 V are recommended for general applications (Cole and Coles, 1964).

3.2 Cell Constant and Geometrical Factors

3.2.1 The Theory of the Potential and the three cases of uniform current density distribution.

The theory of the potential relates primarily to the study of the distribution of potential energy between spatial configurations that represent levels of potential energy. These spatial configurations are the electrodes at different potentials (the anode and cathode). In the theory of the potential, a single configuration (electrode) is considered to be entirely at one level of potential energy and hence is an *equipotential* surface. It is convenient to consider the variation of potential from the anode to the cathode, or vice versa, also in terms of equipotential surfaces.

If any restrictions are placed upon the space in which these equipotential surfaces

can unfold, these restrictions enter into determining the form and position of the equipotential surfaces.

In trying to determine the form and position of the equipotential surfaces in a conductive medium, the following restrictions are observed (Kasper, 1940; Gilmont and Walton, 1956):

(1).- the medium is such that the rate of dissipation of energy is a linear function of the difference in potential level. This condition demands that a linear law of conduction be obeyed. In electricity this is known as Ohm's law which generally holds for electrolytes (Kasper, 1940; Gilmont and Walton, 1956). Ohm's law states that the current flowing in any part of the system should be a linear function of the potential gradient, which can be expressed by

$$i = -\kappa \, \nabla V \tag{3.1}$$

$$with \quad \nabla V = \frac{\partial V}{\partial x} + \frac{\partial V}{\partial y} + \frac{\partial V}{\partial z} \quad (for \ rectangular \ coordinates) \tag{3.3}$$

where i is the vector current, κ is the specific conductivity, and ∇V is the potential gradient at any point.

We know in addition that a total constant current enters the system at the anode, flows throughout it, and leaves through the cathode. If the electrodes are specified, then in accordance with the law of conservation of current the following must be true: If any volume of the conducting medium is selected, the net resultant of the current entering and leaving will be zero. In formal mathematical language this is expressed by the statement that *divergence of the current* is zero and written in symbols

$$\nabla i - 0 \qquad\qquad (3.4)$$

However, since $i = -\kappa \nabla V$, and if the medium is homogeneous electrically (κ is constant), the divergence of the gradient of the potential is zero, i.e.

$$\nabla \cdot \nabla V - \nabla^2 V - 0 \qquad\qquad (3.5)$$

This mathematical formulation is known as Laplace's equation, and it has within it the expression of the laws of electrical flow, although it applies equally to other phenomena which may be treated by the theory of the potential.

(2).- the medium is homogeneous and isotropic electrically. Since heat dissipation is associated with the flow of electrical current, and the conductivity changes with the temperature, electrolytes cannot be said to satisfy this condition in a strict sense, although the currents which are used can be made sufficiently small so that the influence of this effect can be neglected.

(3).- the flow of energy through the electrode does not alter the condition which must be assumed viz, that the surface of the electrode must be equipotential. This condition refers to what is known as the "resistance of the electrode (or terminal effect)". If the electrode is large with respect to the terminal of entry or departure of current and the conductivity of the electrode is sufficiently high as compared with that of the medium, this effect will tend to vanish. Since in most practical applications the ratio of conductivity of metal (i.e. of the electrode) to that of electrolyte ranges from a hundred thousand to a million, this effect can be neglected.

(4).- the flow of energy from the electrode to the medium or vice versa may introduce a discontinuity in potential at the electrode surface but the magnitude of the discontinuity must be uniform over the electrode surface. This condition refers to

electrode polarization which can be avoided, or at least rendered negligible, by using alternating current of a suitable frequency.

The terminal effect and electrode polarization can be further reduced by platinizing the electrodes, thereby increasing the surface area and reducing the current density (Braunstein and Robbins, 1971).

Having established the conditions to be satisfied, the three cases which give a uniform current flow will be discussed. These cases are the flow between (i) infinite parallel planes, (ii) concentric cylinders of infinite length, and (iii) concentric spheres (Kasper, 1940).

a).-   The flow between two infinite parallel planes and the method of sectioning

Consider the surface of the anode and the cathode as two parallel infinite planes each being equipotential. In this situation, the distribution of potential between the planes may be represented by planes parallel to the two initial planes. The lines of current flow must leave the anode normally, intersect every equipotential surface normally, and finally hit the cathode normally. If the medium is electrically isotropic and homogeneous the equipotential surfaces per unit potential difference must be equally spaced; thus it follows that a constant current flows from the anode to the cathode. The current density over the electrodes and over each equipotential surface is uniform. This may be indicated graphically by uniform spacing of lines representing lines of current flow.

Infinitely large planes for the anode and cathode is clearly impractical, so systems must be devised which are equivalent. This is effected by a method known as sectioning. The first type of sectioning considered is the replacement of any equipotential surface by a perfect conductor (electrode) with the same shape and position. This assumes implicity

that with a real electrode the terminal effect can be neglected. In a second type of sectioning it is assumed that the sectioning surfaces are everywhere coincident with lines (surfaces) of current flow and, in accordance with this definition, no current crosses such surfaces. The process of sectioning does not alter the flow within the boundaries created.

In a conductor like that illustrated in Figure 3.1 (which is a section of the initial system) where A and B are the electrodes the resistance is given by

$$R = \frac{drop\ of\ potential}{current} = \frac{V_A - V_B}{I}$$
(3.6)

In the case of a linear conductor the current density on any equipotential surface is constant, hence

$$i = -\kappa \frac{\partial V}{\partial x} = \frac{I}{A}$$
(3.7)

where i is the current density, k is the conductivity, I is the total current, and A is the cross-sectional area.

Integrating we obtain

$$K = \kappa \frac{A}{l}$$
(3.8)

where K is the conductance ($= 1/R$), and l is the length of the conductor.

b).-   The flow between concentric cylinders of infinite length.

The cross section of two concentric circular cylinders of infinite length is

illustrated in Figure 3.3(a), which can be sectioned out to obtain the equivalent system shown in Figure 3.3(b). The radius of the inside cylinder is r_1, and that of the external cylinder is r_2. The imaginary equipotential surfaces are a series of cylinders (of circular cross-section) between the two electrodes, with which they are coaxial The lines of flow, which must be normal to all of the cylinders, will hence be radii, which may be drawn from the center of the cylinder.

The actual separation of the equipotential surfaces per unit potential difference can be obtained. Since in this case the current density over any equipotential surface is uniform, the current density per unit area will be

$$ i = -\kappa \, \frac{\partial V}{\partial r} = \frac{I}{(2 \pi r)^{*}} \tag{3.9} $$

that is, the total current divided by the area of the equipotential surface, where r is the radius of the cylinder representing the equipotential surface. Integrating we have

$$ V_1 - V_2 = \frac{I}{2\pi\kappa} \ln \left(\frac{r_2}{r_1} \right) \tag{3.10} $$

the conductance per unit length is

$$ K = \frac{2\pi\kappa}{\ln (r_2 / r_1)} \tag{3.11} $$

---

* area of the cylinder per unit length = $2\pi r$
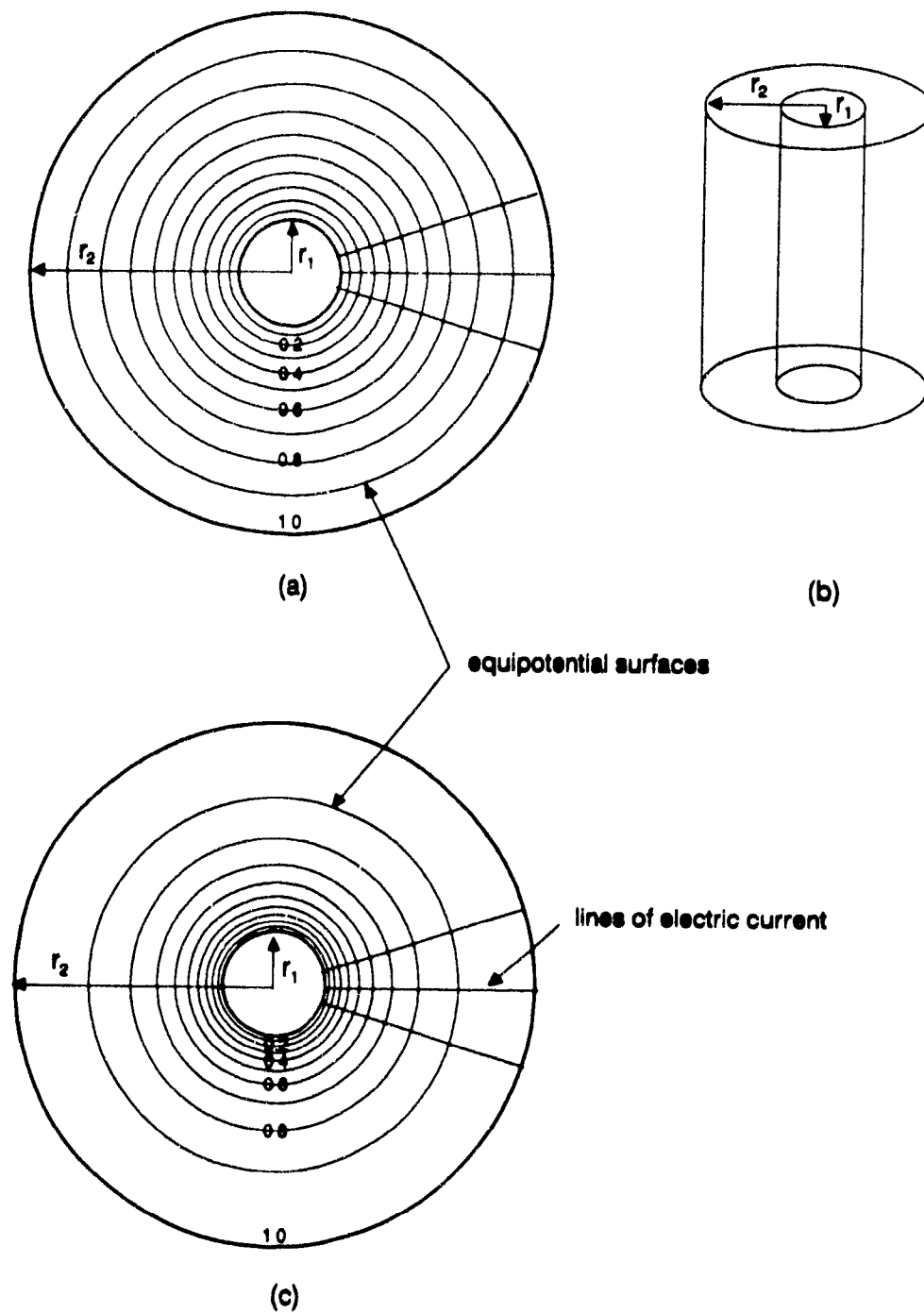
Figure 3.3 Equipotential surfaces and current lines between: (a) concentric cylinders, and (c) concentric spheres. (b) Sectioning to form a system equivalent to the concentric cylinders (after Kasper, 1940)

c).-The flow between concentric spheres

An arrangement of two concentric spheres represents the third and last case in which it is possible to obtain uniform current distribution over the electrodes. This is illustrated in Figure 3.3(c). The equipotential surfaces form a system of concentric spheres existing between the two spheres considered as the electrodes. The lines of flow must be radial lines, which may be drawn from the center. The separation of the equipotential surfaces per unit potential difference can be established. The current density over the equipotentials is

$$i = -\kappa \frac{\partial V}{\partial r} = \frac{I}{4\pi r^2} \tag{3.12}$$

where $4\pi r^2$ refers to the area of any equipotential surface.

Integrating we obtain

$$V_1 - V_2 = \frac{I}{4\pi\kappa} \left(\frac{1}{r_1} - \frac{1}{r_2} \right) \tag{3.13}$$

For the conductance of this system we have:

$$K = 4\pi\kappa \left(\frac{r_1\, r_2}{r_2 - r_1} \right) \tag{3.14}$$

3.2.2 Geometries that depart from the three cases of uniform current density distribution

In a cell with parallel electrodes filling the entire cross section (like the one illustrated in Figure 3.1), a uniform current density may be expected because of

symmetry. In this type of cell the electrical conductivity of the medium can be calculated by using Equation (3.2). For any other cell geometry where uniform current density is not developed, the relationship between the geometrical and electrical parameters of the cell, and the conductivity of the medium should be derived from the basic principles of the theory of the potential, namely that the current density lines must be orthogonal to the equipotential surfaces. Accordingly, in a solution of uniform electrical conductivity, the propagation of electrical energy in the steady state will be such as to satisfy the Laplace equation everywhere, i.e., including the boundaries of the system under consideration (Wagner, 1962; Meredith and Tobias, 1962). The physical consequence of the above statements imply that the lines of flow describing the path of the electric charge show no discontinuities, the flow is "smooth", and that at all points within the system, including the boundaries, lines of flow are orthogonal to equipotential surfaces.

The potential over the cathode is constant if polarization is negligible. The same is also true for the anode. At insulating walls the potential gradient normal to the wall must vanish. Then the solution of the differential Equation (3.5) for the boundary conditions as stated can be calculated. From it, one may obtain the local current density as the product of the electrical conductivity and the potential gradient normal to the surface of the electrode. Results of such calculations are found in papers by Kasper (1940), Hine et al. (1956), and Gilmont and Walton (1956).

An example of this type of analysis is given by Gilmont and Walton (1956) for an electrolytic cell (Figure 3.4) which consists of a container with two straight sides intersecting at 45° and two curved sides consisting of rectangular hyperbolic cylinders orthogonal to each other, and each in turn orthogonal to one of the straight sides. One of the straight sides and its opposite curved surface are insulators, the other straight side is the cathode while the remaining curved surface is the anode. In this geometry the equipotential surfaces and the current density lines appear as rectangular hyperbolas in the x-y plane being mutually orthogonal in accordance with the theory of potential. Also,
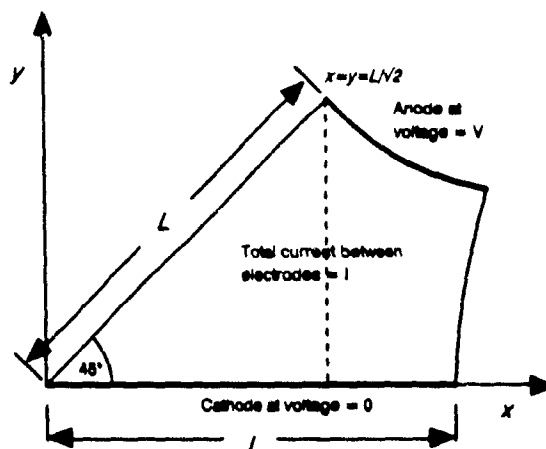
Figure 3.4 Electrolytic cell in which the current density along the cathode is linear and can be calculated directly from the electrical parameters (after Gilmont and Walton, 1956)

(a)   (b)
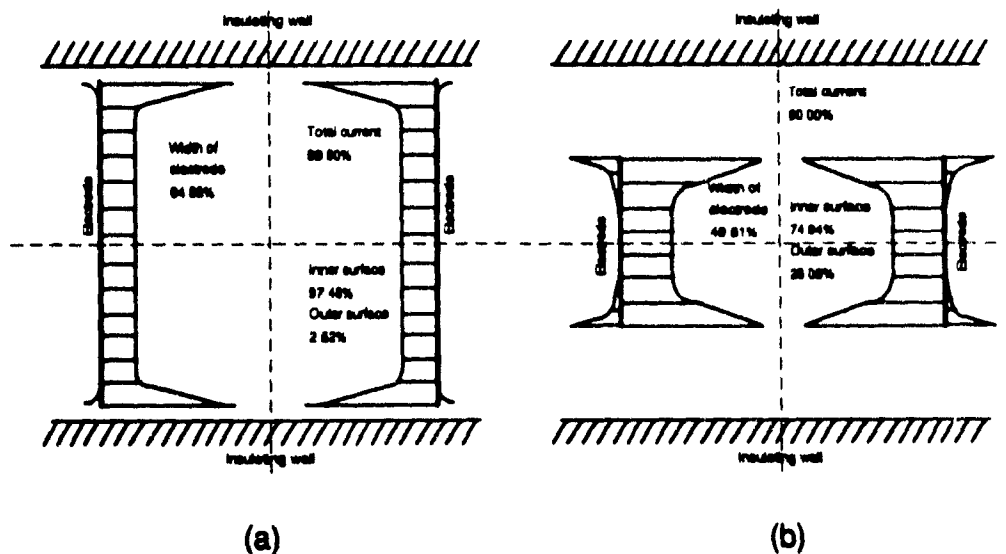
Figure 3.5 Current distribution when the electrode width is: (a) 94.95%, and (b) 49.81% of the bath width (after Hine et al., 1956)

the current density along the cathode is linear and can be calculated directly from the total current and voltage of the cell. The equation relating the conductivity of the medium and electrical and geometrical parameters is

$$K - \kappa \frac{A}{L} \tag{3.15}$$

where K is the conductance ($=I/V$; I the total current flowing between the electrodes, and V the voltage drop across the electrodes); κ is the conductivity of the medium; L is the length of the cathode; and A is the area of the cathode receiving current.

Hine et al. (1956) have calculated the current distribution in cells where the electrodes fill the cross section of a trough only in part and current lines originate and terminate at both the front side and the back side of the electrodes (Figure 3.5). The analysis considers only the effect of the side walls on the current distribution and assumes that the back walls are far removed from the electrodes: "The problem is treated as a two-dimensional one, and the Schwarz-Christoffel transformation is used. If the effect of four walls in a rectangular cell are considered, a hyper-elliptic integral appears, and the analysis is beyond possibility" (Hine et al., 1956).

Numerical methods, such as the finite-difference method, have been proposed to obtain numerical solutions for problems whose analytical solutions are complex (Binns and Lawrenson, 1963). Appendix 2 presents the basis of the method.

3.3   Electrical Conductivity of Two and Three Phase Systems

Electrical conductivity methods to measure holdup in two- and three-phase systems appear to be a standard laboratory technique. This section gives a brief description of the most well-known models as well as some of the applications.

3.3.1 Definition

The electrical conductivity of two or three phase dispersions (a continuous phase plus one or two dispersed phases) has been termed "effective conductivity" (De la Rue and Tobias, 1959; Hashin, 1968; Neale and Nader, 1973; Fan et al.,1989), "apparent conductivity" (Turner, 1976) or simply "conductivity". In the present Thesis the term effective conductivity -to distinguish the conductivity measured for a multiphase system from that for a single phase- will be used together with the letter kappa, κ, and appropriate subindices indicating the type of system, e.g. κ_{l-s} refers to the conductivity of a liquid-solids-gas system. For convenience, cgs units (S/cm) will be used.

3.3.2 Available models

a).-   Electrical conductivity of two-phase dispersions

In general terms, the electrical conductivity of a liquid-gas, κ_{l-g}, or liquid-solid, κ_{l-s}, system depends on the electrical conductivities of the two phases and their relative amounts. However, as noted early by Maxwell (1892), the conductivity of dispersions do not follow the additivity rule, i.e. the relation between conductivity of the dispersion and the concentration of the dispersed phase is not linear.

As far as it is known, Maxwell (1892) was the first to investigate the phenomenon. Maxwell considered a sphere of different conductivity from the material around it and the effect of this sphere on the current flow, and potential field, in the surrounding material. If many such spheres -at distances from each other large enough so that their effects in disturbing the course of the current may be taken as independent of each other- are contained within a larger sphere of the continuous medium, then the *effective conductivity*, κ_{l-d}, of the large sphere for a volume fraction ε_d of the dispersed phase of conductivity κ_d is given by

$$\kappa_{l\text{-}d} - \kappa_l \left(\frac{1 + 2\beta\epsilon_d}{1 - \beta\epsilon_d} \right) \tag{3.16}$$

where κ_l is the conductivity of the continuous phase, and β is given by

$$\beta - \frac{\alpha - 1}{\alpha + 2}; \qquad \alpha - \frac{\kappa_d}{\kappa_l} \tag{3.17}$$

Hashin (1968) studied the electrical and thermal conductivity properties of solid heterogeneous media (polycrystalline aggregates and bimetallic composites, for example) and proposed a universal expression for electric and thermal conduction equivalent to Maxwell's equation, namely

$$\frac{\kappa_{c\text{-}d}}{\kappa_c} - \frac{k_{c\text{-}d}}{k_c} - \left(\frac{1 + 2\beta\epsilon_d}{1 - \beta\epsilon_d} \right) \tag{3.18}$$

where $\kappa_{c\text{-}d}$ and $k_{c\text{-}d}$ stand for the electrical and thermal conductivity of the continuous-dispersed phase, respectively, and κ_c and k_c are the electrical and thermal conductivity of the continuous phase, respectively.

Neale and Nader (1973), based on a model for an homogeneous and isotropic swarm of dielectric spherical particles and through the analogy between the problem of electrical conduction and the problem of diffusion, reported an expression equivalent to Maxwell's equation for non-conducting dispersed phase, namely

$$\frac{\kappa_{l\text{-}d}}{\kappa_l} - \frac{1 - \epsilon_d}{1 + 0.5\,\epsilon_d} \tag{3.19}$$

The agreement between the experimental data (acidified aqueous copper sulphate solution-glass spheres less than 0.2 mm diam.) and the model proved to be satisfactory for packed beds ($\varepsilon_s > 0.55$) and excellent for suspensions ($\varepsilon_s < 0.55$).

Maxwell's model has been successfully used by Turner (1976) for measuring holdup in liquid-fluidized beds of spheres. A range of solid particle diameters (0.15-1.0 mm) and conductivities (0 ~ 0.03 S cm^{-1}) were used. The conductivity of the aqueous solution was varied by NaCl additions. Although Maxwell's model considers dilute dispersions (Maxwell, 1892), solid volume fractions of up to 60% were adequately fitted by Maxwell's equation. In that work, two platinized-platinum wire grid electrodes were immersed in the fluidized bed contained in a 7.4 cm diameter column, and the resistance between them was measured as a function of their separation. The slope of the straight line portion of the graph of resistance against separation was used to calculate the effective conductivity of the suspension.

Bruggeman (1935), as reported by Nasr-El-Din et al. (1987), extended Maxwell's work to the case of spheres of various sizes and random distribution. His equation should, therefore, be valid for a mixture of a wide size distribution at *any concentration*. For a mixture of solids conductivity κ_s, liquid conductivity κ_l and solids concentration ε_s, Bruggeman's equation is

$$(\kappa_{l-s} - \kappa_s) \left(\frac{\kappa_{l-s}}{\kappa_l} \right)^{-1/3} = (1 - \varepsilon_s) (\kappa_l - \kappa_s) \qquad (3.20)$$

For a mixture of nonconducting solids in a conducting liquid, this reduces to

$$\frac{\kappa_{l-s}}{\kappa_l} = (1 - \epsilon_s)^{3/2} \tag{3.21}$$

De la Rue and Tobias (1959) measured the conductivities of random suspensions of glass spheres, polystyrene cylinders and sand particles (0.175 to 0.21 mm) in aqueous solutions of zinc bromide of approximately the same densities as the particles. Solids holdups up to 40% were tested. They found the suspension conductivity could be calculated from the expression

$$\kappa_{l-s} = \kappa_l (1 - \epsilon_s)^m \tag{3.22}$$

where m = 1.35 to 1.56 depending on the "irregularity" and size distribution of particles. The authors reported that Maxwell's model performed well for uniformly sized spheres ($m \sim 1.35$), while Bruggeman's equation applied best for irregular particles and random distribution of sizes ($m = 1.5$).

Lord Rayleigh (1892) treated the cases of parallel cylinders in a square array and spheres of uniform size in cubical array. In each case, the effect of a large number of "shells" of cylinders (and spheres) surrounding a central one was considered. For the cubical array of spheres where the field is perpendicular to a side of the cube, using the principle of superposition for potentials, Lord Rayleigh obtained

$$\kappa_{l-d} = \kappa_l \left[1 + \frac{3\beta\epsilon_d}{1 - \beta\epsilon_d - 0.525[(\kappa_d - \kappa_l)/(\kappa_d + \frac{4}{3}\kappa_l)]\beta\epsilon_d^{10/3}} \right] \tag{3.23}$$

The upper limit of ε_d is implicitly set by the geometry of the model; Equation (3.23) loses physical significance above $\varepsilon_d > \pi/6$ ($\sim 52\%$), i.e. above the holdup corresponding to a cubical packing of spheres.

In the case of cubic array of spheres, using a different function for the potential and considering higher terms in the series expression for the potential in the continuous phase, Meredith and Tobias (1962) derived a similar expression for κ_{1d}.

Yianatos et at.(1985) developed a geometrical model based on the concept of tortuosity to estimate local gas holdup from conductance measurements in a two-phase (water-air) bubble column. This model considers the ratio between the conductance of the liquid-gas dispersion and the conductance of the aqueous-phase

$$\gamma = \frac{K_{l-g}}{K_l} = \frac{\kappa_l A(1 - \varepsilon_g)/l_e}{\kappa_l A/l} = \frac{1 - \varepsilon_g}{l_e/l} \tag{3.24}$$

where γ is the relative conductance, A is the cross-sectional area of conducting material, l is the length of the path between electrodes and l_e is the effective length of the path at gas holdup ε_g.

This model considers the tortuosity as a function of the gas holdup in both the froth and bubbling zones. Assuming spherical bubbles in a homogeneous regime for the bubbling zone,

$$\frac{l_e}{l} = 1 + 0.55 \, \varepsilon_g \tag{3.25}$$

and assuming a cellular bubble shape in the froth zone with the ions preferentially migrating along the borders,

$$\frac{l_e}{l} - 2.315 \, \epsilon_g \tag{3.26}$$

The model was tested in a two-dimensional column, $2.5 \times 10 \times 100$ cm, using facing rectangular electrodes, 1×2.5 cm, glued on the walls and for a range of gas holdups in both the bubbling (0-30%) and froth (60-95%) zones.

Considering a dispersion of air bubbles ($\kappa_{air} \approx 0$) in a continuous aqueous-solution, an equation similar to that of Maxwell is obtained by substituting Equation (3.25) into Equation (3.24), namely

$$\frac{K_{l-g}}{K_l} - \frac{1 - \epsilon_g}{1 + 0.55 \, \epsilon_g} \tag{3.27}$$

except Equation (3.27) considers conductances K, rather than conductivities κ.

Figure 3.6 shows the comparison between models by Maxwell (Equations (3.16) and (3.17)), Rayleigh (Equation (3.23)) and Bruggeman (Equation (3.20)).

b).-   *Electrical conductivity of three-phase dispersions*

Three-phase systems are common in fluidized bed and packed column reactors used mainly in hydrocarbon and coal processing applications. In a typical three-phase system the liquid forms the continuous phase while the gas and solids are discontinuous phases.
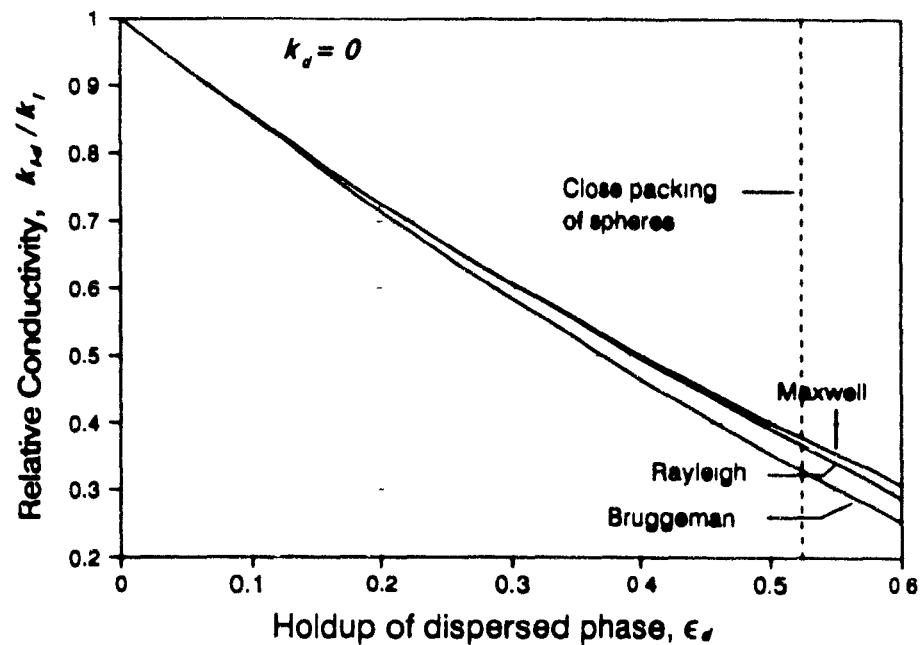
Figure 3.6 A comparison of model by Maxwell (Equations (3.16) and (3.17)), Rayleigh (Equation (3 23)) (uniformly sized spheres in cubical array), and Bruggeman (Equation (3 21)) (distribution of sizes)

Achwal and Stepanek (1975,1976) report an experimental method to determine the gas and liquid holdups in packed columns using electrical conductivity. The method is based on the following considerations: The conductivity of a liquid system with a fixed concentration of ions at a fixed temperature is proportional to the cross-sectional area of conducting material and inversely proportional to the length of the path between two electrodes. The fraction of the cross-sectional area occupied by the liquid in a multi-phase system is equal to the volumetric fraction of the liquid. The length of the path in a multi-phase system is obtained by multiplying the distance between the electrodes by some tortuosity factor. If the tortuosity factor does not change substantially with the amount of gas in the ternary system (gas-liquid-solid), then the conductivity should vary in proportion to the liquid holdup in the bed.

These authors found that in a 5 cm diameter column packed with non-conductive 1/4" Rashing rings or 6 mm ceramic cylinders, (both giving $\varepsilon_s = 0.543$), the conductivity of the liquid-solid-gas system κ_{l-s-g} did vary in proportion to the liquid holdup in the bed

$$\frac{\kappa_{l-s-g}}{\kappa_{l-s}} - \varepsilon_l \qquad (3.28)$$

where κ_{l-s-g} is the effective conductivity of the ternary system and κ_{l-s} is the conductivity of the packed bed filled with the aqueous solution, S/cm.

This method involves the use of two electrodes made of coiled tungsten wire located one at the bottom of the bed and the other 60 cm above, close to the column overflow. It is worth noticing that the authors do not explicitly consider the solids holdup (54.3% in this case) in Equation (3.28) and that 100% liquid holdup in the two-phase system liquid-gas actually represents 45.7% in the ternary system liquid-solid-gas.

Dhanuka and Stepanek (1987) also found Equation (3.28) to be applicable in determining the liquid holdup in a three-phase fluidized bed (glass spheres 1.98 to 5.86 mm diameter). The authors made clear that ε_l in Equation (3.28) is "on solid free basis".

Begovich and Watson (1978) used a technique based on electrical conductivity to measure the axial variation of holdups in three-phase fluidized beds. In this work 4.6-6.3 mm glass, alumina and Plexiglas beads were fluidized by air and water in either a 7.62 cm or 15.2 cm diameter column. Two 1.4 cm^2 platinum electrodes were attached 180° apart on the inside of a movable Plexiglas ring. The pressure gradient in the bed was obtained by using eleven liquid manometers located at 9 cm intervals along the column. The three-phases holdups were calculated using the equations

$$\varepsilon_l + \varepsilon_g + \varepsilon_s - 1 \qquad (3.29a)$$

$$\frac{dP}{dh} = g \ (\rho_l \varepsilon_l + \rho_g \varepsilon_g + \rho_s \varepsilon_s) \tag{3.29b}$$

$$\frac{\kappa_{l-s-g}}{\kappa_l} = \varepsilon_l \tag{3.29c}$$

where dP/dh is the pressure drop along the fluidized bed (Pa/m), g is the acceleration due to gravity (m/s^2), and d_i is the density of the i (i=liquid, or solid or gas) phase (kg/m^3).

Kato et al. (1981) used a conductivity technique to measure liquid holdup in a gas-liquid-solid fluidized bed. The authors found that for fluidized beds of uniform glass beads (0.42, 0.66, 1.2, and 2.2 mm diameter) the following empirical equation fit their data

$$\frac{\kappa_{l-s-g}}{\kappa_l} = \varepsilon_l^{1.2} \tag{3.30}$$

3.4 Summary

The physical/chemical phenomena involved in the measurement of electrical conductivity of electrolytes were described. The geometric constraints of the cell designs used to measure conductivity were discussed in the light of the theory of the potential.

Several models proposed in the literature to define the effective conductivity of two and three phase dispersions were presented.

CHAPTER 4

INTERFACE LEVEL: EXPERIMENTAL TECHNIQUES AND RESULTS

4.1   Introduction

In Section 2.2.1, the importance of the interface level in the performance of flotation columns was discussed and the different ways of measuring it were presented. This chapter describes the steps followed in the development of a conductivity based technique to measure interface level in flotation cells.

The froth zone and the collection zone in flotation columns have substantially different gas contents. Since the electrical conductivity of a dispersion depends on the amount of dispersed phase, as described in Section 3.3, it should be possible, in principle, to distinguish one zone from the other based upon their effective conductivities. Furthermore, the position at which the substantial change in gas contents occurs, i.e. the interface position, should be also detectable. The Pulp height-Froth depth monitor (Kitzinger et al., 1979) exploits this principle.

In a two-phase (liquid-gas) laboratory flotation column, Yianatos et al. (1985) found that for gas holdups in the bubbling zone of 0 to 30%, the gas holdup in the froth zone ranged from 60 to 90%. Further work (Yianatos et al., 1986 and 1987) revealed that for a variety of operating conditions, the gas holdup in the base of the froth ranged from 52 to 67%. Thus, under the extreme circumstances of a combination of gas holdup of 30% in the bubbling zone and 52% in the base of the froth zone, a conductivity ratio ($\kappa_{bubbling\ zone} / \kappa_{froth\ zone}$) of 1.50 is obtained by using Yianatos correlations (Equation (3.24) to (3.26)). This conductivity ratio will increase if: (a) the temperature of the froth phase is lower than that of the slurry (a proportional relationship between conductivity and

temperature exists); and (b) the water in the froth phase contains less dissolved electrolytes (as will typically be the case as reagents are not usually added to wash water). In most circumstances, the ratio is large enough to be exploited for level detection purposes (Moy_ and Finch, 1988a; Gomez et al., 1990).

4.2   Laboratory Scale Columns

4.2.1   Previous work

Conductivity based techniques for level detection in laboratory scale columns has been explored by Moys and Finch (1988a). These authors analyzed the liquid-gas system using a rectangular Plexiglas column (180 cm high with a 10 cm × 2.5 cm cross-section). Two general methods to locate the level were explored: (i) interpretation of the conductivity signal of a pair of vertical plates (15 cm × 1.5 cm) facing each other; the signal is proportional to the level position provided the level is within the "detecting" length of the electrodes; and (ii) interpretation of a conductivity measurement along the vertical axis of the column. The measurement was performed with two electrodes (1 0 cm × 2.5 cm) located above one another (20 cm of separation).

The results presented in Figure 4.1 showed that method (i) gave a conductivity signal more or less proportional to the level, whereas in method (ii), the inverse of the conductivity signal, i.e. resistivity, was proportional to the position of the level.

More recently, Moys (1989) reported the results of laboratory testwork in the development of a simple conductivity sensor capable of detecting level under conditions of drastic changes in conductivity of the flotation pulps such as those encountered in most flotation circuits.
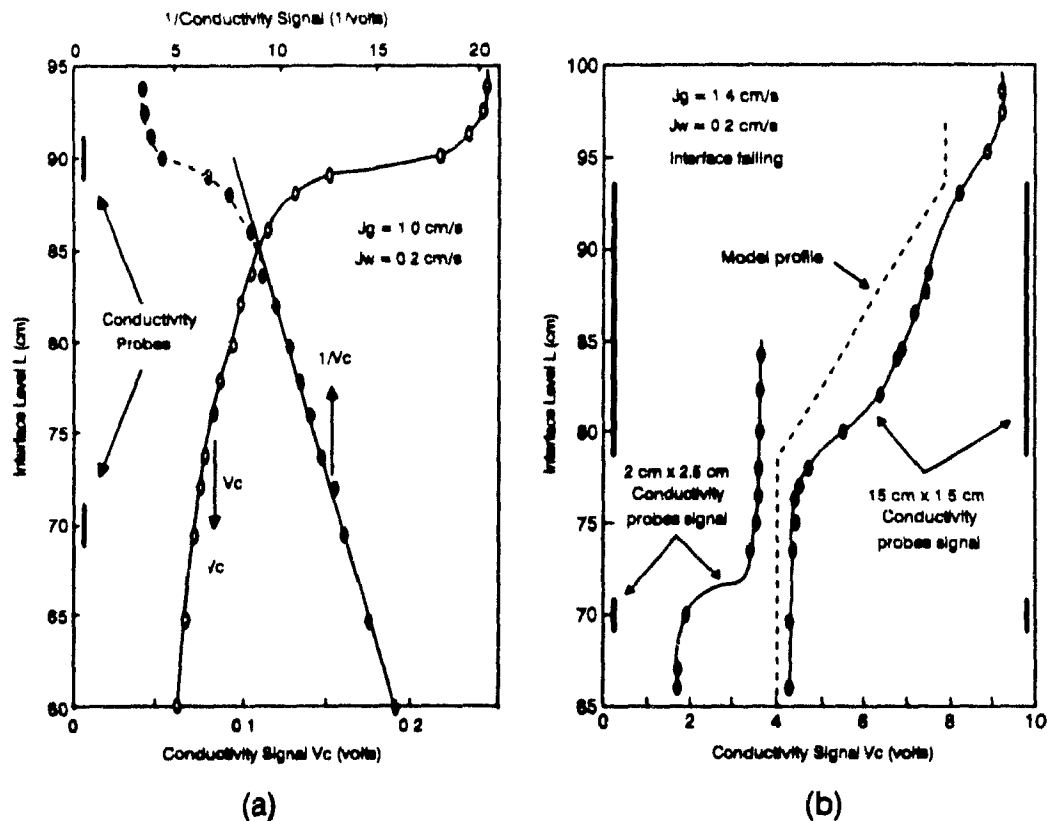
Figure 4.1 Conductivity response as a function of interface level for: (a) two electrodes measuring conductivity along the vertical axis, and (b) long parallel vertical electrodes; the response of a pair of short electrodes located at 70 cm is also shown (after Moys and Finch, 1988a)

4.2.2 Preliminary work on the detection of level using conductivity

In order to explore the potential use of conductivity as a technique for level detection in three phase (slurry-air) systems, an experimental program to be completed with a laboratory column was designed.   The program consisted in measuring conductivity according to two methods: the first, similar to method (i) used by Moys and Finch (1988a), namely, interpretation of a conductivity signal generated by means of a pair of facing plates (100 cm × 1 cm) installed in the top section of a 5.04 cm diam.
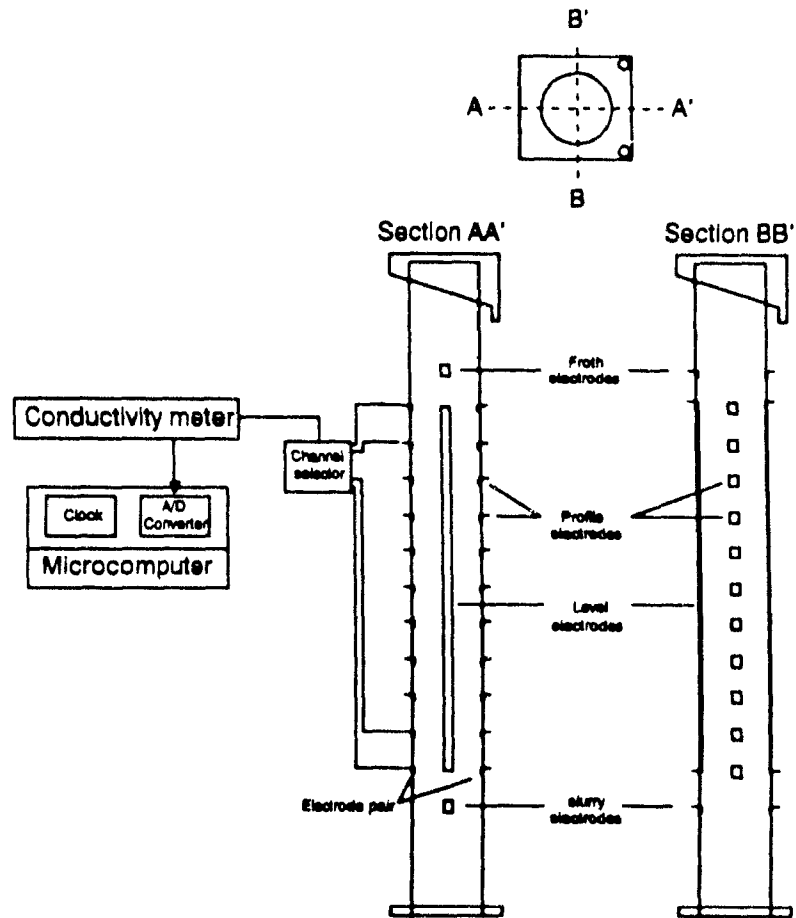
Figure 4.2 Schematic representation of electrodes arrangement in the top section of the 5.04 cm diam. column and attached data acquisition system

laboratory column (Figure 4.2). The signal was expected to be proportional to the position of the level along the electrodes. Two pair of facing electrodes (2 cm × 1 cm), one above and the other below the long ones were used to measure the conductivities of the froth and collection zones. The second method comprised the collection of conductivity profiles around the interface by means of a series of electrode pairs equally spaced along the vertical axis of the top section of the column. The level position was to be inferred from the sharp change in conductance across the interface.

The experimental apparatus consisted of a 5.04 cm diam. × 10.5 m height Plexiglas column. A porous stainless steel sparger installed at the bottom of the column was used to generate the air bubbles. Feed was introduced at about 2 m from the top of the column. Wash water was added at about 1 cm below the lip through a perforated 0.64 cm (1/4") copper tube ring. The air fed to the column via the gas sparger was measured using a calibrated rotameter. Three peristaltic pumps (Masterflex Cole Parmer, model 7520) were used to supply and control the flows of feed, tailings and wash water.

The top section of the column (Figure 4.2) comprised a suitable arrangement of electrodes to obtain conductance profiles and conductance readings that allow the calculation of the interface position within the column. In the case of conductance profiles, 11 electrode pairs (stainless steel plate, 1×2 cm), were glued to the column walls following vertical lines 180° apart, and with a separation of 10 cm starting at 50 cm from the top of the column. For level estimation, 3 electrode pairs were installed in the same way but on vertical lines displaced 90° from those of the profile electrodes. A pair of long parallel electrodes (stainless steel plate, 1×100 cm), was installed at 50 cm from the top of the column. Two pairs of small electrodes for measuring froth and collection zone conductances were installed at 40 and 160 cm from the top of the column, respectively.

The data were collected using a data acquisition system formed by a microcomputer (Mackintosh, Apple compatible, 64 K of memory), a conductivity meter (Tacussel, Mod. CD 810), an interface board which includes a clock and an 8-bit A/D converter, and a manual 10-channel selector.

The acquisition of the data during the experiments was as follows:

i).- Electrode pairs were connected to the different positions in the channel selector according to a pre-established reading sequence.

ii).- The first electrode pair was connected to the conductivity meter through the channel selector.

iii).- After six time constants (the time constant of the conductivity meter limits this value to a minimum of 3 seconds, see part 4.2.3(d) in this section) had elapsed the meter output to the computer A/D converter was read and stored in the computer memory (this value corresponds to the conductance through the selected pair of electrodes).

iv).- Another pair of electrodes was connected to the conductivity meter via channel selector and step (iii) was repeated until all the electrode pairs had been scanned.

A stream of the copper circuit (PRC, primary rougher concentrate) of the Strathcona mill (Falconbridge Ltd.) was used. Four runs were completed with combinations of two solids contents (30% and 47%), and two different tailings rates (0.9 and 1.26 cm/s). The interface level was controlled varying only one of two variables: feed or wash water flowrate. The air rate was maintained constant at around 2 cm/s. After the column was operated at the selected conditions for 2 residence times, the data acquisition was initiated. The actual position of the level was determined by visual inspection. Typical results obtained are presented in Figures 4.3 which shows conductance profiles for normal, intermediate and low levels.

There are two important findings to stress: first, a large difference between the conductance of the froth and collection zone does exist, thus, satisfying the condition for level detection using conductivity; and second, a conductance variation within the zones exists; in other words, the conductance varies within a zone as the position of the measuring point moves away from the interface. This finding has significant impact in the calculation of level using two long electrodes, which will be discussed next.
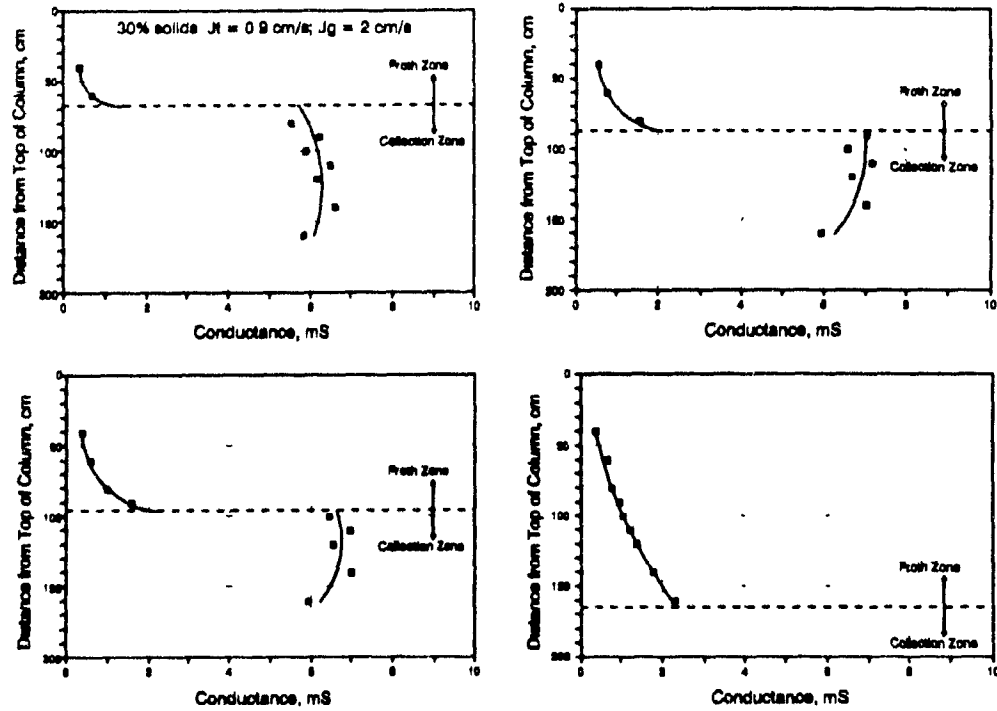
Figure 4.3   Conductance profiles obtained in the 5.04 cm diam. column while processing a
mineral slurry (Primary Rougher Concentrate)
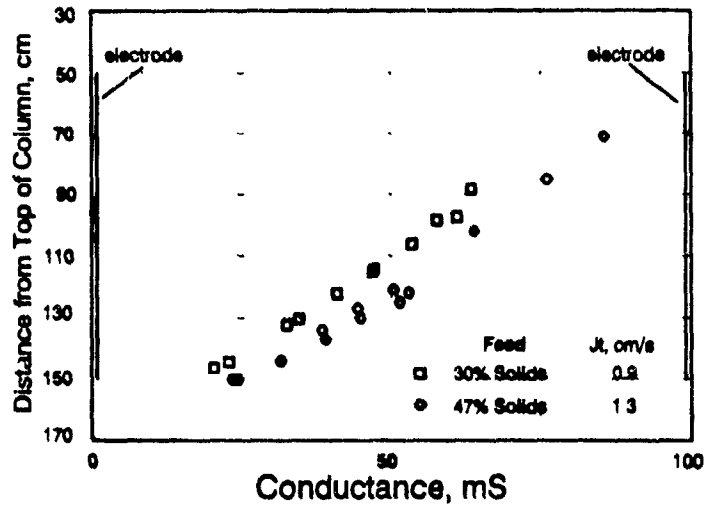
Figure 4.4   Response of the "level" electrodes to interface level variations

In principle, the relationship between conductance and level was substantially linear as shown in Figure 4.4. This figure also shows that the conductance response depends on the operating conditions; for example, the same conductance value in Figure 4.4 holds for two different level "locations" corresponding to two % Solids in the feed (30 and 47%). Thus, knowledge of the conductance of the froth and collection zones is required to compensate for variations in operating conditions. This was done by using the conductance measured with the electrodes at 40 and 160 cm from top of the column for the froth and collection zones, respectively, and by using the expression (Appendix 3)

$$l = L \times \frac{(K_{fw}/K_{lw})\ K_l - K_f}{(K_{fw}/K_{cw})\ K_c - K_f} \tag{4.1}$$

where l is the position of the interface within the long electrodes; L is the length of the long electrodes (cm); K_{fw}, K_{lw} and K_{cw} are the conductances measured in water with the froth, "level" and collection (zone) electrode pairs (mS), respectively; and K_f, K_l and K_c are the actual conductances measured during normal operation with the froth, level and slurry electrodes (mS), respectively.

Figure 4.5(a) presents the comparison between the interface position calculated by using Equation (4.1) and that from visual inspection. A constant offset was observed which is most likely due to the existence of a conductance profile in both zones. Since values measured with the electrode pairs located at 40 and 160 cm were assigned to the conductance of the froth and collection zone, it is clear from Figure 4.3 that those values are unlikely to represent the average conductance value of the zone (or at least that portion of the zone which lies within the "level" electrodes). Better accuracy is obtained if an average value of the conductance for both zones is considered in the calculation, as shown in Figure 4.5(b). Since this approach for measuring level requires the measuring of conductivity for the froth and collection zones above and below the probe, the problem posed by the existence of a profile cannot be avoided.
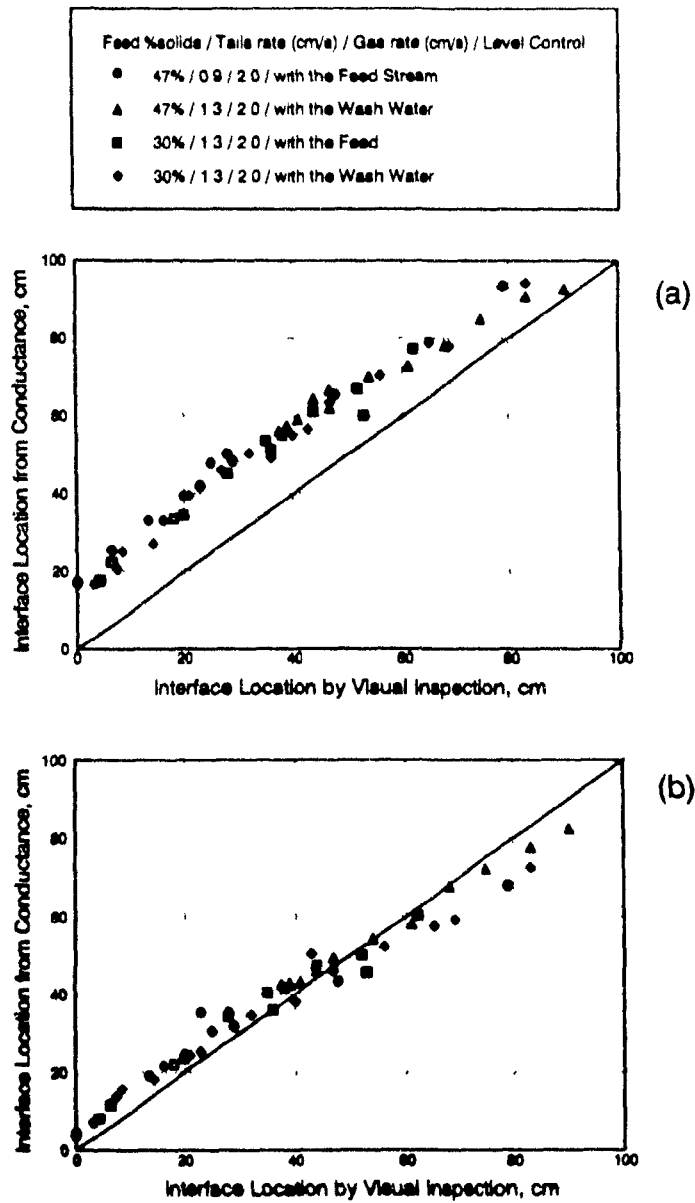
Figure 4.5 Computation of interface level: (a) using "local" values for the conductance of the froth and collection zone, and (b) using the averaged conductance values for both zones

4.2.3 Level detection from conductance profiles

a).-   Physical/chemical nature of the profile

The conductance profiles, the second alternative for level detection, clearly show the interface position (Figures 4.3). As a first approximation, it can be said that the conductance measured in the froth or collection zone, since the conductivity cell (geometry) is fixed, is a function of the amount of non-conductive phase (gas holdup) and the conductivity of the conductive phase (liquid). Thus, the differences in conductance between the froth and collection zones observed are most probably due to a combination of: a).- a difference in gas holdup between both zones, and b).- a difference in conductivity between the wash water and pulp water. These effects are illustrated by considering the conductance profiles in Figure 4.6, collected in a two-phase (liquid-gas) system.

Figure 4.6(a) shows that for the same operating conditions, the nature (chemistry) of the water used as feed and wash water has an impact on the conductance values. When using the same source of water (recycled water, $\kappa_{25°C} = 2.16$ mS/cm) for the feed and wash water, the difference in conductance between the bubbling and froth zone (conductance ratio ~ 2.5) is essentially due to the difference in gas holdup. A bubbling to froth zone conductance ratio of 2.5 is in good agreement with the values expected from the correlations of Yianatos et al.(1985)(ratio $\geq$ 1.5). When tap water ($\kappa_{25°C} = 0.26$ mS/cm) is used for wash water instead of recycled water, the difference (conductance ratio ~ 8) is a combination of both effects.

Changes in operating conditions leading to changes in gas holdup (gas rate variations, for example) and changes in the chemistry of the water in the flotation pulp (reagent addition, for example) are commonly encountered in industrial operation.
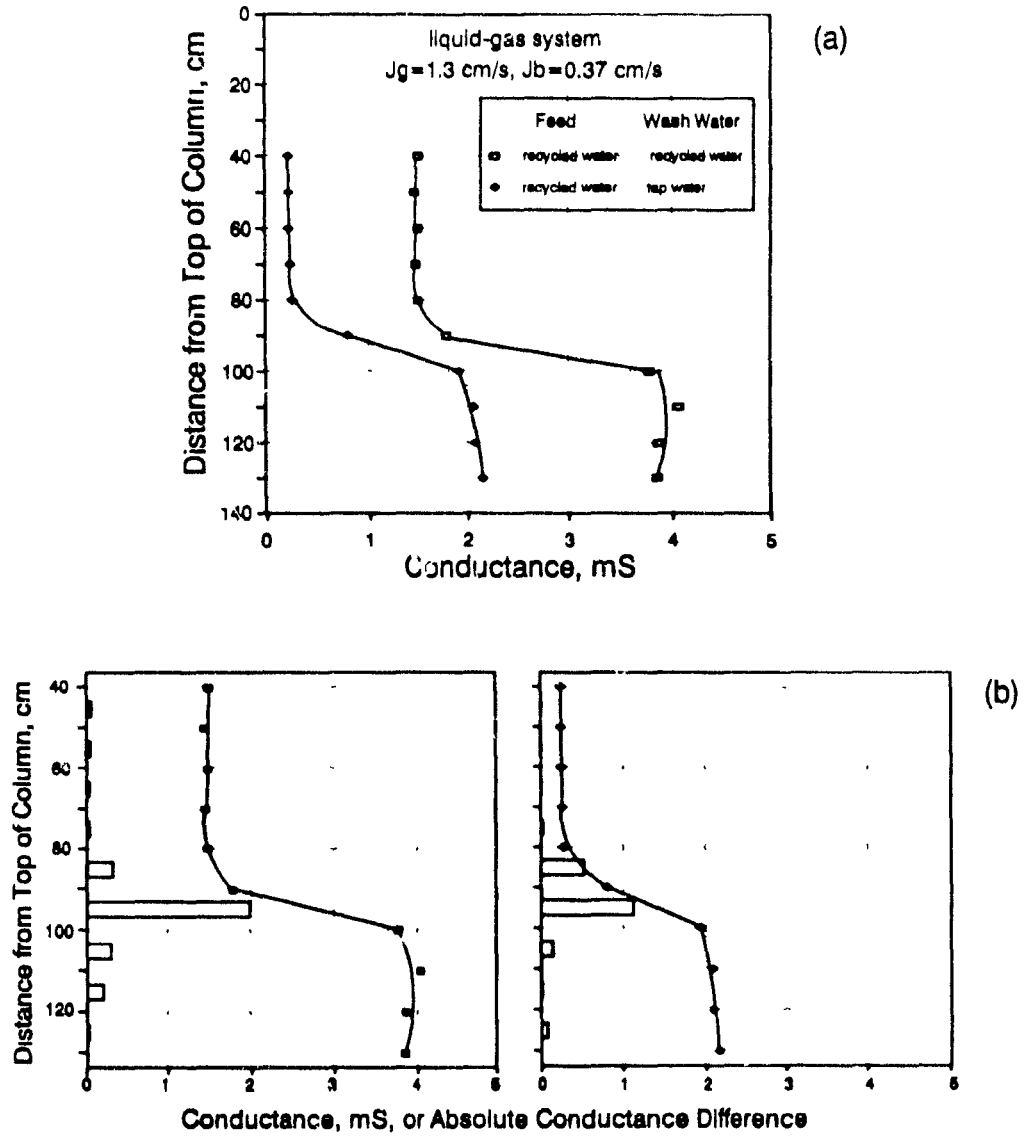
Figure 4.6   Conductance profiles collected in a water-air system showing: (a) the effect of
the chemistry of the water, and (b) the basis of the "largest slope" level
detection algorithm

b).-   Level detection algorithm

The position of the interface level can be inferred from the conductance profiles simply because the largest difference in conductance between adjacent points occurs when crossing the interface. Thus, the interface level is defined as the loc. tion at which the largest conductance difference (largest slope in mathematical terms) occurs. The application of this definition to the conductance profiles of Figure 4.6(a) is illustrated in Figure 4.6(b). The conductance difference values are located midway between the position of the adjacent electrode pairs producing a specific conductance difference value. For example, when wash water is tap water and the feed is recycled water, the conductance measured at 80 and 90 cm from top of the column are 0.27 and 0.80 mS, respectively; therefore, the absolute difference, 0.53 mS, is assigned to the intermediate position, i.e., 85 cm.

More elaborated approaches that involve the fitting of the data to a conductance vs distance equation and obtaining the point at which the largest slope occurs (largest first derivative) or the point at which there is an inflection point (second derivative equals zero) were discarded because of the lack of a simple mathematical expression capable of describing all the possible profile shapes encountered.

c).-   Performance of level detection algorithm

Given the nature of the level detection algorithm which only discriminates the position at which the largest slope occurs, the accuracy of the detection is mainly dictated by the axial separation between electrode pairs. The algorithm will report a level position of 95 cm, for example, as long as the largest conductance difference occurs between electrodes at 90 and 100 cm; if the level moves in such a way that the new largest difference occurs between electrodes at 80 and 90 cm, the value reported by the algorithm will jump from 95 to 85 cm. Therefore, the accuracy of the detection is

expressed as being $\pm\frac{1}{2}$ the axial separation between electrode pairs, e.g., ± 5 cm for the experimental results presented.

Figure 4.7 shows the performance of the algorithm for the column operated with a level set point of 95 cm. In all the cases, the accuracy of the detection was ± 5 cm as compared to the interface position obtained by optical inspection.

d).-   Time constant of the technique

Collecting a conductance profile takes a period of time that depends on the number of measurements (conductance points) and on the time constant of the instrument (conductivity meter). The number of points depends on the span and on the accuracy required: given the span the accuracy will increase by increasing the number of points, and vice versa. The response of the commercially available conductivity sensors are described by the equation of a first order system, that is to say, the response to a change in the conductivity of the medium is not instantaneous but a function of time and follows the first order lag equation

$$\kappa(t) - \kappa_\infty (1 - e^{-t/T}) \tag{4.2}$$

where $\kappa(t)$ is the time-dependent conductivity measurement, mS/cm; κ_∞ is the actual value of conductivity of the medium whose conductivity is being measured, mS/cm; t is the time, sec; and T is the time constant of the sensor, sec.

Figure 4.8 presents the response of the commercial meter being used (Tacussel, Mod. CD 810) to a sudden change in conductance from zero to -5.25 mS. A time constant of about 0.46 s is obtained by fitting the data in Figure 4.8 to Equation (4.2). Therefore, in accordance with the first order lag model, 99% of the actual conductance value would be obtained when a period of time of *five time constants*, e.g, 2.3 s in the
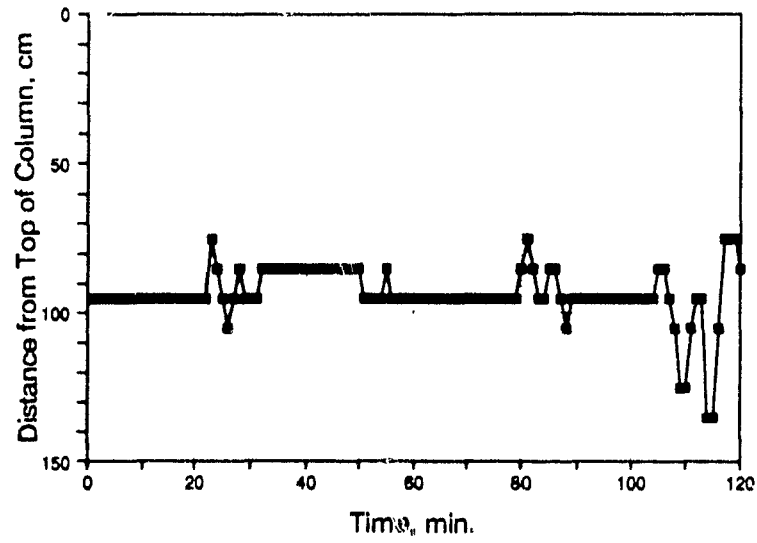
Figure 4.7 Performance of the level detection algorithm in a water-air laboratory column
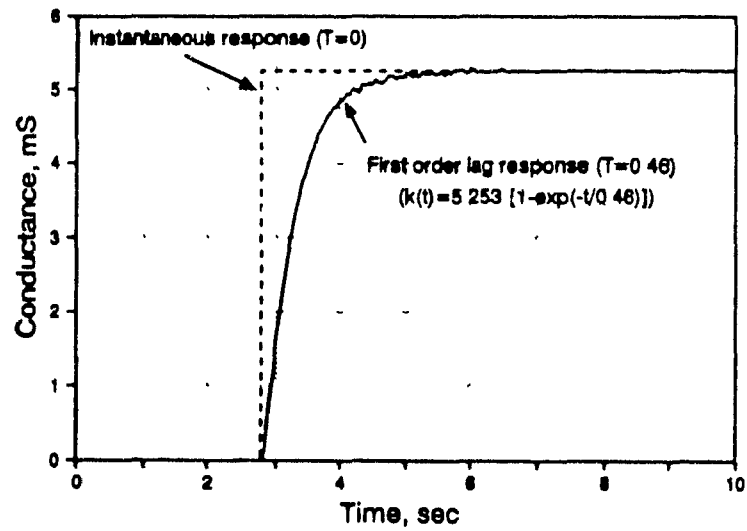
Figure 4.8 First order lag response of a commercial conductivity meter

case being discussed here, has elapsed. This essentially means that each conductance measurement will take at least 2.3 s, which translates into 23 s for a full scan of ten points to be completed. Obviously, the level is updated every time a new profile is collected, and therefore, this gives rise to a lag in level detection that has to be accounted for within a level control scheme.

These two drawbacks of the technique, namely, the step shape of the response and the lag in the detection of level, can be minimized by using a sensor with a shorter time constant (Omega Mod. CDTX-101, for example) and by interpretation of the conductance measurement collected; this latter option is discussed next.

4.2.4 Basic studies on the effect of cell configuration

The possibility of increasing the accuracy of the detection by interpreting the response of alternative electrode arrangements was experimentally explored.

The experiments were carried out in a 10 cm diam. $\times$ 3.6 m height water-air laboratory column. In this column, twelve pairs of stainless steel facing circles (0.71 cm^2) were installed in the column wall starting at 28 cm from the top and with and axial separation of 10 cm. The data acquisition system described in Section 4.2.2 was improved by replacing the apple-compatible computer by an IBM-compatible computer, the 8-bit A/D board for a 12-bit A/D board (Mod. DAS-8PGA), and the manual channel selector for a 24-channel electromechanical relay board (Mod. ERB-24) driven by an I/O interface (Mod. PIO 12).

Two different electrode arrangements were tested, the "facing electrodes" arrangement, already introduced, and a "coaxial electrodes" arrangement which consists in measuring conductance between an electrode (positive, for example) and a negative one located 10 cm below (or above). The conductance value is then assigned to the

intermediate position. It is worth mentioning that in order for this arrangement to work, it is necessary to alternate the electrical sign of the electrodes installed in the same vertical axis as schematically shown in Figure 4.9.

Typical conductance profiles collected with both arrangements are shown in Figure 4.9. The interface level is at 70 cm from the top, e.g. in between electrodes located at 68 and 78 cm. The normalized conductance introduced in this figure refers to the conductance value measured while in operation divided by that measured in water only (~ 2.7 mS; $K_{water\ 25\,^\circ C} = 3.4$ mS/cm).

a).-   Performance of the facing electrodes arrangement

To evaluate the performance of the facing electrodes arrangement an experiment where the level was slowly moved up (or down) around the electrodes located at 68 and 78 cm, was designed. Figure 4.10 presents the results obtained showing that the response of this arrangement can be said to be on-off in the sense that it reports the conductance number for the bubbling zone (~ 0.8, normalized) when the level is above the electrodes, and the conductance number for the froth zone (~ 0.38, normalized) for the levels below the electrodes. Under these circumstances, more precise level location is not possible because of the lack of a simple relationship between the response and the level position.

The performance of the level detection algorithm is expected to be satisfactory according to Figure 4.11 which presents the absolute value of the conductance (normalized) difference. The figure shows that the difference is close to zero for levels outside the range 68-78 cm, and is maximized (~ 0.04) for levels between the electrodes.

b).-   Performance of coaxial electrodes

This arrangement was experimentally evaluated in a similar way as described
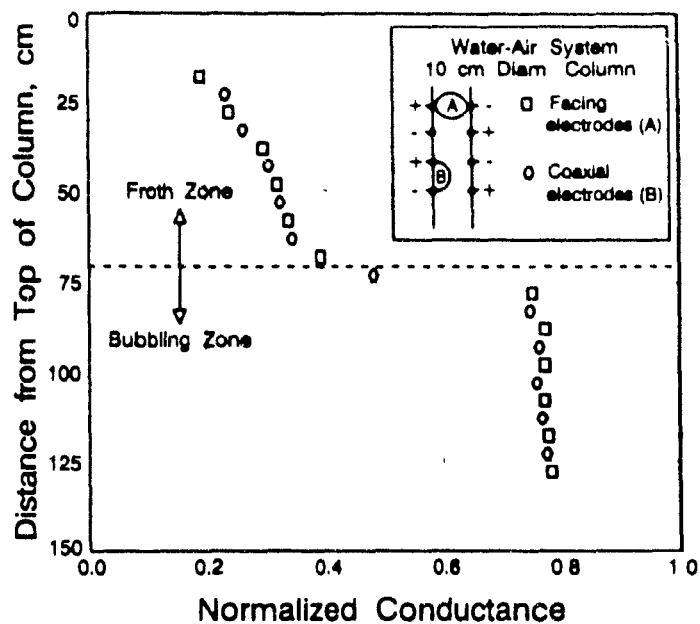
Figure 4.9   Conductance profiles collected with facing electrodes and coaxial electrodes
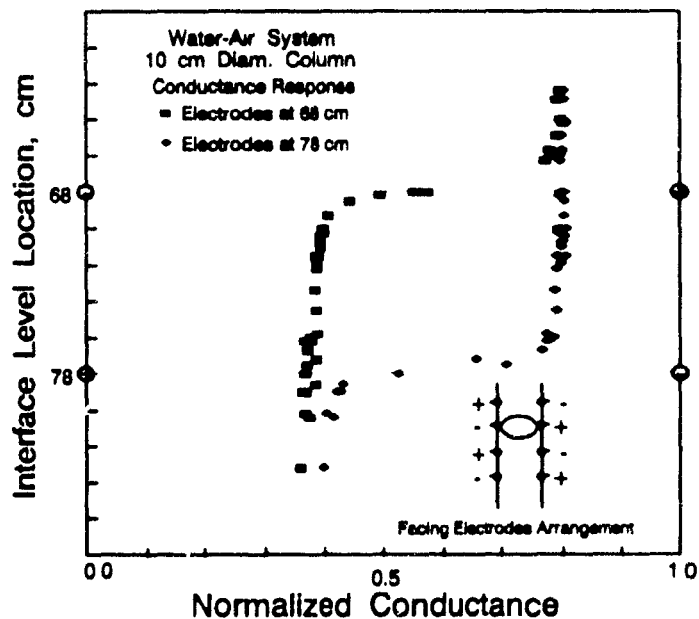
Figure 4.10   Response of the facing electrodes to interface level variations
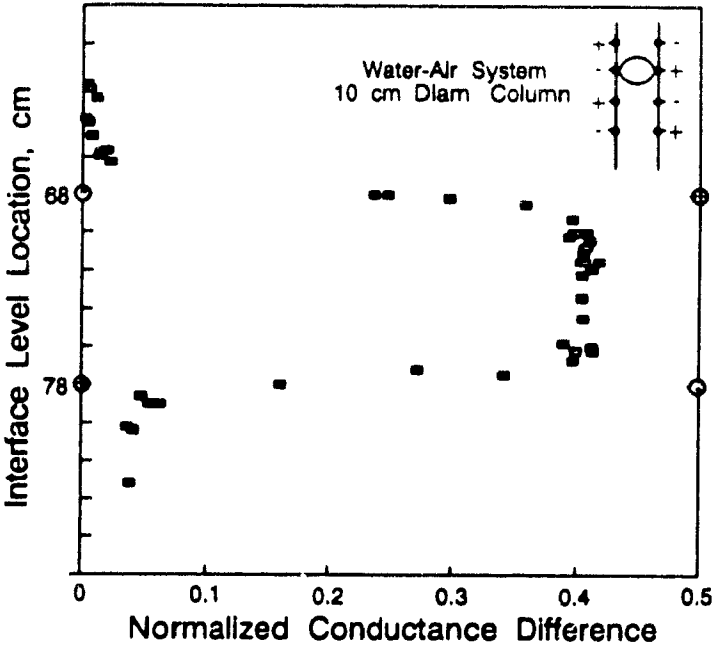
Figure 4.11   Normalized conductance difference for data in Figure 4.10
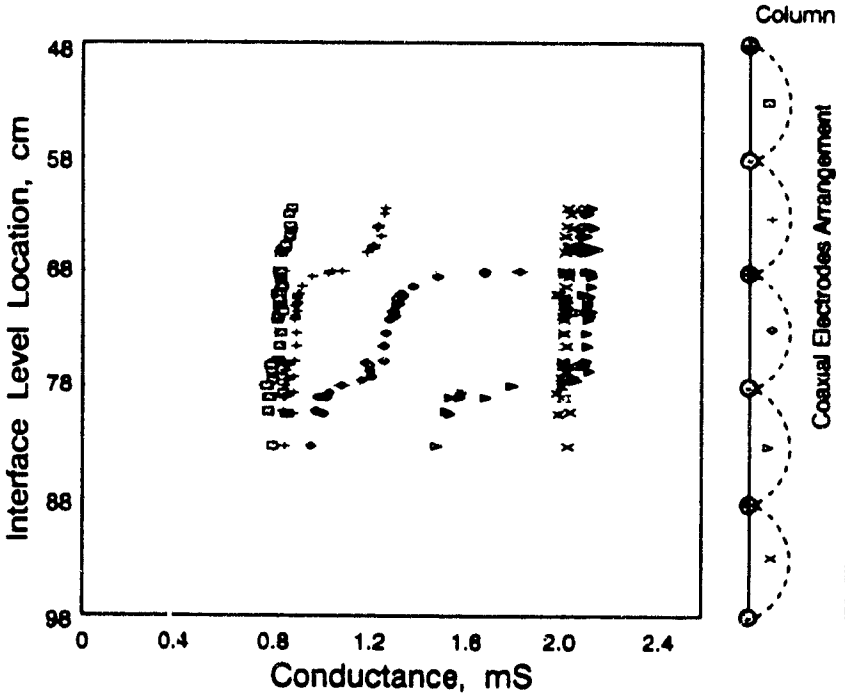
Figure 4.12   Response of coaxial electrodes to interface level variations

above for the facing electrodes In the experiments the level was slowly moved in the range from 62 to 83 cm, while conductance readings were continuously collected The method of measuring conductance is illustrated in Figure 4 12 together with the experimental results obtained. This plot shows that the electrodes located at 48 and 58 cm report the conductance value of the froth zone (~ 0 9 mS) simply because they were always immersed in that zone; for similar reasons the electrodes located at 88 and 48 cm report the value of the bubbling zone (~ 2.1 mS) The numbers collected with the electrodes between these two pairs were affected by the level The electrodes at 68 and 78 cm, for example, present a step shape response to level values between 68 and 78 cm This response is broadly described as follows: the conductance is that of the bubbling zone (~ 2.1 mS) for levels above 68 cm, then drops to an intermediate value of around 1.3 mS for levels between 68 and 78 cm, and finally attains the value of the froth (~ 1 mS) for levels below 78 cm.

The conductance response shown in Figure 4.12 is not useful for gaining accuracy in the detection of level because a clear relationship between the two variables does not exist. Characterizing or modelling this response by using the basic elements of electricity is not possible due to the complexity of the system, this complexity arising basically because of the existence of a non-uniform current field. The modelling of the geometries discussed in Section 3.2.1, in which a uniform current field exists, should be possible.

c).-   Performance of an ideal cell

The performance of an adaptation of an ideal cell was experimentally evaluated in order to verify the applicability of the basic principles of electricity to well defined conditions. This time, a 5.7 cm diam. Plexiglas column was used. Grid electrodes filling the entire cross-sectional area of the column (25.5 cm^2) and separated 17.2 cm (cell constant=25.5 cm^2/17.2 cm = 1.48 cm^2/cm) were used. This geometry is an adapted section of the general case of parallel infinite plates that has been used for measuring

holdup in two and three phase dispersions (Turner, 1976; Achwal and Stepanek, 1975 and 1976; Dhanuka and Stepanek, 1987).

A grid electrode consists of a three concentric rings (2.7, 4.3 and 5.7 cm diam.) soldered to a cross Copper wire 0.14 cm diam. was used. The grid electrodes are located one above the other along the vertical axis of the column (Figure 4.13). This geometry simulates full plate electrodes and at the same time provides space for the air bubbles to enter and leave the cell. No substantial disturbance of the hydrodynamics of the system caused by the presence of such grids was observed.

The resistance (inverse of conductance) for the physical situation depicted in Figure 4.13 is represented by the equation of two resistances in series, namely

$$R - R_f + R_b \tag{4.3}$$

where the resistance of the froth (R_f) and bubbling zone (R_b) will depend on the size of the zones, namely

$$R_f - \frac{l}{A_c \, \kappa_f} \, , \quad and \quad R_b - \frac{L - l}{A_c \, \kappa_b} \tag{4.4}$$

where l is the distance from the top electrode to the interface level, cm; L is the separation between electrodes, 17.2 cm; A_c is the cross-sectional area of the column, 25.5 cm^2; κ_f and κ_b are the effective conductivities of the froth and bubbling zones.

Considering the conductivity ratio $n = \kappa_b/\kappa_f$, substituting Equation (4.4) into Equation (4.3) and rearranging, one obtains

$$K - \frac{1}{R} - \frac{A_c \, \kappa_b}{(n-1)\, l + L} \tag{4.5}$$
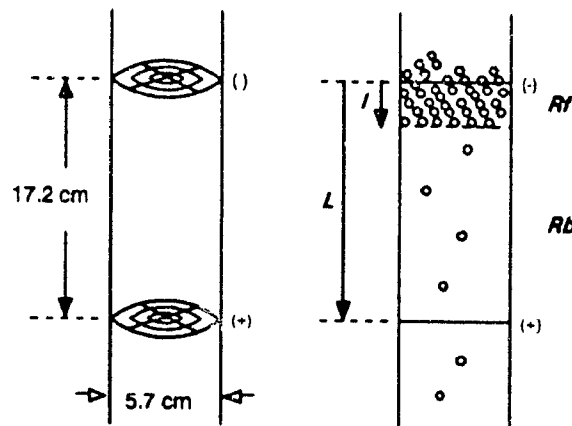
Figure 4.13   Schematic representation of the adaption of an ideal cell (grid electrodes) and resistances associated with the froth and bubbling zones
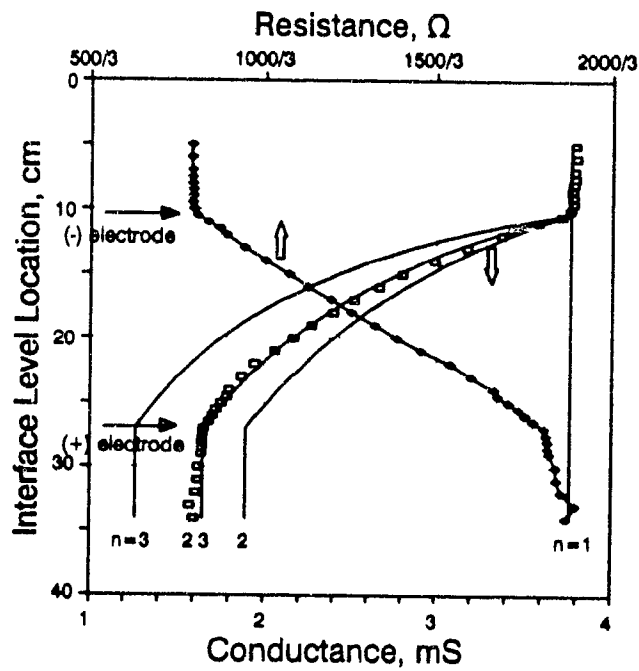
Figure 4.14   Response of the grid electrodes to interface level variations. "n" is the bubbling to froth zone conductivity ratio

With the geometrical parameters A_c and L being fixed, testing the equation requires knowledge of κ_b and κ_f; thus, for a given conductance number K, the level position in between the electrodes, l, will be given by Equation (4.5).

The experimental results obtained, presented in Figure 4.14, were fitted by Equation (4.5) for $n = 2.3$ and $\kappa_b = 2.55$ mS/cm ($\kappa_{liquid} - 3$ mS/cm). The value for the effective conductivity of the bubbling zone was calculated by using Equation (3.8), namely

$$\kappa_b = \frac{K_b}{A_c / l} = \frac{3.78 mS}{25.5 \ cm^2 \ / \ 17.2 \ cm} = 2.55 \ mS/cm$$

Curves for other values of n are also presented; the curve for $n = 1$ corresponds to a single, homogeneous phase.

Figure 4.14 also shows the resistance has a linear relationship with level and therefore, appears to be the appropriate parameter to use for the purposes of interpolating the position of the interface. These results are similar to those reported by Moys and Finch (1988a) presented in Figure 4.1.

This result demonstrates that the laws electricity hold provided the restrictions introduced in Section 3.2 are respected.

4.3 Industrial Scale Columns

The satisfactory performance of the conductivity technique for level detection at the laboratory scale, led to its implementation at the industrial scale.

4.3.1 Development of a conductivity probe for industrial applications

The first step in adapting the technique to the industrial environment was the development of an appropriate probe. Such a probe should meet several requirements, namely: i).- be sensitive to the physical/chemical property to be measured (conductivity); ii).- be of a simple geometry to facilitate construction and maintenance, and iii).- be robust (but not very heavy) in order to withstand the harsh environment prevailing in a mineral processing plant.

a).-   Selection of the cell geometry

The cell geometry, that is, the size, shape and arrangement of the positive (or positively charged) and negative (or grounded) electrodes, has a definitive impact on the performance of the cell. This is intimately related to the nature of the phenomena involved (introduced and discussed in Section 3.2). As a general rule, measurements conducted with large cells more closely represent the average of the property, and therefore are less "noisy" (i.e., show a small relative standard deviation); on the other hand, measurements conducted with small cells are more localized and, in two or three-phase systems they are affected by changes in local holdup of the phases. Besides dimensions, the shape and arrangement are also important. For example, two large parallel plates facing each other are, most probably, well described by Equation (3.8), whereas an explicit equation to describe the response of the same plates but in a rearward arrangement does not exist and cannot be derived by using conventional mathematics (Kasper, 1940). As mentioned before, this latter behaviour is mainly related to the complexity of the current field established in such a situation.

The development of the industrial prototype probe started with the selection of the appropriate cell geometry. This was experimentally addressed by evaluating the performance of different alternatives. The experiments simply consisted in collecting conductance profiles around the interface level in a slurry-air flotation column. That geometry presenting good sensitivity to the difference in conductance across the interface

and easy construction and maintenance would be the most appropriate one. Electrode arrangements such as facing plates, parallel rings and rearward plates were tested (Figure 4.15).

To collect a profile the specific cell needs to be moved up, or down, known distances. To achieve this the cell was mounted in a structure of aluminum and PVC tubing (Figure 4.16). Wiring between the electrodes and the conductivity meter was completed through the interior of the tubing. The vertical aluminum tube was graduated to indicate the depth of the cell relative to the top of the column. The probe was maintained in its working position by two guides that allowed smooth vertical displacement of the structure. The experiments were completed in a 91 cm diam. × 1300 cm height column (Strathcona mill, Falconbridge Ltd) while processing a stream of the copper circuit. Figure 4.17(a) presents the conductance profiles collected and shows that substantial difference in the magnitude of the conductance from one cell to another exists. This is simply a consequence of the difference in geometry. Nevertheless, when the profiles are normalized, all the cells show similar abilities to detect the interface (Figure 4.17(b)). In this particular case the conductance profiles were normalized by dividing the conductance values by the maximum value on the profile. The geometry offering easiest construction and maintenance is the ring (A in Figure 4.17); in addition, the ring gave the second best sensitivity after the facing plates (D in Figure 4.17). Thus, overall, the ring geometry fulfilled requirements (i) and (ii).

b).-   The ring electrodes and the portable conductivity probe

A portable conductivity probe to locate the interface level in flotation columns was designed and built with two objectives: first, to substantiate the performance of the ring electrodes, and second, to provide operators with a simple and reliable device to locate level in flotation cells.
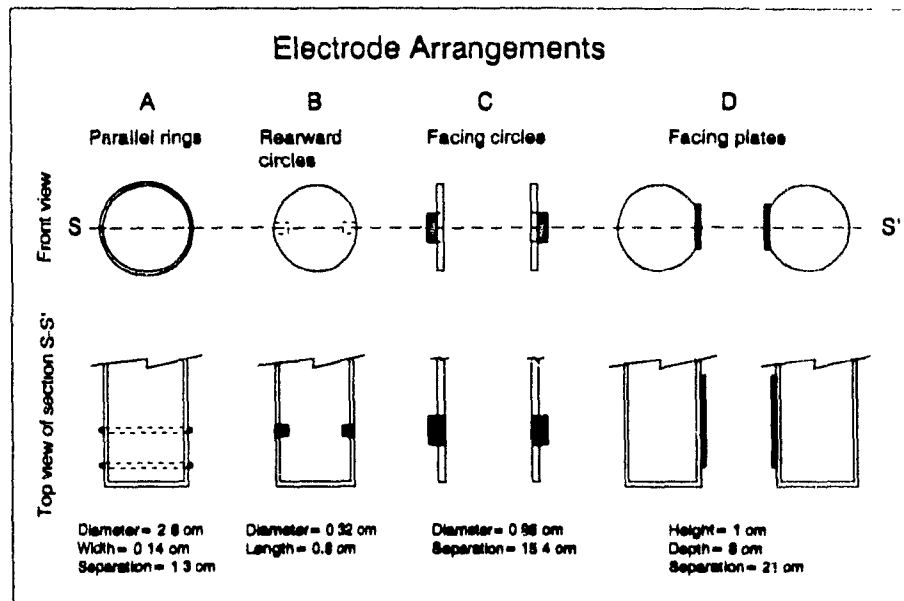
Figure 4.15 Electrode arrangements tested for detection of interface level in a slurry-air 0.91 m diam. column

Figure 4.16 Illustration of the portable probe (not to scale). Details of the commercial electrode are given. The same structure was used to evaluate the performance of the electrode arrangements in Figure 4.15
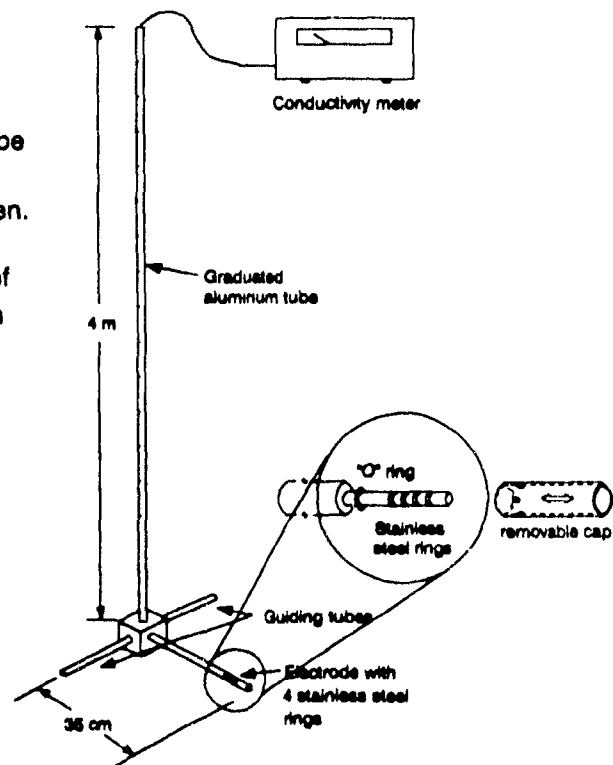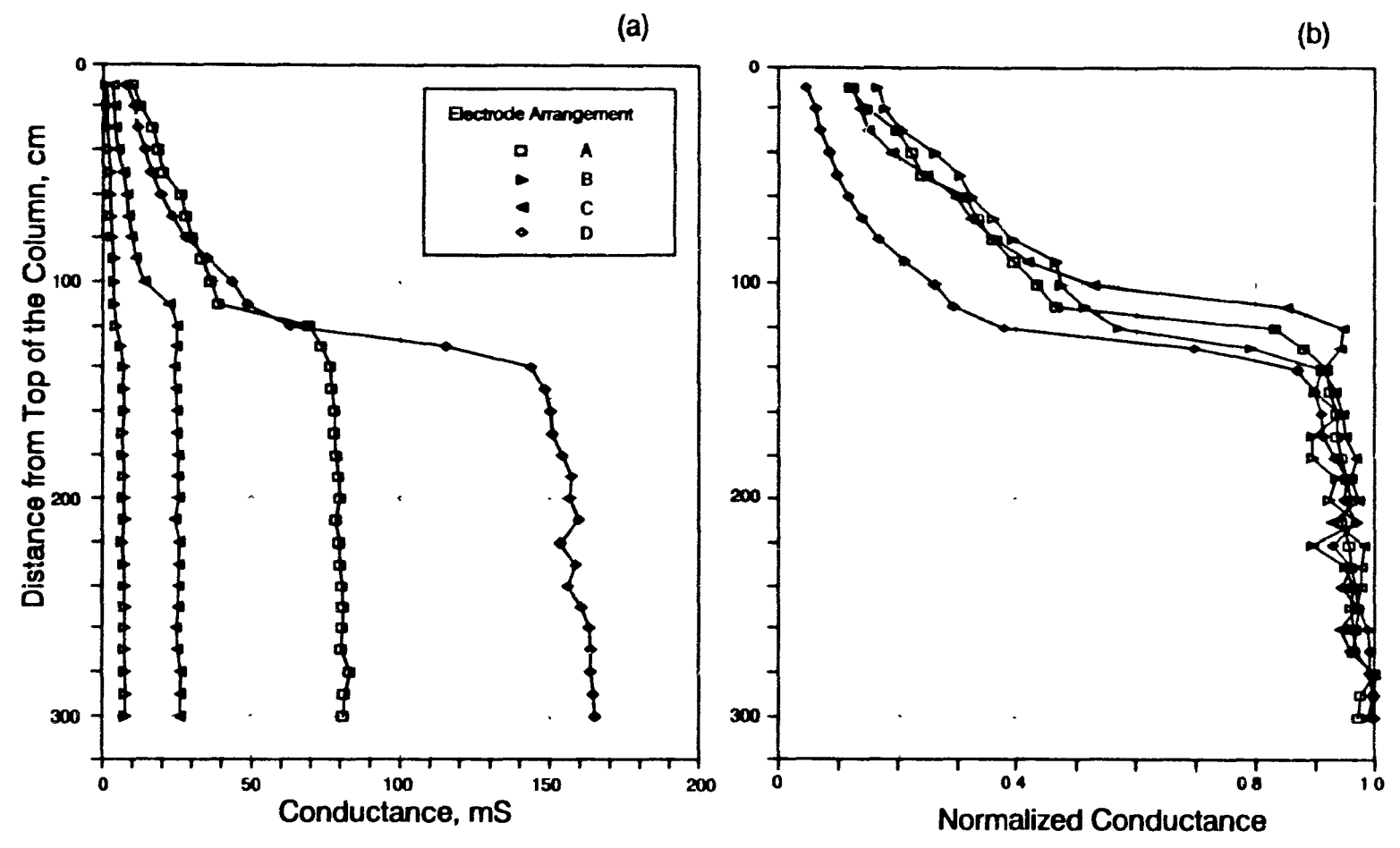
Figure 4.17 Performance of electrode arrangements of Figure 4.15: (a) conductance profiles, and (b) normalized conductance profiles
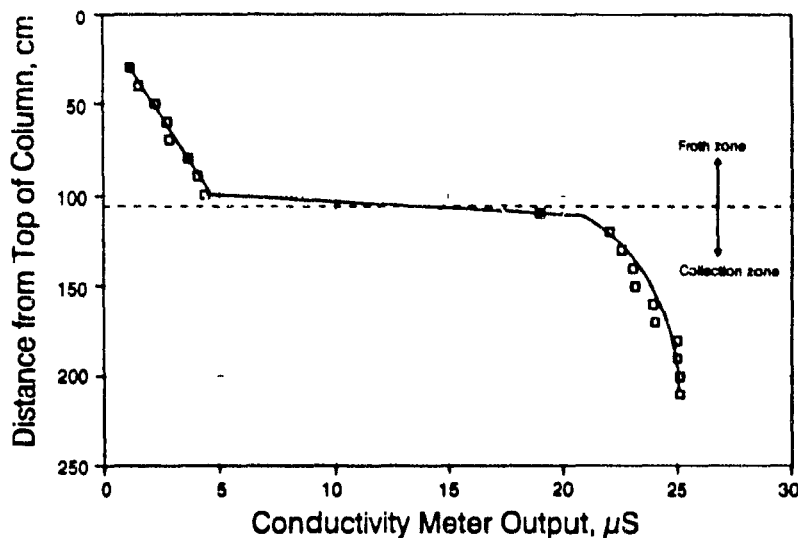
Figure 4.18   Conductance profile collected with the portable probe in a slurry-air system

The probe, illustrated in Figure 4.16, consisted of the aluminum structure described above supporting a commercial 4-electrode conductivity cell (Hanna Instruments HI 76302). Comments on the selection of such a cell are offered in Appendix 4. A portable meter (Hanna Instruments HI 8633) was attached to the probe.

Originally, the commercial cell came enclosed in a cap, as illustrated in Figure 4.16, whose main purpose is to shape and constrain the flow of electric current in such a way that a fixed cell constant is achieved allowing conductance measurements to be directly translated into conductivity values. This array is adequate when dealing with homogeneous solutions but in slurry-air systems it was impractical and the sensor had to be used without the cap; thereby, conductances rather than conductivities are reported here since the cell constant is now not known.

The portable probe was operated in a similar manner as described above for the evaluation of the different electrode geometries. Figure 4.18 presents a typical profile collected with this probe.

The excellent results obtained with the portable probe, as judged from the resolution of the profile in Figure 4.18, reinforced the decision to use ring electrodes to construct the prototype probe, and met the objective of providing a simple instrument to locate level in flotation cells. Probes based on this concept have been successfully used to check or calibrate level detection systems based on pressure (Huls et al., 1989; Gomez et al., 1990; Huls et al.,1990), and Metritape (Sepulveda, 1990); and to judge the performance of various level detection devices tested in a 38 m³ mechanical flotation cell (Macnamara, 1990).

c).-   Preliminary version of the stationary probe

To exploit the conductivity profiling technique for level detection at the industrial scale, the manual profiling procedure needed to be translated into a fully automated one. Thus, a stationary probe supporting the series of electrodes and covering the required span was envisaged.

The preliminary version of the stationary probe is shown in Figure 4.19. It included 11 stainless steel rings (electrodes), 1.27 cm diam. (1/2") × 0.4 cm height, installed every 10 cm on 1.27 cm diam. (1/2") PVC tubing. Each of the rings was soldered to a wire that ran through the interior of the PVC tube. The probe was driven by the data acquisition system described in Section 4.2.4, allowing the collection of conductance profiles along 1 m of the column. The probe was designed to be installed at the center of a column and parallel to its walls.

Initially, the conductance was measured between adjacent electrodes, one positively charged and the other grounded. However, because of the presence of the column wall which is grounded, having a grounded electrode or not on the probe did not make any difference to the magnitude of the conductance value; in other words, conductance was being measured between the positive ring of the probe and the column
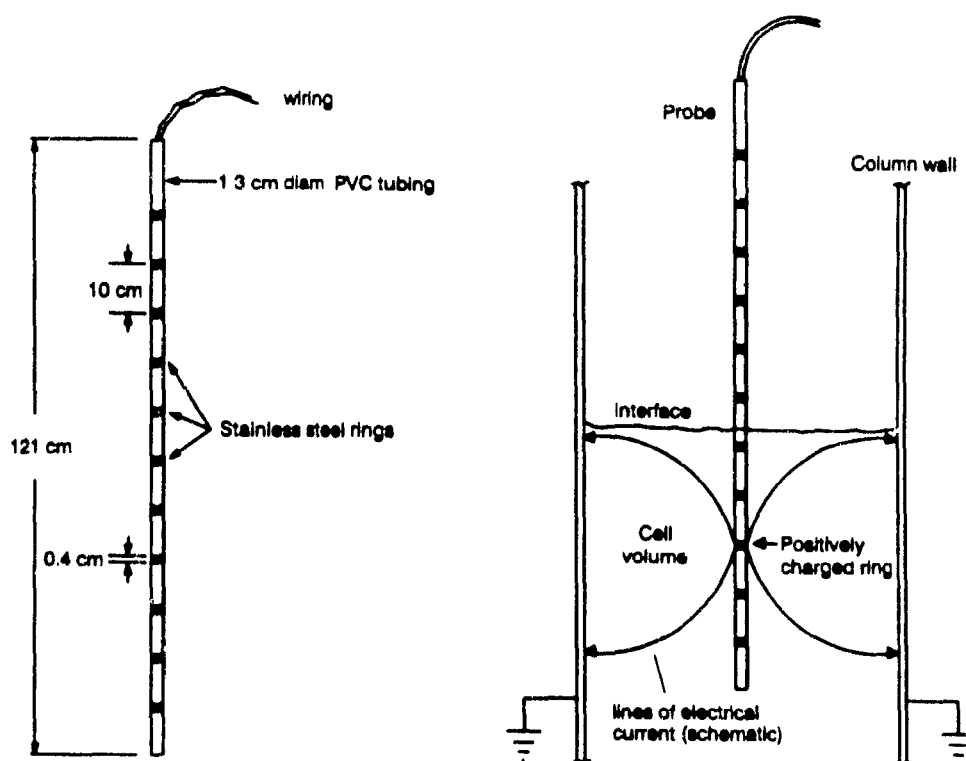
Figure 4.19 Geometrical details of the preliminary version of the stationary probe and schematic representation of the use of the column wall as grounded electrode

wall. Because of this, it was decided to take advantage of the situation and the probe was re-wired to make measurements between the eleven positive electrodes on the probe and the grounded wall, as depicted in Figure 4.19. It is worth remembering that a profile is collected by sequentially connecting one positive ring and one grounded (the column in this particular case) to the conductivity meter. A typical conductance profile collected with this probe is presented in Figure 4.20, which shows that the froth/collection zone interface is readily detectable although there is an appreciable loss in sharpness compared to the profile collected at the same time with the portable probe (Figure 4.18). This loss in sharpness is most probably caused by an effect of the column wall acting as the grounded electrode: the lines of flow describing the path of the electric charge going from the positive to the grounded electrode, schematically shown in Figure 4.19, will
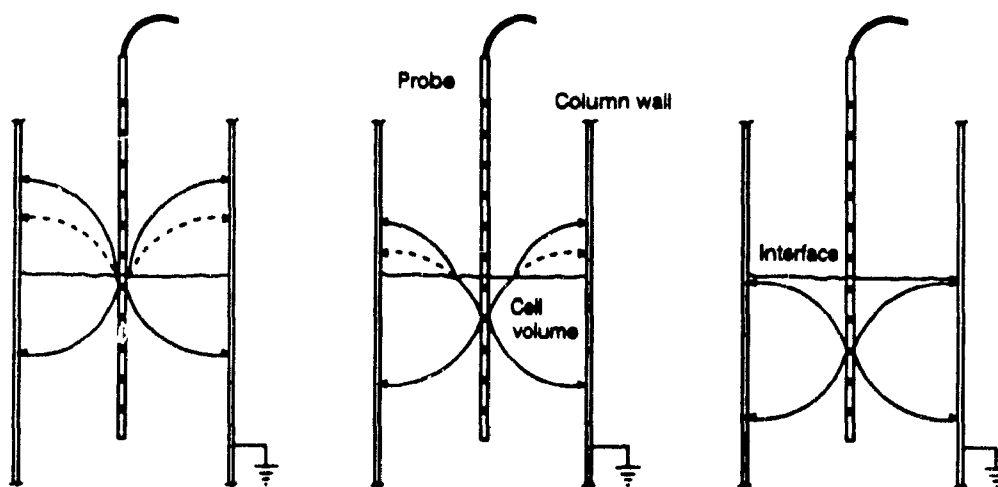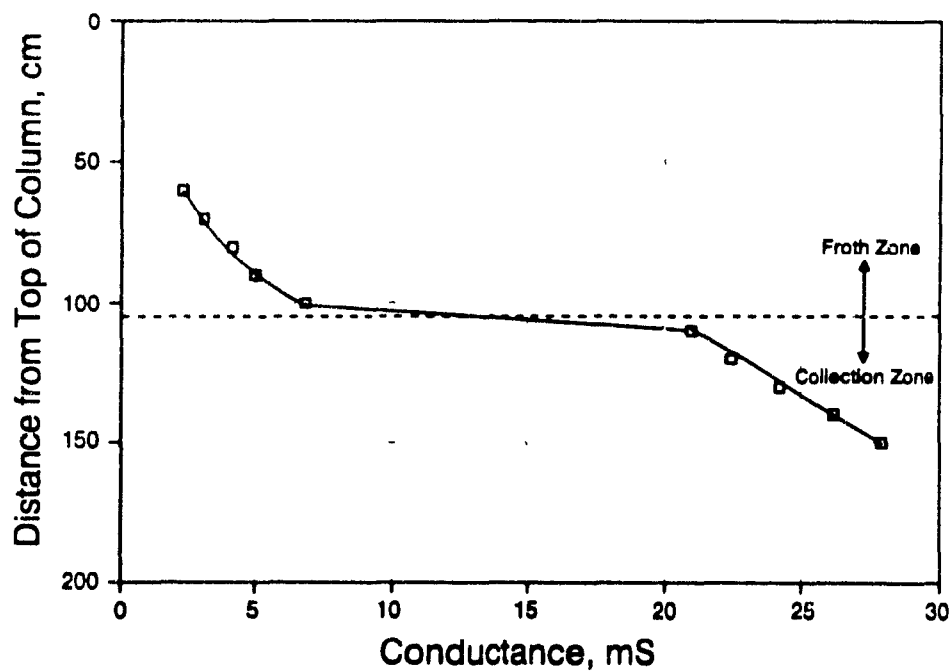
Figure 4.20 Conductance profile collected with the preliminary version of the stationary probe and schematic representation of the effect of the froth zone on the "refraction" of the lines of flow of electric current

converge in regions of high conductivity and diverge in regions where the conductivity is low (Meredith and Tobias, 1962). This phenomenon can be visualized as a "refraction" of the lines of flow on crossing the interface between the two regions (Binns and Lawrenson, 1963). In accordance with this, the electrodes in the probe will experience the phenomenon with an intensity depending on how close they are to the froth/collection zone interface. The net macroscopic effect is that a conductance value in between that of the collection and froth zones is measured, the magnitude of the value depending on the position of the particular electrode with respect to the interface. This is depicted in Figure 4.20.

The results showed that conductance profiles collected with a stationary probe were good enough for level detection; however, the effect of the grounded wall on the degradation of the profile was a problem that needed to be solved by either rubber lining the top section of the column wall (some industrial columns are rubber lined), or by increasing the area, and thus the "electrical strength" of the grounded electrodes mounted on the probe in order for them to compete with the column wall. The latter alternative was preferred and the appropriate modifications were addressed.

d).- The prototype stationary probe

The second version of the stationary probe consisted of a series of basic modules mounted around a 5.08 cr. (2") pipe. Each module was formed by a non-conductive PVC cylinder machined to support a stainless steel ring (electrode). Every other ring was grounded while those in between, termed positive electrodes, were connected to a relay board driven by a computer which activated them sequentially. The conductance was measured between the activated ring (positively charged) and those grounded on both sides. Figure 4.21 shows geometrical details of the probe and illustrates the data acquisition system (described in Section 4.2.4) attached to the probe.
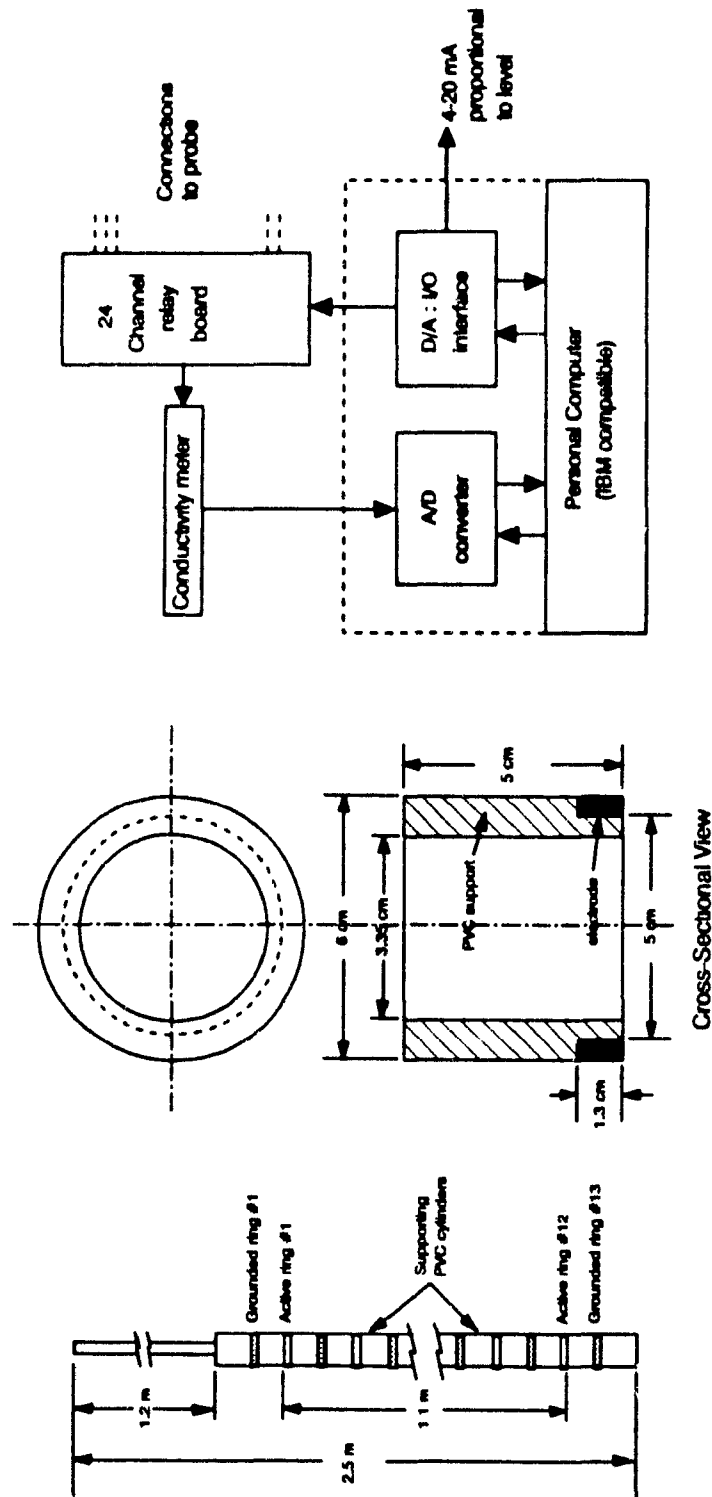
Figure 4.21 Details of geometry of the stationary level detection probe and data acquisition system

To collect a profile the computer sequentially connected positive electrodes to the conductivity meter. The signal emitted by the conductivity meter, which is proportional to the conductance, was continuously fed to the A/D converter, a reading was collected every 3 seconds (this value is dictated by the time constant of the conductivity meter, see Section 4.2.3(d)) and stored in the computer memory. Once a scan had been completed, the conductance values were processed by the level detection algorithm introduced in Section 4.2.3(b); the resulting value of level was either displayed on the computer monitor or converted into an analogical signal (4-20 mA) and outputted (an analog output board Mod.DDA-06 was used).

e).- Testing of the probe

The probe was tested in both slurry-air and water-air systems. Figure 4.22 present typical conductance profiles collected for a number of operating conditions. In principle, as noticed in Figure 4.22, the profiles showed an obvious change in conductance across the interface; in addition, the branches of the profile in both zones did not have the shallow slope observed in Figure 4.20, suggesting that the deleterious effect of the grounded column wall on degrading the shape of the profile was largely eliminated by the electrode arrangement used in the probe.

The magnitude of the difference in conductance between the froth and collection zone, which is the working parameter for level detection, depends on the operating conditions. In water-air systems tested the difference was due to differences in gas holdup between both zones since the same source of water was used for the feed and the wash water; in general, however, the difference is due to a combined effect of the difference in gas holdup and a difference in the relative amounts of feed/wash water in both zones Normally, the conductivity of the flotation pulp liquor is larger than that of the wash water (~ 3 mS/cm for the pulp water compared to ~ 1.3 mS/cm for the wash water, in the profiles presented in Figure 4.22(a)), most probably due to the addition of chemicals
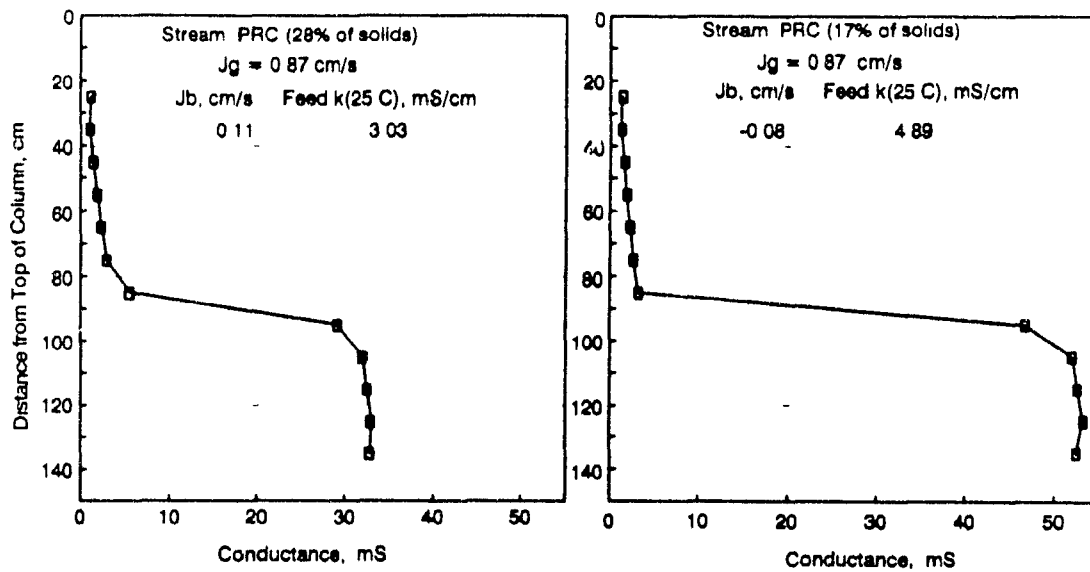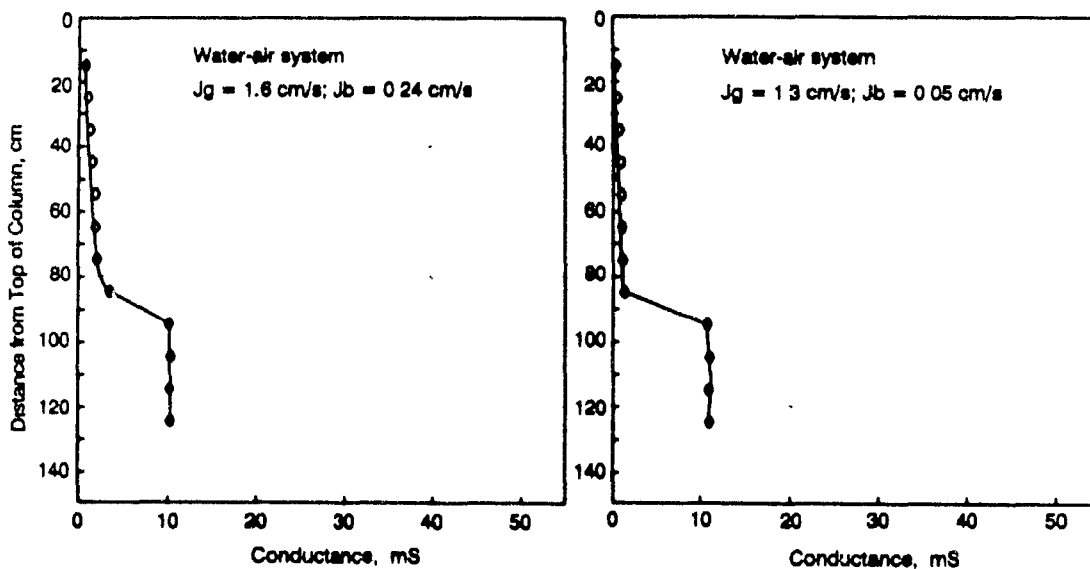
Figure 4.22 Typical conductance profiles collected with the level detection probe: (a) slurry-air system (Primary Rougher Concentrate), and (b) water-air system
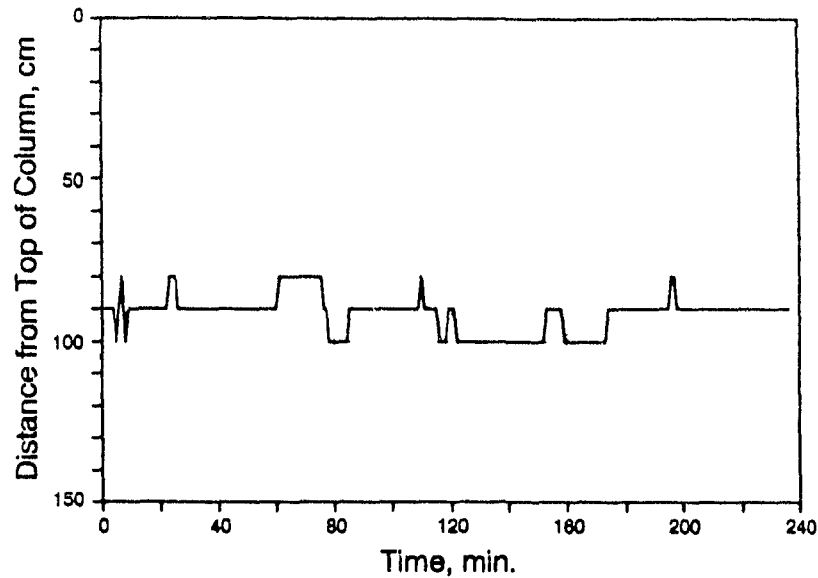
Figure 4.23   Performance of the level detection ("largest slope") algorithm (slurry-air system)

(NaCN and lime are used in the copper circuit at the Strathcona mill (Huls et al., 1991)) to the flotation pulp.

f).-   Level detection algorithm

The level detection algorithm based on the "largest slope" was used with the probe. Figure 4.23 shows the performance of the algorithm in the slurry-air system for the profiles in Figure 4.22(a). A conductance profile every minute was collected which means that the level position was updated every minute. Figure 4.23 shows the step shape response of the algorithm to a change in level. The explanation of this behaviour given for the laboratory column in Section 4.2.3 also applies to the present results.

4.3.2 Analysis of the performance of the electrode geometry of the stationary probe

a).-   Effect of an "external" grounded electrode

The performance of the probe in the presence of an "external" (with respect to the probe) grounded electrode was experimentally addressed with the aim of finding an explanation for the negligible effect of the column wall in degrading the conductance profiles collected with the probe.

To accomplish this, measurements of conductance were performed in the presence and absence of an "external" grounded electrode. Three electrode combinations were used: a).- a positive against a ground immediately above (or below), b).- a positive against the two grounded electrodes on both sides, and c).- a positive against four grounded electrodes on both sides.

The experiments were conducted in a 91 cm diam. × 1 m height PVC tank filled with a solution of known conductivity at room temperature ($\sim 24\,^\circ$C). KCl was used to vary the conductivity of the solution. A calibrated conductivity meter (Hanna Instruments HI 8633) was used to measure conductivity. A shortened version of the probe comprising two positive and four grounded electrodes was used (Figure 4.24). Arrangements were made to allow for the measurement of conductance between any desired combination of positive and grounded electrodes. The probe was positioned in the center of the tank and an aluminum tube (3.8 cm diam.) located close to the wall was used to simulate the "external" grounded electrode (Figure 4.24).

The results, presented in Figure 4.25, show that by increasing the number of grounded electrodes used in the measurement, the conductance value increases and asymptotically levels off (an arithmetic relationship between conductance and surface area of grounded electrodes does not appear to exist). It is evident from this behaviour that the contribution of the external electrode to the overall measurement decreases as the number of grounded electrodes in the probe increases. This explains, at least qualitatively, the better performance, in terms of sharpness and resolution of the conductance profile, of the stationary probe compared with the "preliminary" one.
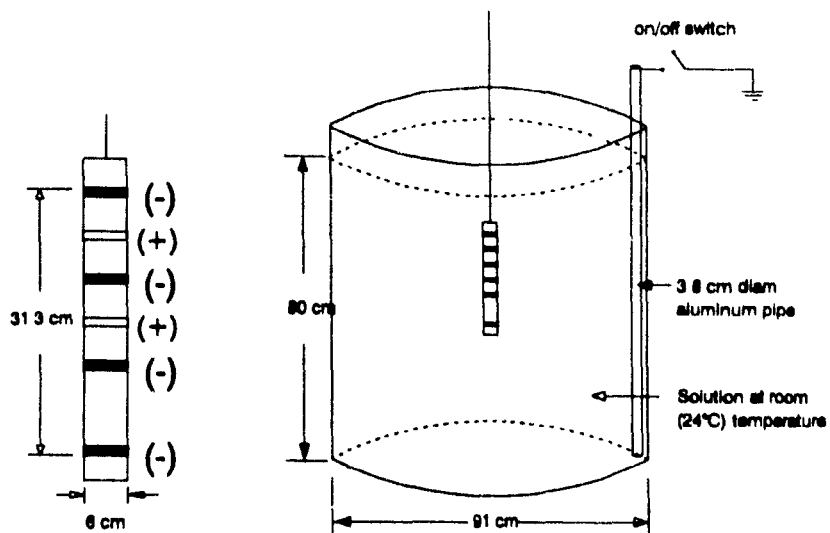
Figure 4.24 Shortened version of stationary probe and experimental set up used to evaluate the effect of an "external" grounded electrode (not to scale)
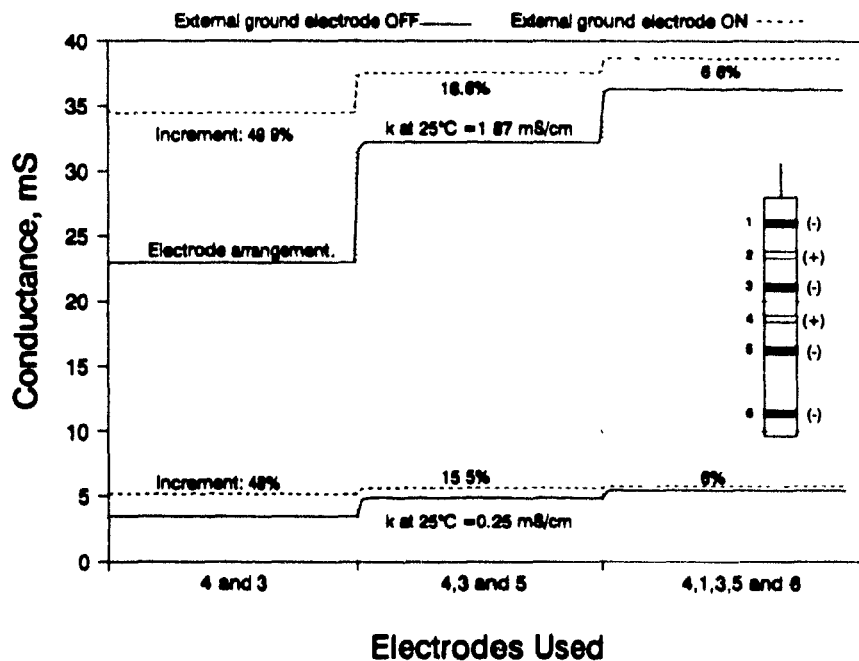
Figure 4.25 Effect of an "external" grounded electrode on the response of different electrode arrangements for solutions of conductivity 0.25 and 1.87 mS/cm

Another interesting finding is the experimental fact that positive and grounded electrodes are interchangeable provided an external electrode is not present, that is to say, in the absence of an external electrode a similar conductance measurement is obtained by using a positive against two grounded electrodes or vice versa; when an external grounded electrode is introduced this interchangeability does not apply any more.

b).-   Performance of the conductivity cell of the stationary probe

The performance of the conductivity cell of the stationary probe was experimentally studied with the aim of establishing whether the conductance values of the profile could be used to infer the level position with more accuracy. It is worth keeping in mind that the largest slope algorithm locates the level in between those electrodes giving rise to the largest conductance difference, and therefore, with an accuracy of ± 5 cm for this particular geometry. The experiments were conducted at the industrial and laboratory scale.

At the industrial scale the experiments were completed in the 91 cm diam. column at the Strathcona mill (Falconbridge Ltd.) while processing a stream from the copper circuit. The experiments consisted of collecting simultaneously conductance profiles and measurements of the level within ~ 1 cm accuracy. A probe to achieve this degree of accuracy was developed (the "high accuracy" probe). This probe is intended to be manually operated from the top of the column. The sensing element is a 1 cm Plexiglas cube open at the bottom and the top, that has two of its internal opposing faces formed by stainless steel plates. Figure 4.26 illustrates the probe and its accuracy when tested in a 10 cm diam. Plexiglas (transparent) column using a water-air system. This probe proved to be quite effective; displacements of 1 cm were sufficient to produce large conductance variations as the cube was moved up and down across the interface.

Inspection of a conductance profile around the interface shows either high or low
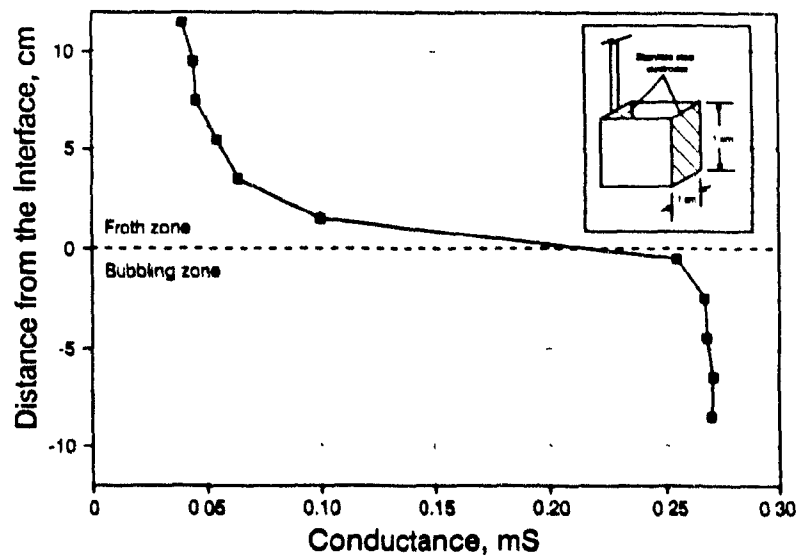
Figure 4.26 Performance and geometrical details of the "high accuracy probe" (10 cm diam. water-air column)

conductances typical of the collection or froth zones, respectively. In most cases, however, the conductance measured by the ring closest to the interface ranges between these two extremes, as point A in Figure 4.27. This figure also shows the levels determined by the "high accuracy" probe and that calculated by the "largest slope" algorithm. Figure 4.28 presents the data obtained from twenty consecutive profiles collected when the level was around ring electrode 8, which was located at 87 cm from the top of the column; the response of electrode 8 to different levels measured with the high accuracy probe is shown.

Similar experiments but under a more controlled environment were performed at the laboratory scale in a water-air system (tap water of conductivity ~0.3 mS/cm was used). The shortened version of the probe and a 20 cm diam. × 100 cm Plexiglas column (Figure 4.29) were used. The advantage of the laboratory set up over the industrial one is that the position of the probe in the column and the location of the interface level during the experiments can be defined with an accuracy in the order of
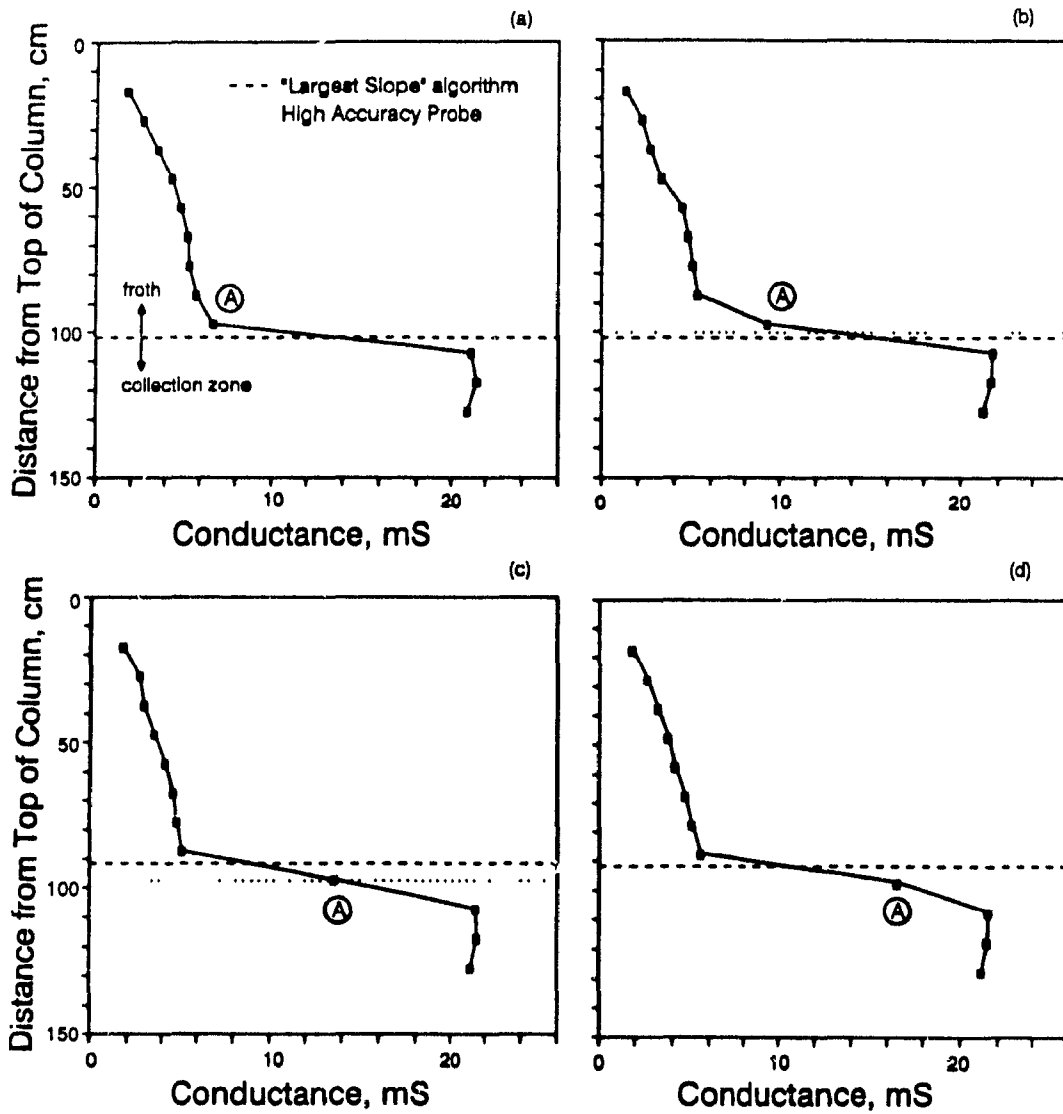
Figure 4.27 Conductance profiles showing the effect of the position of the interface level on the response of the conductivity cell of the stationary probe. Measurements performed with the "high accuracy probe" are shown in (b) and (c)
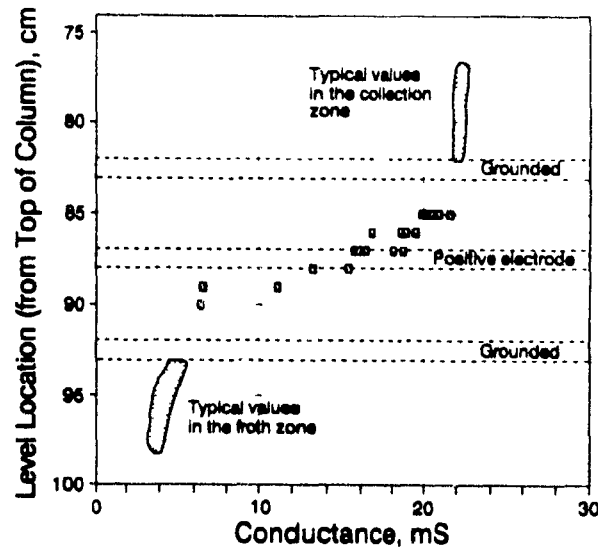
Figure 4.28 Response of the conductivity cell of the stationary probe to fluctuating interface level in a slurry-air system (accurate location of level (squares) achieved using the "high accuracy" probe)

millimeters, thereby allowing more precise measurements to be made. In these experiments, the interface level was slowly moved up or down by varying the underflow (tails) rate. Conductance measurements were continuously collected with the probe and, simultaneously, the interface level obtained from visual inspection was recorded. The electrode arrangement of the stationary probe was simulated by measuring conductance between a positively charged electrode and the two grounded electrodes, one on either side. Figure 4.30 presents the results obtained.

Figure 4.30 shows that the response of the cell to level variations within its dimensions (i.e. between the positive electrode and the two grounded electrodes) can be approximated by a straight line from the middle position of the top grounded electrode to the middle position of the bottom grounded electrode. The accuracy of the interpolation of level that results from using this linear relationship is in the range from +1.08 to -0.9 cm, for the experimental results presented in Figure 4.30.

Figure 4.29   Experimental set up to evaluate the response of the conductivity cell of the stationary probe
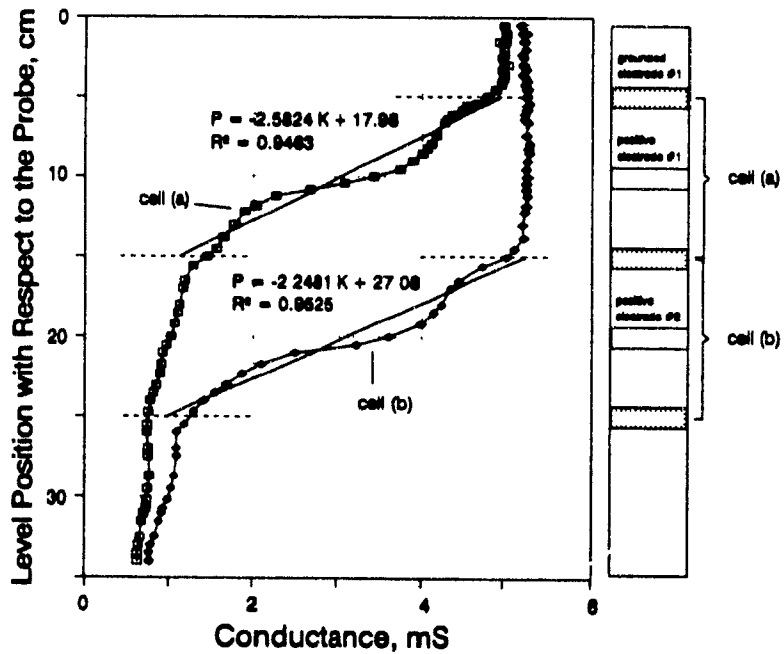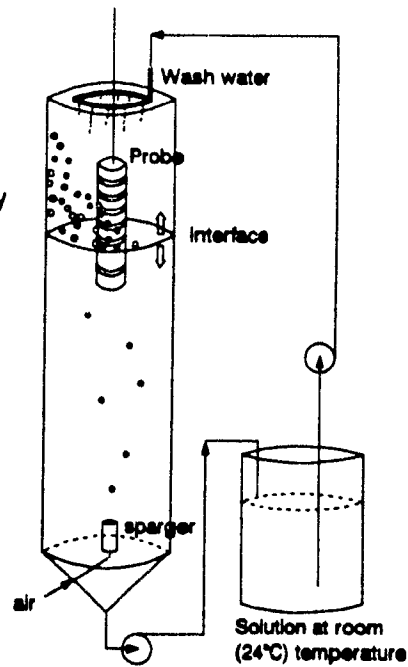
Figure 4.30   Response of the conductivity cell of the stationary probe to interface level variations (water-air system). The equation is the relationship between the level position, P, and the measured conductance, K

Based on the previous results, a level detection algorithm that incorporates the interpolation of level between those two positive electrodes producing the largest conductance differences was developed. The algorithm is described next.

c).-   Level interpolation algorithm

Once a conductance profile is completed, the following steps are followed:

1).-   The largest conductance difference is located. For the purpose of the discussion, let us assume it occurs between the positive rings "p" and "$p+1$" in Figure 4.31.

2).-   The conductance of the froth (K_f) and collection zone (K_c) are approximated by the measurements performed with the positive rings "$p-1$" and "$p+2$", respectively. Thus, by using an "idealized" representation of Figure 4.30, which is presented in Figure 4.32, the slope of the straight line defining the transition from the collection to the froth zone is given by

$$slope \; - \; - \frac{K_c - K_f}{l_{g+1} - l_g} \; - \; - \frac{K_c - K_f}{10 \; cm} \tag{4.6}$$

3).-   From the two rings producing the largest conductance difference, the conductance on the froth side, denoted "F", is given by electrode p (Refer to Figure 4.31), and that on the collection zone side is given by electrode $p+1$ and is denoted "C".

Now, from inspection of typical profiles (profiles in Figure 4.27, for example), three general cases emerge (see Figure 4.32):
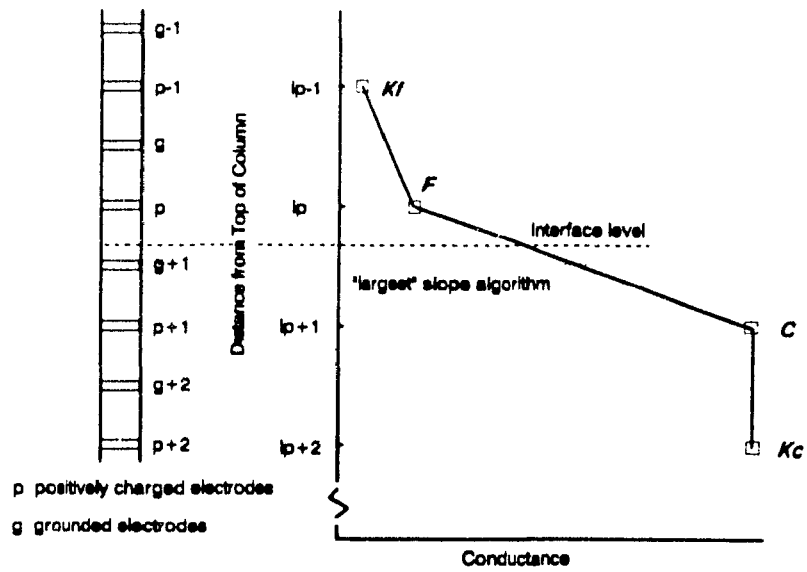
Figure 4.31   Definition of terms involved in the "interpolation" algorithm
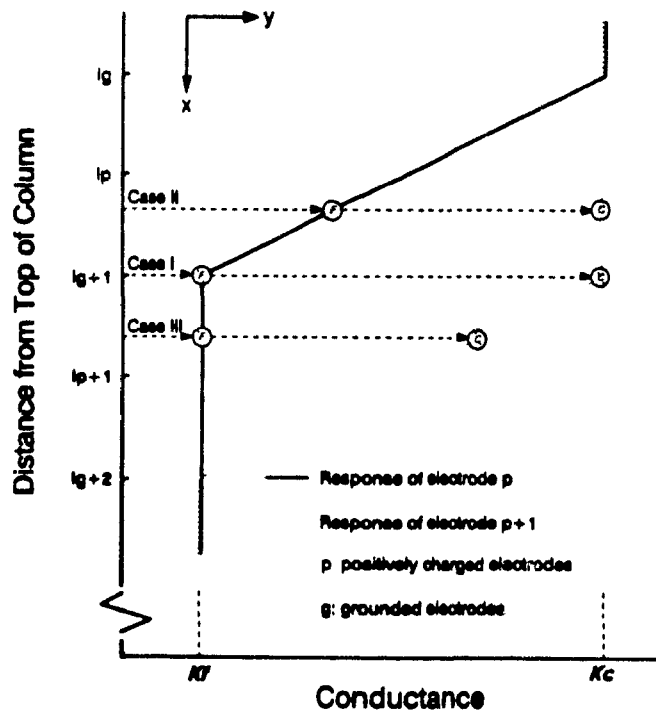
Figure 4.32   Idealization of experimental results in Figure 4.29

CASE I.-The values F and C are <u>similar</u> to the values of K_f and K_c, respectively (profile (a) in Figure 4.27). Under these conditions, the level is given by the "largest slope" algorithm which locates the level in the position of the grounded electrode "$g+1$"

$$level = l_{g+1} = l_p + 5 \qquad (4.7)$$

CASE II.-F is <u>larger</u> than K_f. This condition prevails when the level is between rings p and $g+1$ (profile (b) in Figure 4.27); the level is then given by

$$level = -10 \times \frac{F - K_f}{K_c - K_f} + l_p + 5 \qquad (4.8)$$

CASE III.-F is <u>similar</u> to K_f and C is <u>smaller</u> than K_c. This situation represents levels between rings $g+1$ and $p+1$ (profiles (c) and (d) in Figure 4.27); the level is given by

$$level = -10 \times \frac{C - K_c}{K_c - K_f} + l_p + 5 \qquad (4.9)$$

The next problem to solve in putting the algorithm to work is the definition of <u>similar</u>, <u>larger</u> and <u>smaller</u>. By trying different factors it was decided that those presented in the block diagram of the algorithm, showed in Figure 4.33, were appropriate for most conditions.

Figure 4.34 presents the comparison between the estimations of the "interpolation" algorithm, the estimations of the "largest slope" algorithm, and actual measurements performed with the independent "high accuracy" probe. Fairly good agreement is observed between the "interpolation" algorithm and the measurements, thus validating the algorithm.
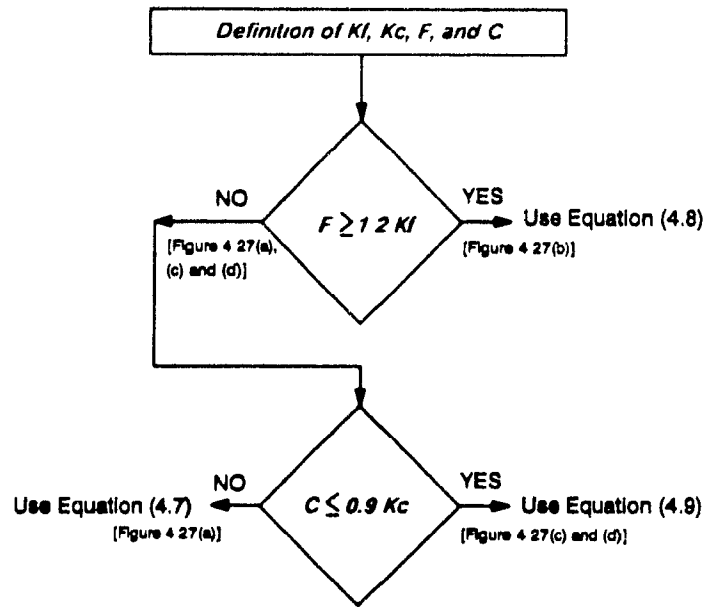
Figure 4.33 Block diagram of the "interpolation" algorithm
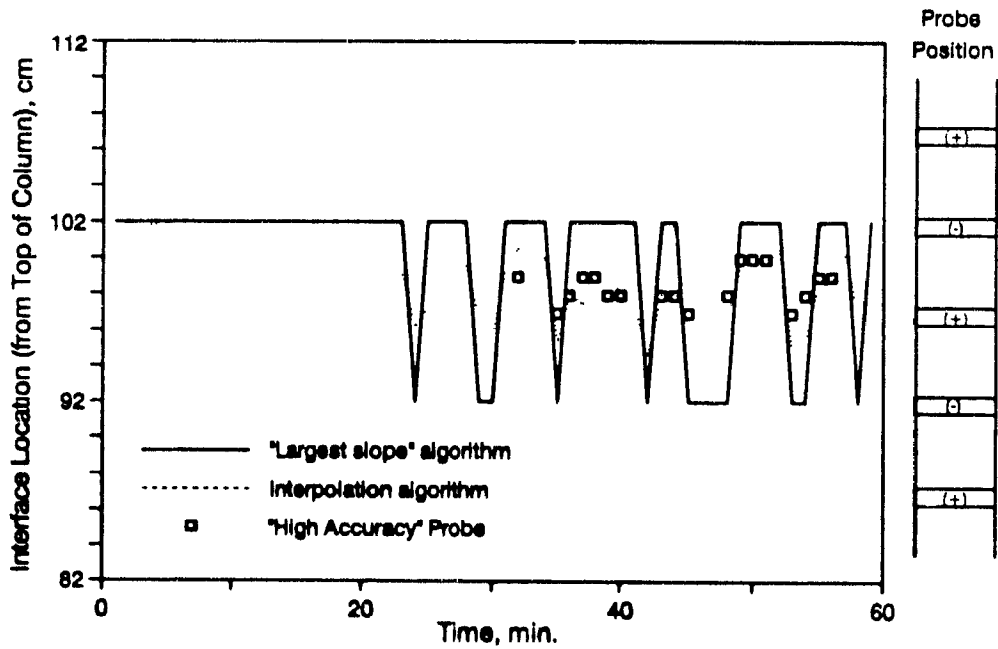
Figure 4.34 Comparison between the "largest slope" algorithm, the "interpolation" algorithm and measurements performed with the "high accuracy probe"

d).-   An alternative algorithm

An alternative level detection algorithm that locates the level with an offset that ranges from 0 to 5 cm is presented next. The algorithm originates from the experimental results obtained when testing an alternative way of collecting conductance profiles. The basic idea consisted in collecting the conductance profile by measuring between pairs of neighbouring electrodes, one positively charged and the other grounded.

Laboratory experiments to evaluate the performance of this electrode arrangement were conducted in a water-air system making use of the set up illustrated in Figure 4.29. The experiments basically consisted in collecting conductance measurements while the level was slowly moved (less than 0.5 cm/min) up (or down). For a given level position, obtained from visual inspection and time-recorded, timed conductance measurements were sequentially performed making use of the shortened version of the probe (thus allowing four measurements). A set of measurements was collected every minute. Figure 4.35 presents the results obtained and Figure 4.36 presents the behaviour of the conductance difference between adjacent cells. For any particular position of level, these differences were computed by subtracting the conductance values of adjacent cells such that the measurements collected with the four cells translated into three conductance differences.

Inspection of Figure 4.36 reveals that the use of the "largest slope" (equivalent to the largest conductance difference) algorithm to analyze the data is promising. This plot shows, for example, that for levels between ~ 10.7 and ~ 15.6 cm the conductance difference generated by cells (b) and (c) is the largest; thus, by assigning the level to the position of the common electrode of these two cells (the grounded #2 located at 15 cm), the level is estimated with an offset that ranges from ~ -0.6 cm to ~ 4.6 cm, in other words, the level estimation can be up to -0.6 cm lower or up to 4.3 cm higher than the actual one. This is neatly shown in Figure 4.37 which presents the step shape response of this algorithm when applied to the results of Figure 4.35.
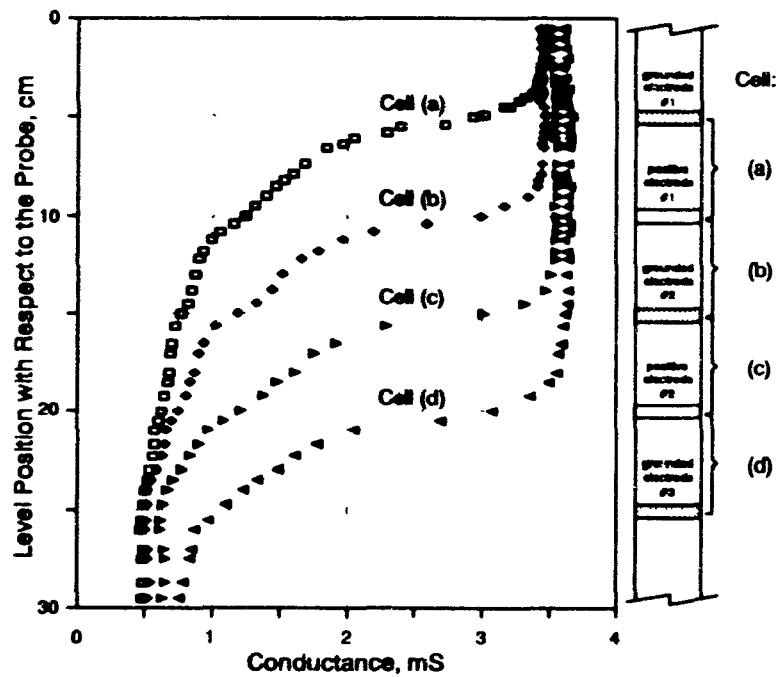
Figure 4.35 Response of adjacent electrodes (a positive and a grounded) to interface level variations (water-air system)
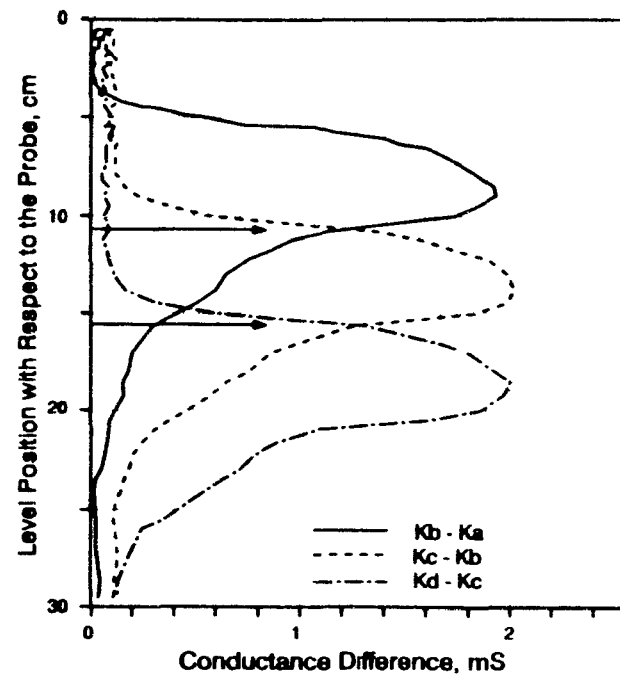
Figure 4.36 Conductance difference between adjacent cells
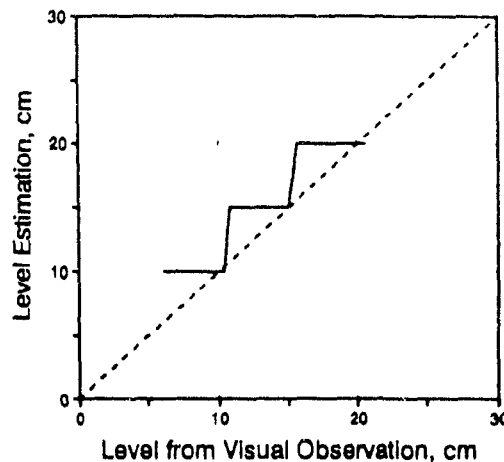
Figure 4.37 Performance of the "largest slope" algorithm for the experimental results in Figure 4.35

The main disadvantage of this approach is that the number of measurements required to complete a profile increases by a factor of two with respect to that required with the arrangement introduced first. The same factor of two applies to the time required to update the level. This problem can be mitigated, as mentioned before, by using a conductivity meter with a shorter time constant. The main advantage is the accuracy gained in the detection of level without the need to involve more elaborate computations besides those simple ones required to locate the largest slope. Finally, it is worth mentioning that the effect of an "external" grounded electrode (the column wall), which increases as the number of grounded electrodes on the probe decreases, could represent a problem when testing this alternative algorithm under industrial conditions.

e).- Modelling the electrode arrangements

The performance of the two electrode arrangement introduced above, namely a cell that consists of a positive electrode in between two grounded electrodes and a second

consisting of a positive and a grounded electrode, were analyzed in the light of the basic laws of electricity. This was attempted even though, as stated before, the cells do not fulfil the requirement of uniform electric current distribution and, therefore, their performance is unlikely to be described by simple relationships.

The conductance measurements conducted with the first cell, schematically shown in Figure 4.38, is represented by the equivalent electric circuit consisting of two resistances in parallel, R_1 and R_2, which stand for the resistances between the central positive electrode and the grounded electrodes above and below it, respectively,

$$K - \frac{1}{R} - \frac{R_1 + R_2}{R_1 \cdot R_2} \qquad (4.10)$$

Now, depending on the position of the level, l, R_1 or R_2 will correspond to two resistances in series, R_f and R_b that stand for the resistance of the froth and bubbling zones, respectively, whose magnitude will depend on the actual position of the level. For the position of level illustrated in Figure 4.38, that is $l=7$ cm, the relationship is as follows

$$R_1 - R_f + R_b - \frac{l - 5}{\kappa_f A} + \frac{10 - l}{\kappa_b A} \qquad (4.11)$$

and

$$R_2 - \frac{15 - 10}{\kappa_b A} \qquad (4.12)$$
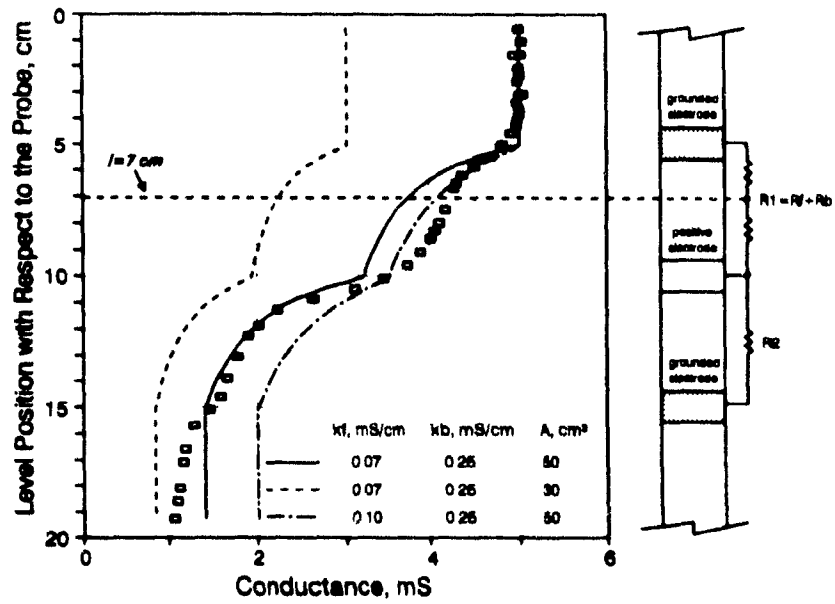
Figure 4.38 Comparison between experimental results and predictions of Equation (4.10) (The case when I=7 cm is discussed in the text)
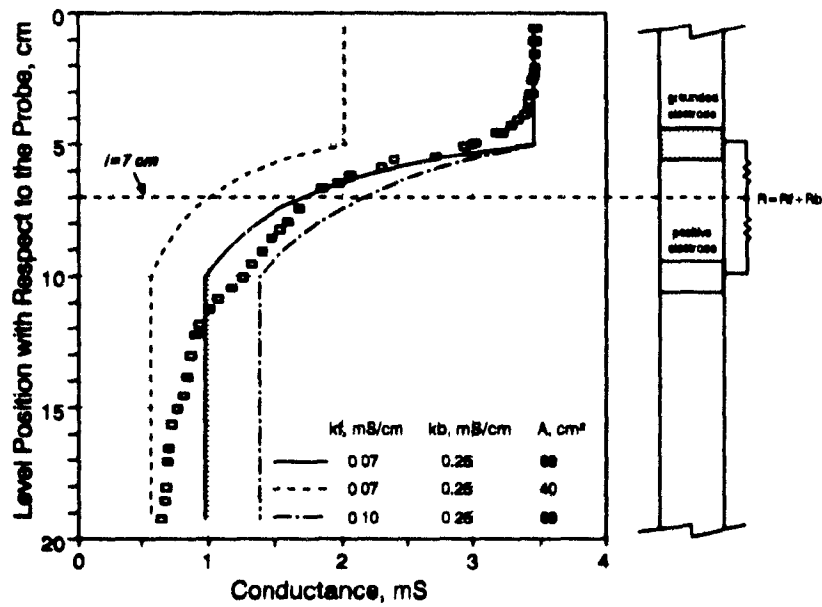
Figure 4.39 Comparison between experimental results and predictions of Equation (4.13) (The case when I=7 cm is discussed in the text)

where κ_f and κ_b are the effective conductivities of the froth and bubbling zones, mS/cm, respectively, and A is the "cross-sectional area", cm^2.

In ideal geometries like the ones discussed in Section 4.2.4(c), A, and therefore the cell constant of the cell, is well defined and κ_f and κ_b can be estimated from conductance measurements when the cell is completely immersed in the respective zone. In the present situation this is not the case and a different approach was taken.

Since tap water of conductivity ~ 0.3 mS/cm and an average gas holdup of around 12% was used in these experiments, the effective conductivity of the bubbling zone κ_b was estimated by using Maxwell's correlation which gave a value of ~ 0.25 mS/cm. Fixing this value, combinations of values for κ_f and A were tested to determine the set of values best fitting the experimental data. The results of the computations showing the effect of the different parameters are presented in Figure 4.38.

The performance of the second cell, that is, the one formed by a single positive and grounded electrode, was analyzed in a similar way. This time, the equivalent electric circuit consists of two resistance in series, as depicted in Figure 4.39 and expressed as follows

$$K - \frac{1}{R} - \frac{1}{R_f + R_b}$$
(4.13)

The resistance of the froth zone, R_f, and the bubbling zone, R_b, depends on the position of the level, l, in between the electrodes (l varies from 5 to 10 cm) as follows

$$R_f - \frac{l - 5}{\kappa_f A} \quad and \quad R_b - \frac{10 - l}{\kappa_b A}$$
(4.14)

Since these experiments were conducted in parallel with those described previously, the effective conductivity of the bubbling zone is again fixed at ~0.25 mS/cm. Figure 4.39 presents the results of the computations for three different set of values.

The conclusion that arises from Figures 4.38 and 4.39 is that none of the set of values is capable of describing the data, which basically means that the complexity of the cell geometry prevents its modelling by using simple principles of electricity. Consequently, empirical correlations like the one presented under the heading "Level Interpolation Algorithm", must be used in the attempt to increase the accuracy of the level detection.

4.4   Mechanical Flotation Machines

Level detection in conventional mechanical flotation machines has been conventionally done in a number of ways. Devices based on the response of a float (Outokumpu), devices based on conductivity (Duval Corp. Patent; Kitzinger et al., 1979; Miettunen, 1982; Koivistoinen and Miettunen, 1985), and devices based on pressure, such as bubble tubes and pressure cells, are commonly encountered. The advantages and disadvantages of these devices have been presented in Section 2.2.1.

It is of interest to determine if the conductivity probe has a potential use in mechanical cells.

The experiments were conducted in a slurry-air system at the Strathcona mill, Falconbridge Ltd., in two different flotation cells: a 38 m³ mechanical flotation cell (Dorr-Oliver), and a 1.4 m³ mechanical cell (Denver). The stationary probe described in Section 4.3.1(d) was used in the larger mechanical cell; the cell was in the copper

circuit. A smaller version of the probe, which will be described latter, was used in the Denver cell on a stream in the nickel circuit.

4.4.1 Level detection in the 38 m³ mechanical (Dorr-Oliver) cell

The conductance profiles presented in Figure 4.40 show that level detection in large mechanical cells is, in principle, possible. The difference in the shape of the profiles with respect to those encountered in flotation columns are mainly due to the absence of wash water addition in the mechanical cells, which gives rise to typical conductance ratios (collection/froth) around 2.5. In these cells the interface level is not as well defined as in the flotation column. This translates into a more noisy signal output from the system as depicted in Figure 4.41. This problem can be mitigated by filtering the signal.

Figure 4.41 illustrates the performance of the largest slope algorithm showing the step response of the level detection system. This is related to the specific geometrical arrangement of the electrodes in the probe and to the algorithm used to process the data.

4.4.2 The small version of the probe and the detection of level in 1.4 m³ Denver cells

A smaller version of the probe intended for situations where minimizing the volume occupied by the probe is important was constructed. In this probe, seventeen electrode rings (2.5 cm × 0.4 cm width) are mounted on a 2.2 cm diam. PVC pipe. The rings are equally spaced by PVC spacers (9 cm width). The distance between active rings is 2.6 cm which gives a level accuracy of ± 1.3 cm.

The probe was characterized in a similar way to that done for the large probe. Figure 4.42 shows, for example, that in tap water (~0.3 mS/cm), the conductance measured between a positive electrode and one, two, four, six or eight grounded
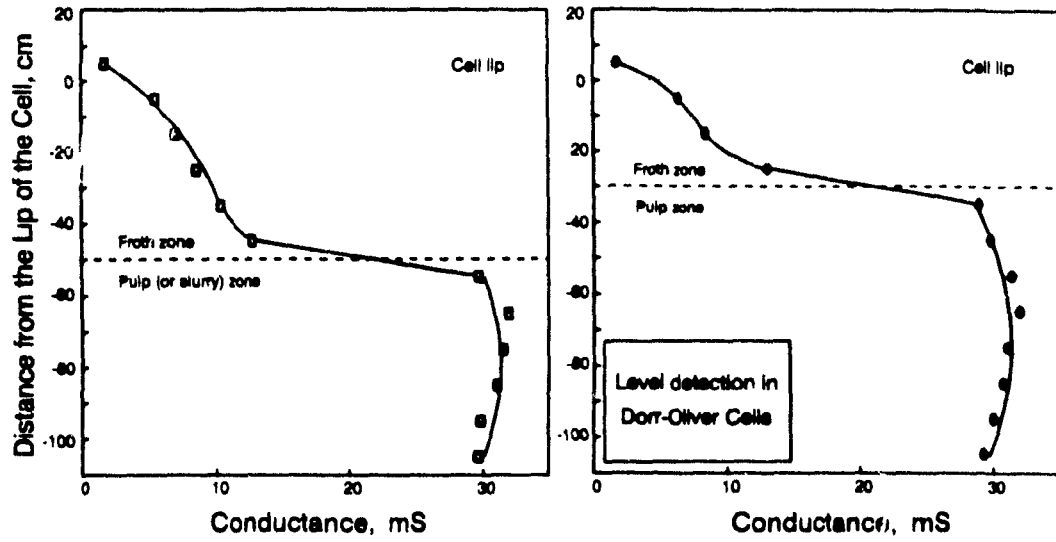
Figure 4.40 Typical conductance profiles collected in the 38 m^3 mechanical (Dorr-Oliver) cell (stream: Scavenger Feed)
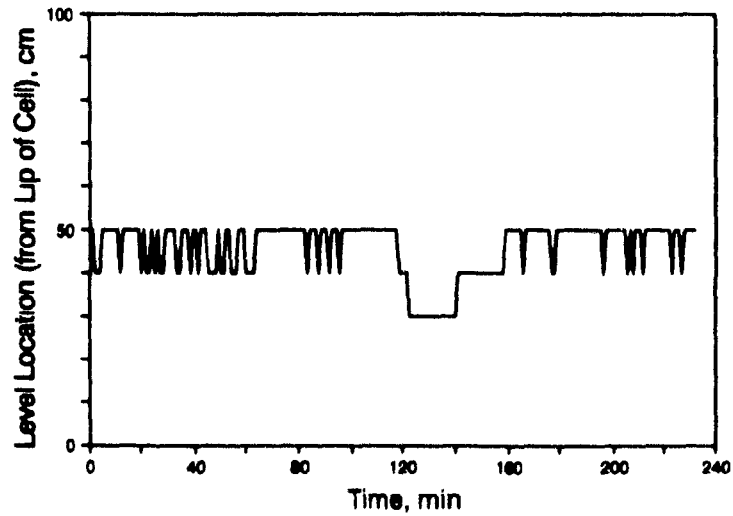
Figure 4.41 Performance of "largest slope" algorithm in the 38 m ^{3} mechanical cell
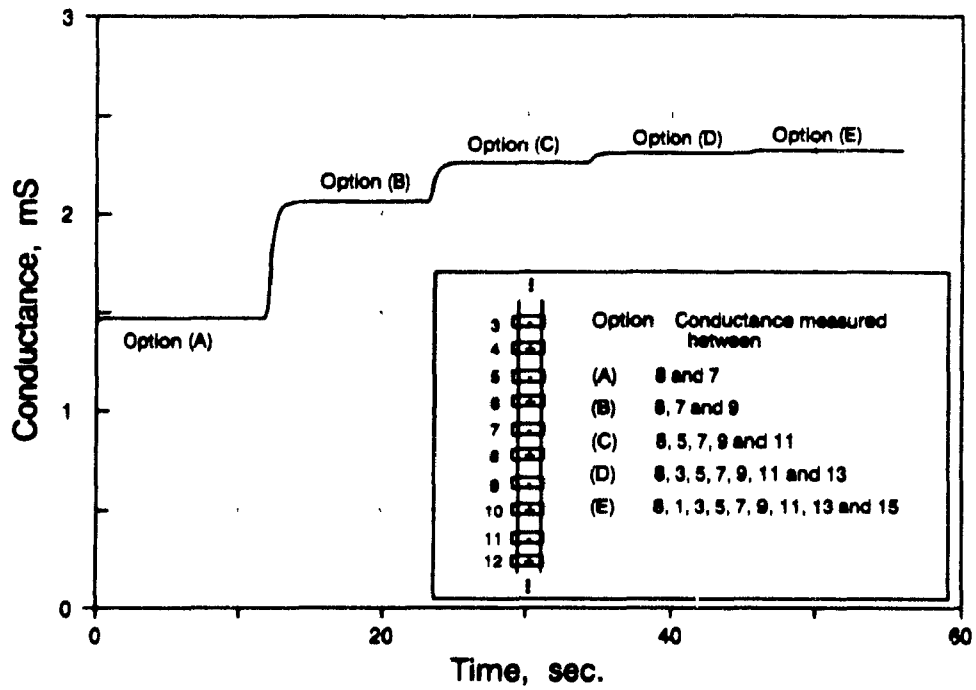
Figure 4.42 Conductance response for different electrode arrangements
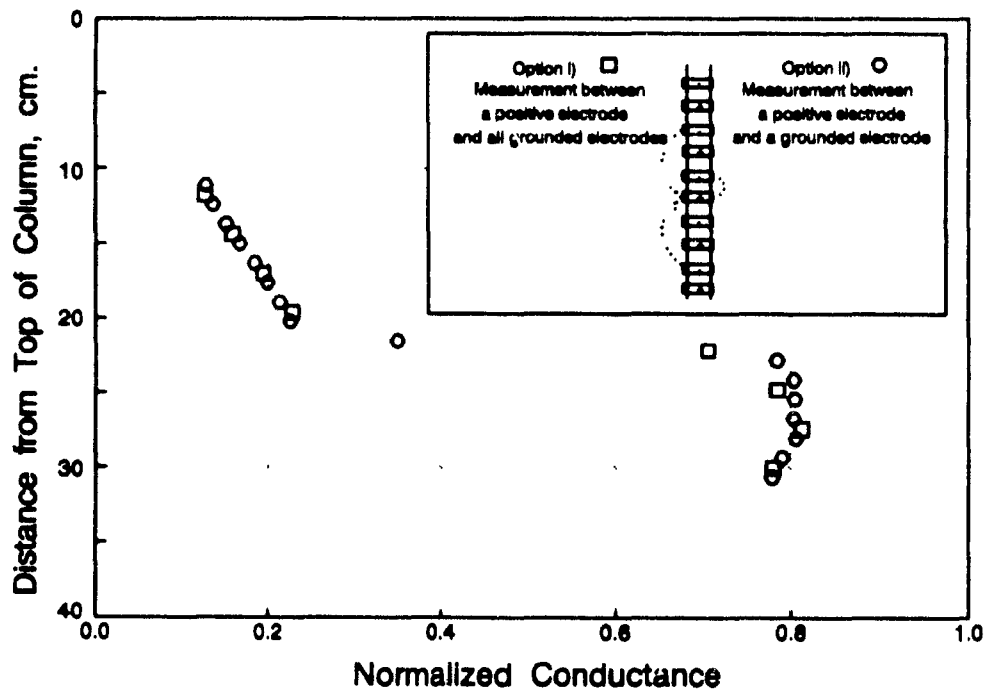
Figure 4.43 Normalized conductance profiles for two different electrode arrangements showing similar performance in the detection of interface level

electrodes increases and asymptotically levels off as the number of grounded electrodes increases, a behaviour similar to that encountered with the large probe. Figure 4.43 presents conductance profiles collected with this probe in a 10 cm diam. water (0.3 mS/cm)-air laboratory column. This figure shows that the shape of the profiles (relative position of the arms in the froth and bubbling zone, and their slope) for two different cell arrangements, namely, a positive electrode and a grounded one, and a positive electrode and eight grounded ones, is equivalent. The profiles were normalized by dividing the conductance values collected in water-air by those collected in water only. These results suggest that the performance of the small probe is similar to that of the large one.

As mentioned above, the probe was tested in a 1.4 m³ mechanical flotation cell. In order to estimate the true froth depth (i.e. allow for the layer above the lip of the cell), profiling was started 21 cm above the lip. It is evident from Figure 4.44 that the top of the froth as well as the interface level can be inferred from the conductance profile (to cover the length shown in Figure 4.44, the probe was moved).

4.5 Summary

A technique for locating the froth/collection zone interface in flotation columns was presented. The technique involves the collection of conductance profiles around the interface and the location of the position at which a sharp change in the conductance value occurs. Such a change in conductance across the interface is due to the difference in gas holdup) between the zones. The development and testing of a conductivity probe suitable for industrial application were described along with the data acquisition system and level detection algorithm. The step shape output of the system and the time delay in the detection of level were discussed. Modelling of the response to interface level of different conductivity cells was described.

The detection of level in mechanical flotation cells and the measurement of the
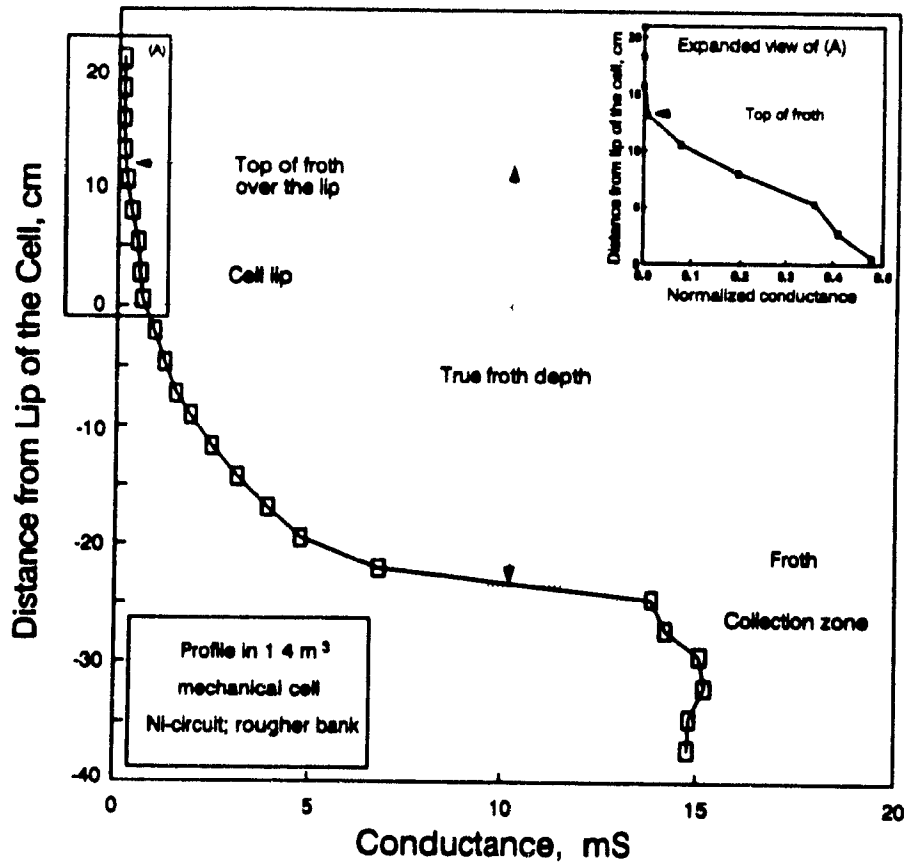
Figure 4.44 Conductance profile collected in a 1.4 m³ mechanical cell. Conductance was normalized in the expanded view by zeroing the actual reading obtained in air

"true froth depth" were addressed.

CHAPTER 5

GAS HOLDUP: EXPERIMENTAL TECHNIQUES AND RESULTS

5.1 Laboratory Scale Columns

5.1.1 Preliminary work

Preliminary work conducted in a 10 cm diam. laboratory column equipped with 12 pairs of facing circles (0.71 cm^2) intended for level detection showed that the conductance measured in the bubbling zone (water-air system) varied with the gas holdup. In these experiments the gas holdup was calculated from pressure readings collected with two water manometers and by using Equation (2.23)(according to Yianatos et al. (1985), the fractional gas holdup calculated from pressure drop measurements using water manometers separated 10 cm has an absolute ± 0.005 estimated error).

Since values of conductance for different gas holdups plus that for the clear liquid were available, it was decided to try to estimate the gas holdup using the equation proposed by Yianatos et al.(1985), namely

$$\varepsilon_g - \frac{1 - \gamma}{1 + 0.55\, \gamma} \qquad (3.43)$$

which gives the volumetric fraction of gas holdup as a function of the relative conductance K_{l-g}/K_l. Figure 5.1 presents the results obtained, showing that a substantial deviation existed between the values obtained from pressure measurements and those estimated from conductance measurements.

The question at that time was: is the difference in experimental set up here
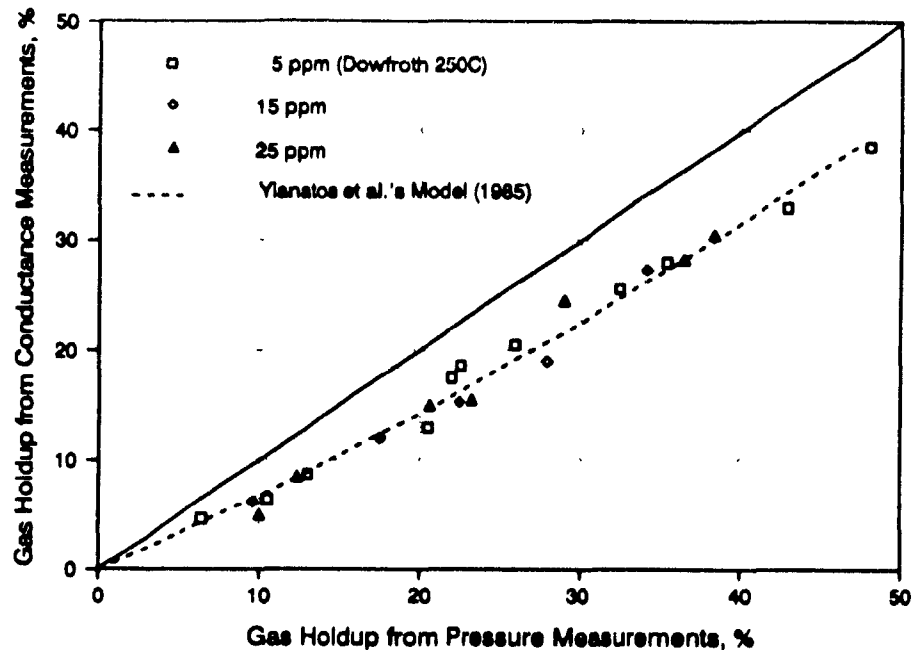
Figure 5.1   Preliminary results on gas holdup estimation using electrical conductivity

compared with that used by Yianatos et al. (1985) the cause of the discrepancy? As will be shown, it became evident that the cell geometry was playing a role. It is worth remarking that Yianatos et al. (1985) developed their model based upon results obtained in a two-dimensional column (2.5 cm width × 10 cm length) equipped with 2.5 cm width × 1 cm height facing electrodes; in this geometry uniform current distribution exists to some degree (for example, a cross-sectional view of the column, at the position of the electrodes, is an exact representation of a cross-sectional view of one of the three ideal cells -the infinite parallel plates (Section 3.2.1)).

To substantiate these findings, a set of experiments to investigate the effect of the shape and dimensions of the electrodes was conducted. This time, facing electrodes of three different sizes, 0.08 cm^2, 0.71 cm^2 and 6 cm^2, and an electrode arrangement consisting of two concentric rings were tested (Figure 5.2). These sets of electrodes were installed in a 10 cm diam. column with an axial separation of about 14 cm. The cells
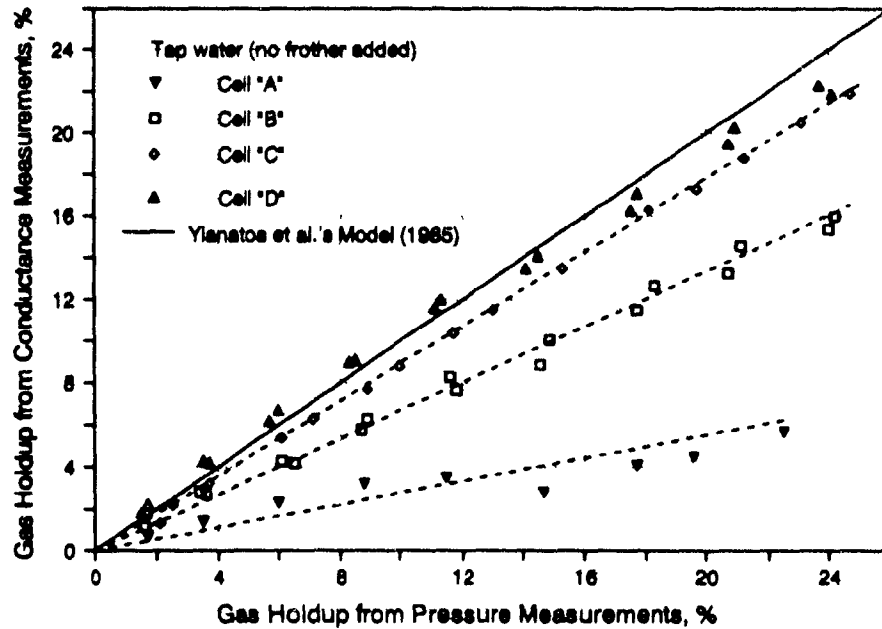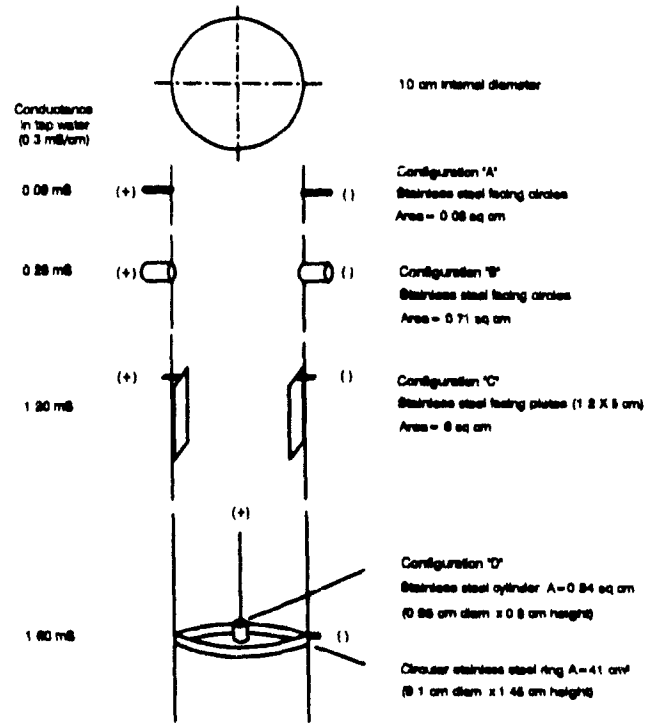
Figure 5.2   Electrode geometries tested for gas holdup estimation and experimental results

were located in between two pressure taps separated by 60 cm. The gas holdup was estimated from pressure readings obtained with water manometers. Figure 5.2 presents the results obtained.

The performance of the cells depends on their shape and dimensions (Figure 5.2). In the case of the facing electrodes, the gas holdup estimate improved as the surface area of the electrodes increased. This is due, as will be shown latter, to two factors: (a).- the appearance of a polarization resistance which varies inversely with the size of the electrodes, and (b).- by increasing the size of the electrodes, the geometry of the cell approaches that of two infinite and parallel plates, and therefore comes closer to an ideal cell where uniform electric current distribution exists. The same comments apply to cell "D" (concentric rings). In this case, the relatively large dimensions of the rings (compared to the facing electrodes), and its resemblance to a section of the infinite concentric cylinders explains the fairly good gas holdup estimates with this cell.

5.1.2 Testing Maxwell's model

A literature review on the estimation of holdup in two and three phase dispersions (see Section 3.3.2) revealed that the most widely accepted model characterizing the conductivity of a two phase dispersion is that due to Maxwell (1892). The use of Maxwell's equations requires knowledge of the effective conductivity of the dispersion and that of the continuous phase. As mentioned before, the electrical conductivity of a conductive medium can be obtained from conductance measurements only when the relationship between conductance and conductivity is known. This is the case of the cells introduced in Section 3.2.1, namely, the infinite parallel plates, the infinite concentric cylinders, and the concentric spheres. Measurement of the effective conductivity of a water-air dispersion should be performed, therefore, with an adaption of one of these three cells. In these types of cells, if polarization appears, it is uniform over the entire surface of the electrode and, therefore, the theory of the potential still applies (Kasper,

1940).

For convenience, an adaption of the infinite parallel plates was selected. This cell was described in detail in Section 4.2.4 under the heading "Performance of an ideal cell". As was pointed out at that time, such a cell has been used for measuring holdup in two and three phase dispersions (Turner, 1976; Achwal and Stepanek, 1975 and 1976; Dhanuka and Stepanek, 1987).

a).-   Experimental approach

An experimental program to evaluate the performance of the selected cell design in a water-air system was conducted. Variables such as gas content, frother content (Dowfroth 250 C), conductivity and temperature of the continuous phase (water) were explored. The experiments were conducted in a 5.7 cm diam. × 93 cm height laboratory column. Figure 5.3 illustrates the experimental set up.

Gas holdup was measured with a water manometer located at 62 cm from the lip of the column. With this arrangement the gas holdup of the aerated column is calculated by dividing the distance from the column lip to the water level in the manometer by the length of the column of water in the absence of air (62 cm). This measurement represents the average value of the gas holdup in the section of the column between the pressure tap and the column lip.

An immersion circulator (Cole-Parmer Mod. 1266-02) was used to maintain the temperature of the solution constant (at 25°C unless otherwise specified). Potassium chloride (KCl) was used to increase the conductivity of water over that of the tap water (~0.3 mS/cm). A small flow of water (less than 0.05 cm/s) was fed to the column through the underflow port to avoid the formation of a layer of froth which would invalidate the pressure-based technique to estimate holdup. The overflow was returned
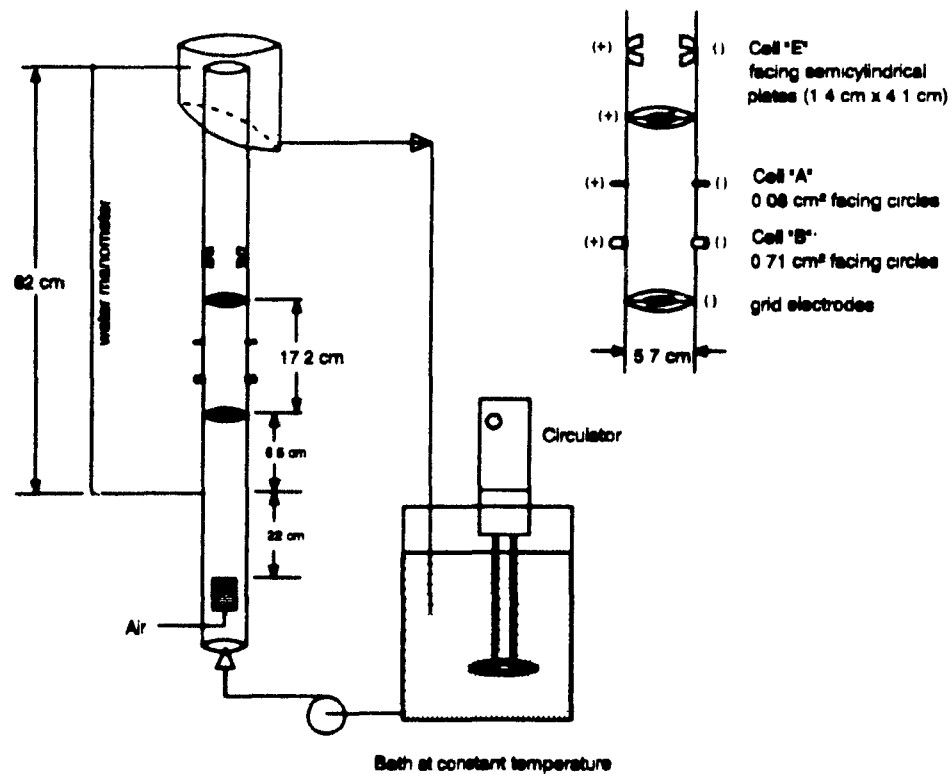
Figure 5.3 Experimental set up to evaluate the performance of the grid electrodes

to the constant temperature bath and then recycled to the column.

"Grid" electrodes were tested in parallel with three other cells namely, the 0.08 and 0.71 cm^2 facing circles (introduced earlier) and a cell formed by two semi-cylindrical facing plates (1.4 height × 4.1 length, Cell "E" in Figure 5.3). Preliminary results obtained with this latter cell in a water (0.3 mS/cm)-air system were promising in terms of gas holdup estimation.

b).-   Experimental procedure.

The column was filled with KCl solution at constant temperature. A constant overflow was allowed and compensated by a small feed flowrate (less than 0.05 cm/s)

through the underflow port. Conductance measurements of the clear liquid were performed with the four conductivity cells. Ten measurements, one every second, were performed with each cell.

An air flowrate (0 to ~2.5 cm/s) was established and, after the column reached stable operating conditions (as judged from the fairly constant reading of the water manometer), the water manometer was read and simultaneously, the conductance measurement of the liquid-air dispersion was measured with the four cells. A new air rate was then established and the above procedure repeated. After the desired range of gas holdup was covered, the air was turned off and the column was filled with solution. For comparison purposes, a second set of conductance measurements on the solution only was collected. Excellent reproducibility was encountered (relative difference less than 0.2%).

Analysis of the data was conducted using Maxwell's equation. The averaged values of the conductance measurements were directly used in the computation of gas holdup according to

$$ e_g = \frac{1 - K_{l-g} / K_l}{1 + 0.5 \, K_{l-g} / K_l} \times 100 $$

Although Maxwell's model considers conductivities rather than conductances, the relative conductance is equivalent to the relative conductivity provided the cell constant remains constant. Figure 5.4 shows the relationship between the apparent cell constant (conductance/conductivity) and conductivity for the cells tested in this work. For comparison purposes, the results obtained with a section of an ideal cell are also presented. This cell consisted of a Plexiglas cylinder 5.7 cm diam. having two circular stainless steel plates filling the entire cross-sectional area of the cylinder and separated by 22 cm. The calculated cell constant of 1.16 cm (25.5 cm²/22 cm) is in good agreement with the experimental results (Figure 5.4). The apparent variation of the cell constant with conductivity (Figure 5.4, cell "E") has been attributed to polarization,
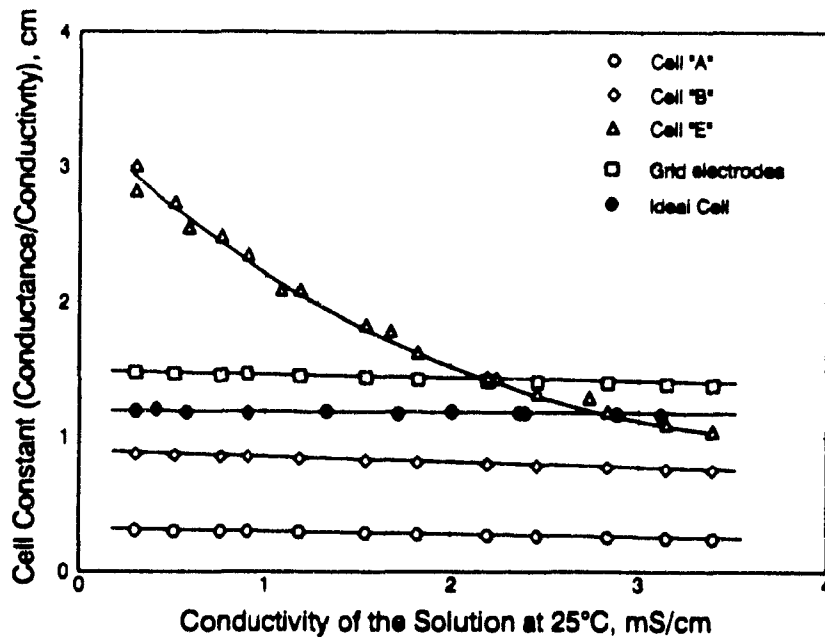
Figure 5.4 Behaviour of the apparent cell constant of the different cells tested in this work

which intensifies as the conductivity increases (Davies, 1930), or to interference from effects other than the resistance of the solution (William, 1990).

The gas holdup obtained from conductance using Maxwell's model was plotted against that obtained from pressure. For comparison purposes, two other models are also presented. Figures 5.5 to 5.8 present the experimental results.

c).-   Performance of the cells

Effect of electrode size

The use of platinized platinum electrodes to measure the conductivity of electrolytes is a common laboratory practice. The reason for this is that by platinizing the electrodes the surface area increases, the current density decreases and so does the
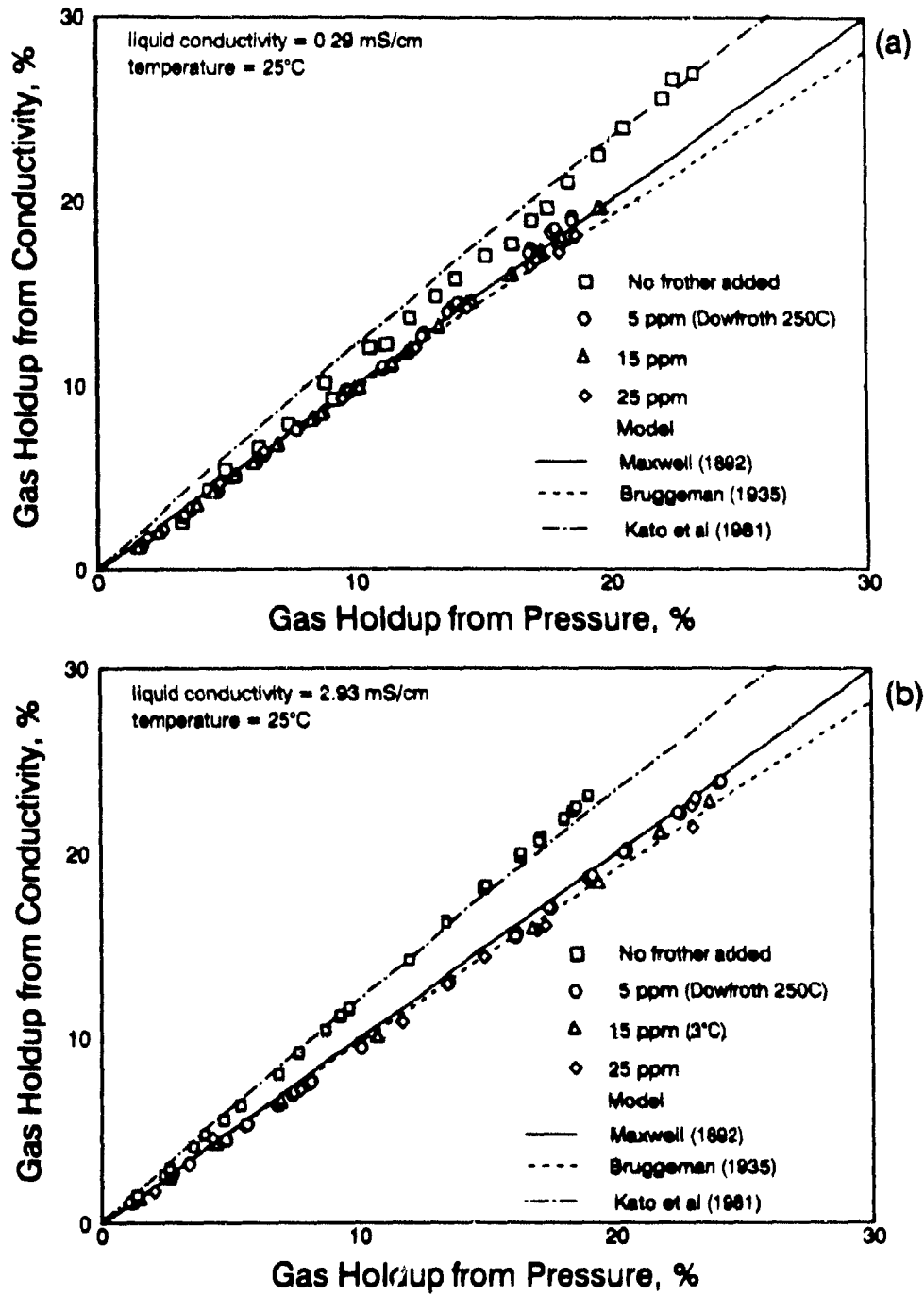
Figure 5.5 Experimental results obtained with the grid electrodes
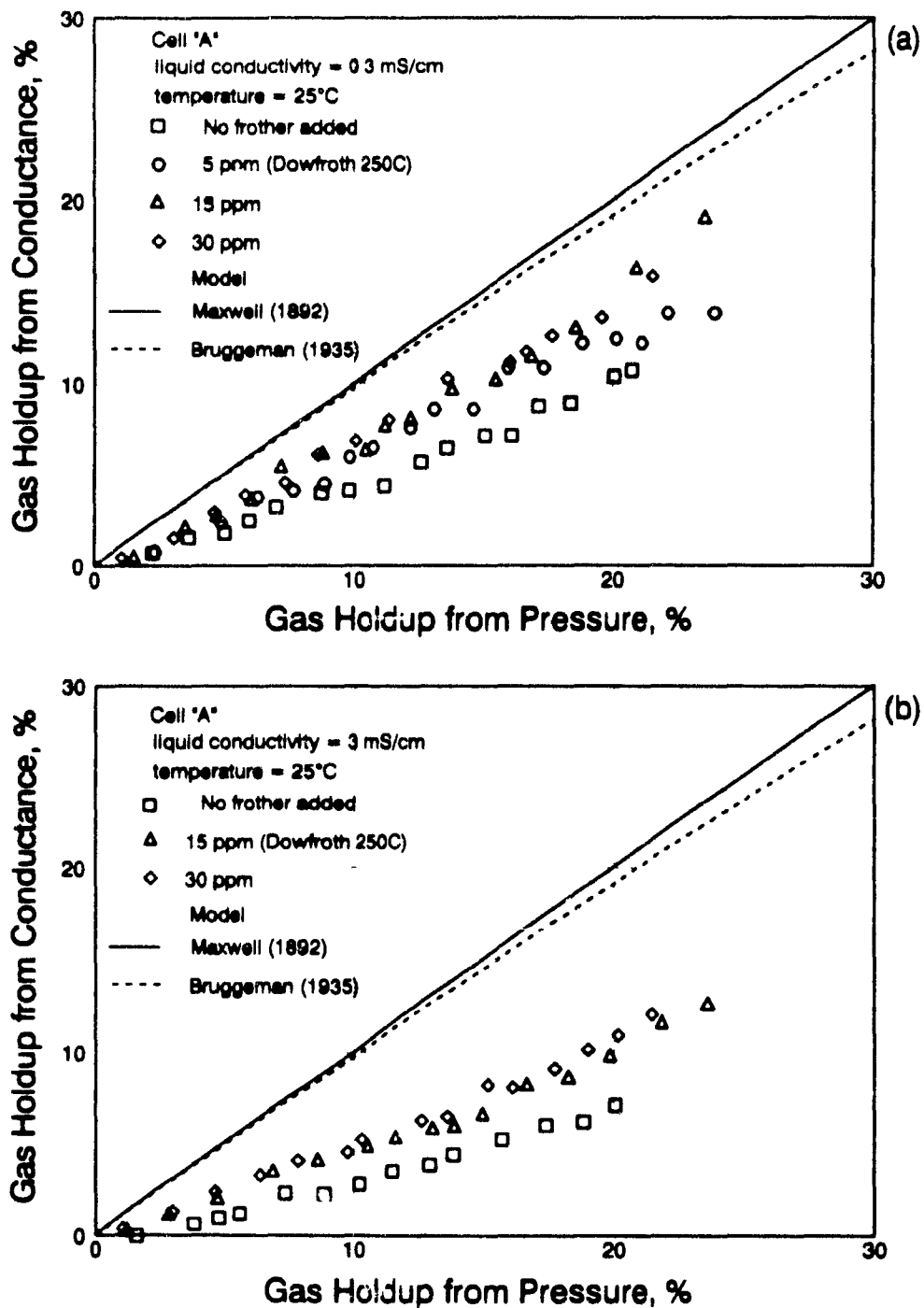
Figure 5.6   Experimental results obtained with Cell "A" (0.08 cm² facing circles)
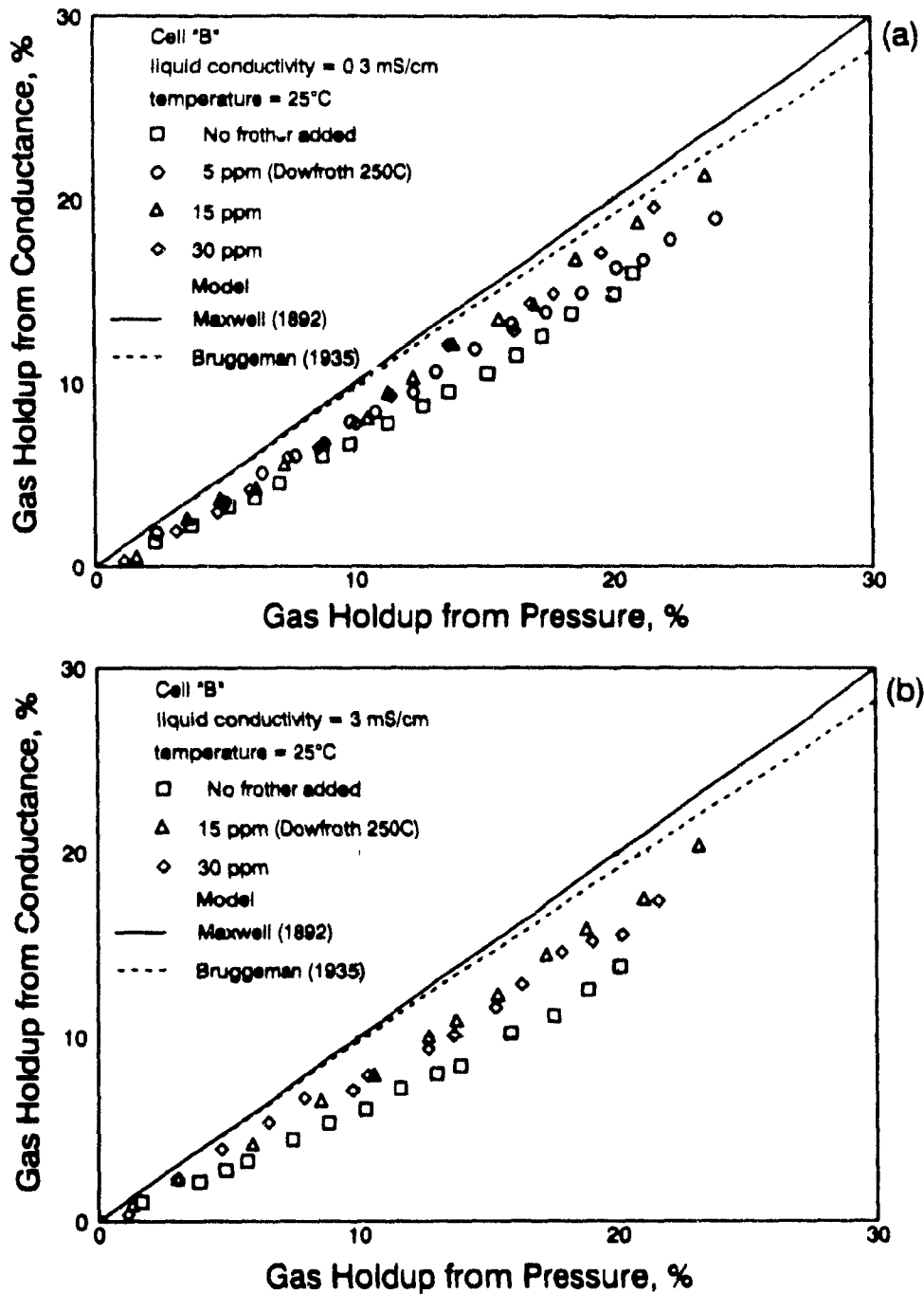
Figure 5.7 Experimental results obtained with Cell "B" (0.71 cm² facing circles)
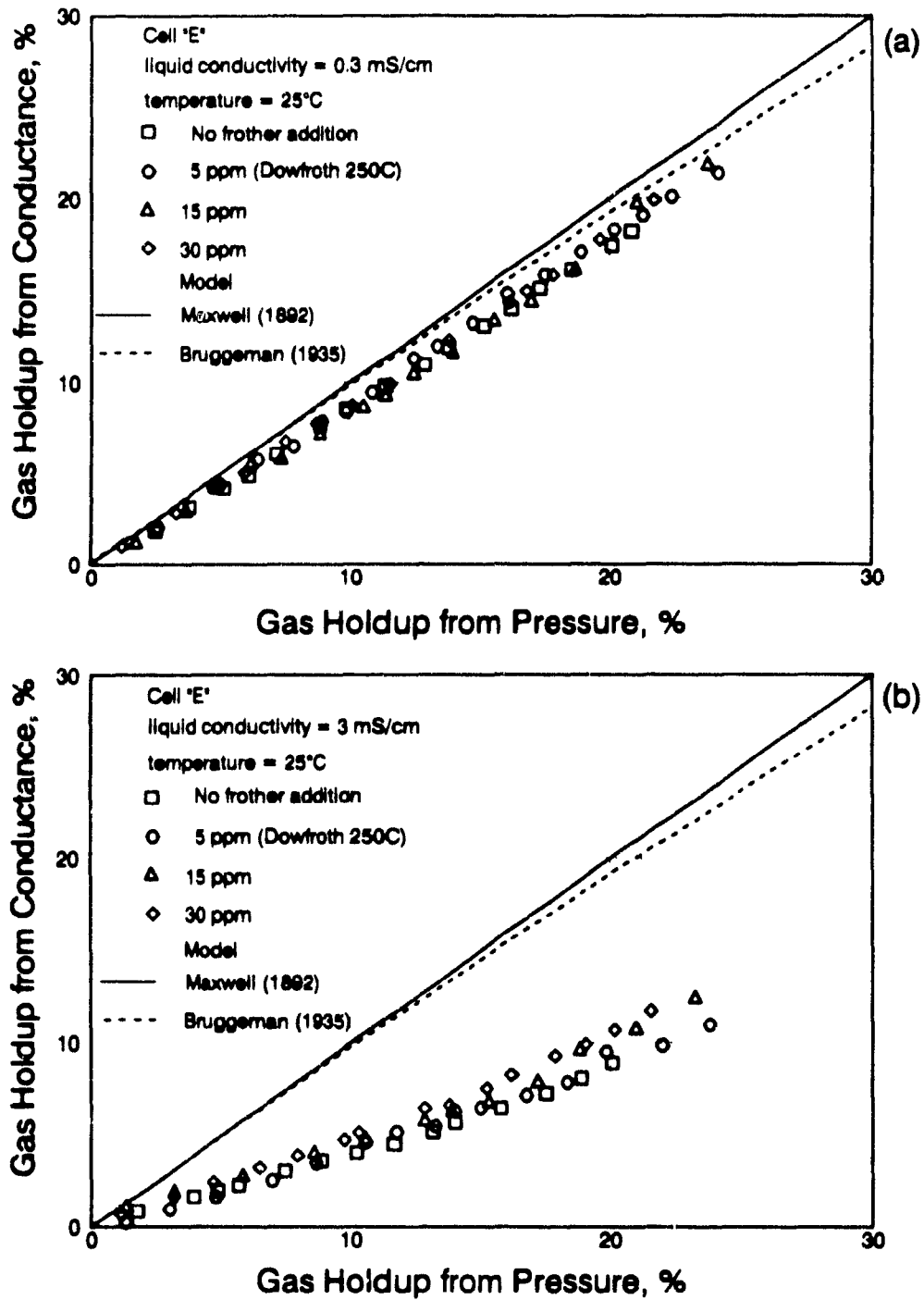
Figure 5.8 Experimental results obtained with Cell "E" (semicylindrical 1.4 cm x 4.1 cm facing plates)

polarization resistance (Braunstein and Robbins, 1971). The polarization resistance depends on current density; it increases as the size of the electrodes, or more exactly, their surface area, decreases (Kasper, 1940). This is most probably the basis of the explanation of the better performance of the larger electrodes observed in Figures 5.6 to Figure 5.8.

The fit to the models improved as the size of the electrodes increased. Since uniform current density does not exist over the entire surface of the electrodes, polarization can develop in areas where the current density is larger (e.g the edges of the electrodes (Meredith and Tobias, 1962)). If polarization exists, the conductance measurements will be a function not only of the effective conductivity of the dispersion and size of the electrodes but also of the degree of polarization developed (which is a function of size of electrodes). Polarization can be reduced either by increasing the surface area of the electrodes or by increasing the frequency of the (alternating) current (Davies, 1930). Meredith and Tobias (1960 and 1961) reported that with liquid-conductive solids systems, the presence of polarization is important up to frequencies in the order of 10 kHz. Having the frequency fixed at 1 kHz (as in most commercial meters), the use of larger electrodes will provide a more resolved measurement of the effective conductivity of the dispersed system and, therefore, give gas holdup estimates closer to those expected from Maxwell's model.

Effect of bubble size

The performance of the cells in tap water (no frother added) was, in general, not satisfactory. Under this conditions relatively large bubbles occur (much larger than 2 mm).

Interestingly, the results using the grid electrodes were well described by empirical equations developed for fluidized beds. Figure 5.5 shows that the equation of

Kato et al. (1981) (Equation (3.30)) fits the experimental data obtained with the grid electrodes in tap water reasonably well. This is probably due to the similarities between the present conditions and those in fluidized beds where no surface active chemicals are added and, therefore, relatively large bubble sizes are encountered. However, these are not conditions prevailing in flotation where frother addition to decrease the bubble size is common practice.

When frother was present performance of all the cells improved. The qualitative explanation for this comes from Maxwell's model. It is worth recalling that Maxwell's treatment examined the case of spheres at distances from each other large enough so that their effect in disturbing the path of the electric current may be taken as independent of each other. This condition is approached by solutions containing frother since spherical bubbles of sizes less than 2 mm are achieved (Klassen and Mokrousov, 1963). Application of Maxwell's model for a dispersed phase of size less than about 2 mm is supported by, for example: Neale and Nader (1973) (glass spheres less than 2 mm); Nasr-El-Din et al. (1987) (polystyrene particles 0.3 mm diam.); De la Rue and Tobias (1959) (glass spheres 0.175 to 0.21 mm diam.); Turner (1976) (conductive and non-conductive resin beads 0.15 to 1 mm diam). On the other hand, fluidized systems, where relatively large bubbles and solids are commonly used are not well described by Maxwell's model. This is the case for the data reported by Achwal and Stepanek (1975, 1976)(1/4" Rashing rings and 6 mm ceramic cylinders), Dhanuka and Stepanek (1987)(glass spheres 1.98 to 5.86 mm diam.), and Begovich and Watson (1978)(glass, alumina and Plexiglas beads 4.6 to 6.3 mm diam.). Although the work of Kato et al.(1981) is for a fluidized bed, the small size of solids they used (glass beads 0.42 to 2.2 mm diam.) may explain the proximity of their empirical correlation ($\kappa_{1-g}/\kappa_1 = \varepsilon_1^{1.2}$) to that of Maxwell (Maxwell's equation for a non-conductive dispersed phase is well represented by the expression $\kappa_{1-g}/\kappa_1 = \varepsilon_1^{1.4}$ up to about 40% of holdup of the dispersed phase).

Effect of the conductivity of the continuous phase

Two electrical conductivities of the aqueous solution were used: 0.3 mS/cm, the conductivity of tap water normally used in laboratory studies; and ~ 3 mS/cm, as a representative of typical pulp water conductivity (copper circuit, Strathcona mill (Uribe-Salas and Finch, 1990)). KCl was used to increase the conductivity of the solution over that of the tap water.

As shown in Figures 5.6 to 5.8, the increase in the conductivity of the solution has a dramatic effect on the performance of cells "A", "B", and "E". The performance of the grid electrodes, however, was insensitive to the conductivity variations. This behaviour is thought to be, again, related to polarization since the conductivity of the conductive medium plays an important role in polarization (Wagner, 1962). As the effective conductivity of the dispersion increases (by increasing the conductivity of the liquid phase), the contribution of the polarization resistance increases. This can be visualized by considering the measuring cell as an electric circuit consisting of two resistances in series (William, 1990): the polarization resistance at the electrode/electrolyte interface and the effective resistance of the liquid-air mixture. Thus, the conductance measurement will include the contribution of the polarization resistance which could become a significant proportion of the total value as the resistance of the system decreases.

Effect of the temperature

The conductivity of an electrolyte depends on the temperature according to the expression (in the region near 25°C) (Glasstone, 1930 and 1942; Condon, 1967)

$$\kappa = \kappa_{25^{\circ}C} \left[1 + \alpha_{25^{\circ}C} \left(t - 25^{\circ}C \right) \right] \tag{5.1}$$
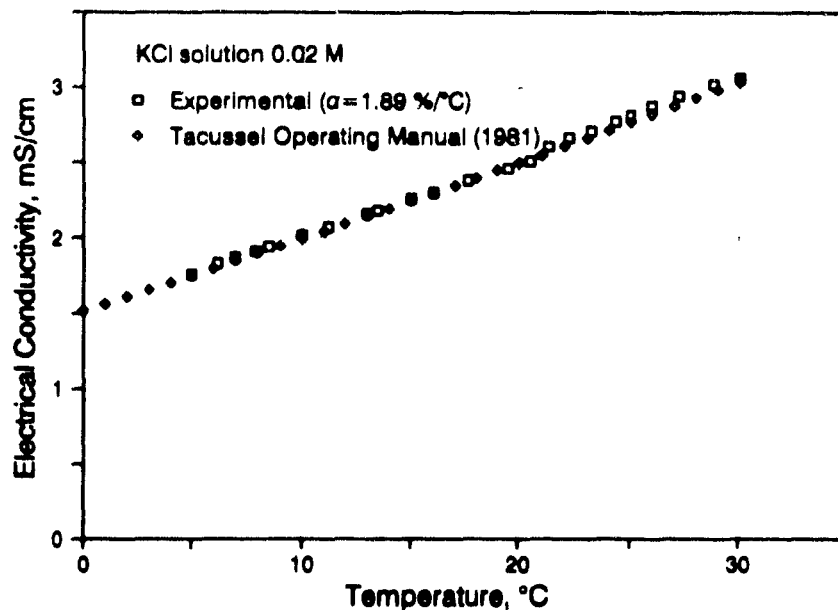
Figure 5.9   Effect of temperature on the conductivity of a 0.02 M KCl solution

where κ and $\kappa_{25^\circ C}$ are the conductivities (mS/cm) of the electrolyte at the temperature t and 25°C, respectively, and $\alpha_{25^\circ C}$ is the coefficient of variation of the conductivity per degree Celsius with respect to the conductivity at 25°C.

For most electrolytes, the conductivity increases with temperature presenting temperature coefficients around 2 (Glasstone, 1942).

Figure 5.9 presents experimental data on the effect of temperature on the conductivity of a 0.02 M KCl solution. For comparison purposes, values for a standard KCl solution of the same concentration are also presented (Tacussel Operating Manual, 1981). According to Equation (5.1), the coefficient of variation $\alpha_{25^\circ C}$ obtained for the experimental data in Figure 5.9 is 1.89 %/°C for 5 to 25°C.

The effect of temperature on the performance of the cells is directly related to the effect of the conductivity. Since the net effect of temperature is to vary the conductivity

of the electrolyte according to Equation (5.1), cells whose *cell constant* is not affected by conductivity variations such as the grid electrodes will not be affected by temperature variations. This obviously requires the measurements of $\kappa_{l,g}$ and κ_l to be performed at the same temperature. Figure 5.5(b) presents the results obtained with the grid electrodes when a KCl solution ($\kappa_{25^\circ C}$=2.94 mS/cm) at 3°C was used.

Those cells whose performance is affected by the conductivity of the electrolyte, cells "A" and "E", for example, will also be affected by the temperature.

d).- Error propagation analysis

Analysis of error propagation in the estimation of gas holdup using Maxwell's model was performed for the case of the grid electrodes.

As already mentioned in the experimental part, in these experiments ten conductance measurements in the water-air dispersion and clear liquid were performed, the average of which were used in the computation of gas holdup. The relative standard deviation (or coefficient of variation) of the conductance samples varied from ~0.4% for the clear liquid to ~1.5% for the dispersions of relatively high gas content. Table 5.1 presents some values of the experiments conducted with a frother concentration of 5 ppm, liquid conductivity 2.93 mS/cm, and temperature 25°C.

Table 5.1 presents the gas holdup obtained from pressure, the average conductance of the dispersion and its standard deviation, the gas holdup estimated by using Maxwell's equation and the standard deviation (obtained by error propagation analysis), and finally, the 95% confidence interval.

Table 5.1   Experimental results and error propagation analysis for gas holdup experiments at 5 ppm frother concentration, 2.93 mS/cm liquid conductivity, and 25°C temperature.

Gas holdup from pressure, %	Conductance, mS	Standard deviation, mS	Gas holdup from conductivity, %	Standard deviation, %	95% confidence interval, %	
0 00	4 2681	0 0181	0 00	0 400	-0 8	0 8
4 84	3 9824	0 0214	4 51	0 445	3 62	5 40
10 08	3 6838	0 0321	9 51	0 612	8 28	10 73
16 13	3 3333	0 0403	15 70	0 776	14 14	17 25
20 40	3 0906	0 0425	20 20	0 843	18 52	21 89
24 11	2 8987	0 0382	23.90	0 786	22 33	25 47

To perform the error propagation analysis, the function of interest

$$\varepsilon_g = \frac{\overline{\kappa}_l - \overline{\kappa}_{l-g}}{\overline{\kappa}_l + 0.5 \, \overline{\kappa}_{l-g}} \times 100 \qquad (5.2)$$

needs to be linearized by expanding it in a (truncated) Taylor series

$$\varepsilon_g = \varepsilon_g(\overline{\kappa}_l, \overline{\kappa}_{l-g}) + \frac{\partial \varepsilon_g(\overline{\kappa}_l, \overline{\kappa}_{l-g})}{\partial \kappa_l} (\kappa_l - \overline{\kappa}_l) + \frac{\partial \varepsilon_g(\overline{\kappa}_l, \overline{\kappa}_{l-g})}{\partial \kappa_{l-g}} (\kappa_{l-g} - \overline{\kappa}_{l-g})$$

$$(5.3)$$

where $\overline{\kappa}_l$ and $\overline{\kappa}_{l-g}$ are the average conductance values.

Thus, the variance of ε_g is given by

$$S^2_{\varepsilon_g} - \left(\frac{\partial \varepsilon_g}{\partial \kappa_l}\right)^2 S^2_{\kappa_l} + \left(\frac{\partial \varepsilon_g}{\partial \kappa_{l-g}}\right)^2 S^2_{\kappa_{l-g}} \tag{5.4}$$

which gives

$$S^2_{\varepsilon_g} - \left(\frac{150\,\overline{\kappa}_{l-g}}{(\overline{\kappa}_l + 0.5\overline{\kappa}_{l-g})^2}\right)^2 S^2_{\kappa_l} + \left(\frac{-150\,\overline{\kappa}_l}{(\overline{\kappa}_l + 0.5\,\overline{\kappa}_{l-g})^2}\right)^2 S^2_{\kappa_{l-g}} \tag{5.4}$$

An example of the calculations involved is given for the fourth row in Table 5.1, (gas holdup from pressure 16.13%, etc.). The conductance in the clear liquid and its standard deviation, 4.2681 and 0.0181 mS, respectively, are also needed in the computation.

$$\left(\frac{\partial \varepsilon_g}{\partial \kappa_l}\right) - \frac{150 \times 3.3333}{(4.2681 + 0.5 \times 3.3333)^2} - 14.1958\ mS^{-1}$$

and

$$\left(\frac{\partial \varepsilon_g}{\partial \kappa_{l-g}}\right) - \frac{-150 \times 4.2681}{(4.2681 + 0.5 \times 3.3333)^2} - -18.1769 mS^{-1}$$

$$S^2_{\varepsilon_g} - 14.1958^2 \times 0.0181^2 + (-18.1769)^2 \times 0.0403^2 - 0.6026$$

and therefore,

$$S_{\varepsilon_g} - 0.7763$$

which gives a relative standard deviation of

$$C_{\epsilon_g} = \frac{S_{\epsilon_g}}{\overline{\epsilon}_g} \times 100 = \frac{0.7763}{15.76} \times 100 = 4.92 \ \%$$ (5.5)

and a 95 % confidence interval defined by

$$\overline{\epsilon}_g - 2 \ S_{\epsilon_g} \leq \mu_{\epsilon_g} \leq \overline{\epsilon}_g + 2 \ S_{\epsilon_g}$$ (5.6)

that is

$$14.15 \leq \mu_{\epsilon_g} \leq 17.25$$

where μ_ϵ is the mean of the population.

Figure 5.10 presents the results of the computations.

5.1.3 Solids holdup measurement

Preliminary conductance measurements performed in flotation pulps (Strathcona mill, Falconbridge Ltd.) showed that the effect of solids was to decrease the conductance of the aqueous phase even though a large percentage of highly conductive solids, chalcopyrite, for example, was present. These measurements were collected with a 4-electrode conductivity cell similar to that used in the portable level calibration probe (see Section 4.3.1(b)). The technique consisted in following the change in conductance of an initially well mixed slurry after switching off the mixer and allowing the suspended particles to settle, eventually leaving the conductivity cell immersed in clear liquid.
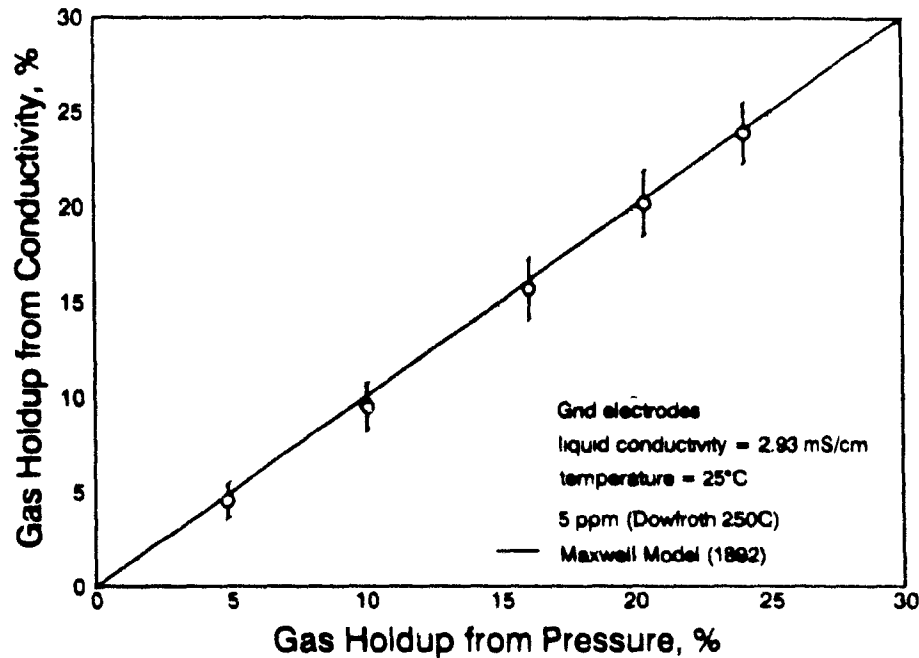
Figure 5.10 95% confidence interval of typical results obtained with the grid electrodes

Figure 5.11 presents these results.

Independent work conducted at Mount Isa Mines, Australia, encountered similar trends (Espinosa-Gomez, 1990). Figure 5.12 shows the variation of conductance with solid percentage in the LGM (low grade middlings of Pb and Zn sulphides) rougher concentrate fed to a flotation column circuit. Typical assays for this stream are 8% PbS, 32% ZnS, 34% pyrite + pyrrhotite, and 26% non-sulphide gangue (Espinosa-Gomez et al., 1989). Figure 5.12 includes the fitting of the Maxwell and Bruggeman models for an average solids density of 4 g/cm^3 (calculated by stoichiometry considering non-sulphide gangue as silica). The translation of the curves is simply due to a change in the conductivity of the aqueous medium from day to day.

It is evident from these results that conductive solids (sulphides, for example) in
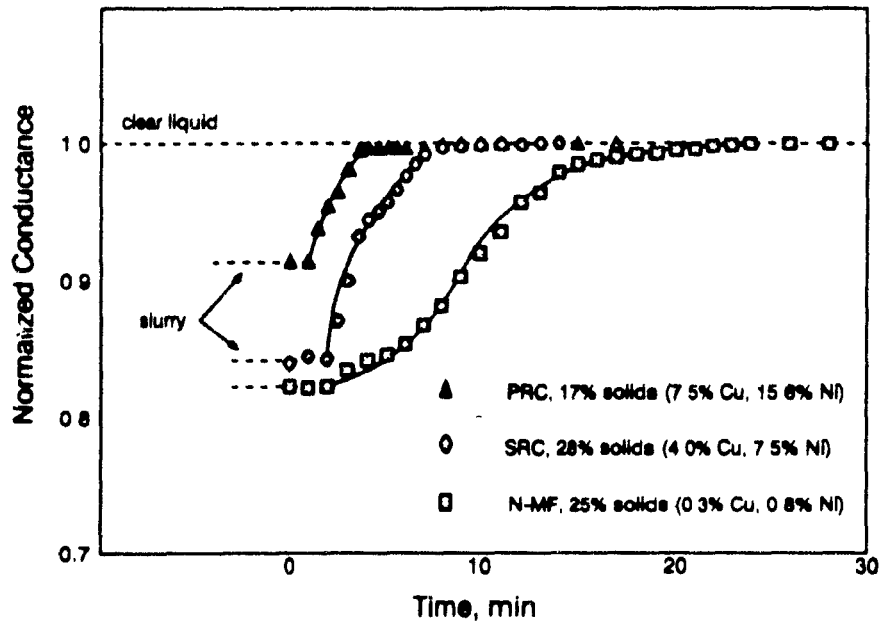
Figure 5.11 Preliminary results on the behaviour of typical flotation slurries (PRC, primary rougher concentrate; SRC, secondary rougher concentrate; N-MF, non-magnetic feed)
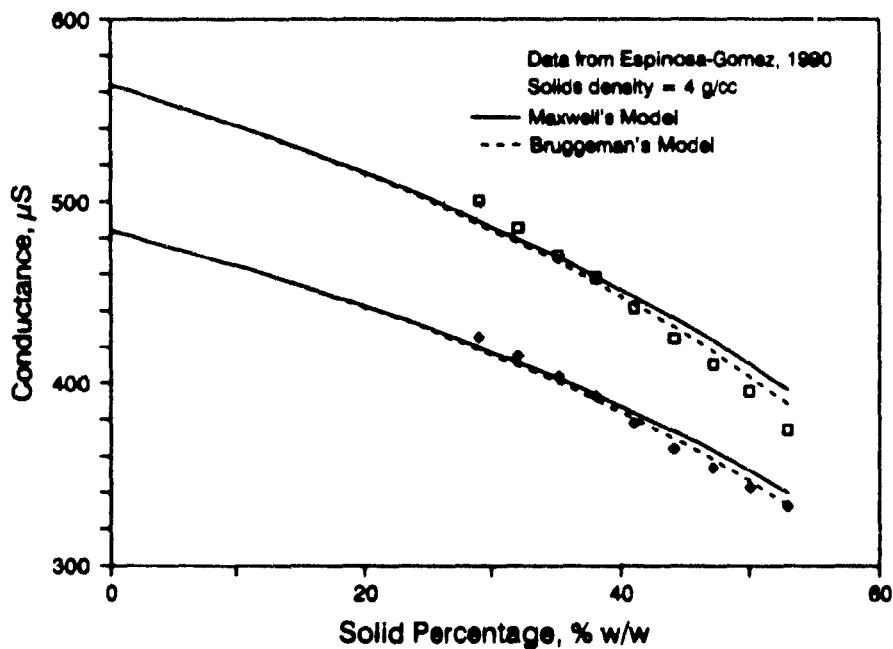
Figure 5.12 Conductance vs solid percentage for a Mt. Isa Mines Pb/Zn flotation slurry (after Espinosa-Gomez, 1990)
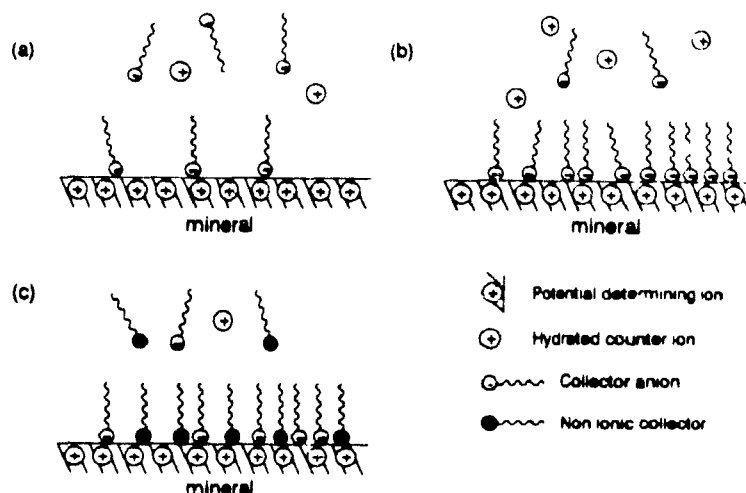
Figure 5.13 Schematic representation of the mineral-solution interface in the presence of an anionic collector (a) Single ion adsorption at low concentration (b) Hemi-micelle formation at higher concentrations. (c) Coadsorption of neutral molecules. (After Kelly and Spottiswood, 1982)

flotation pulps behave as a non conductive phase. This may be due to the nature of the mineral-solution interface that develops when the particles are slurried in aqueous solutions containing surface active organic compounds (Figure 5.13)(Kelly and Spottiswood, 1982; Fuerstenau et al., 1984). The presence of flotation collector reagents on the sulphide surface may prevent electron transfer across the solid-water interface. This proposed mechanism clearly needs further study. The preliminary finding, however does indicate that solids holdup can be estimated from conductivity using an approach similar to that developed here for gas holdup.

An experimental program was designed to investigate measuring solids holdup by this approach in more detail. The experiments consisted of measuring the conductance in a well mixed slurry followed by the measurement of the conductance in the clear liquid, after the solids had settled. The experimental apparatus is shown in Figure 5 14. It consisted of a 5.7 cm diam. × 38 cm length Plexiglas cylinder having a PVC piston at both ends. One of the pistons was fixed while the other was removable. Two grid
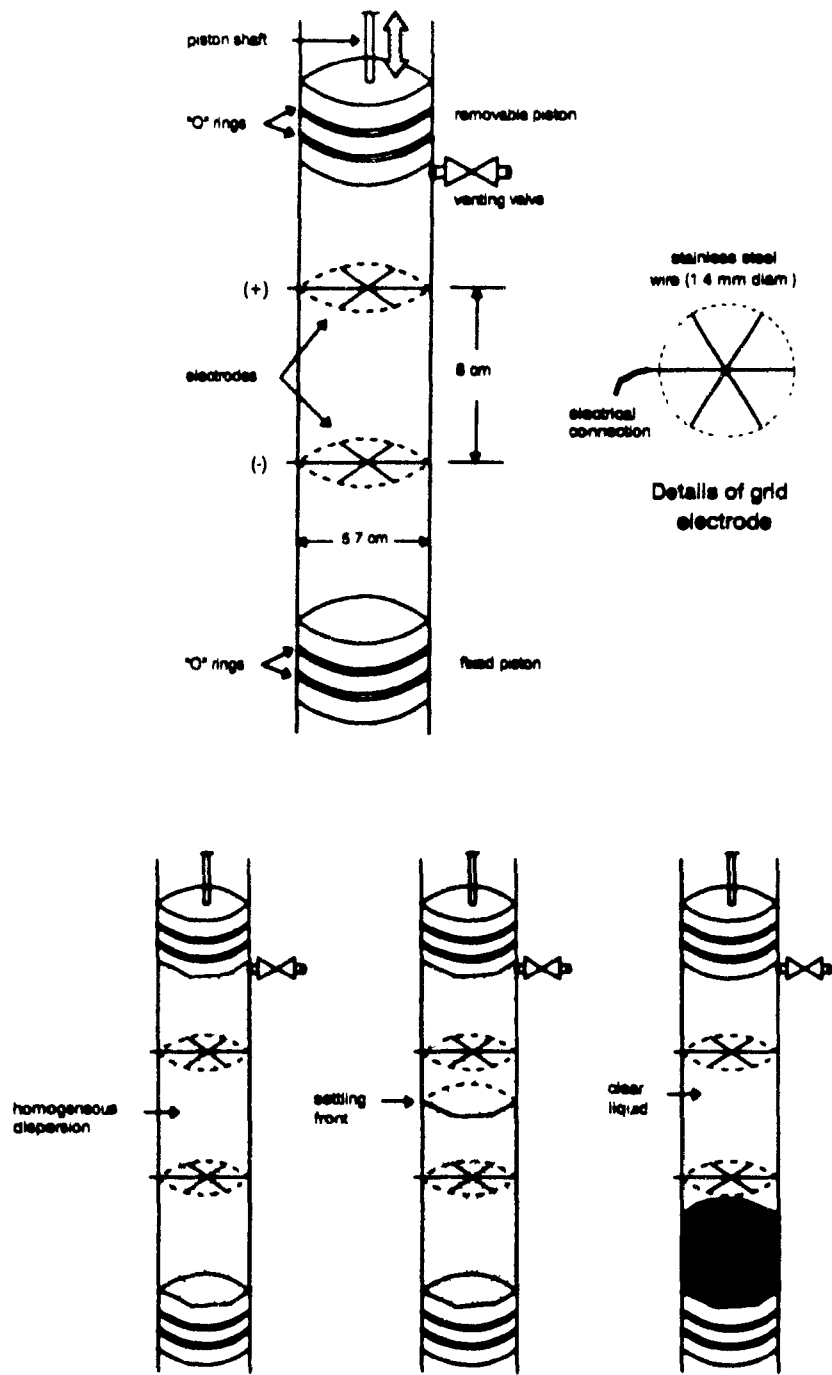
Figure 5.14 Experimental apparatus used in the sedimentation experiments and illustration of the stages of the sedimentation process

electrodes separated by 8 cm are located in the middle section of the cylinder (thus having a cell constant ~ 3.19 cm^2/cm). A venting valve was used to remove the gas trapped in the chamber after the cylinder was closed was available.

The experimental procedure consisted in feeding ~ 700 cm^3 of slurry of known solid percentage to the cylinder which was then closed by sliding in the removable piston. The air trapped in the cylindrical chamber was removed through the venting valve. The grid electrodes were connected to a conductivity meter (Tacussel Mod. CD 810) and the analog output of the meter was fed to a channel of an A/D board (DAS-8PGA) in an IBM compatible computer. The slurry inside the tube was mixed by subjecting the tube to a rhythmic rotation (this technique was used in sedimentation studies by Richardson and Zaki (1954) and in sedimentation-conductivity studies by Nasr-El-Din et al. (1987)). After a homogeneous dispersion had been obtained, as judged from the fairly constant conductance value being measured, the recording of conductance was started. After enough data were collected (around 60 measurements) to define the conductance of the slurry, the cylinder was stood vertically to allow the solid particles to settle eventually leaving the conductivity cell immersed in the clear liquid only, as illustrated in Figure 5.14.

Experiments were conducted with water-silica slurries and flotation slurries.

a).-   Water-silica slurries

In these experiments, measured amounts of silica sand (94.3% -208 μm, $\rho = 2.6$ g/cm^3) were mixed with known volumes of water (~ 500 cm^3). Volume percentages of solids ranging from 4% (9.74 % w/w) to 20% (39.4% w/w) were tested. Two different conductivities of the water were used: 0.27 to 0.29 mS/cm (tap water) and ~ 2.6 mS/cm (by adding KCl). Figures 5.15 to 5.17 present the results.
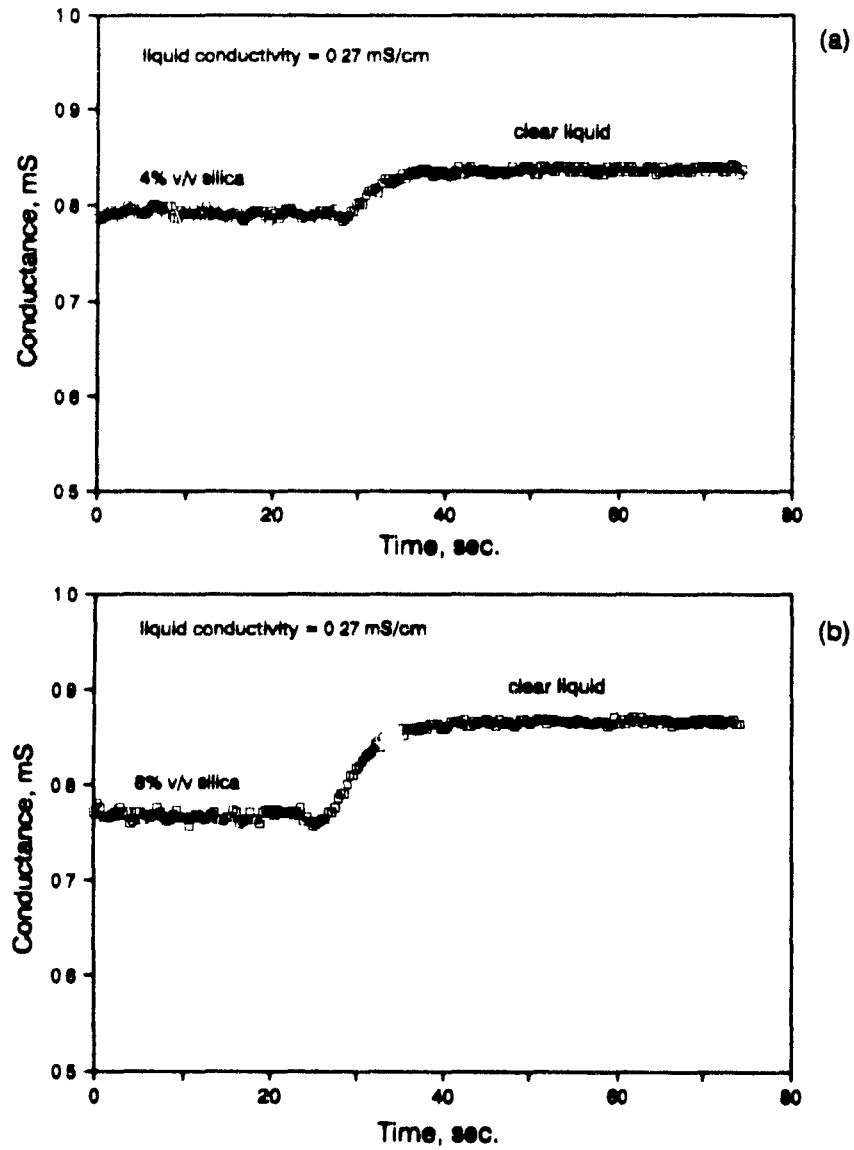
Figure 5.15 Settling experiments results: (a) 4% v/v silica, and (b) 8% v/v silica
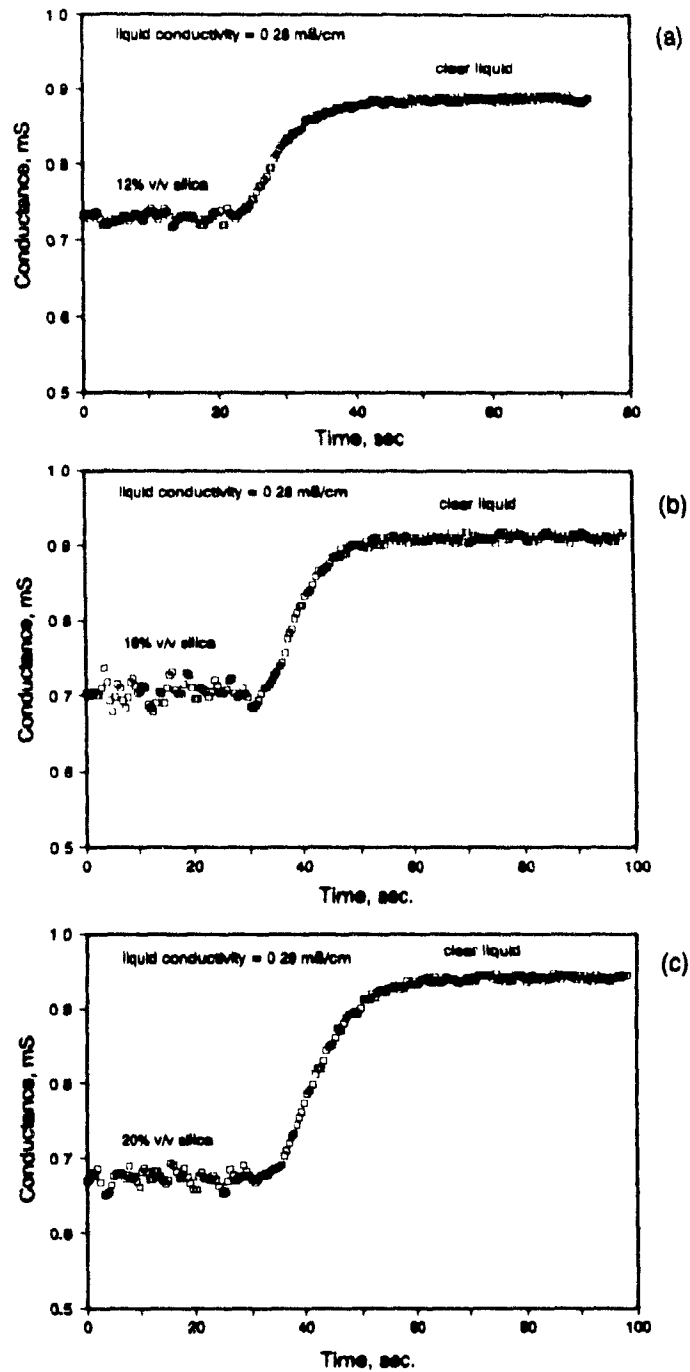
Figure 5.16   Settling experiments results: (a) 12% v/v silica, (b) 16% v/v silica, and (c) 20% v/v silica. Liquid conductivity around 0.28 mS/cm
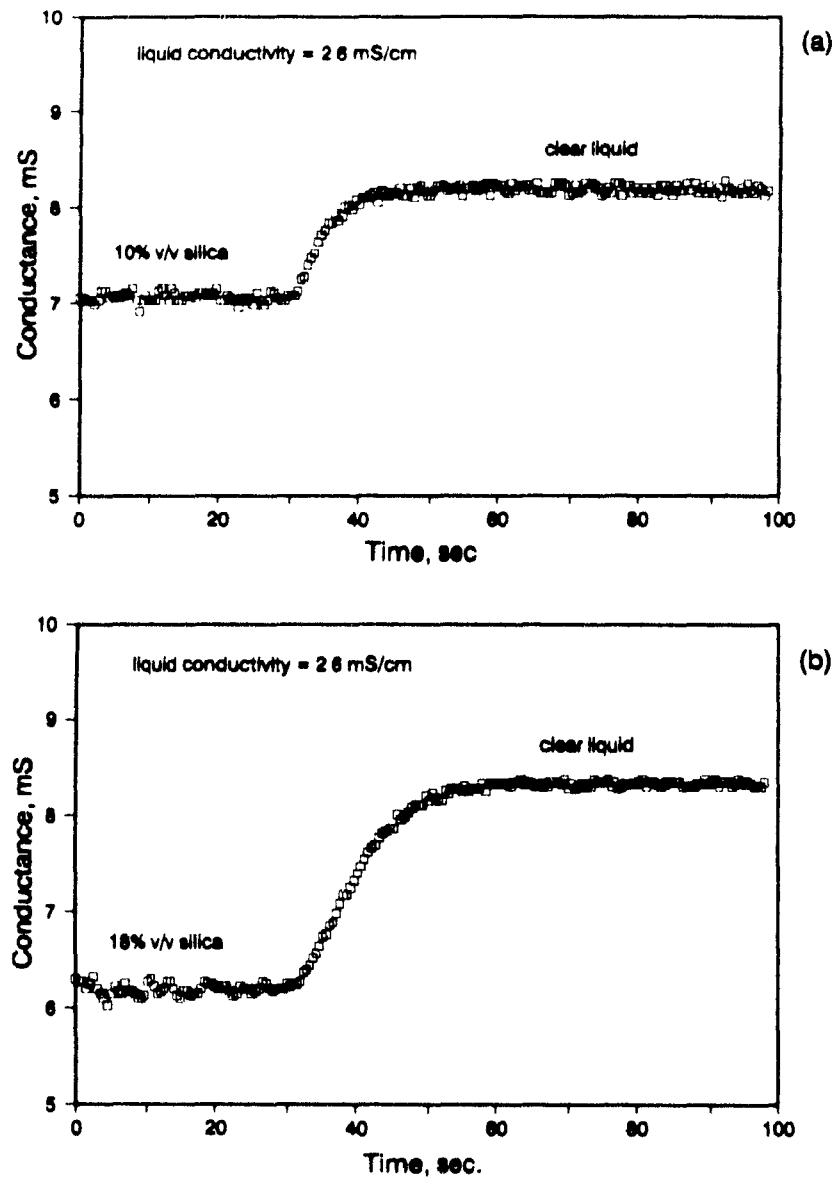
Figure 5.17 Settling experiments results: (a) 10% v/v silica, and (b) 18% v/v silica. Liquid conductivity 2.6 mS/cm
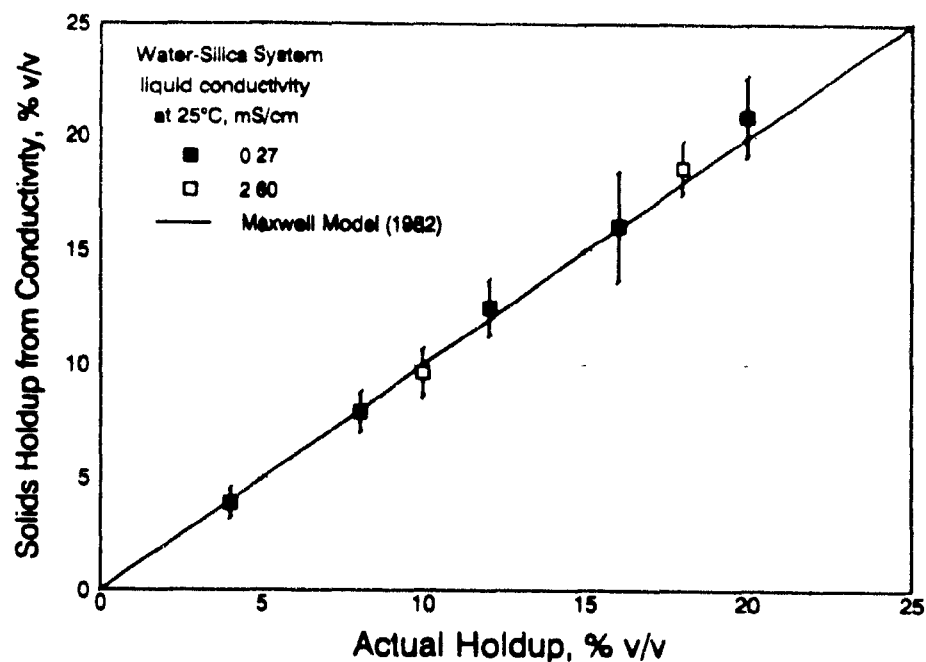
Figure 5.18   Estimation of non-conductive solids holdup using electrical conductivity and Maxwell's model

It is noticed in Figures 5.15 to 5.17 that the average conductance of the slurry and clear liquid is readily obtainable. With these two numbers Maxwell's equation was used to estimate the solids holdup. Figure 5.18 presents the results of the estimations showing that Maxwell's model fitted the experimental data fairly well. Figure 5.18 also presents the 95% confidence interval for the measurements. These statistical parameters, presented in Table 5.2, come from an analysis of error propagation similar to that performed before for the gas holdup estimates.

Table 5.2   Experimental results and error propagation analysis for the water-silica sedimentation experiments.

Solids holdup, % v/v	$K_{1.s}$, mS/ Standard deviation, mS	K_1, mS/ Standard deviation, mS	Solids from conductance, %/ Standard deviation, %	95 % confidence interval, %
4 00	0 7890/0 0031	0 8370/0 0027	3 88/0 3320	3 22 to 4 54
8 00	0 7680/0 0050	0 8670/0 0020	7 91/0 4408	7 03 to 8 79
10 0C	7 0630/0 0470	8 1950/0 0400	9 65/0 5211	8 61 to 10 69
12 00	0 7310/0 0070	0 8880/0 0020	12 49/0 6096	11 27 to 13 71
16 00	0 7080/0 0137	0 9120/0 0039	16 07/1 1975	13 67 to 18 47
18 00	6 1980/0 0570	8 3290/0 0262	18 65/0 5763	17 50 to 19 80
20 00	0 6740/0 0100	0 9420/0 0028	20 93/0 8809	19 17 to 22 69

b).-   Mineral slurries

Preliminary laboratory experiments showed that a slurry of highly conductive solids did have a higher conductivity than that of the clear liquid. Figure 5.19 shows the effect of the presence of highly conductive solids (Zn particles, -850 μm) and the effect of the frequency of the ac excitation voltage. As already mentioned, the frequency becomes important as the conductivity of the solids increases (Meredith and Tobias, 1960 and 1961). The results suggest that high frequencies should be used when dealing with slurries of conductive solids. According to this, the highest frequency available in the Tacussel meter (16 kHz) was used in the experiments with mineral slurries.

Figure 5.20 presents the settling curve of a freshly ground pyrite ore ($\sim$62% pyrite; 25% +75 μm, 49% -38 μm; no flotation reagents added). The curve suggests, and visual observation tended to corroborate that the particle size may play a role in the behaviour observed. It was experimentally observed that the relatively large mineral particles originally present in the well mixed slurry, settled faster moving out of the conductivity cell. This phenomenon may correspond to the decrease in conductivity of
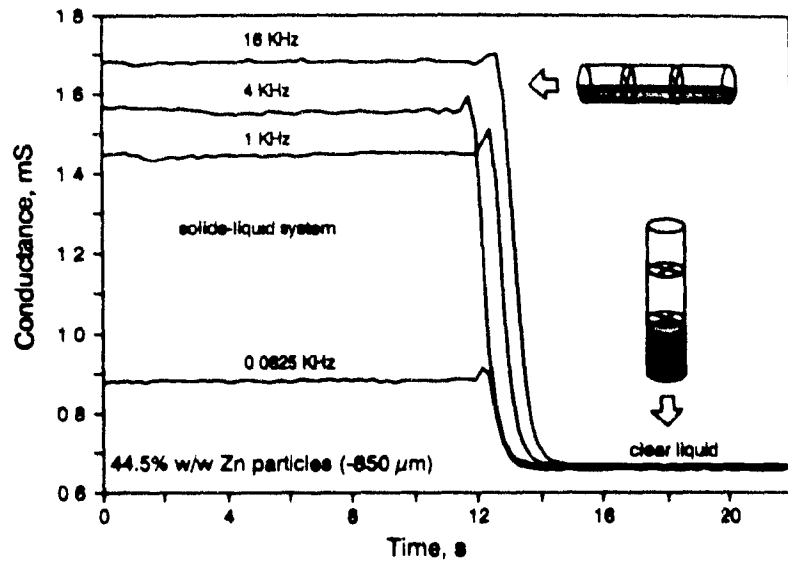
Figure 5.19 Effect of conductive solids (zinc particles) on the conductivity of a liquid-solid system. The effect of the frequency is also shown
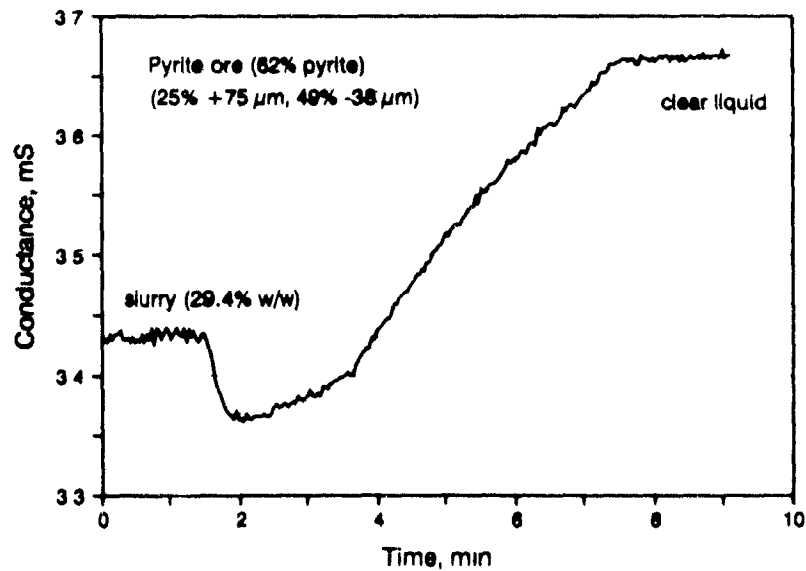
Figure 5.20 Settling curve for a pyrite ore (freshly ground, no reagents)

the slurry observed in the first moments after the cylinder was stood vertically. The smaller size classes having a slower settling velocity, may be responsible for the following gradual increase in conductivity. This may suggest that larger particles behave as conductive solids while smaller particles behave as non conductive ones. This is probably related to the size itself, or with a gradient of grade among the size classes.

The experiments with mineral slurries were conducted at the Strathcona mill, Falconbridge Ltd. The objective of the experiments was to investigate the suitability of the conductivity technique to measure holdup of conductive solids present in flotation slurries. To accomplish this, slurry samples of the concentrate of the copper circuit assaying ~32% Cu (mainly present as chalcopyrite; 22% +75 μm, 46% -38 μm) and of the combined Cu-Ni concentrate (4.9% Cu, 7.5% Ni; 19% +75 μm, 61% -38 μm)) were used. To vary the solid percentage (thus, the volume fraction), the samples were diluted (using the water obtained by filtration of additional samples), or a fraction of the water was decanted. After filling the cylinder with the sample, enough time was allowed for the sample to attain thermal equilibrium with the room temperature. For each sample, the sedimentation process was repeated until it was determined that the temperature variation during the sedimentation process was negligible. The sample was then collected and the solid percentage was measured. Volume percentages of solids ranging from 3.51% (12.97% w/w) to 18.60% (48.37% w/w) were tested. The density of the solids was measured making use of a Null Pycnometer (Mod. Quantachrome). The density of both samples was ~4.1 g/cm^3. Figures 5.21 to 5.23 present the sedimentation curves and Table 5.3 presents the results obtained as well as the error propagation analysis performed.

Figure 5.24 presents the results of the estimations showing that Maxwell's model fitted the experimental data reasonably well. The plot also presents the 95% confidence interval for the measurements.
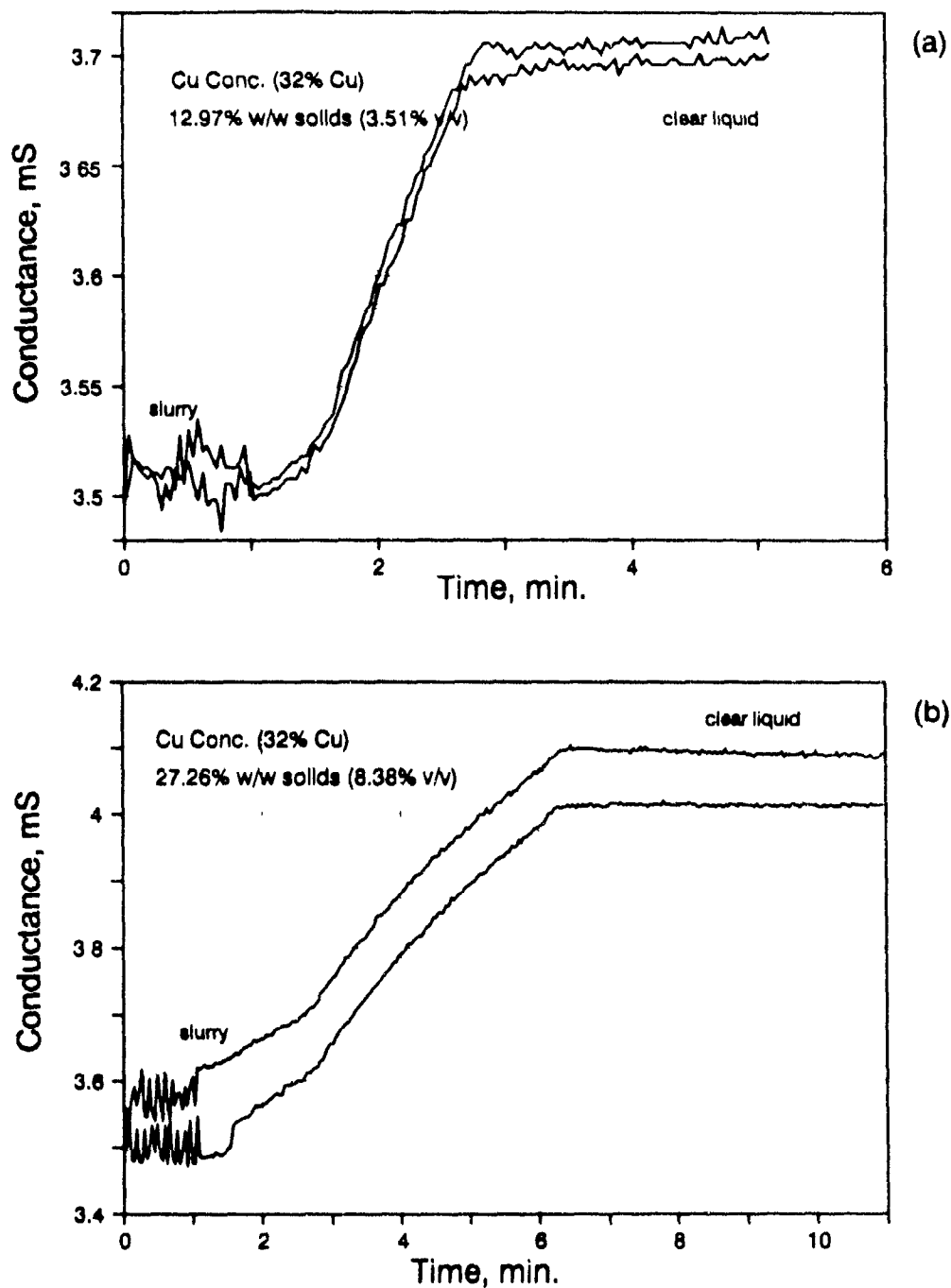
Figure 5.21   Settling curves for a mineral slurry: (a) 12.97% w/w, and (b) 27 26% w/w
solids (32% Cu). (Note that the two curves in each graph are repeats)
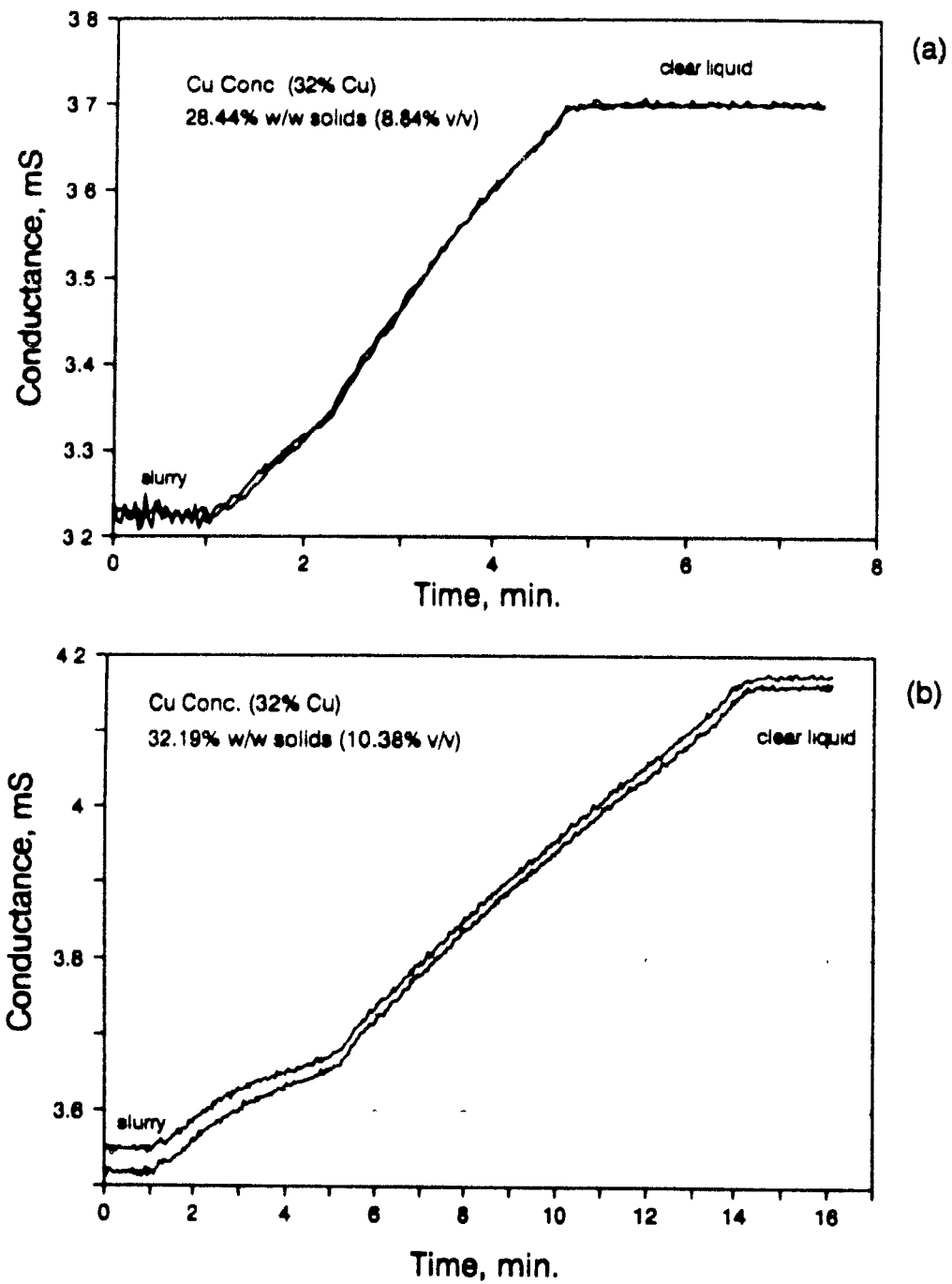
Figure 5.22 Settling curves for a mineral slurry: (a) 28.44% w/w, and (b) 32.19% w/w solids (32% Cu). (Note that the two curves in each graph are repeats)
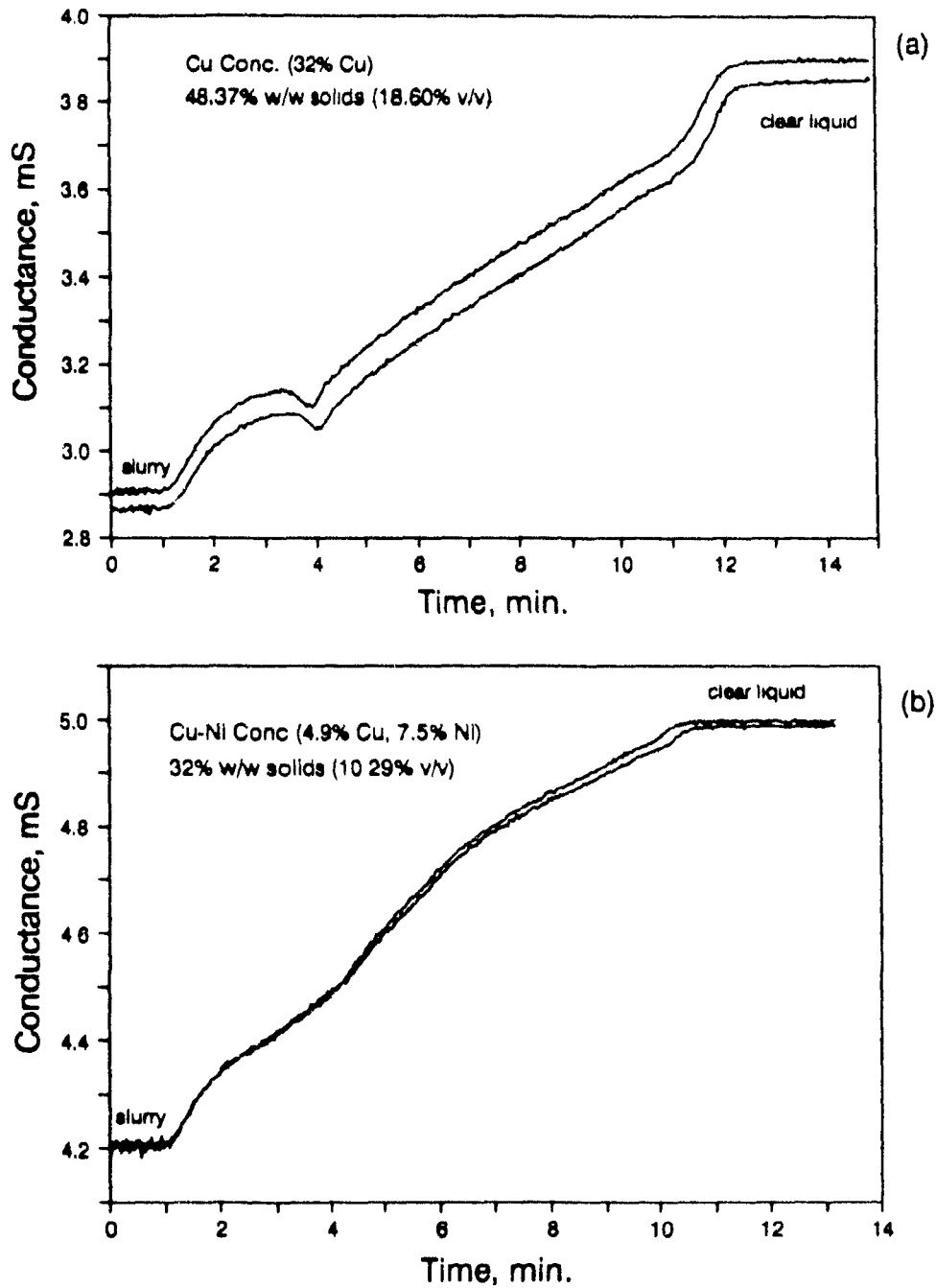
Figure 5.23 Settling curves for a mineral slurry· (a) 48 37% w/w solids (32% Cu), and (b) 32% w/w solids (4.9% Cu, 7.5% Ni). (Note that the two curves in each graph are repeats)
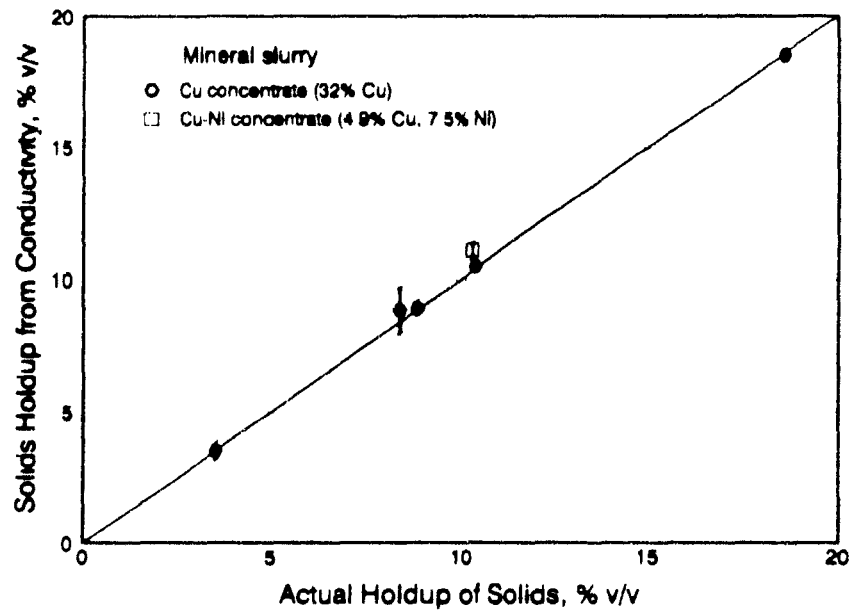
Figure 5.24 Estimation of holdup of solids (sulphides in flotation pulps) using
conductivity and Maxwell's model

Table 5.3 Experimental results and error propagation analysis for the mineral
slurry sedimentation experiments.

Solids holdup, % v/v	$K_{l,s}$, mS/ Standard deviation, mS	K_l, mS/ Standard deviation, mS	Solids from conductance, %/ Standard deviation, %	95% confidence interval, %
3 51	3 5050/0 0077	3 6964/0 0028	3 51/0 1521	3 21 to 3 82
8 38	3 5727/0 0237	4 0925/0 0036	8 84/0 4246	7 99 to 9 69
8 84	3 2279/0 0053	3 7013/0 0023	8 91/0 1114	8 68 to 9 13
10 29	4 2025/0 0092	4 9872/0 0019	11 07/0 1390	10 79 to 11 35
10 38	3 5498/0 0023	4 1739/0 0022	10 49/0 0525	10 39 to 10 60
18 60	2 9079/0 0051	3 8991/0 0027	18 52/0 1119	18 29 to 18 74

The sedimentation curves in Figures 5.21 to Figure 5.23 are in contrast to the
behaviour observed with the freshly ground pyrite (Figure 5.20), supporting the

preliminary results that sulphide particles exposed to flotation reagents behave as non conductive solids.

5.1.4 Gas holdup in a silica slurry-air system

The determination of gas holdup in three phase systems using electrical conductivity was experimentally addressed in a water-air-silica laboratory column For this, an independent technique to measure the actual holdup of gas and solids in the section of the column where the conductivity measurements are performed, was developed. The technique, called "isolating technique" here, has been reported in the literature (Jepsen and Ralph, 1969-70; Flint, 1974; Watson and Grainger-Allen, 1974) and it consists in cutting (instantaneously) a section of the three phase system to trap the phases present in the section.

Figure 5.25 presents the experimental set up used which consisted of a 3.8 cm diam. x 246 cm height Plexiglas column having two ball valves (3.81 cm internal diam . Withley mod. MS-135-SR) enclosing the section where the conductivity was measured The dimensions of the ball of the valves was such that, when open, the internal diameter of the ball equalled that of the column, thus ensuring negligible disturbance of the hydrodynamics of the system The valves were air actuated having a response time of around ~ 150 ms when a pressure of 690 kPa (100 psi) was used. The valves were connected to a compressed air cylinder via a solenoid valve (ASCO) which released the pressure of the cylinder in 5 to 10 ms closing both valves at the same time Facility was available to open one of the valves while keeping the other closed and vice versa.

Two conductivity cells were used; one located between the valves (conductivity cell 1: cell constant 0.49 cm^2/cm), and the other located below the sparger (conductivity cell 2: cell constant 1 cm^2/cm) where air bubbles are not present. The idea behind this arrangement was to attempt on-line measurement of gas holdup. To accomplish this using
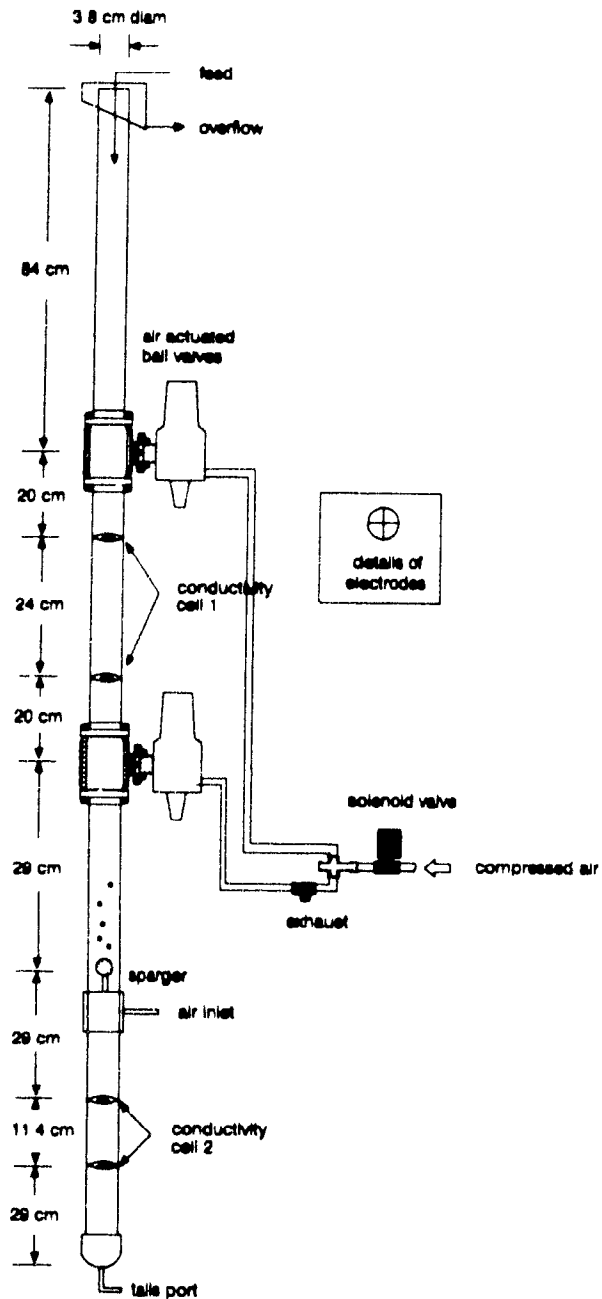
Figure 5.25   Experimental set up for the preliminary study on the determination of holdup in three phase systems (not to scale)

the models, two conductivity measurements are required: one of the liquid-solids-gas system and one of the liquid-solids system. By using the arrangement shown in Figure 5.25, it was assumed that the concentration of solids was uniform along the column. For the purpose of this preliminary work and because of the lack of a better alternative to perform the measurement, such an assumption was deemed reasonable

The experimental technique consisted in slurring a sample of silica powder (100% -75 μm/+38 μm) in tap water (κ ~0 3 mS/cm) containing 25 ppm frother (Dowfroth 250C) to obtain a slurry of ~32% w/w silica. A baffled pail and a conventional stirrer were used to keep the silica in suspension. The slurry was fed to the column close to the top, discharged by gravity through the tailings port and recycled to the pail Overflow was avoided, as far as possible, to ensure that all the solids being fed would, eventually, leave through the tails port and therefore, would necessarily pass through the measuring section and conductivity cells

The experiments were started by filling the column with the liquid only and measuring its conductivity (this was done by allowing the solids to settle leaving a layer of clear liquid). The column was emptied and the stirring started; the slurry was then fed to the column and the tailings flow controlled to achieve correct balance of flows The column was operated with slurry only for around 10 minutes (~4 liquid residence times) The conductivity of the water-silica slurry was then measured and recorded Values of clear liquid and slurry conductivities obtained with the two conductivity cells were in good agreement. A gas flowrate was established and 10 minutes were allowed to achieve steady operation as judged by the stability of the conductivity of the three phase system. The conductivity of the water-silica-air and water-silica systems was measured using cell 1 and cell 2, respectively. Immediately after the last conductivity measurement, the solenoid valve was activated and the ball valves closed trapping a sample of the three phase system. The gas holdup was obtained by measuring the empty volume in the measuring section (after all the air bubbles had disengaged) and dividing it by the total
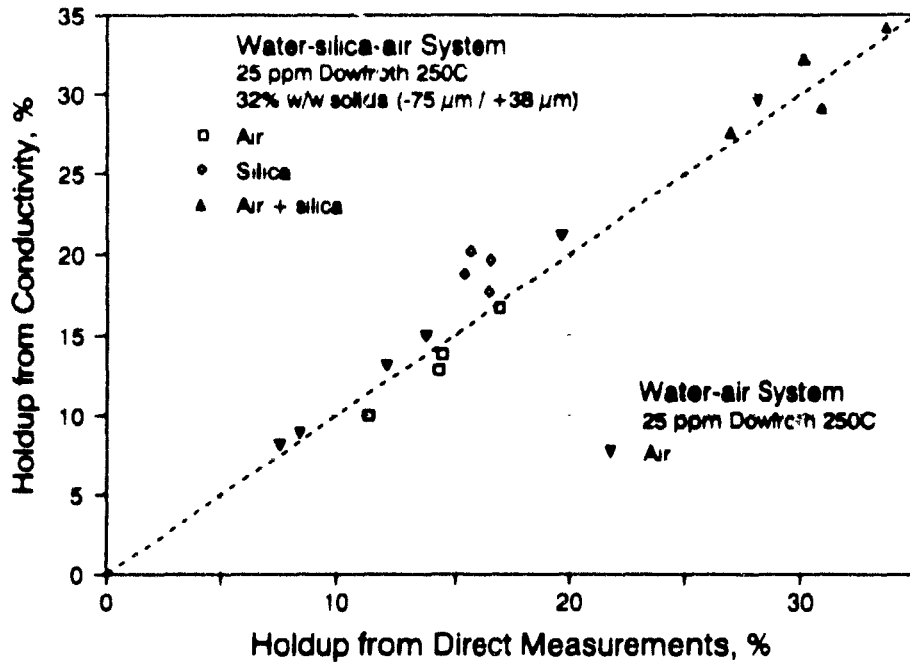
Figure 5.26 Holdup estimated by direct measurements against that obtained from conductivity using Maxwell's model

volume of the section (700 cm³). The remaining liquid-solid sample was collected, after the bottom section of the column was emptied, by opening the bottom ball valve and allowing the sample to leave through the tailings port. The volume and weight of the sample was measured and recorded, and laboratory analysis to determine solids percentage and solids density was performed. The above procedure was repeated for four different gas rates. Table 5.4 presents the results obtained and Figure 5.26 presents the holdup of the phases obtained by direct measurements against those obtained from conductivity using Maxwell's model. For comparison purposes, Figure 5.26 also presents gas holdup values obtained in a water-air system.

Table 5.4   Experimental results on the determination of holdup in three phase systems.

κ, mS/cm			ε, % calculated			ε, % Experimental		
κ_l	$\kappa_{l\cdot}$	$\kappa_{l\cdot g}$	ε_l	$\varepsilon_\cdot$	$\varepsilon_{l\cdot\cdot}$	ε_l	$\varepsilon_\cdot$	$\varepsilon_{l\cdot\cdot}$
0.2888	0.2113	0 1622	16.79	19 65	34 23	17 01	16 60	33 61
0.2891	0.2186	0 1787	12 96	17 70	29 17	14 30	16 56	30 86
0 3027	0 2196	0 1768	13 90	20 15	32 19	14 46	15 66	30 12
0 3024	0 2249	0 1925	10 09	18 68	27 57	11 43	15 38	26 81

κ_l and $\kappa_{l\cdot g}$ w\ e obtained with cell 1, $\kappa_{l\cdot}$ was obtained with cell 2
Relative standard deviations $x_l \sim 0$ 10%, $\kappa_{l\cdot} \sim 0.20\%$, and $\kappa_{l\cdot g} \sim 0$ 25%

Figure 5 26 shows that good holdup estimations were possible. The results do suggest that the holdup of the phases is additive.

Deviations from Maxwell's model are probably related to two factors (a) the source of error that arises form the assumption that the holdup of solids in the column (in the presence and absence of air) is uniform. More work is required to clarify this point, probably by simultaneously sampling different locations along the vertical axis of the column; and (b) the fact that Maxwell's model is better suited for uniformly sized particles (bubbles or solids) whereas the present system involves quite different sizes. Also, the experimental errors involved in the measurements, mainly those related with the collection and managing of the sample, have to be taken into account.

5.2   Industrial Scale Columns

5.2.1   Preliminary work

Gas holdup estimation in a two phase (water-air) industrial scale column (91 cm diam.) was attempted making use of the level detection probe described in Section 4.3.1(d).

The calculation of holdup of the dispersed phase using Maxwell's equation requires the effective conductivity of the dispersion and the conductivity of the phases involved, all measured under the same conditions. These measurements can be easily accomplished in the laboratory but they are difficult to perform in large industrial columns. However, the probe developed to detect the froth/slurry interface was found to produce fairly good estimates of gas holdup.

To test the accuracy of gas holdup determination using the probe two experimental programs were designed: (i) to compare gas holdup from pressure readings and conductance measurements in an air-water system; and (ii) to test the limitations imposed by the probe geometry.

a).-   Experimental approach

The experiments were performed in the pilot column installed at the Strathcona Mill, Falconbridge Limited (Sudbury, Ontario). The column is approximately 1350 cm high and has a diameter of 91 cm. It is equipped with three Taylor pressure transducers (model 532TB04112A) and three water manometers (Huls et al., 1990)(Figure 5.27). Table 5.5 summarizes the location of the six pressure sensing devices, their range, and the output obtained when the column was filled with still water. Excellent agreement between the depths calculated from their respective outputs and their measured locations
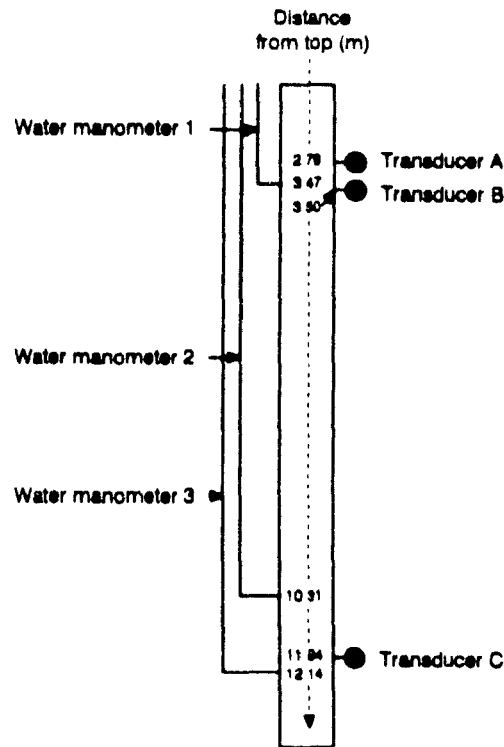
Figure 5.27   Pressure sensing devices in the 91 cm diam. column at the Strathcona mill, Falconbridge Ltd.

was shown.

Table 5.5   Characteristics of pressure sensing devices installed in the 91 cm diam. column at the Strathcona mill, Falconbridge Ltd.

Device	Distance from top, m	Range, kPa (m water)	Output when column filled with water, mA (m water)	Calculated depth, m
Transducer A	2 79	68 97 (—)	10 367 (—)	2 80
Water manometer 1	3 47	— (5 36)	— (3 47)	--
Transducer B	3 50	47 59 (—)	15 593 (—)	3 50
Water manometer 2	10 31	— (12 22)	— (10 31)	--
Transducer C	11 94	206 9 (—)	13 070 (—)	11 95
Water manometer 3	12.14	— (14 03)	— (12 14)	--

b).- Experimental procedure

After the column was filled with water containing frother (process water of conductivity ~ 1.3 mS/cm), an air flowrate was established through the column. No tailings flow was used but a small amount of wash water or feed flow was added to compensate for the water carried away by the air bubbles thus keeping the column always filled. After about 30 minutes, the outputs of the six pressure sensing devices installed along the column were recorded while conductance measurements were automatically collected once every second for a full minute using the level detection probe.

The gas holdup was calculated from pressure readings at three different locations along the column: at the top of the column from the output of pressure transducer B, at the middle using the readings of water manometers 1 and 2, and at the bottom using the readings of water manometers 2 and 3. An average value for the column was calculated from the output of pressure transducer C. The results of all these calculations for the different runs (Table 5.6) show a consistent gas holdup increase of about 100% from bottom to top. (Further exploration of this phenomenon has been carried out (Uribe-Salas et al., 1991)).

Table 5.6   Gas holdup calculated from pressure readings of pressure sensing devices

Run	Air Rate (cm/s)	Pressure, m of water						Gas Holdup, %			
		PTA	WM1	PTB	WM2	PTC	WM3	Top	Middle	Bottom	Average
1	—	2 80	3 47	3 50	10 31	11 96	12 14	--	--	--	--
2	0 72	2 66	3 30	3 32	9 93	11 53	11 72	4 92	3 11	2 08	3 56
3	0 93	2 61	3 26	3 26	9 79	11 39	11 57	6 67	4 64	2 78	4 77
4	1 22	2 58	3 17	3 21	9 61	11.24	11 37	8 22	5 84	4 17	5 97
5	1 51	2 50	3 09	3 10	9 40	10 97	11 12	11 32	7 79	5 90	8 21
6	--	2 72	3 46	3 49	10 31	11 95	12 14	--	--	--	--
7	2 59	2 01	2 54	2 56	8 17	9 58	9 74	26 82	17 81	13 89	19 84
8	2 23	2 18	2 74	2 77	8 61	10 13	10 25	20 89	14 29	10 42	15 27
9	1 67	2 17	3 01	3 05	9 26	10 82	10 96	12.80	8 72	6.94	9 50

WM = water manometer, PT = pressure transducer

c).- Results

The calculation of gas holdup from conductance measurements has been summarized in Table 5.7, which includes the average conductance (K) measured in the different runs by using the deepest active ring in the probe (1.25 m from top) and the values of gas holdup calculated using Maxwell's equation. Conductance values of runs 1 and 6 were used as K_i for runs 2 to 5 and for runs 7 to 9, respectively.

Table 5.7   Experimental results and error propagation analysis for the estimations of gas holdup in the 91 cm diam. (water-air) column.

Run	Air rate, cm/s	Average conductance, mS/Standard deviation, mS	Estimated gas holdup, %/Standard deviation, %	95% confidence interval, %
1	0 00	13 462/0 0140	—	
2	0 72	12 531/0 0733	4 72/0 39	3 95 to 5 49
3	0 93	12 233/0 0653	6 28/0 35	5 58 to 6 98
4	1 22	11 945/0 0575	7 81/0 31	7 18 to 8 43
5	1 51	11 407/0 0651	10 72/0 36	9 99 to 11 45
6	0 00	13 305/0 0123	—	
7	2 59	8 842/0 0878	25 18/0 56	24 06 to 26 30
8	2 23	9 571/0 0964	20 64/0 59	19 46 to 21 82
9	1 67	10 800/ 0622	13 39/0 36	12 67 to 14 11

A comparison between the gas holdup calculated from pressure measurements at B (i.e. at the top) and that from conductivity shows good agreement (Figure 5.28). The gas holdup from conductivity corresponds to that at 1.25 m while the value from pressure transducer B, corresponds to an average of the top 3.5 m of the column. The results clearly show that the location of the measurement is an important consideration in making the comparison. The agreement between techniques suggests that, under the experimental
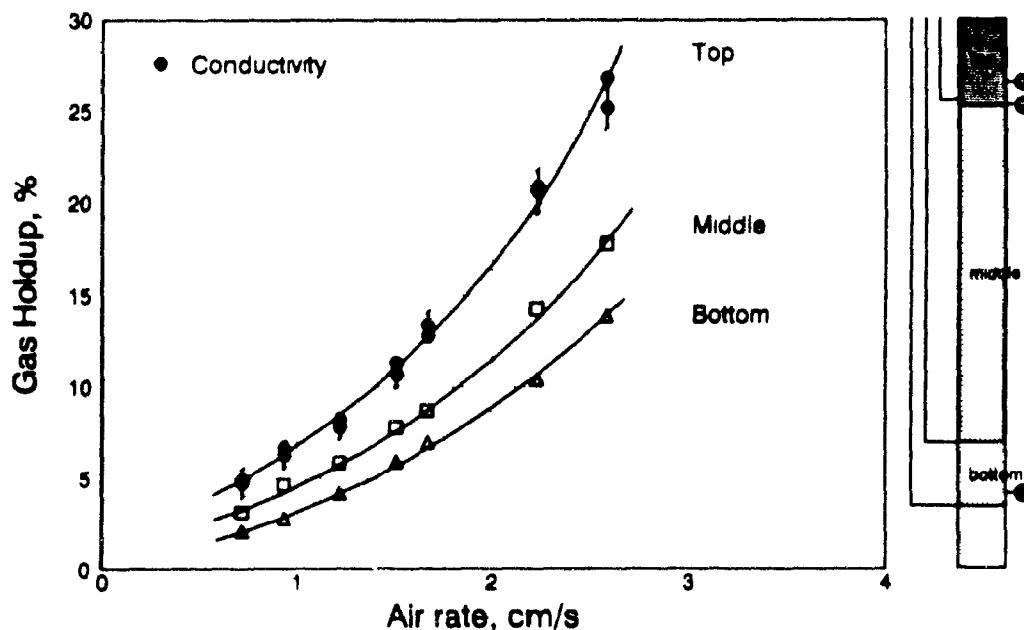
Figure 5.28 Comparison of gas holdup determination using the pressure sensing devices and the conductivity probe. 91 cm diam. column; water-air system The 95% confidence interval for gas holdup estimations from conductivity is also shown

conditions imposed. the electrode configuration of the level detection probe appears to be an appropriate geometry to measure gas holdup continuously. This geometrical consideration is discussed below.

d).- Cell constant of the probe

According to Maxwell's equation, the ratio of conductivity with and without the dispersed phase (air in this case) is needed. Estimating the conductivity from conductance measurements requires a knowledge of the cell constant. The ratio of conductances, however, can be substituted provided the cell constant remains relatively fixed over the range of conductivity values encountered. This is not always the case, depending on cell geometry.

One way of analyzing the magnitude of the problem is by experimental means. The apparent cell constant of a specific cell geometry is given by the ratio conductance (mS) over conductivity (mS/cm), (K/κ).

Experimental procedure and results

By performing conductance measurements in solutions of known conductivity, the behaviour of a particular cell geometry can be evaluated. The experiments were conducted in a 91 cm diam. × 100 cm height PVC tank. The probe was located in the center of the tank as depicted in Figure 5.29. The tank was filled with a solution of known conductivity and the conductance of the solution measured with the positive electrode positioned halfway between the surface of the solution and the bottom of the tank. The conductivity of the solution was varied by adding KCl, and measured by using a calibrated conductivity meter (Hanna Instruments HI 8633). Figure 5.29 presents the results obtained. For comparison purposes, the cell constant of a conductivity cell close to the ideal case (section of two infinite and parallel plates) is also included.

The apparent change in the cell constant of the probe's cell with conductivity shown in Figure 5.29 was similar to that observed for Cell "E" (discussed in the Section 5.1.2). Such a behaviour was interpreted in terms of polarization (Davies, 1930), or as unresolved components of the conductivity measurements (William, 1990). The successful determination of gas holdup using the level detection probe (successful by comparison with gas holdup from pressure readings) can be interpreted with the help of Figure 5.29, and comparison with performance of Cell "E" (See Figures 5.4 and 5.8). Typical gas holdup values, for example <20%, translate into changes in apparent conductivity of <27% between the system with and without gas. In other words, given a typical value of the liquid conductivity of 1.3 mS/cm (Strathcona process water), 20% gas holdup translates into an apparent conductivity of 0.95 mS/cm. It is shown in Figure 5.29 that such a variation in conductivity falls in the "upper" part of the Cell constant
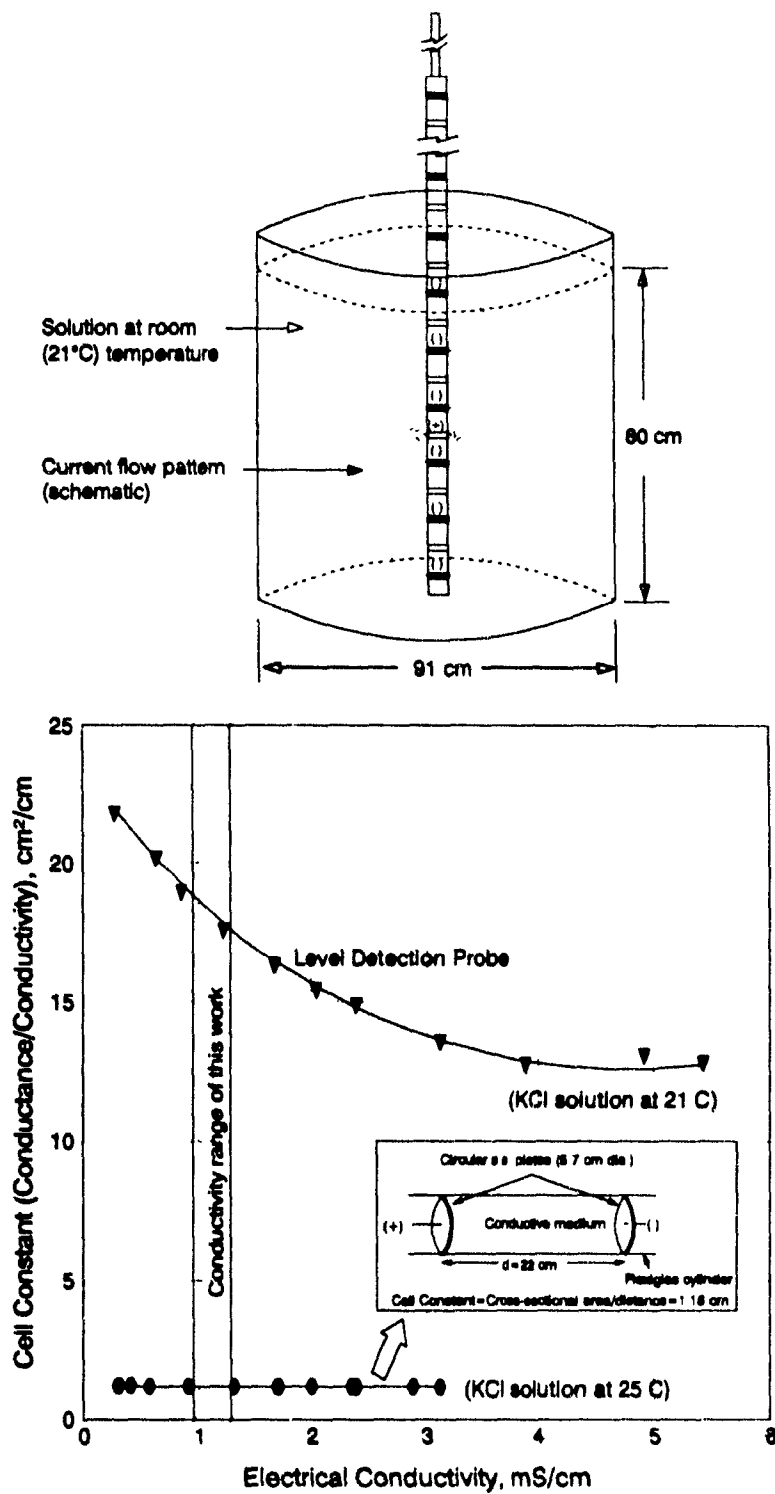
Figure 5.29   Experimental set up for experiments on the cell constant of the level detection probe and behaviour of the conductivity cell of the probe as a function of the conductivity of the medium (KCl solution)

vs conductivity curve. This is a.so the case of the fairly good gas holdup estimates obtained with Cell "E" for the experiments conducted with a liquid of conductivity ~ 0.3 mS/cm (Figure 5.8(a)); however, when the liquid conductivity was increased to ~ 3 mS/cm the cell constant of Cell "E" falls to the "lower" part of the curve (Figure 5.8(b)) and a dramatic deterioration of the estimates was observed. Due to a similar behaviour of the cell constants of Cell "E" and the probe's cell, it is also reasonable to expect similar behaviour in terms of gas holdup estimation. Thus, extra precautions should be taken when attempting gas holdup estimation using the level detection probe in solutions of conductivities higher than ~ 1.3 mS/cm.

5.3 Summary

A conductivity technique to estimate gas holdup of a non-conductive phase in two and three phase systems was presented.

A conductivity cell consisting of two grid electrodes covering the entire cross-sectional area of a cylinder containing the two (or three) phase system was presented. The importance of the geometry and characteristics of such a cell were discussed. Models available in the literature were used to fit the experimental data. It was observed that Maxwell's model (1892) best described the data.

The estimation of holdup of non-conductive solids (silica) and conductive solids (sulphides in flotation slurries) is considered. It was observed that sulphides in flotation slurries behave as non-conductive material: Maxwell's model appeared to fit the data. Gas holdup estimation in a water-silica-air system was described. The results showed that the gas holdup estimates from conductivity were in good agreement with those obtained with an independent technique (the isolating technique).

CHAPTER 6

BIAS RATE: EXPERIMENTAL TECHNIQUES AND RESULTS

6.1   Laboratory Scale

6.1.1   Preliminary work in a two phase system

Results obtained in the water-air laboratory 10 cm diam. column (described in Section 4.2.4) showed that the conductance profiles collected around the interface were related to the operating conditions. Figure 6.1(a) shows, for example, that for a constant wash water rate the slope of the branch of the profile in the froth zone changed as the bias rate was varied from positive to negative.

Under normal operating conditions, a large fraction of the wash water added on the top of the froth flows downwards under gravity. Also because of gravity, the water carried to the froth by the rising air bubbles tends to concentrate in the base of the froth. This produces a gradient of gas holdup (and liquid holdup) in the froth zone. Relatively low gas holdups are expected in the base of the froth compared to those in the top of the froth (Yianatos et al., 1987). The qualitative explanation given to the behaviour observed in Figure 6.1(a) is that as the gas rate is increased, more water is carried to the froth until conditions are met where the wash water (or at least a large fraction of it) is unable to flow downwards, thus giving rise to an inversion of the gradient of gas holdup. This gradient is reflected by the conductance profile.

A similar explanation is offered for the results in Figure 6.1(b). For a constant gas rate, it is expected that the volume flowrate of water being carried to the froth zone by the bubbles is constant. Therefore, by varying the wash water flowrate, the gas
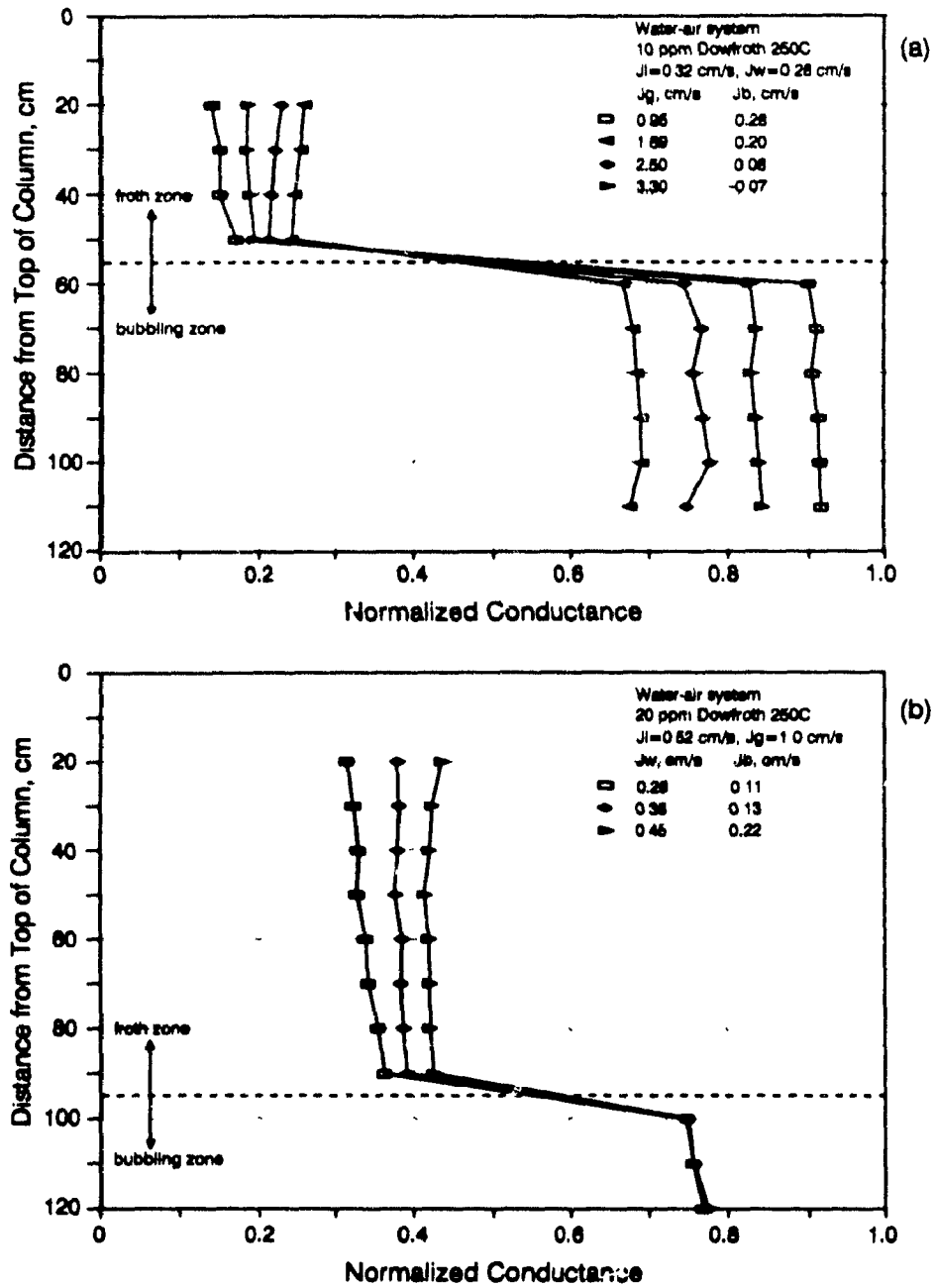
Figure 6.1 Preliminary results showing the effect of operating parameters on the conductance profiles around the interface

holdup in the froth zone will vary. The smaller the wash water flowrate, the larger the gas holdup and vice versa

Although the bias rate appears to be difficult to relate to the behaviour of the profiles in Figure 6.1, an experimental program was designed to investigate in more detail the phenomenon. Conditions encountered in the laboratory (where the same liquid is normally used for feed and wash water) and conditions prevailing in industrial operations (Stratlicona mill, Falconbridge Ltd.), where the pulp water conductivity is often higher than that of the wash water, were examined.

6.1.2 Feed water entrainment and feed water recovery

The working hypothesis is that, to maximize froth washing the bias should be positive; that is the tailings water flow should be greater than the feed water flow (this difference in flow being provided by the wash water). The use of bias as a measurement parameter, however, has recently been challenged. The measurement is subject to error (Finch and Dobby, 1990a; Moys and Finch, 1988b) and cases are being reported where grade is maintained under negative bias conditions (Finch and Dobby, 1990b; Furey, 1990). Measurements other than bias have been introduced and shown to be related to grade. Moys and Finch (1989) used the fraction of feed water in the overflow water, called here feed water entrainment or simply entrainment; Maachar et al. (1990) measured feed water recovery to the overflow. Both these latter parameters have an attraction: they focus on the feed water reporting to the overflow which ultimately dictates hydrophillic particle recovery by entrainment.

Provided there is a difference in feed water and wash water conductivity, which is frequently the case, conductivity measurements enable the two waters to be "traced" through the column. Similar reasoning was used by Moys and Finch (1988b) and Maachar et al.(1990) regarding the use of temperature measurements.

a).-   Theory

In preliminary experimental work, it became evident that the shape and location of the conductance profiles through the froth were related to bias. This is considered here. In addition, the use of conductivity measurements in the four streams around the column: the feed, overflow (or concentrate). underflow (or tails) and wash water, to trace the feed and wash water is also examined.

The rule of additivity for conductivity states that the conductivity of a mixture of two electrolytes of different conductivity, κ_A and κ_B, is proportional to the *volumetric fractions*, ν_A and ν_B, of the electrolytes in the mixture:

$$\kappa_{A-B} = \nu_A \, \kappa_A + \nu_B \, \kappa_B \tag{6.1}$$

where κ_{A-B}, κ_A and κ_B are the conductivities (mS/cm) of the mixture, and electrolytes A and B, respectively; and ν_A (volume of A/volume of mixture) and ν_B (volume of B/volume of mixture) are the volumetric fractions of A and B.

Figure 6.2 shows that Equation (6.1) describes well such mixtures.

Accordingly, the following can be derived for the column presented in Figure 6.3: for the overflow water,

$$\kappa_c = \frac{Q_{fc}}{Q_c} \, \kappa_f + \frac{Q_{wc}}{Q_c} \, \kappa_w \tag{6.2}$$

and, for the underflow water,

$$\kappa_t = \frac{Q_{ft}}{Q_t} \, \kappa_f + \frac{Q_{wt}}{Q_t} \, \kappa_w \tag{6.3}$$
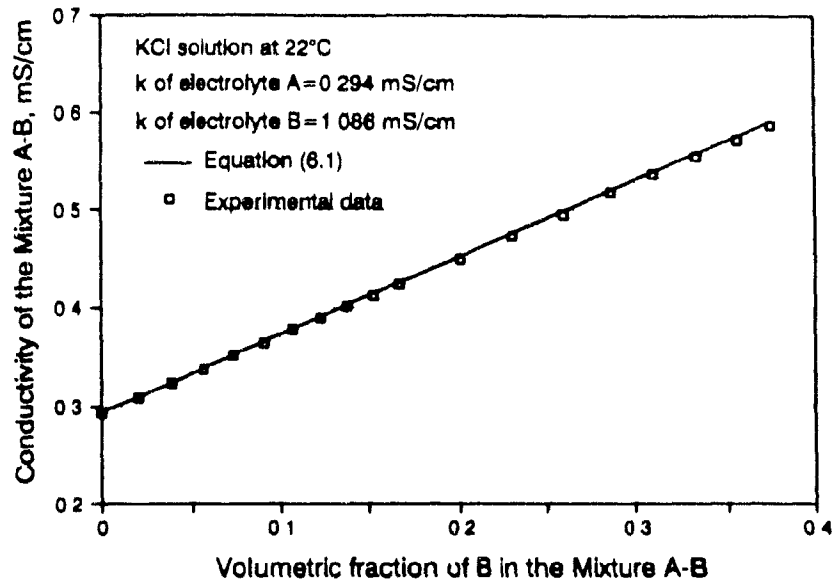
Figure 6.2   Experimental validation of the rule of additivity for conductivity
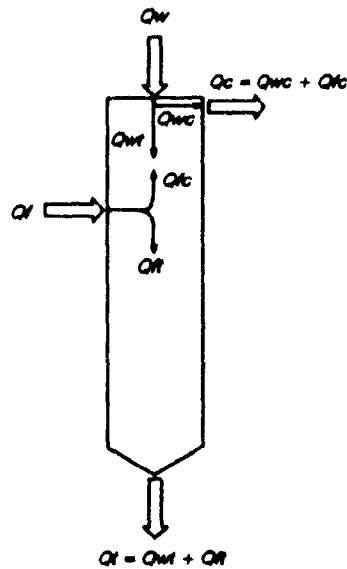
Figure 6.3   Water distribution in and around a flotation column and definition of bias rate, feed water recovery and feed water entrainment

where κ_c, κ_f, κ_w and κ_t, are the conductivities (mS/cm) of the overflow, feed, wash water and underflow streams, respectively; Q_{fc} and Q_{ft} are the volumetric flowrates (cm^3/s) of feed water reporting to the overflow and underflow, respectively; Q_{wc} and Q_{wt} are the volumetric flowrates (cm^3/s) of wash water reporting to the overflow and underflow, and Q_c and Q_t are the volumetric flowrates (cm^3/s) of the overflow and underflow.

From Equations (6.2) and (6.3) the required parameters can be obtained.

Bias: The net flow of water to the underflow is given by

$$Q_B = Q_t \left(\frac{\kappa_f - \kappa_t}{\kappa_f - \kappa_w} \right) - Q_c \left(\frac{\kappa_c - \kappa_w}{\kappa_f - \kappa_w} \right) \tag{6.4}$$

This is often converted to a superficial rate, J_B, by dividing by the column cross-sectional area, A_c. (Other definitions of bias are in use, see Figure 6.1 and Appendix 5).

Feed water entrainment: This is defined here as the fraction of feed water in the overflow stream, Q_{fc}/Q_c, and is given by

$$\frac{Q_{fc}}{Q_c} = \frac{\kappa_c - \kappa_w}{\kappa_f - \kappa_w} \tag{6.5}$$

Feed water recovery: Defined as the fraction of the feed water that reports to the overflow, Q_{fc}/Q_f, and given by

$$\frac{Q_{fc}}{Q_f} = \frac{Q_c}{Q_f} \left(\frac{\kappa_c - \kappa_w}{\kappa_f - \kappa_w} \right) \tag{6.6}$$
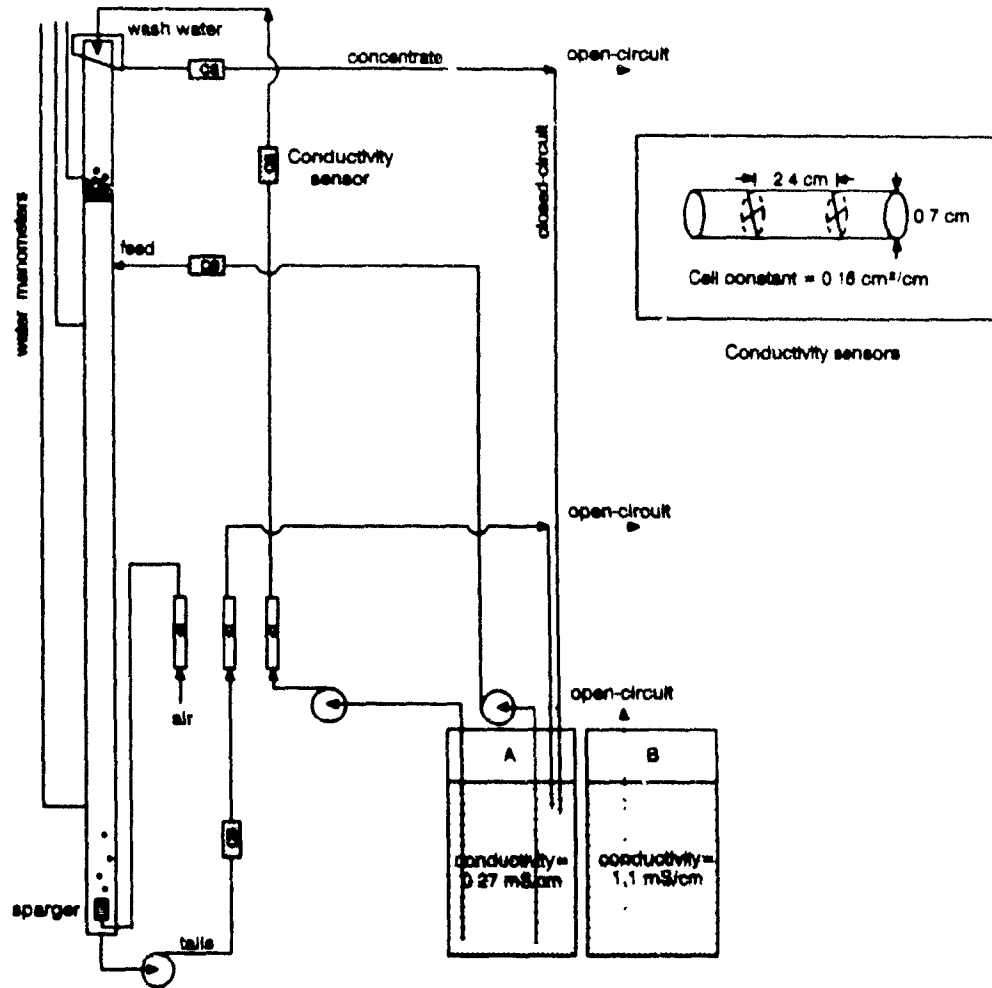
Figure 6.4 Experimental apparatus and details of conductivity sensors used

where Q_f is the volumetric flowrate (cm^3/s) of the feed stream.

b).- Experimental Approach

Apparatus

A laboratory column, 5.7 cm diam. × 391 cm height was used (Figure 6.4). The feed entered at 146 cm from the lip. The wash water distributor consisted of a perforated

copper ring (~ 0.4 cm diam.) located about 3 cm below the lip. A cylindrical stainless steel sparger (surface area$=84$ cm^2) was used to generate the bubbles. Calibrated rotameters and peristaltic pumps (Masterflex Cole Parmer, model 7520) were used to monitor and control the underflow, wash water and feed streams. The air flowrate was measured with a mass flowmeter (Tylan Model FM-380).

There was facility to operate the column under closed or open circuit conditions. In closed circuit, the column feed and wash water was from tank A (Figure 6.4) (200 l of 15 ppm Dowfroth 250C solution at room temperature; $\kappa_{24^\circ C} \sim 0.27$ mS/cm) and the underflow and overflow streams were recycled. In open circuit, the wash water was from tank A and the feed stream from tank B (500 l of 15 ppm Dowfroth 250C solution at room temperature; $\kappa_{24^\circ C} \sim 1.1$ mS/cm); the underflow and overflow were discarded. Potassium chloride was used to increase the conductivity of the solution in tank B over that of the tap water in tank A.

In the top section of the column conductance profiles were collected by using twelve electrode pairs (stainless steel facing circles, 1 cm diam.) installed in the column wall following vertical lines 180 degrees apart, and with a separation of 10 cm starting at 31 cm from the column lip. The conductivity of the streams around the column was extracted from conductance measurements collected with sensors consisting of a PVC tube (0.7 cm diam.) supporting two facing electrodes (a cross of stainless steel wire, see Figure 6.4) separated by 2.4 cm. The calculated cell constant, ~ 0.16 cm^2/cm, was in good agreement with those obtained experimentally by performing conductance measurements on KCl solutions of known conductivity (Table 6.1).

Table 6.1   Experimental cell constants of conductivity sensors used for on line
measurement of conductivity in the streams around the column

KCl solution $\kappa_{25°C}$ (mS/cm)	Sensor 1 K (mS) / K_{cell} (cm/cm)	Sensor 2 K (mS) / K_{cell} (cm²/cm)	Sensor 3 K (mS) K_{cell} (cm²/cm)	Sensor 4 K (mS) K_{cell} (cm²/cm)
0 310	0 0495 / 0 160	0 0498 / 0 161	0 0496 / 0 160	0 0489 / 0 158
0 443	0 0707 / 0 160	0 0708 / 0 160	0 0706 / 0 159	0 0701 / 0 158
0 532	0 0852 / 0 160	0 0845 / 0 159	0 0847 / 0 159	0 0841 / 0 158
0 726	0 1158 / 0 160	0 1154 / 0 159	0 1149 / 0 158	0 1140 / 0 157
0 860	0 1371 / 0 159	0 1358 / 0 158	0 1354 / 0 157	0 1349 / 0 157
1 037	0 1654 / 0 159	0 1628 / 0 157	0 1628 / 0 157	0 1625 / 0 157

The performance of these sensors was consistent and reliable as reflected by the value of their relative standard deviation, $\sim 0.75\%$ for low conductivities (~ 0.3 mS/cm), and $\sim 0.2\%$ for high conductivities (~ 1.1 mS/cm). Data collection was performed by using a data acquisition system similar to the one described in Section 4.2 4.

Procedure

Two options for varying the bias rate were used: option i), varying the gas rate (0.65 to 2.25 cm/s) while keeping the underflow and wash water constant (0.81 and 0.41 cm/s, respectively) and maintaining the interface level with the feed stream; and option ii), varying the wash water rate (0 to 0.36 cm/s) while keeping the underflow and gas rate constant (0.81 and 1.2 cm/s, respectively) and maintaining the interface level with the feed stream. Two froth depths were tested, 55 ± 5 and 95 ± 5 cm. Experiments were completed for both open and closed circuit conditions.

For option (i) the system was initially operated in closed circuit and when steady

conditions were established the system was opened. For option (ii) the system was started open.

c).-   Experimental Results

Conductance profiles

Figures 6.5 and 6.6 present sets of conductance profiles for both options (i) and (ii) for closed and open circuit. The usual marked step in conductance across the bubbling/froth zone interface is observed reflecting the difference in gas holdup between these zones. This step is more pronounced for open circuit conditions because of the added effect of the lower conductivity of the wash water (the water in the bubbling zone is predominantly feed water, in the froth zone predominantly wash water).

The behaviour of the conductance profiles appears to be related to the bias as observed in Figure 6.6. For open circuit (the relevant conditions for industrial operation) the profiles shift towards larger conductance values when the bias decreases.

This increase in bubbling zone conductance reflects the increased proportion of feed water in the bubbling zone water; because bias is reduced, the volume of wash water entering the bubbling zone is reduced. The increase in conductance in the froth zone may similarly be related to an increased proportion of feed water in the froth zone water, but possible changes in gas holdup are a complication: for example, in Figure 6.6(a) the increase in gas rate increases the conductance in the froth zone even in the closed circuit case as the gas holdup in the froth has decreased (as is known to occur when gas rate is increased (Yianatos et al., 1987)).

The behaviour of the conductance profiles for closed circuit conditions (the same source of water was used for wash water and feed water) was similar to that observed
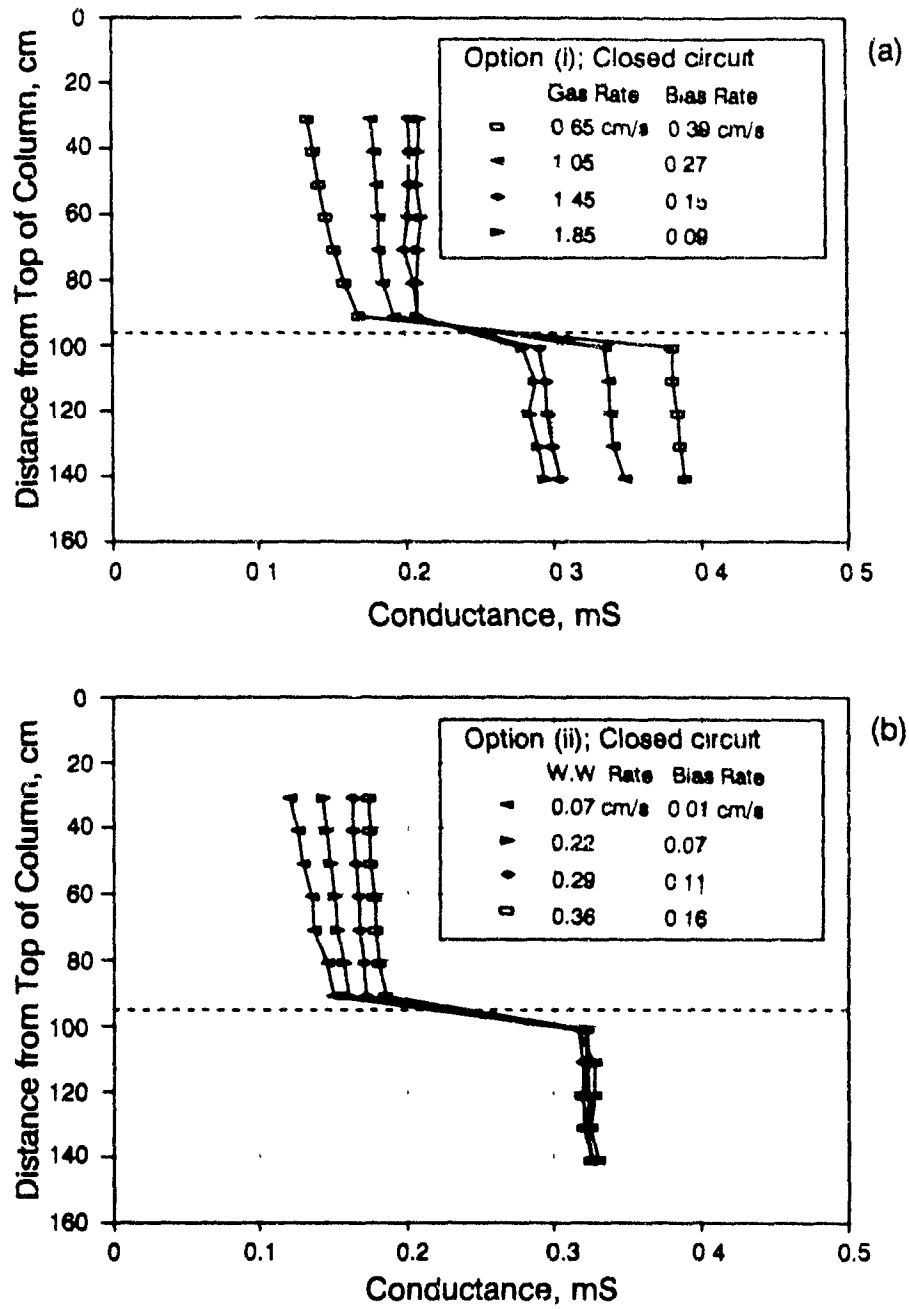
Figure 6.5   Conductance profiles for closed circuit conditions. Froth depth=95 cm.
Option (i): Jt=0.8 cm/s and Jw=0.41 cm/s. Option (ii): Jt=0.8 cm/s and
Jg=1.2 cm/s
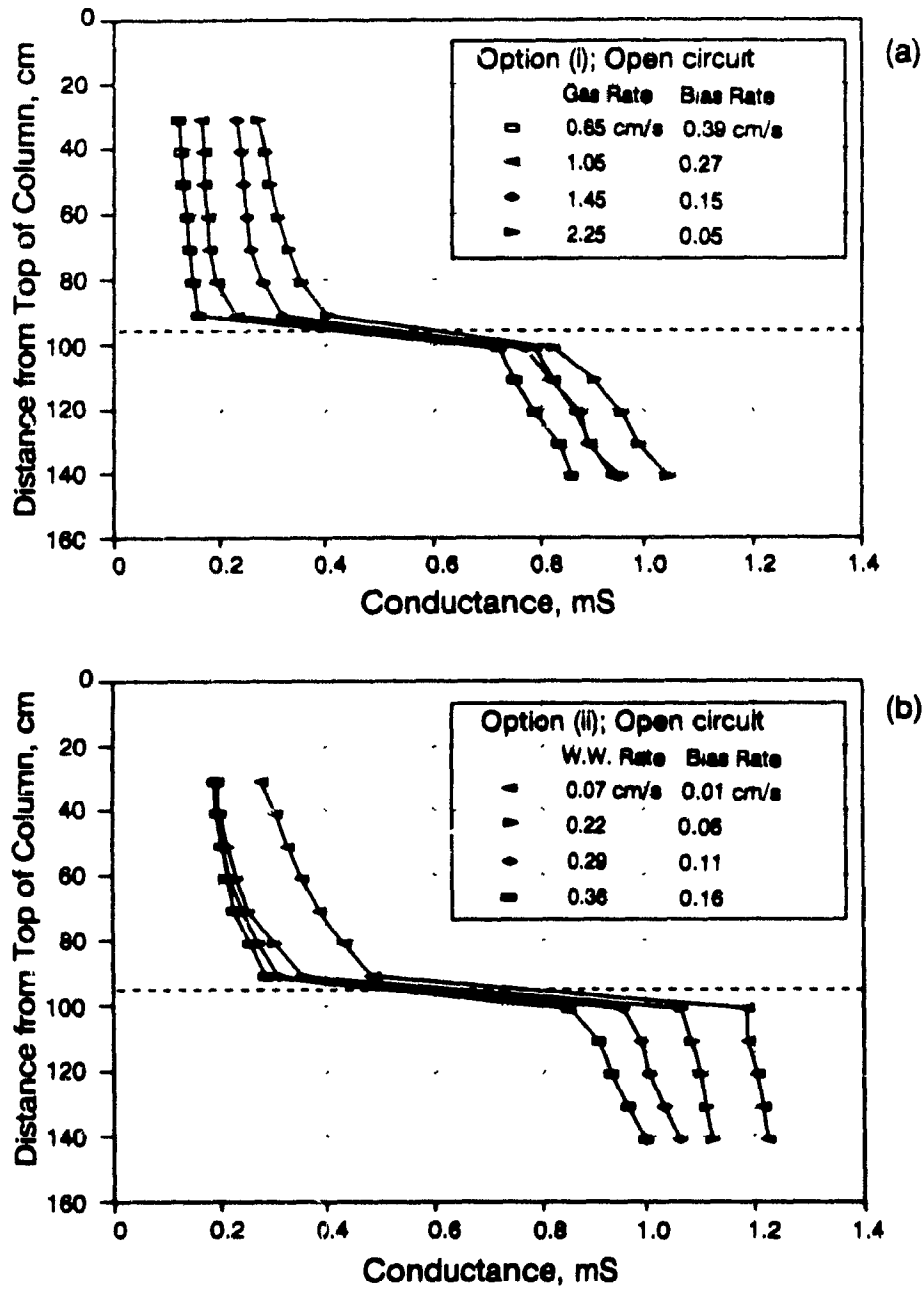
Figure 6.6 Conductance profiles for open circuit conditions. Froth depth=95 cm. Option (i): Jt=0.8 cm/s and Jw=0.42 cm/s. Option (ii): Jt=0.8 cm/s and Jg=1.2 cm/s

in the preliminary results presented in Figure 6.1. Explanation for such a behaviour was given.

Work recently reported by Bergh and Yianatos (1991) showed that the (normalized) conductivity profiles obtained in a water-air column (feed water of higher temperature than the wash water) were insensitive to bias variations; no explanation was offered.

Bias rate, feed water entrainment and feed water recovery

Figure 6.7 presents typical variation of the conductivity of the streams vs time as a function of gas rate (option i). Table 6.2 and Table 6.3 present the operating parameters, bias rate, entrainment and recovery results for these experiments. A few points of note are: (1) before the circuit is opened the same conductivity value is reported for all the streams (as should be the case); (2) for the first two air rates (0.65 and 1.05 cm/s) the overflow conductivity is practically that of the wash water indicating that no feed water is reaching the overflow, while for higher air rates feed water starts showing up in the overflow; (3) the volumetric fraction of wash water flowing downwards decreases as gas rate increases; (4) feed water entrainment occurs even if a downward flow of wash water exists; and (5) the stability of the column operation decreased as the gas rate increased: at the lower gas rates (0.65, 1.05 and 1.45 cm/s) the interface level was maintained within ± 5 cm, while at higher gas rates (1.85 and 2.25 cm/s) the level could only be maintained within 95 ± 10 cm and 55 ± 20 cm. This instability is revealed by the wide variations observed in the overflow conductivity at high gas rates, specially at 55 cm froth depth (Figure 6.7(b)).
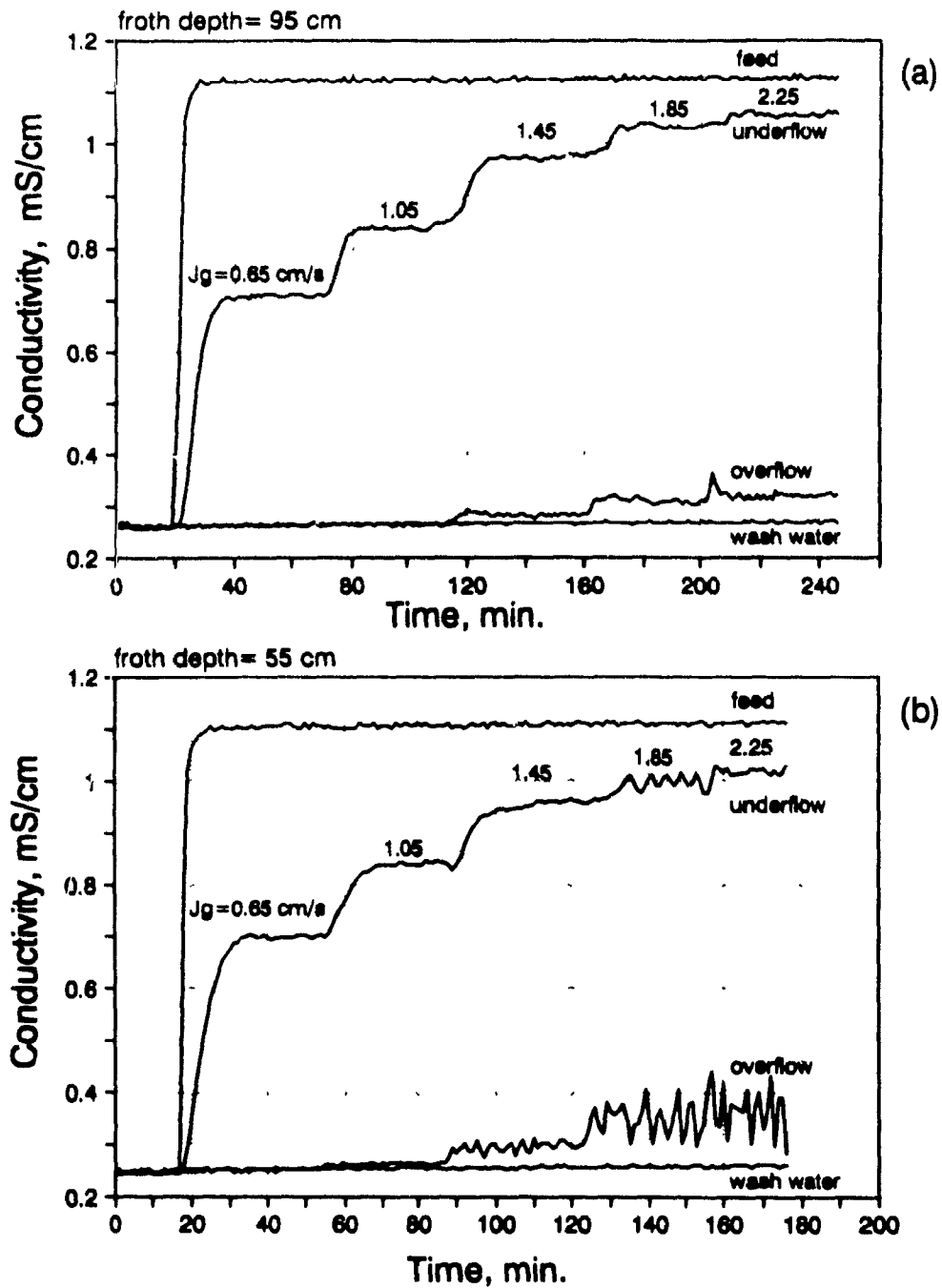
Figure 6.7   Conductivity vs time for option (I), Jt=0.8 cm/s, Jw=0.4 cm/s, 15 ppm Dowfroth
250C, for (a) froth depth=95 cm, and (b) froth depth=55 cm

Table 6.2   Operating parameters, bias rate, entrainment and recovery results for options (i)-open circuit experiments; froth depth = 95 cm.

J_g, cm/s	J_l, cm/s	J_w, cm/s	J_c, cm/s	J_f, cm/s	J_b, cm/s	Q_{fc}/Q_c, %	Q_{fc}/Q_f, %
0 65	0 81	0 42	0 03	0 42	0 39	0 27	0 02
1 05	0 81	0 42	0 15	0 54	0 27	0 38	0 11
1 45	0 80	0 42	0 27	0 65	0 15	1 68	0 71
1 85	0 80	0 42	0 34	0 72	0 08	4 55	2 15
2 25	0 80	0 42	0 37	0 75	0 05	6 02	2 86

Table 6.3   Operating parameters, bias rate, entrainment and recovery results for options (i)-open circuit experiments; froth depth = 55 cm..

J_g, cm/s	J_l, cm/s	J_w, cm/s	J_c, cm/s	J_f, cm/s	J_b, cm/s	Q_{fc}/Q_c, %	Q_{fc}/Q_f, %
0 65	0 80	0 41	0 04	0.43	0 37	0 00	0 00
1 05	0 81	0 41	0 17	0 57	0 24	0 88	0 27
1 45	0 80	0 41	0 28	0 67	0 13	4 75	2 12
1 85	0 80	0 41	0 34	0 73	0 07	10 14	4 68
2 25	0 81	0 41	0.38	0 78	0 03	12 19	6 00

Figure 6.8 presents typical plots of stream conductivity vs time for option (ii). Table 6.4 and Table 6.5 present the operating parameters, bias rate, entrainment and recovery results for these experiments. At 95 cm froth depth, $J_w = 0.07$ cm/s was the minimum wash water rate that could maintain a stable froth bed; at 55 cm froth depth, the column could be operated with no wash water addition. Note that the overflow conductivity decreased as the wash water rate increased indicating an increasing proportion of wash water in the overflow. The operation of the column was again more stable at 95 cm froth depth than at 55 cm.

froth depth=95 cm

(a)

froth depth=55 cm

(b)
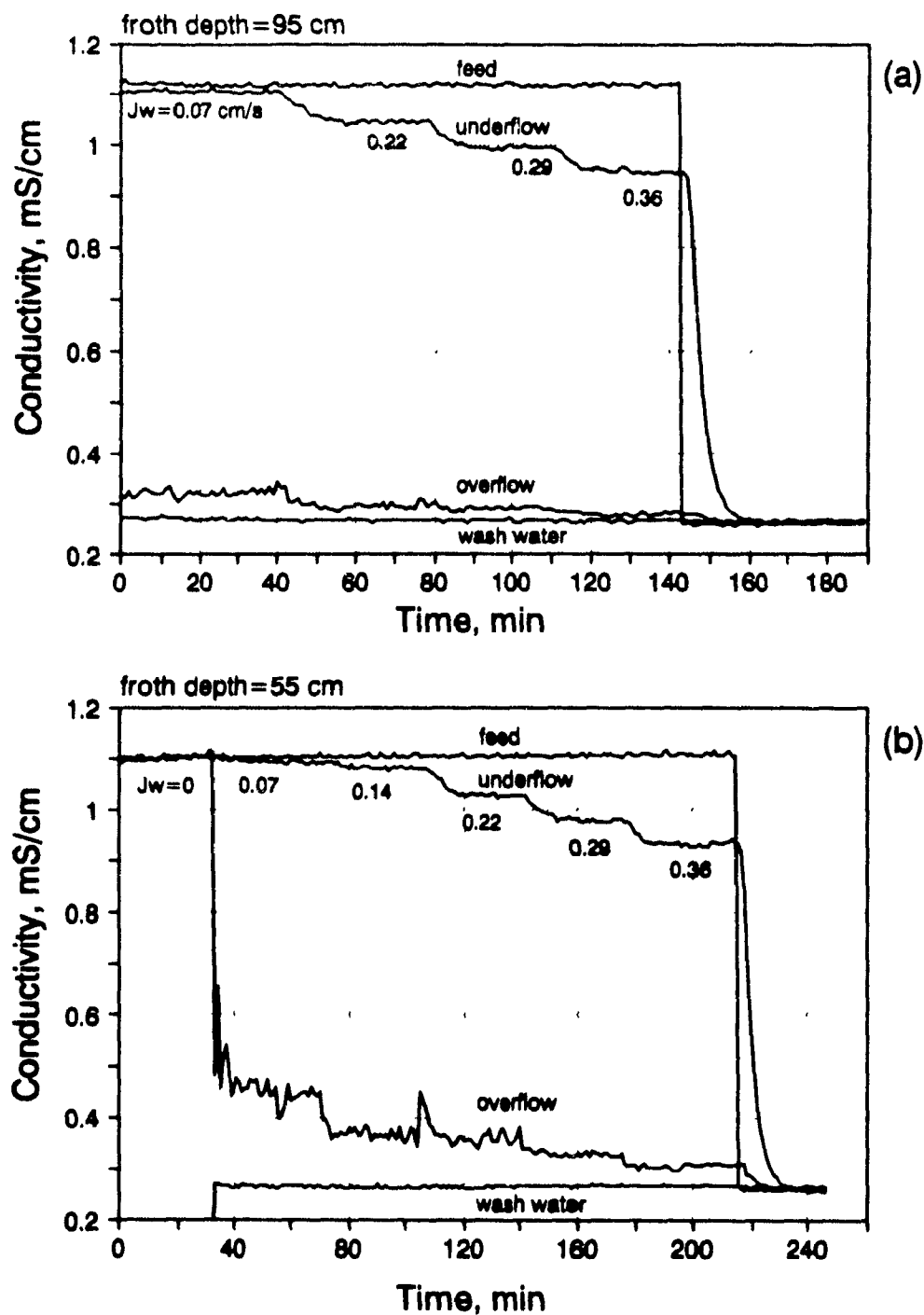
Figure 6.8   Conductivity vs time for option (ii), J_t=0.82 cm/s, J_g=1.2 cm/s, 15 ppm Dowfroth 250C, for (a) froth depth=95 cm, and (b) froth depth=55 cm

Table 6.4   Operating parameters, bias rate, entrainment and recovery results for options (ii)-open circuit experiments; froth depth = 95 cm..

J_g, cm/s	J_1, cm/s	J_w, cm/s	J_c, cm/s	J_f, cm/s	J_b, cm/s	Q_{tc}/Q_c, %	Q_{tf}/Q_f, %
1 20	0 82	0 07	0 06	0 80	0 01	5 88	0 42
1 20	0 82	0 22	0 16	0 75	0 06	3 04	0 62
1 20	0 82	0 29	0 18	0 70	0 11	2 80	0 70
1 20	0 82	0 36	0 20	0 65	0 16	1 40	0 42

Table 6.5   Operating parameters, bias rate, entrainment and recovery results for options (ii)-open circuit experiments; froth depth = 55 cm.

J_g, cm/s	J_1, cm/s	J_w, cm/s	J_c, cm/s	J_f, cm/s	J_b, cm/s	Q_{tc}/Q_c, %	Q_{tf}/Q_f, %
1 20	0 81	0 00	0 02	0 83	-0 02	100 00	2 76
1 20	0 82	0 07	0 08	0 82	-0 01	22 27	2 20
1 20	0 81	0 14	0 14	0 81	0 00	12 39	2 15
1 20	0 82	0 22	0 17	0 76	0 05	11 14	2 45
1 20	0 82	0 29	0 18	0 70	0 11	7 26	1 85
1 20	0 81	0 36	0 19	0 64	0 17	4 67	1 37

Estimation of bias rate. The bias rate was estimated in two different ways: (a) from a water balance around the column performed by using timed samples collected in the streams around the column under stable operating conditions (as judged from the constant values of conductivity of the overflow and underflow streams): these bias rate values are presented in Tables 6.2 to 6.5; and (b), by using Equation (6.4), the "punctual" values of the conductivities of the streams, and the overflow and underflow rates for stable operating conditions. This assumes that the overflow rate obtained for stable operating conditions holds for the entire period of time when the column was operated under such conditions (i.e. the system was at steady state). Although the

assumption introduces a limitation in describing the dynamics of the transition between different operating conditions, it does not affect the trends observed under steady state conditions. The underflow rate was kept constant at around 0.81 cm/s throughout the experiments. Figures 6.9(a) to 6.12(a) show the evolution of bias rate.

Estimation of feed water entrainment and recovery. Feed water entrainment was calculated using Equation (6.5) and the conductivities of the streams around the column (error propagation analysis is presented in Appendix 6). Feed water recovery was calculated using Equation (6.6) and the overflow and feed rates obtained for stable operating conditions. The comments offered above for the estimation of bias rate also apply for the recovery. Figures 6.9(b) to 6.12(b) show the evolution of feed water entrainment and recovery for the data in Figures 6.7 and 6.8. They clearly show that feed water enters the overflow even though bias is positive.

The values of entrainment and recovery presented in Tables 6.2 to 6.5 were obtained by averaging 10 to 20 values (representing a period of 10 to 20 minutes) of stable operation.

Figure 6.13 presents the bias rate and feed water entrainment and recovery as a function of (a) the gas rate (option (i)), and (b) the wash water rate (option (ii)). For (a), bias rate decreased and feed water entrainment and recovery increased as gas rate increased. No substantial difference was observed between 55 and 95 cm froth depth in terms of bias rate, but entrainment and recovery were higher for the shallower froth. For (b), the bias rate increased and the entrainment decreased when the wash water was increased but recovery was essentially constant. Again, the bias rate behaviour was similar for both froth depths, while entrainment and recovery were higher for the shallower froth.
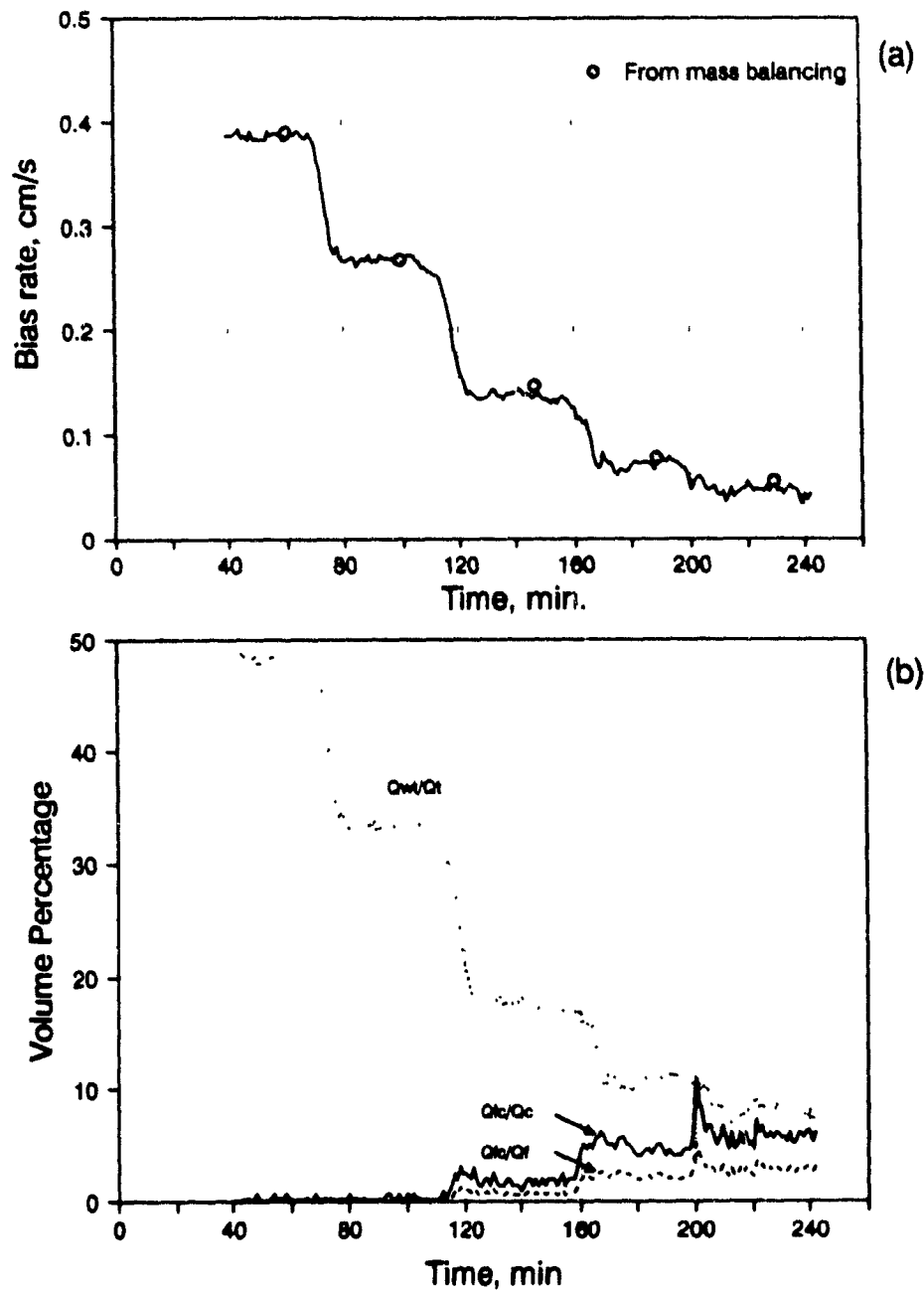
Figure 6.9 Evolution of: (a) bias rate and (b) feed water entrainment, Qfc/Qc, and feed water recovery, Qfc/Qf, for results in Figure 6.7(a). The percentage of wash water in the underflow, Qwt/Qt, and steady state mass balancing results for bias rate are also shown.
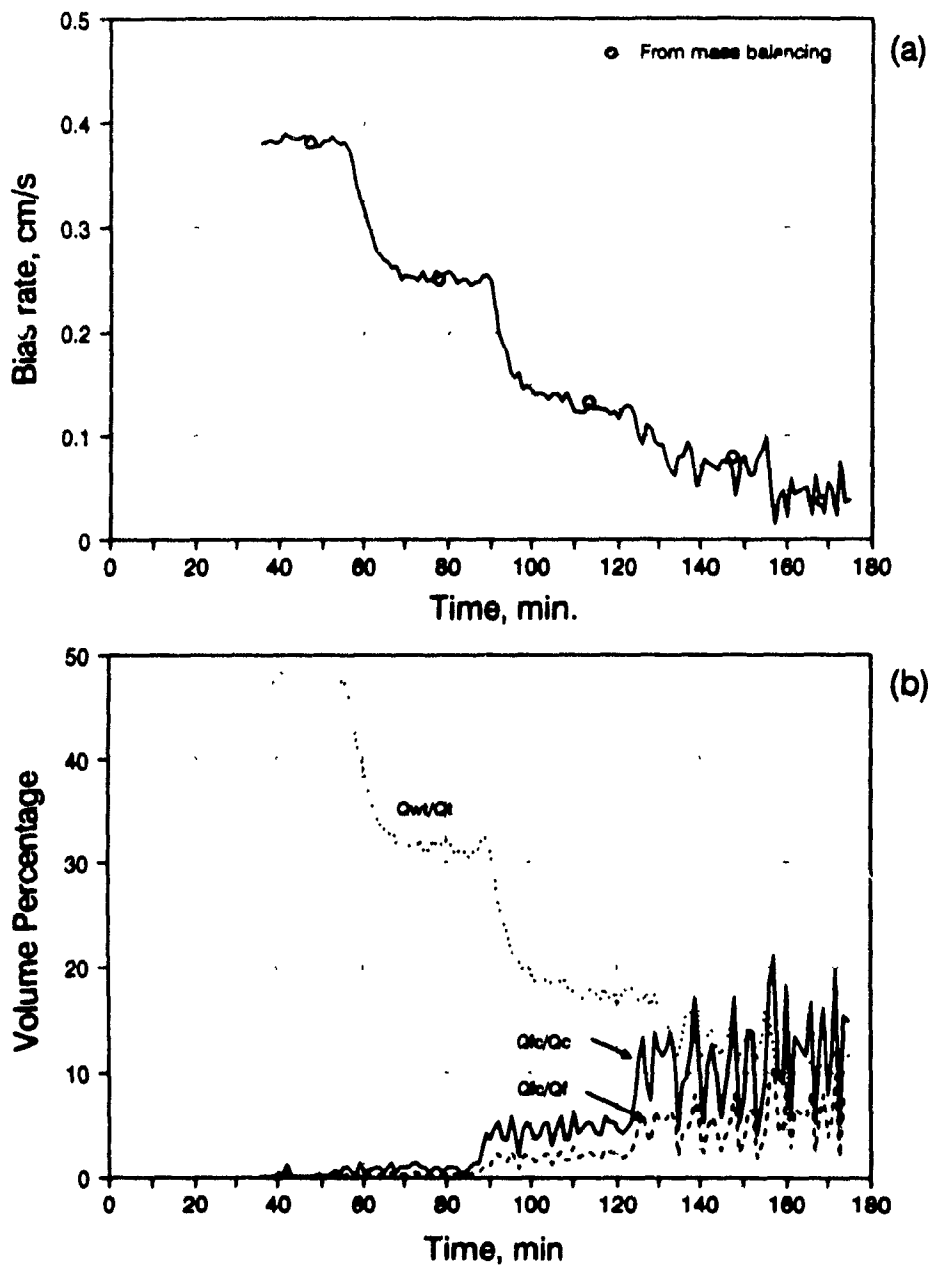
Figure 6.10 Evolution of: (a) bias rate and (b) feed water entrainment, Qfc/Qc, and feed water recovery, Qfc/Qf, for results in Figure 6.7(b)
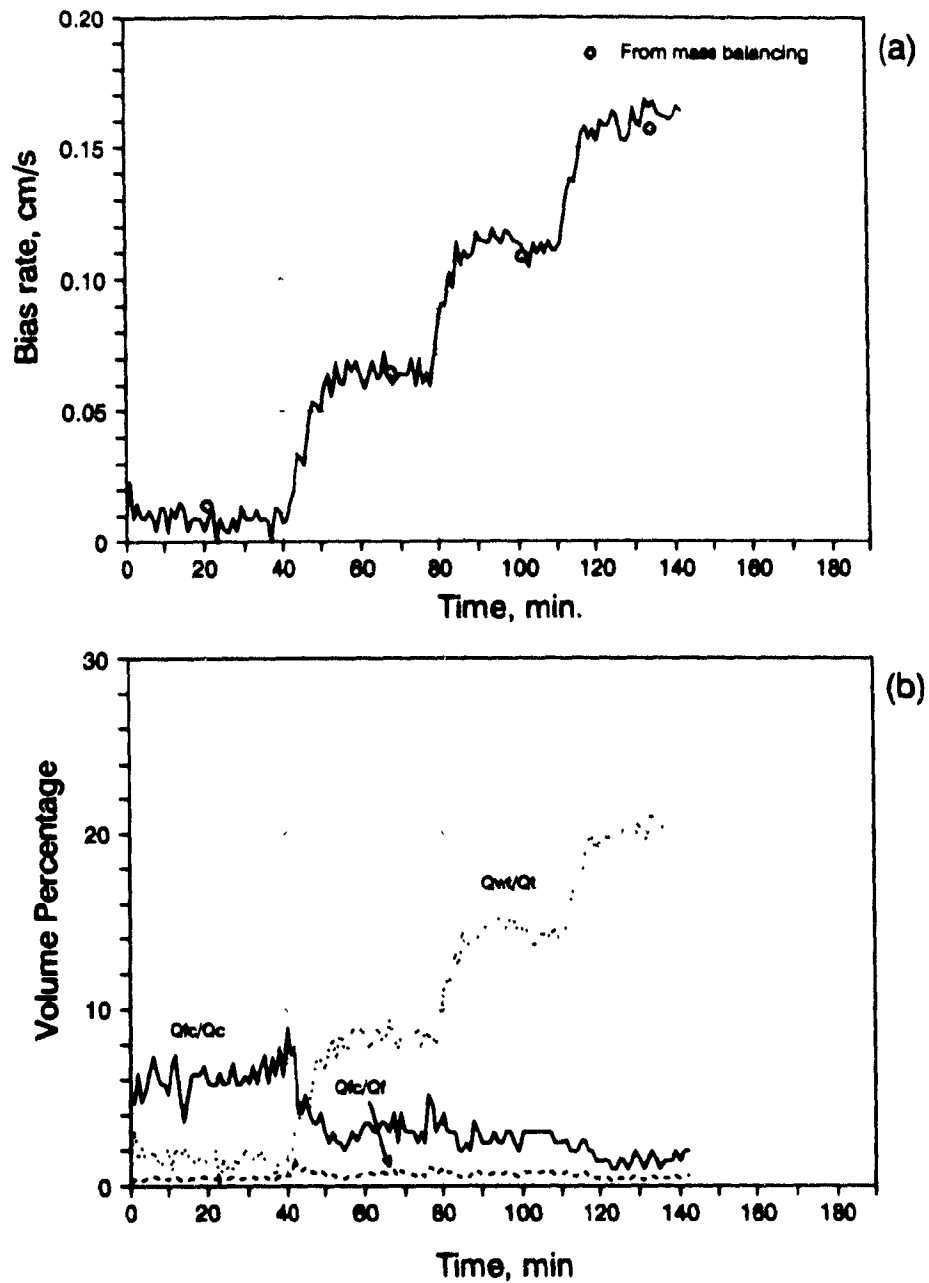
Figure 6.11 Evolution of: (a) bias rate and (b) feed water entrainment, Qfc/Qc, and feed water recovery, Qfc/Qf, for results in Figure 6.8(a)
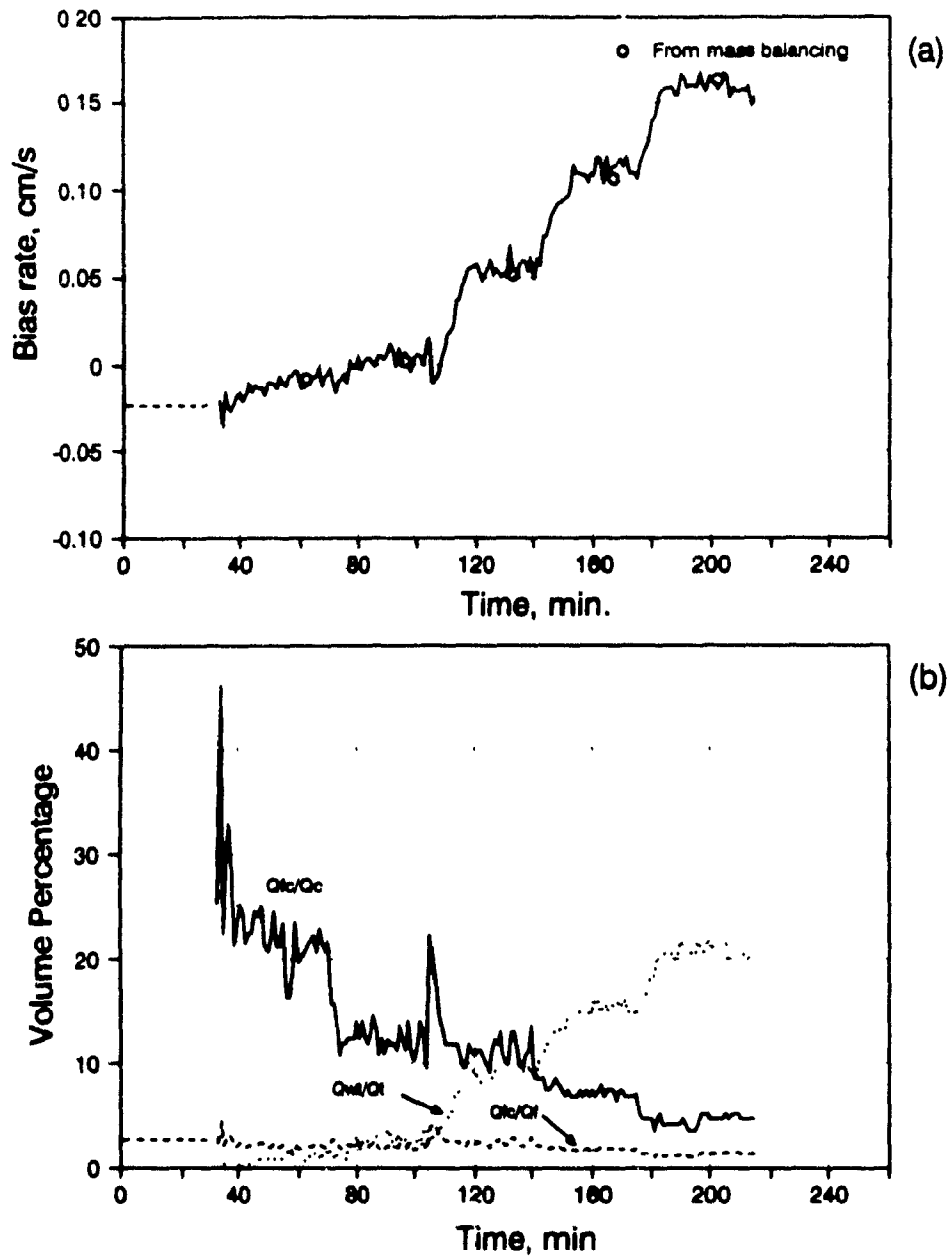
Figure 6.12 Evolution of: (a) bias rate and (b) feed water entrainment, Qfc/Qc, and feed water recovery, Qfc/Qf, for results in Figure 6.8(b)
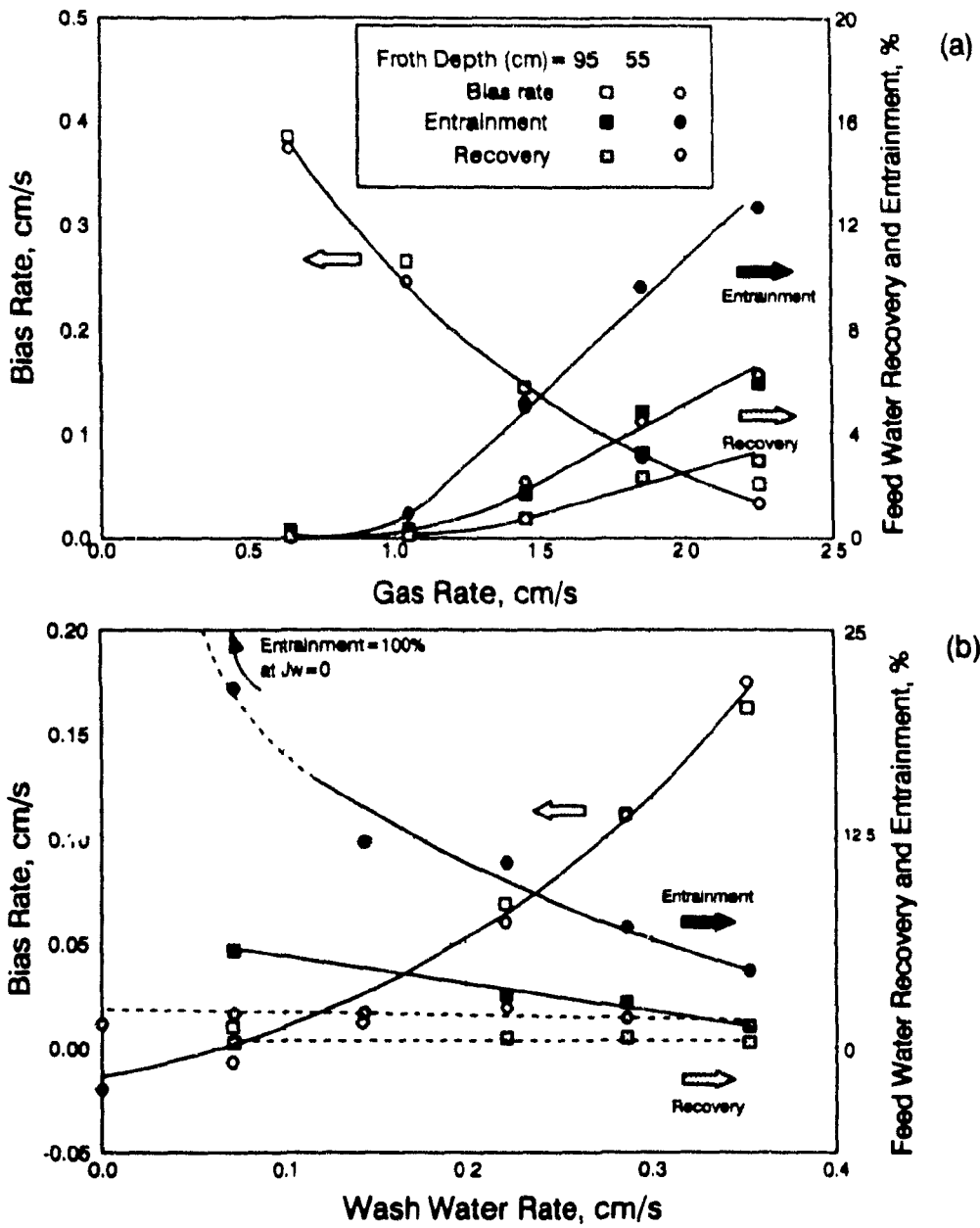
Figure 6.13 Bias rate, feed water entrainment and feed water recovery for: (a) option (i), Jt=0.8 cm/s and Jw=0.4 cm/s; (b) option (ii), Jt=0 8 cm/s and Jg=1.2 cm/s
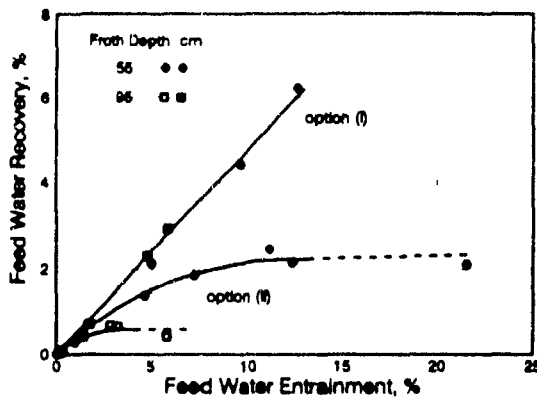
Figure 6.14   Feed water entrainment vs
feed water recovery
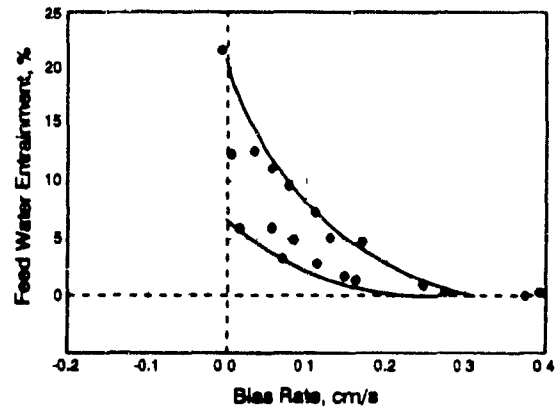
Figure 6.15   Feed water entrainment vs
bias rate

Figure 6.14 presents the feed water recovery vs feed water entrainment. The plot shows that recovery and entrainment are related but not necessarily linearly; however, no example was encountered where the two had opposite trends.

This implies that entrainment and hydrophillic fine particle recovery are related, and hence entrainment should be related to metallurgy. Entrainment may well be a satisfactory substitute for feed water recovery for a given design of column (changing the wash water location may alter the entrainment-recovery relationship, for example). A more severe test of the use of entrainment than that executed here would be where gas rate and wash water are manipulated simultaneously as may happen in practice.

Figure 6.15 presents the evolution of entrainment as a function of bias rate clearly showing that having a positive bias did not completely prevent the entrainment of feed water. These results are in good agreement with the work of Yianatos et al. (1987) who found that to minimize the hydraulic entrainment of fine particles in flotation columns bias rates of 0.2-0.4 cm/s were needed.

6.1.3 Conductance profiles in a three phase system

The effect of operating conditions on the behaviour of the conductance profiles was explored in a three phase system while performing amenability tests on some of the streams of the flotation circuit of the Strathcona mill, Falconbridge Ltd. In these tests, the flotation rate in the column was changed by varying the liquid residence time (by varying the tailings flowrate) while keeping the wash water and gas rate constant. The level was adjusted at around 100 cm from top of the column by manipulating the feed flowrate. When stable operating conditions had been reached (normally three residence times were allowed after each operating change), timed samples of the streams around the column were collected. Solid percentage analysis and chemical assays were performed on the samples. The tests were conducted making use of a 5.04 cm diam. x 1050 cm high laboratory column. The column, the arrangement of electrodes and the data acquisition system used in this application were described in Section 4.2.2.

These types of tests are suitable for exploring the feasibility of correlating the profiles with the bias rate since a wide range of bias, including negative values, was covered. It is worth mentioning that tap water of conductivity ~ 0.3 mS/cm was used for wash water while the conductivity of the flotation pulp water was around 2 to 3 mS/cm. As already discussed, this condition is well suited for the conductance measurements to reflect the proportion of feed and wash water around the interface. Figure 6.16 presents the conductance profiles collected when processing a sample of the Magnetic Flotation Concentrate (MFC), and a sample of the Secondary Rougher Concentrate (SRC).

Figure 6.16 shows that, as expected, the profiles did shift towards larger values of conductance as the bias decreased (from positive to negative values), indicating that the proportion of feed water in both the collection and froth zones increased. These results are in good agreement with the observations made in the two-phase system discussed before. Furthermore, the metallurgical results appeared to be related to the bias
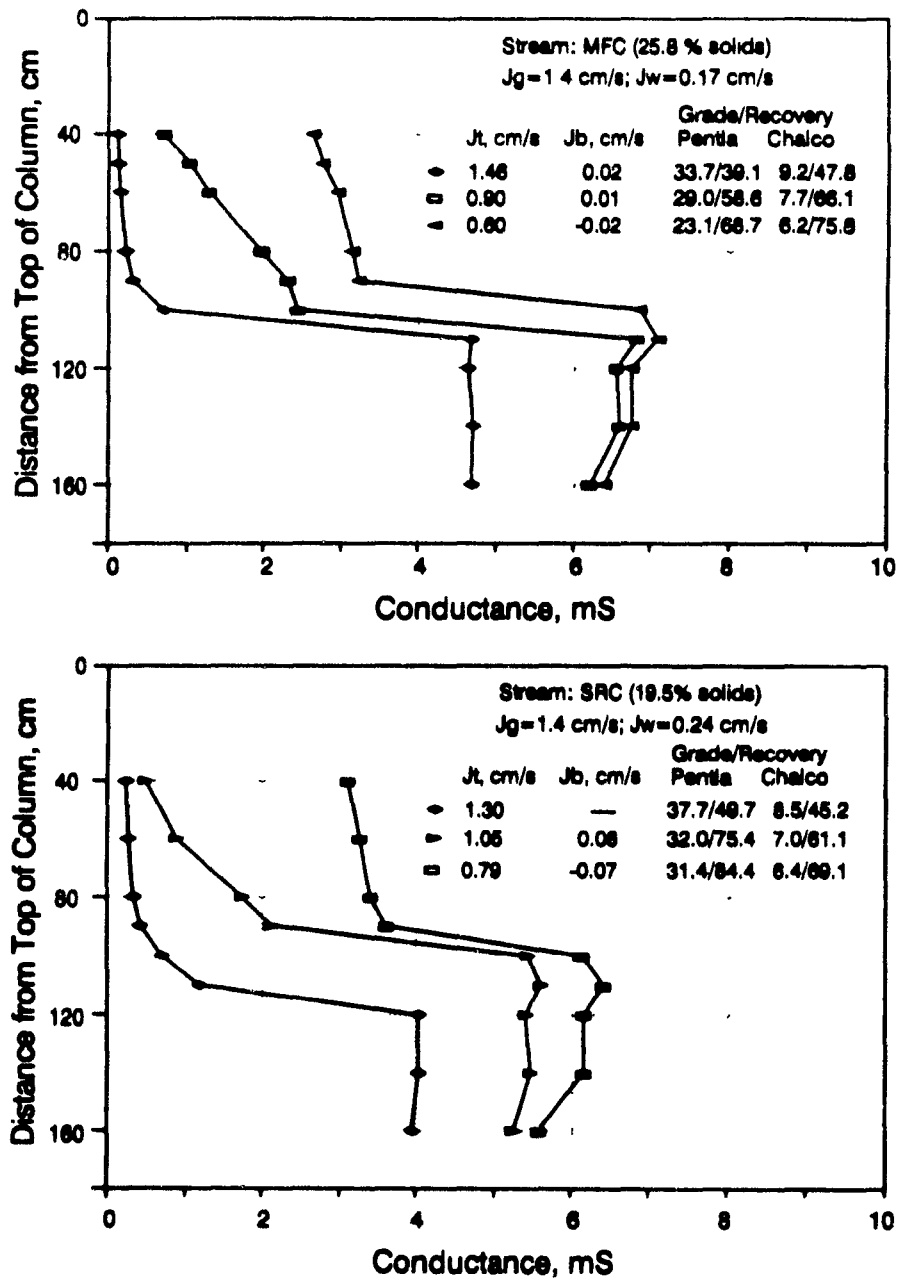
Figure 6.16 Conductance profiles, operating conditions and metallurgical results in a three phase laboratory (5.04 cm diam.) column. MFC is Magnetic Flotation Concentrate and SRC is Secondary Rougher Concentrate

rate. For both streams, MFC and SRC, the grades of Pentlandite (Pentla) and Chalcopyrite (Chalco), decreased in the direction of negative biases, while the recovery increased (see Figure 6.16). This finding supports the general hypotheses on the relationship between grade, recovery and bias (the grade improves at the expense of recovery as the bias increases in the positive direction).

6.2 Industrial Scale

Conductance profiles in a 91 cm diam. x 1350 cm high column (described in Section 5.2) were collected for both water-air and slurry-air systems by using the level detection probe. The objective of the testwork was to assess the feasibility of correlating the conductance profiles obtained with the level probe in large columns with the operating conditions, particularly with the bias rate.

In these tests, bias transitions were produced by varying the feed flowrate at constant gas and tailings flowrates while controlling the interface level (at around 100 cm froth depth) with the wash water stream. This scheme was mainly dictated by the available method of control. The instrumentation of the column included magnetic flow meters to measure wash water, feed and tailings flows and densities, and a calibrated rotameter for gas rate.

6.2.1 Water-air system

The water-air experiments were conducted using a closed circuit, that is, the feed and the wash water were from the same source. Water containing frother (Dowfroth 250C, to around 15 ppm) was used. Once the selected air, tailings and feed flowrates were set, the column was automatically operated for about 45 minutes. Conductance profiles were continuously collected one every minute. One of the profiles collected at the end of this period of time was selected to represent the specific operating conditions.

Figure 6.17 presents the operating conditions an the results obtained.

The results in Figure 6.17 are consistent with those obtained in the laboratory when using a similar approach (option (i), closed circuit experiments; see Figure 6.5(b)). Since constant gas and tailings rate were used (a fairly constant gas holdup is expected), the conductance of the bubbling zone remained essentially constant regardless of variations in wash water addition. However, in the froth zone the profiles shifted towards larger conductance values as the wash water addition was increased, thus indicating the expected increase in liquid holdup of the froth zone.

The results do indicate that similarities exist between the laboratory and the industrial unit in terms of the effect of operating parameters on the behaviour of the profiles in water-air systems.

6.2.2 Slurry-air system

Preliminary experiments in a slurry-air system were conducted at the Strathcona mill, Falconbridge Ltd., by processing a stream of the copper circuit (Primary Rougher Concentrate).

a).- Experimental approach

The experiments were designed to generate a bias transition by increasing the feed flowrate at constant air and tailings flowrate while keeping the interface level constant by manipulating the wash water stream. Figure 6.18 illustrates the relevant variables monitored by the instruments attached to the column. Based on statistical data available in the mill, solids density in the feed, tailings, and concentrate streams were assumed to be 4.6, 4.6 and 4.3 g/cm^3, respectively. The flow of gland water for the tailings pump was 746 cm^3/s (10 l in 13.4 seconds). After stable operation was reached (a period of
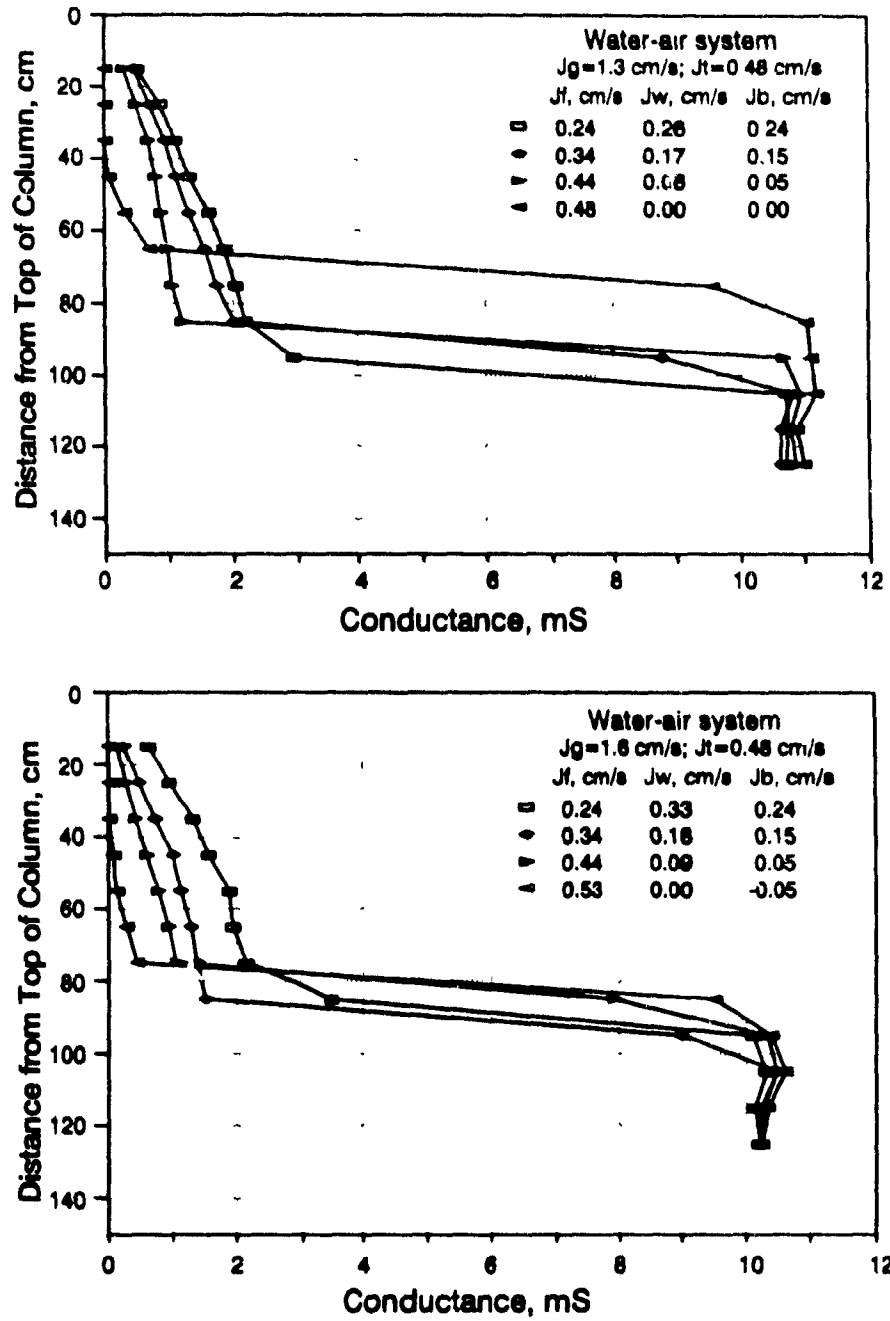
Figure 6.17 Conductance profiles for different bias rates in a 91 cm diam. water-air column
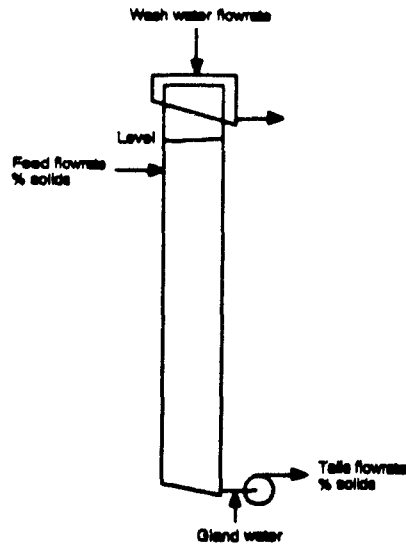
Figure 6.18   Operating variables measured in the slurry-air experiments

around 45 minutes was allowed), conductance profiles were collected (one every minute), and samples of the streams around the column were simultaneously collected for conductivity measurements, solid percentage and chemical assays. Slurry samples were filtered before the conductivity measurements were performed in order to obtain the conductivity of the water in the particular stream. Conductance profiles were collected by using the level detection probe. Four series of tests with a total of 19 runs were completed.

b).-   Results

The operating conditions are summarized in Table 6.6, and the values of the conductivity of the streams and the metallurgical data are presented in Table 6.7.

Table 6.6(a) shows that the bias rate calculated by using the tails and feed streams, Bias (i), substantially differs from that calculated by using the wash water and concentrate streams, Bias (ii). A solids balance performed around the column also

Table 6.6(a)   Operating conditions and bias rate from mass balancing.

Run	Air rate (cm/s)	Tailings rate (cm/s)	solids (%)	Feed rate (cm/s)	solids (%)	Concentrate rate (cm/s)	solids (%)	W w rate (cm/s)	Bias (i) rate (cm/s)	Bias (ii) rate (cm/s)
Bias 01	0 87	0 73	36 00	0 48	27 60	0 16	—	0 29	0 10	---
Bias 02	0 87	0 73	18 74	0 58	29 09	0 19	55 11	0 22	0 05	0 07
Bias 03	0 87	0 73	32 65	0 6?	28 28	0 21	48 73	0 15	-0 07	-0 03
Bias 04	0 87	0 73	38 01	0 73	29 40	0 23	48.62	0 12	-0 13	-0 07
Bias 05	0.87	0 73	38 18	0 78	27 36	0 25	46 51	0 09	-0 18	-0 12
Bias 06	1 16	0 73	42 13	0 48	16 17	0 22	55 98	0 35	0 06	0 18
Bias 07	1 16	0 73	9 84	0 58	17 09	0 26	39 45	0 29	0 04	0 06
Bias 08	1 16	0 73	19 50	0 68	19 38	0 26	40 05	0 19	-0 06	-0 03
Bias 09	1 16	0 73	19 32	0.73	19.84	0 29	39 02	0 17	-0 11	-0 08
Bias 10	1.16	0 73	19 73	0.78	18 46	0 32	39 08	0 16	-0 16	-0 12
Bias 11	1 60	0 73	14 50	0 48	17.14	0.27	28 50	0 40	0 13	0 15
Bias 12	1.60	0 73	10.04	0 58	15 83	0 28	28 13	0 31	0 04	0 05
Bias 13	1 60	0 73	19 23	0.68	17.60	0.30	36 51	0 23	-0 07	-0 03
Bias 14	1 60	0 73	20 54	0 73	16 82	0 31	37 07	0 19	-0 12	-0 08
Bias 15	1 60	0.73	22 54	0 78	17 59	0 32	39 85	0 16	-0 16	-0 12
Bias 16	0 87	0.73	8.50	0.48	16 53	0 23	53 66	0 36	0 14	0 18
Bias 17	0 87	0 73	11.21	0.58	17.34	0 25	54 48	0 28	0 04	0 09
Bias 18	0 87	0 73	15 22	0.68	15.46	0 26	58.14	0.19	-0 06	0 00
Bias 19	0.87	0.73	19 54	0.78	18.27	0 27	58 86	0 11	-0.16	-0 10

Tailings flowrate includes gland water (0.11 cm/s)
Bias (i) = tails water rate - feed water rate
Bias (ii) = wash water rate - concentrate water rate

Table 6.6(b) Adjusted operating conditions and bias rate from mass balancing.

Run	Air rate (cm/s)	Tailings rate (cm/s)	solids (%)	Feed rate (cm/s)	solids (%)	Concentrate rate (cm/s)	solids (%)	W w rate (cm/s)	Bias (i) rate (cm/s)	Bias (ii) rate (cm/s)
Bias 01	0 87	0 76	11 11	0 47	27 60	0 11	—	0 29	0 19	—
Bias 02	0 87	0 76	13 50	0 55	29 09	0 10	55 11	0 19	0 11	0 11
Bias 03	0 87	0 76	15 88	0 65	28 28	0 13	48 73	0 12	0 01	0.02
Bias 04	0 87	0 76	17 34	0 69	29 40	0 14	48.62	0 10	-0 02	-0 02
Bias 05	0 87	0 76	17 95	0 74	27.36	0 14	46 51	0 04	-0 07	-0 07
Bias 06	1 16	0 76	3 98	0 47	16.17	0 06	55 98	0 23	0 19	0 19
Bias 07	1 16	0 76	5 76	0 55	17 09	0.11	39.45	0 20	0.10	0.10
Bias 08	1 16	0 76	6 99	0 65	19 38	0.16	40 05	0 16	0 01	0 01
Bias 09	1 16	0 76	8.37	0.69	19.84	0 17	39 02	0.13	-0 03	-0 02
Bias 10	1 16	0 76	8 37	0 74	18 46	0 16	39.08	0.07	-0 08	-0.07
Bias 11	1 60	0 76	2.59	0.47	17.14	0 20	28.50	0.38	0.19	0.19
Bias 12	1 60	0.76	3 81	0 55	15 83	0.20	28.13	0 29	0 10	0 11
Bias 13	1 60	0.76	5.76	0.65	17 60	0 17	36.51	0 16	0.01	0 01
Bias 14	1 60	0.76	6.60	0.69	16.82	0.16	37.07	0.11	-0 03	-0.03
Bias 15	1 60	0 76	7.32	0 74	17.59	0.16	39.85	0 07	-0.08	-0 07
Bias 16	0 87	0 76	5 09	0.47	16.53	0.05	53 66	0 23	0.19	0.19
Bias 17	0.87	0.76	6 83	0 55	17 34	0 06	54 48	0 15	0.10	0 10
Bias 18	0 87	0.76	8.13	0.65	15.46	0 05	58 14	0.04	0.00	0.00
Bias 19	0 87	0 76	9.95	0 74	18 27	0.10	58.86	0.00	-0.08	-0 07

Tailings flowrate includes gland water (0.11 cm/s)
Bias (i) = tails water rate - feed water rate
Bias (ii) = wash water rate - concentrate water rate

Table 6.7   Metallurgical results and conductivity values at 25°C of the streams around the column.

Run	Tails assay κ (mS/cm)	Cu (%)	Ni (%)	Feed assay κ (mS/cm)	Cu (%)	Ni (%)	Concentrate assay κ (mS/cm)	Cu (%)	Ni (%)	W w κ (mS/cm)
Bias 01	1.96	8 44	14 60	2 82	13 50	10 10	1 52	33 60	0 29	1 45
Bias 02	2 13	7 67	12 90	3 03	13 00	10 70	1 50	33 20	0 30	1 43
Bias 03	2 44	7 55	13 60	2 66	11 80	10 70	1 48	33 10	0 35	1 45
Bias 04	2 28	6 51	13 20	2 64	11 40	10 30	1 57	32 20	0 45	1 35
Bias 05	2 66	8 07	12 30	2 71	11 40	10 00	1 49	31 60	0 47	1 35
Bias 06	1 67	7 20	15.70	3 11	10 30	9 62	1 40	31 70	0 45	1 41
Bias 07	2.45	3 38	14 20	3 81	10 60	10 90	1 43	31 40	0 59	1 50
Bias 08	2 86	3 01	16.00	3.67	10 90	11 80	1 44	31 50	0 62	1 50
Bias 09	2 89	2.36	17.00	3.37	11 50	11 10	1 48	31 40	0 57	1 33
Bias 10	2 66	2.42	17 00	3 05	13 00	11.00	1 45	31 40	0 55	1 37
Bias 11	1 69	2 68	16.20	2 59	11 90	10 60	1 49	29 30	0 78	1 52
Bias 12	2 14	1 36	16 40	2.80	11 90	10.50	1 69	29 20	0 85	1 58
Bias 13	2.78	0 98	17 60	3 47	12 30	10 90	1.68	28 70	0 72	1 63
Bias 14	2 41	1 03	19.20	2 68	11 80	10 90	1.66	28 60	0 81	1 57
Bias 15	2.19	0.91	18.80	2.47	11 30	11 30	1 69	28 70	0 79	1 58
Bias 16	2.34	4 48	16 30	4.36	7 08	15 10	1 68	32 10	0 30	1 54
Bias 17	2.85	3 52	17.60	3 53	7.75	14 60	1 65	31 90	0 33	1 58
Bias 18	3.14	2.99	18 00	4.05	7 43	15.70	1 71	32.50	0 24	1 58
Bias 19	3 60	2.74	18.80	4 89	7 50	15.60	1.73	32.30	0 26	1 57

showed inconsistencies. The problem is most probably due to two factors: (a) problems with the calibration of the instruments, and (b) experimental error introduced in the sampling of the streams, particularly in the sampling of the tailing stream. This sample was taken from a sampling port located at the bottom of the column and not from the tailings stream (facility did not exist), which on reflection would be a more appropriate location. It is believed that the solids accumulating on the bottom of the column led to erroneous solid percentages in the laboratory samples, as compared to those reported from the instruments. When extra precautions were taken (allowing a flushing period of ~ 6-8 minutes), the difference between bias estimates was reduced but did not completely disappear. Samples carefully taken showed, for example, that while laboratory samples reported 8.50, 11.21, 15.22, and 19.54% solids (Runs Bias 16 to Bias 19), the control panel reported 6.00, 8.03, 9.53, and 11.64% (corrected for gland water), respectively. This is not the case with the feed stream where a very close agreement always existed between the laboratory data and the numbers reported by the instruments. Samples of the feed were collected from a sampling port on the stream just before entering the column. Concentrate samples were collected directly from the overflow.

In order to close the mass balance, the data were processed as follows: the numbers reported on the control panel for the solids percentage in the tailings stream were used; the flow rates of the feed and tailings streams were adjusted allowing a 5% error involved in the measurement; and, finally, the mass balance was closed by adjusting the wash water flowrate. Table 6.6(b) presents the adjusted operating variables. Because of the data manipulation, the numbers in Table 6.6(b) have to be considered as approximations only; however, they are good enough for comparison purposes.

Figure 6.19 and Figure 6.20 present the conductance profiles collected for the different operating conditions.
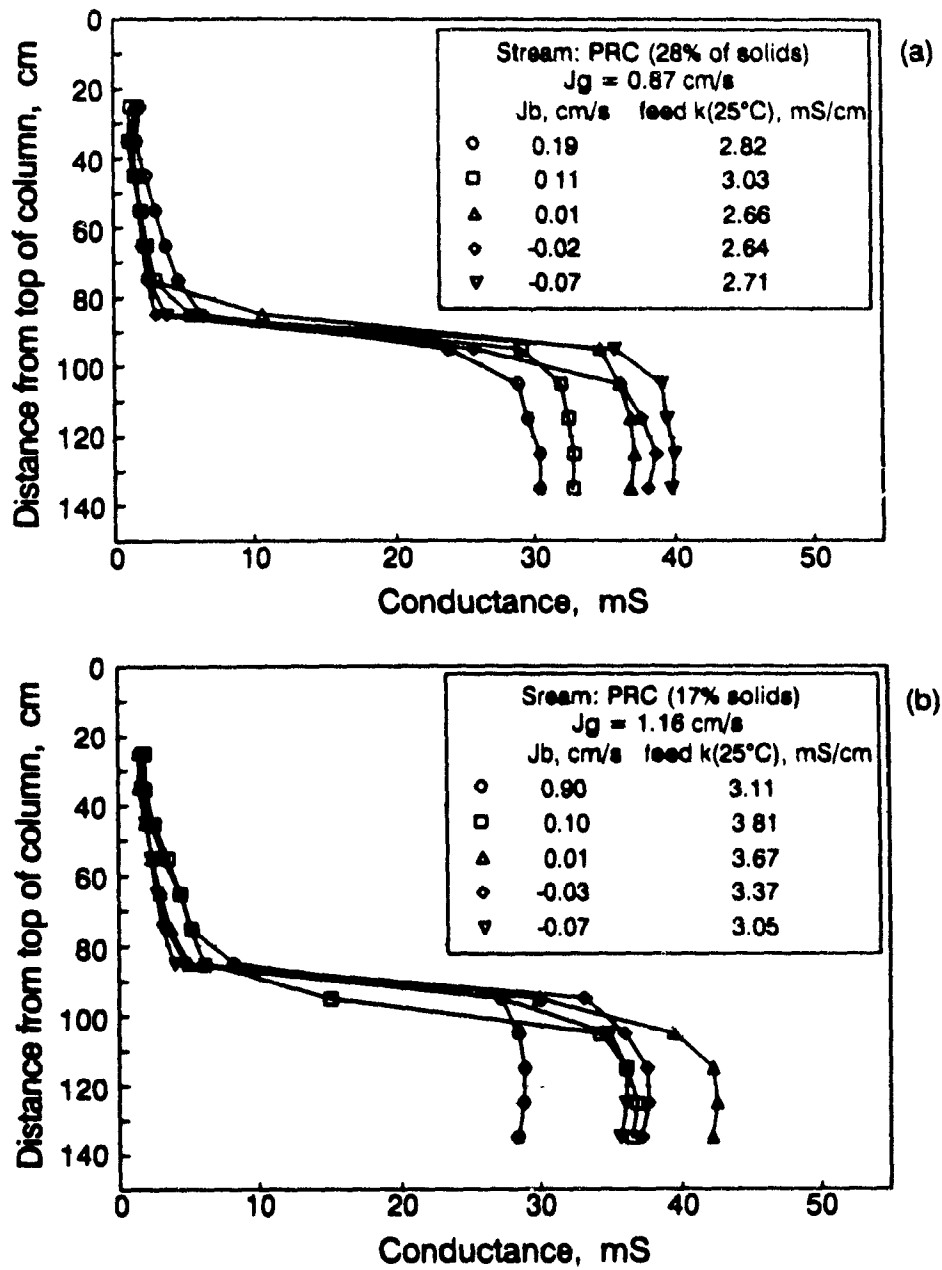
Figure 6.19   Conductance profiles for (a) Jg=0.87 cm/s and 28% solids, and (b) Jg=1.16 cm/s and 17% solids. PRC is Primary Rougher Concentrate
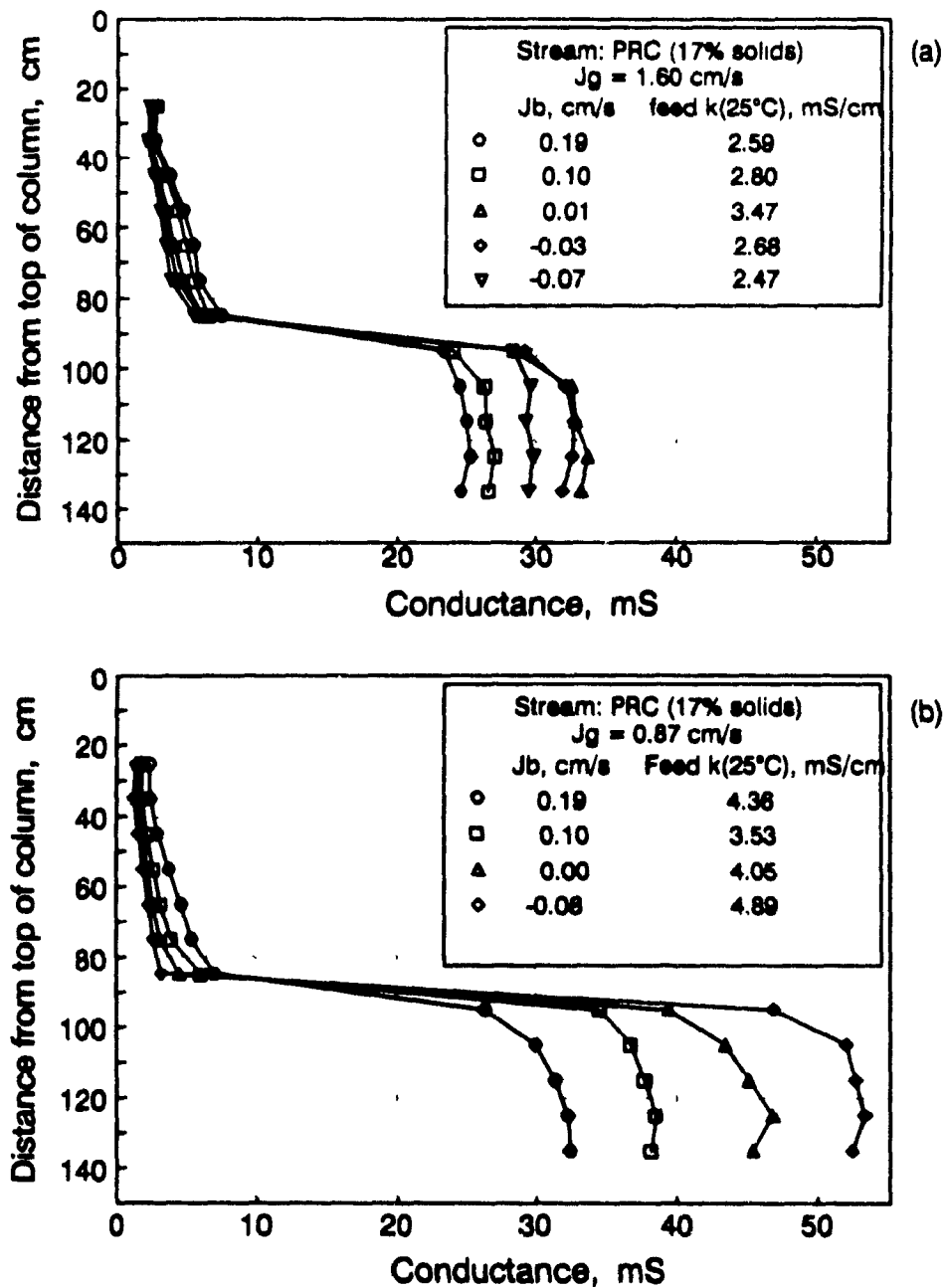
Figure 6.20 Conductance profiles for (a) Jg=1.60 cm/s and 17% solids, and (b) Jg=0.87 cm/s and 17% solids. PRC is Primary Rougher Concentrate

Conductance profiles: collection zone

The behaviour of the conductance profiles in the collection zone seems to be related to the bias rate. As the bias rate varied from positive to negative, the conductance of the collection zone increased as a consequence of there being less washwater flowing downwards to dilute the collection zone. This increase will occur provided the washwater has a lower conductivity than that of the feed water, which was the case under all circumstances here. Another condition that has to be satisfied is that the gas holdup (and solids holdup) in the collection zone, where the conductance measurements were performed, remains constant. This condition was approximated by keeping the gas flowrate and solids percentage in the feed stream constant.

Figure 6.19 and Figure 6.20 also show that changes in the conductivity of the feed water may have played a role in these changes. Figure 6.19(b) and Figure 6.20(a) show, for example, that the profile reached an approximately maximum value of conductance at around zero bias and then shifted back to smaller values of conductance. This shift was probably due to a decrease in the conductivity of the feed water. It is conventionally accepted, and the two-phase study tends to corroborate this, that at zero or negative bias, only small amounts, if any, of wash water flow downwards, which means that the conductance of the collection zone should remain constant provided the gas holdup and the conductivity of the feed remain constant.

A similar explanation is offered for the behaviour of the profiles in Figure 6.20(b). In this case, the position of the profile for the negative bias with respect to that at around zero bias, may well be due to the increase in the conductivity of the feed water observed.

Conductance profiles: froth zone

According to the two-phase study presented above, for a constant tailings and gas rate, a bias transition from positive to negative produced by decreasing the wash water rate, should translate into a shift of the profile towards larger values of conductance (See Figure 6.6(b), open circuit, option (ii)).

In the three-phase system however, the opposite was observed, that is, the profiles moved towards smaller values of conductance as the wash water rate was reduced. With the information available, a complete explanation to this behaviour can not be given although some thoughts are advanced.

During the tests, it was observed that the stability of the froth and its capacity to overflow solids decreased as the wash water rate was reduced. This is to be expected since two objectives of having wash water are to stabilize the froth and help transport solids. This reduction of solids removal rate was associated with an apparent build up of solids in the froth zone, exacerbated by the increase in the feed flowrate (solid flowrate) used to control level (This is in good agreement with the findings of Kosick et al.(1991) who report a substantial increase in froth zone density with a decrease in wash water addition, which is ultimately a consequence of a buildup of solids in the froth). Since, as was shown before, solids in flotation systems behave as a non conductive phase, the net effect was to reduce the conductivity of the froth. Thus, the proposed sequence of events is: as the wash water was reduced, the feed flowrate was increased, the liquid holdup in the froth zone reduced, but the solids holdup increased sufficiently to shift the profile towards smaller values of conductance.

This qualitative explanation is a preliminary one, and other possibilities such as secondary effects in the measurement of conductance introduced by the geometry of the probe, should not be discounted.
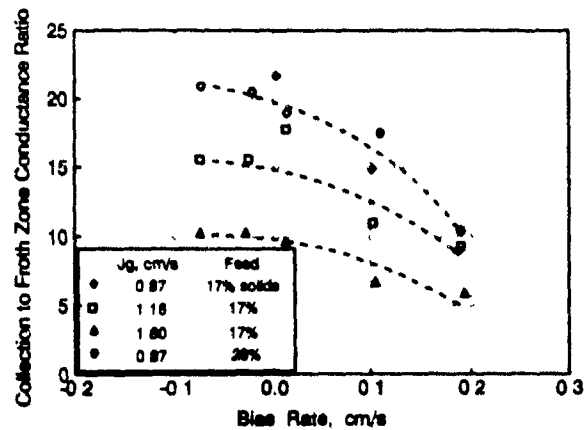
Figure 6.21   Slurry to froth zone conductance ratio vs bias rate

Figure 6.21 presents the collection to froth zone conductance ratio as a function of bias rate. This ratio was computed considering the averaged values of the conductance in both zones (the two measurements immediately on both sides of the interface were discarded because they are strongly affected by the proximity of the other zone). The trend observed in Figure 6.21 is qualitatively explained as follows: At a constant gas rate, the conductance ratio increases as bias rate varies from positive to negative because of a decreasing dilution of the collection zone water by the washwater. Below about zero bias there is no reason to expect further increases in the ratio as dilution is now essentially zero; the ratio does appear to level off. At a constant bias rate, the decrease in conductance ratio with increasing gas rate is expected (a) because of an increase in gas holdup in the collection zone (which causes a decrease in the conductance), and (b) because the liquid holdup in the froth zone increases. This interaction between the effect of gas rate and bias rate on the conductance ratio makes it difficult to relate the ratio to a unique bias rate value. However, Figure 6.21 presents experimental evidences indicating that large conductance ratios are related to negative, or small positive bias rates.

Figure 6.22(a) presents the copper grade in the concentrate as a function of bias
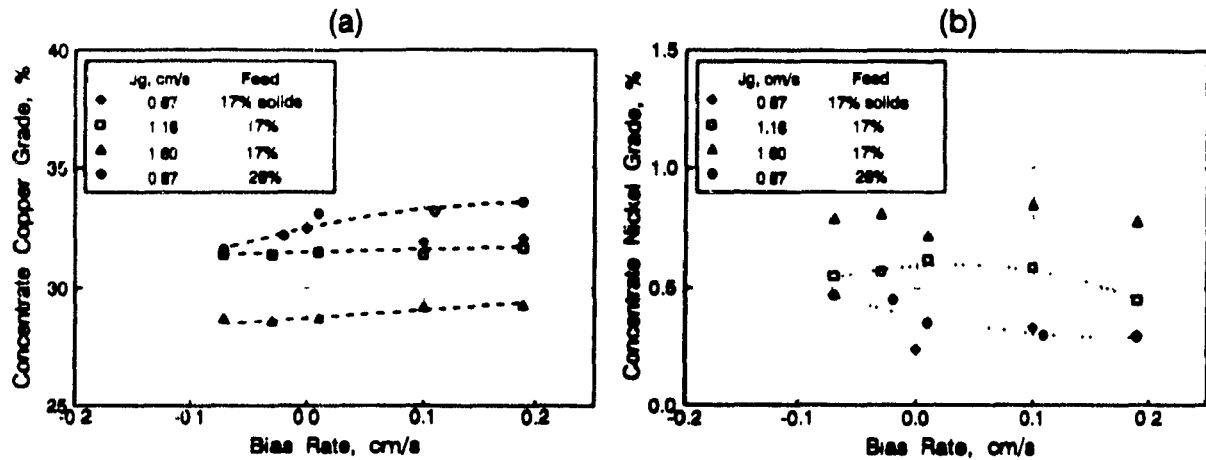
Figure 6.22   (a) Concentrate copper grade and (b) concentrate nickel grade as function of bias rate

rate. As expected, the copper grade decreases (although only slightly) as the bias rate varied from positive to negative. The role of the gas rate is also observed -large gas rates are related to lower grades. Grade/recovery curves cannot be obtained because of the problem (noted earlier) with the sampling of the tailings stream. Figure 6.22(b) presents the nickel grade as a function of bias rate. Here there was no clear trend, although it is possible that a slight increase in nickel grade occurred as the bias decreased. It is worth noticing that the gas rate seemed to play a more important role, concerning final concentrate grades, than the bias rate.

Feed water entrainment and recovery

Feed water entrainment was computed making use of the conductivity values of the water in the streams around the column (Table 6.7) and Equation (6.5). Figure 6.23 presents the results obtained together with 14 values obtained in a previous test performed using a similar experimental technique (Gomez and Finch, 1990). A trend similar to that found in the water-air laboratory study (See Figure 6.15) between bias and entrainment is observed. The plot also shows that substantial scatter existed, reflecting
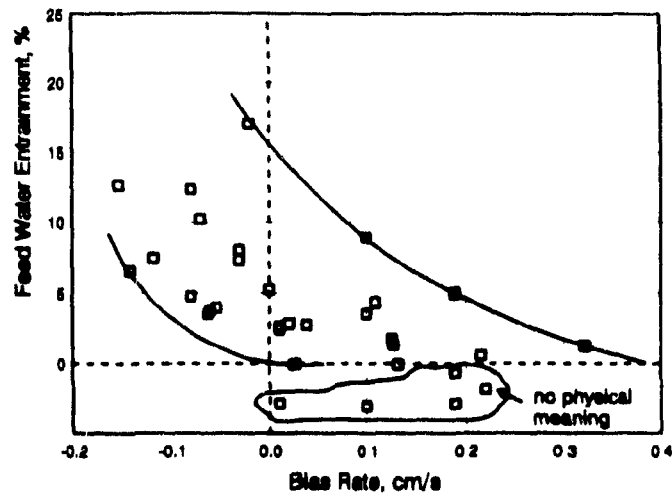
Figure 6.23 Feed water entrainment vs bias rate (solid lines indicate approximated boundaries)
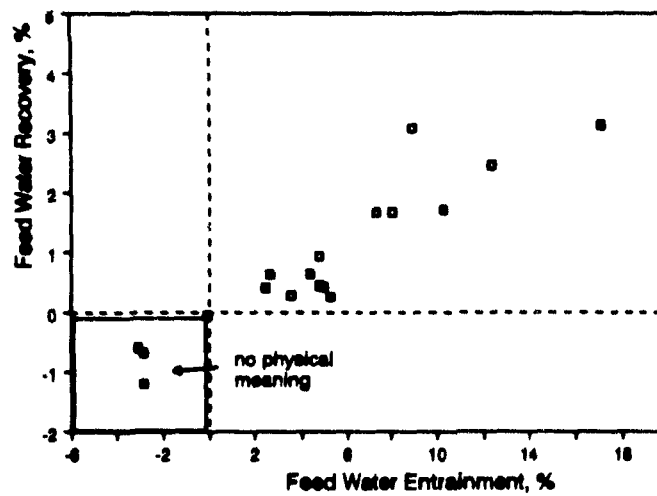
Figure 6.24 Feed water entrainment vs feed water recovery

the experimental error involved in the measurements. The negative values of entrainment, which are physically meaningless, further illustrate the experimental difficulties. However, the set of data demonstrates the feasibility of measuring feed water entrainment in three phase systems using a conductivity technique.

Feed water recovery was computed by using Equation (6.6) and the flowrates of the water in the feed and the concentrate streams obtained from mass balancing. Figure 6.24 presents entrainment vs recovery, showing that, within the limitations of the data, a linear relationship exists between the two parameters. As in the case of the water-air experiments, the range of entrainment values appeared to be better suited to detect trends, compared to the range of recovery values.

Figure 6.25 presents the feed water to tails water conductivity ratio. As expected, the ratio tended to unity as the bias rate varied from positive to negative values. However, ratios larger than one for negative biases are not in good agreement with the laboratory results which suggest that negative biases are connected with conductivity ratios equal to one.

Figure 6.26 presents the fraction of wash water reporting to the tailings stream calculated by using the equation

$$\frac{Q_{wt}}{Q_t} = \frac{\kappa_f - \kappa_t}{\kappa_f - \kappa_w}$$

(6.7)

(symbols were introduced before)

Interestingly, Figure 6.26 shows that the volume percent of wash water in the tails stream varied between ~ 20 and $\sim 70\%$. Such large values are necessarily related with bias rates greater than those obtained from mass balancing. It is worth remarking that although the experimental error involved in the conductivity measurements could be
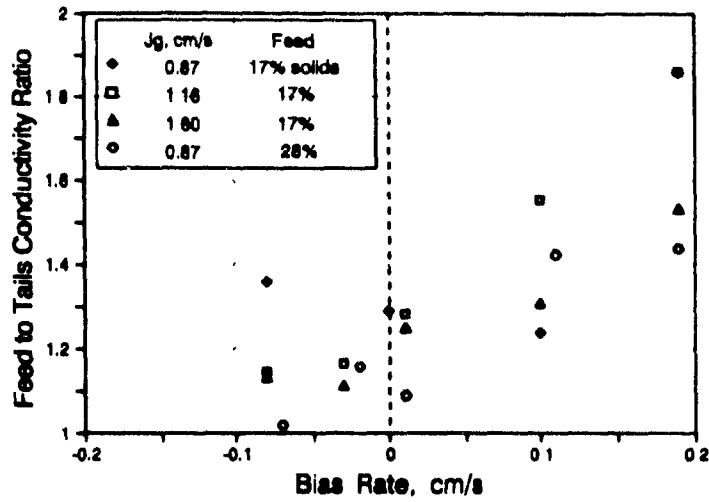
Figure 6.25 Feed to tails conductivity ratio vs bias rate
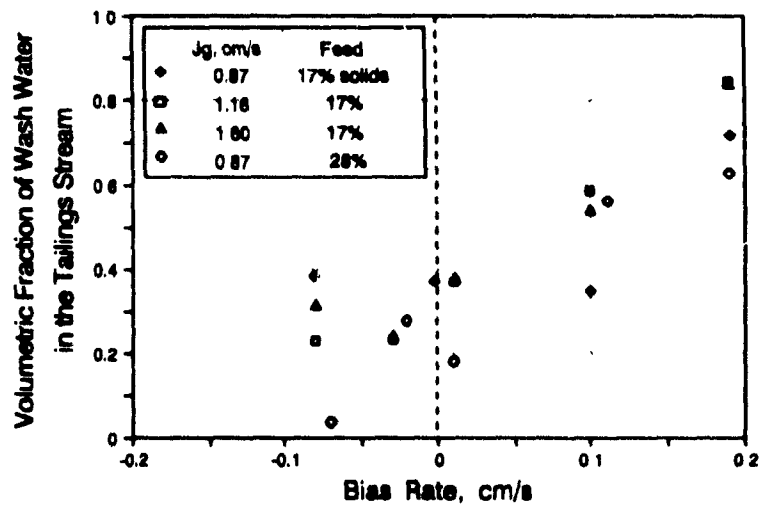
Figure 6.26 Volumetric fraction of wash water in the tails stream vs bias rate
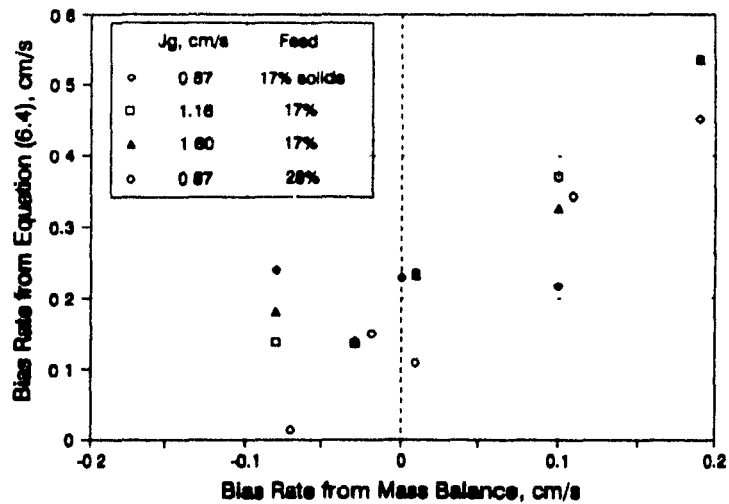
Figure 6.27 Comparison between bias calculated by the conductivity approach
and that from mass balancing

substantial, it is certainly smaller than that associated with the operating data presented in Table 6.6, thus probably being a more confident indicator of bias.

Figure 6.27 presents the bias rate from mass balancing against that obtained from the conductivity approach (Equation (6.4)). The plot shows that although a linear relationship is evident, the relative values indicate a significant discrepancy, again revealing the limitations in the experimental data. It is worth mentioning that both approaches to calculating bias involved the use of liquid flows in two (conductivity approach) and three (mass balancing) streams, making it difficult to judge their relative reliability. Nevertheless, Figure 6.27 does illustrate the magnitude of the error involved in the estimation of bias as pointed out by Finch and Dobby (1990a).

6.3   Summary

The effect of bias rate on the behaviour of conductance profiles collected around the froth/collection zone interface was discussed. For the conditions relevant to the

industrial situation (water in the flotation slurry was of higher conductivity than the wash water), the conductance profiles reflected the relative flows of the two waters across the interface and, therefore, the bias rate. Results at the laboratory and industrial scale were presented.

A case study was presented illustrating the difficulties involved in the estimation of bias rate using conventional methods (i.e. mass balancing). The alternative parameters feed water entrainment and feed water recovery, as measures of metallurgy, were introduced and experimentally explored.

CHAPTER 7

DISCUSSION

In flotation columns the target output variables are grade and recovery. However, because of the lack of a reliable and affordable method to measure these variables on-line (in most flotation columns on-stream chemical analysis is not available), secondary control variables such as level, gas holdup and bias rate have attracted attention.

7.1   Interface Level Measurement with a Conductivity Technique

The pulp level in flotation cells is the prime stabilizing control variable. The large froth depths and the geometry of flotation columns, making level particularly sensitive to disturbances, has prompted several new techniques for level detection in the last decade. Accuracy is one concern, although from the literature it is not clear how accurately level needs to be known. Examples in column flotation can be quoted from ± 20 cm being more than sufficient (Espinosa-Gomez et al., 1989) to ± 10 cm being far too great (Konigsmann, 1990). Accurate level detection, e.g. ± 1-2 cm, is not a trivial problem. It was shown in this work that conductivity profiling around the interface is a technique that has potential for level detection with such an accuracy.

7.1.1   Level detection from conductance profiles

In water-air systems the effective conductivity of the froth and bubbling zone are mainly dictated by the gas holdup in both zones. In industrial situations where the water chemistry of the wash water and slurry water is different, the effective conductivity will depend also on the proportions of the two waters in both zones. Normally, the wash water conductivity is smaller than that of the slurry water due to the addition of flotation

reagents (most of them are electrolytes) to the latter. Thus, for conventional operating conditions (e.g. positive bias), the water in the froth zone is largely made up by wash water while that in the collection zone is largely from the slurry water. This difference in gas holdup boosted by the difference in water conductivity in both zones makes the detection of level using conductivity profiles a reliable and effective technique.

It was shown in this work that the role of solids appears to be in reducing the effective conductivity of the slurry. For typical applications of flotation columns (e.g. as cleaners), the solids percentage in the froth zone, as reflected by the solids percentage in the overflow (concentrate stream), is large compared to that in the collection zone (approximately that of the solids percentage in the feed stream). This basically means that the ratio of the total holdup of non-conductive material in both zones will be larger than that expected from gas holdup considerations only. This will increase, again, the difference in the effective conductivity of the zones, enhancing the ability for discriminating, from conductance profiles, the froth/collection zone interface.

All these factors together, explain the excellent resolution of the profiles obtained in flotation columns as shown in Figures 4.22(a), 6.19 and 6.20 for the pilot column, and Figures 4.3 and 6.16 for the laboratory column.

The situation encountered in mechanical cells is different. Here, no wash water is added (in the conventional practice) and, therefore, the difference in conductivity between the zones will depend only on the total holdup (gas plus solids) in both zones. This translates into a less well resolved profile as illustrated in Figure 4.40.

7.1.2   Time delay in the detection of level

Owing to the nature of the commercial conductivity meter used, which has a time constant of about 0.5 s, the collection of a conductance profile requires a period of time

that depends on the number of points. Assuming that 99% of the actual conductance value is obtained after 5 time constants, e.g. ~2.5 s, have elapsed, collecting a 12 point profile will require a period of 12 points × 2.5 s/point = 30 s. This gives rise to a delay in the detection of level that has to be accounted for.

To qualitatively illustrate the nature of the problem let us consider a 1 m diam. × 11 m high column working in steady state conditions with a gas rate of $J_g = 1$ cm/s (7854 cm³/s). Let us consider also a step change in gas rate to $J_g = 1.2$ cm/s (9425 cm³/s) and qualitatively estimate the expected velocity at which, initially, the level is going to move.

By increasing the gas rate to 1.2 cm/s, the increment of volume of air entering the column will be

$$\Delta V - J_{g_2} A_c - J_{g_1} A_c - 1570 \ cm^3/s \ ^{(*)}$$

This means that the collection zone will increase its volume by 1570 cm³/s which will translate into a level rising with a velocity of

$$u_L - \frac{\Delta V}{A_c} - \frac{1570 \ cm^3/s}{7854 \ cm^2} - 0.2 \ cm/s$$

(*) This volume of air is referred to STP conditions. Inside the column, this volume has to be corrected for hydrostatic pressure head which will depend on the specific position along the vertical axis of the column.

This transition condition will prevail until the collection zone attains a new steady state condition, most probably indicated by a stable value of the (new) gas holdup.

Considering bubbles in the order of 1 mm rising in "contaminated water" with a terminal velocity U_T, of ~ 10 cm/s (Clift et al., 1978), the bubble slip velocity can be obtained by using Richardson and Zaki's (1954) expression for a typical fractional gas holdup of 0.15 and $m=2$ (Xu and Finch, 1990):

$$U_s - U_T (1 - \varepsilon_g)^{m-1} - 10 \ cm/s \ (1 - 0.15) \sim 8.5 \ cm/s$$

The bubble swarm rising velocity, U_b, is related to the slip velocity, U_s, by the definition of the relative or slip velocity

$$U_s - \frac{J_g}{\varepsilon_g} + \frac{J_l}{\varepsilon_l} - U_b + \frac{J_l}{\varepsilon_l}$$

which gives, for a typical slurry downward velocity of 1 cm/s,

$$U_b^{(*)} - U_s - \frac{J_l}{\varepsilon_l} - 8.5 \ cm/s - \frac{1 \ cm/s}{0.85} \sim 7.3 \ cm/s$$

Assuming that the rising of level will occur until the first bubbles of the increment of air reach the interface located 10 m above the sparger, the rising of level will last a period of time of

---

(*) In three phase systems bubbles rise at a lower velocity due to solid particles loading which increases the density of the bubble-particle aggregate.

$$t \sim \frac{L \ (column \ length)}{U_b \ (bubble \ swarm \ velocity)} \sim \frac{1000 \ cm}{7.3 \ cm/s} \sim 137 \ s$$

According to this, the expected change in level caused by the increase in gas rate will be

$$\Delta L \sim v_L \times t \sim 0.2 \ cm/s \times 137 \ s \sim 27 \ cm$$

and the shift in level position in the period of time of a scan (30 s for the present case) of

$$\Delta L_{scan} \sim 0.2 \ cm/s \times 30 \ s \sim 6 \ cm$$

which is 18% of the total expected change[*].

It is evident from the above computations that the potential error introduced by the existence of a delay in the detection of level is of the order of magnitude of the accuracy of the detection (± 5 cm in the probe introduced in this work); also, the period of time when this transition condition prevails is relatively small. It is worth mentioning, however, that the velocity of variation of level could be greater when more than one stream is varied at a time. For example, an increase in gas rate is often accompanied by an increase in wash water addition (to maintain a constant bias rate), both of which produce an initial rise of level. It is, therefore, desirable to decrease the scanning time, probably by using a conductivity meter with a shorter time constant or by developing a dedicated electronic circuitry that enables the measurement of conductivity at "n" points instantaneously. This latter option has the further attraction of providing an instrument

---

(*) After the "new" bubbles reach the interface, the level will drop due to the increase in the amount of liquid being carried to the froth (and eventually to the overflow) by these new bubbles.

to follow dynamic changes in level; also, the size of the probe (number of conductivity measurements) would no longer represent a constraint, and applications where large detection lengths are required (~ 2.5 m) would be satisfied.

7.1.3 Step shape response of the conductivity system

Due to both the specific electrode arrangement used in the level detection probe (Figure 4.21)(and in the laboratory column) and the algorithm used to process the data (the "largest slope" algorithm), the resulting level estimate has a step shape behaviour. A continuous signal is, however, more desirable. It was said in this work that the problem can be mitigated by reducing the separation between the electrodes in the probe, by further interpolation of the raw conductance data, and by filtering the signal.

It was shown that in flotation columns, conductance measurements every 10 cm plus interpolation of the conductance data around the interface allows the detection of level with an accuracy in the order of ± 1-2 cm. In mechanical cells (Dorr-Oliver, for example), the behaviour of the profile (reflecting the nature of the operation) does not allow such an interpolation. Reducing the separation between the electrodes is preferable in this case since an accuracy of ± 5 cm (positive electrodes being separated by 10 cm) may represent a large relative error (typical froth depths are ~ 30 cm). Reducing the electrode separation has the further attraction of providing a measurement of the froth height (by starting the profiling above the froth and detecting the change in slope, see Figure 4.44). This will provide a more complete picture of the cell operation and will enable the detection of conditions where the pulp level is at the set point but the cell is running with no froth.

Figure 7.1 presents an 8 hour strip chart recorded for two different level detection devices tested in parallel in a 38 m³ mechanical (Dorr-Oliver) cell (Strathcona mill, Falconbridge Ltd.). The full line, ROWT LEVEL IND. RUNNING, corresponds to the
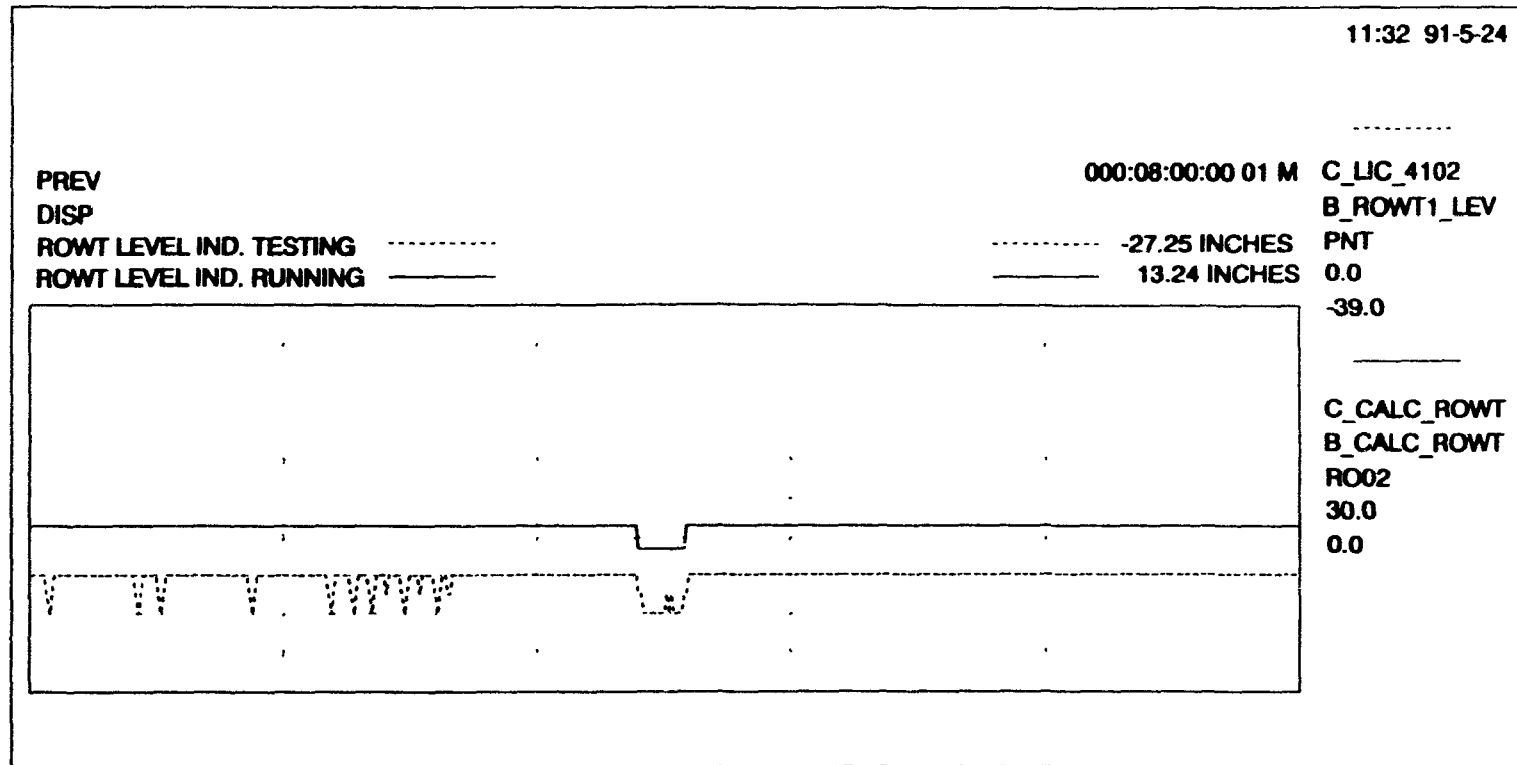
Figure 7.1 Strip chart recorded for two different level detection devices tested in parallel in a 38 m³ mechanical cell (Strathcona mill, Falconbridge Ltd.). The full line is the signal of a bubble tube and the dashed line corresponds to the signal of the conductivity probe

signal of a bubble tube with a span of 0 to 76 cm (0 to 30 in; the base line of the chart corresponding to the cell lip and the top line corresponding to 76 cm (30 in) below the lip), and the dashed line, ROWT LEVEL IND. TESTING, corresponds to the signal of the conductivity probe (Figure 4.1) with a span of 0 to -100 cm (0 to -39 in; the base line corresponding to the cell lip and the top line corresponding to 100 cm (-39 in) below the lip).

Observed in Figure 7.1 is the step shape response of the conductivity system to momentary variations of level. This behaviour is not observed with the bubble tube probably because of the inertia of the pressure-based system and to the filtering of the signal. Figure 7.2 shows that the raw response of the detection algorithm of the conductivity system can be smoothed by filtering the signal using a first order lag model (Equation (4.2)). Figure 7.2 also shows the effect of the magnitude of the time constant, T, on the filtering (when the level changes, five time constants are required to attain 99% of the new level location).

7.1.4   Ranging of the system and detection of high and low levels

Another problem that has to be addressed concerns the "ranging" of the conductivity system and with the detection of levels above and below the detection span of the probe.

The ranging of the system can be solved by implementing the circuitry reported by Moys (1989) (see Figure 2.4). According to Moys, the conductivity meter can be ranged with the resistance measured with an electrode always immersed in the slurry zone. In this way, conductivity changes of the slurry will be accounted for.

The detection of high levels can be solved by simply locating the top probe's electrode a few centimeters (5 cm, for example) above the cell lip. By doing so, this
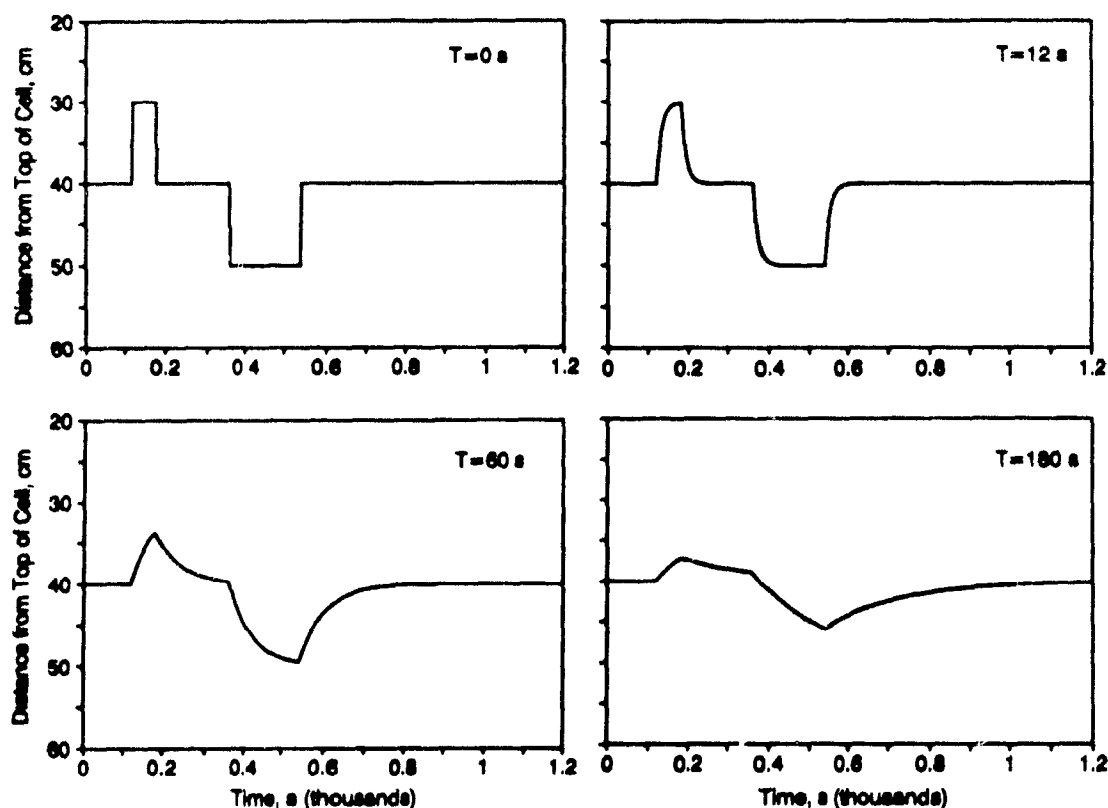
Figure 7.2 Effect of the time constant T (s), on the filtering of the signal of the "largest slope" level detection algorithm (updating time is 60 s)

electrode will always measure the conductance of the froth while those below will report that of the slurry. The largest conductance difference will, therefore, occur between the first and second electrode (from the top) and the level will be reported as being between them, that is, at around the lip level.

Detection of low levels is more complex. Due to the present design of the conductivity system, levels below the span of the probe cannot be discriminated and the system keeps collecting profiles, obtaining the largest difference in conductance and incorrectly assigning the position of the level correspondingly. Several alternatives to

solve the problem have been contemplated.

The immediate alternative consists in comparing the largest conductance value of the largest conductance difference (that should correspond to the pulp conductance), with a *typical* value of pulp conductance, let us say -30 mS (see Figure 4.40). If the largest value is in the order of magnitude of that of the pulp, the difference in conductance is being originated by a real froth/slurry interface. If the value if substantially smaller than the slurry value, the conductance difference is artificial, indicating that the true level is below the probe. This alternative, however, faces the problem of the selection of the *typical* slurry conductance. It has been observed that such a value is subject to sudden and substantial changes (see Figures 6.19 and 6.20).

The second alternative, illustrated in Figure 7.3, consists in having an electrode located below the *working electrodes* that would serve to range the system and to provide the conductance of the slurry to discriminate whether the interface is real or fictitious. This alternative requires an increase in the length of the probe.

The third alternative consists in performing a linear regression on the conductance profile and judging, based on the value of the correlation coefficient, R, whether the interface is real (it is expected that $R^2 << 1$) or fictitious ($R^2 \sim 1$). Figure 4.3 illustrates cases where these two situations apply.

7.1.5 Testing the probe for long term operation

The conductivity probe and the data acquisition system described in Section 4.3 (a TBI-Bailey Mod. 440 conductivity meter was used) were installed in a 38 m^3 Dorr-Oliver cell at the Strathcona mill, Falconbridge Ltd. The 4-20 mA output (proportional to level) of the conductivity system was connected to the mill's control room. A long term evaluation of the system was initiated in May the 19th, 1991. Strip chart printouts
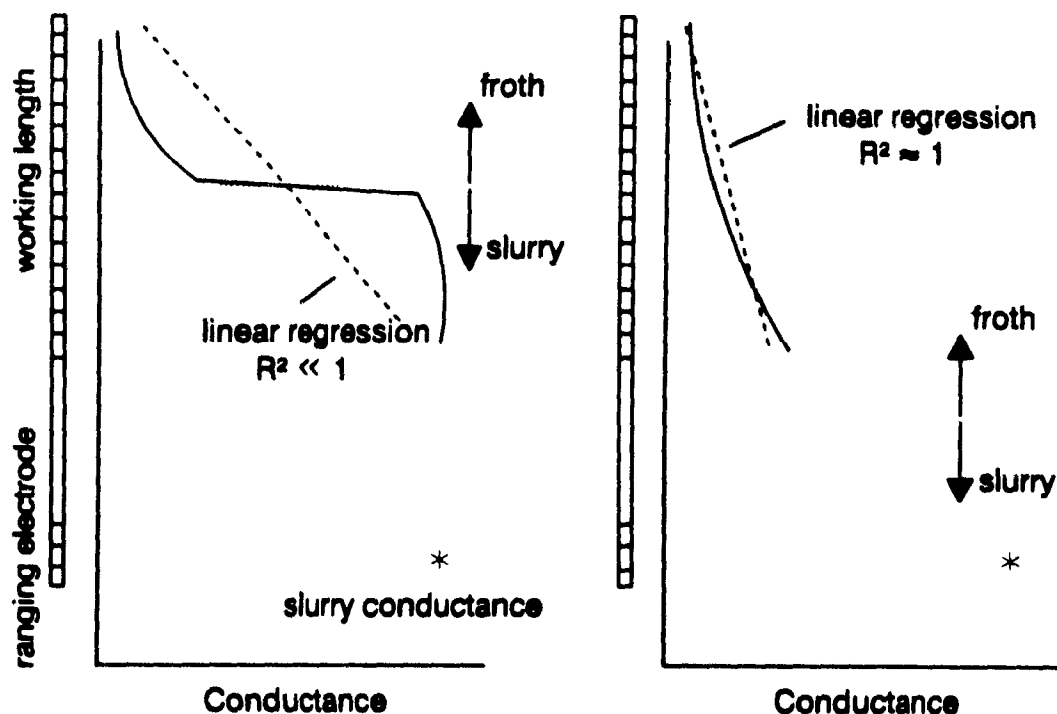
Figure 7.3 Schematic representation of the alternatives for the detection of a low level condition

were obtained every four or five days, or every time interesting events occurred.

After two months of permanent operation the probe was withdrawn from the cell and visually inspected. It was observed that the section of the probe immersed in the slurry zone was completely free of solids deposits; the section immersed in the froth zone ($\sim$35 cm; the froth depth set-point was $\sim$30 cm), however, did show solids deposits. These deposits were relatively small ($<$ 1 cm thick) and not uniformly distributed on the surface of the probe; the deposits were removed by simply hand rubbing the probe surface. Interestingly, the deposits did not affect the performance of the probe as judged from the similar performance of the probe before and after the deposits were removed.

It is believed that the buildup of solids in the section of the probe in the froth is due to the less turbulent flows and to the greater solid percentages, as compared to those encountered in the slurry zone.

Another problem observed during the testing period was the spontaneous appearance (and disappearance) of a "noisy" signal outputted by the system (Figure 7.4). It is believed that the operation of the conductivity meter is temporarily affected by the electrical environment of the plant. Such a problem has been observed (although very rarely) at McGill laboratories and related to the operation of large motors and electric furnaces. When the problem occurs, the conductivity meter simply malfunctions and the conductance profile collected contains random values which translates into random "largest slopes" (outputted signal). The conductivity system is an experimental one whose main objective was to demonstrate the level detection concept, which has clearly been achieved.

7.2 Gas Holdup Estimation from Conductivity Measurements

Conductivity based techniques to estimate gas holdup in fluidized beds are of common use. In flotation columns, Yianatos et al. (1985) were the first to perform such measurements successfully. A model based on the concept of tortuosity was developed.

Classical models such as that of Maxwell (1892) and Bruggeman (1935) appear to be adequate to describe the physical situation encountered in flotation columns. In the end, the problem reduces to one of measuring the effective conductivity of the dispersion.

The electrical conductivity of electrolytes is conventionally performed with a cell that approaches, as much as practically possible, one of the three geometries that allow for uniform current density over the entire surface area of the electrodes (and over all the equipotential surfaces of the potential field established in the electrolyte). For these

10:04 91-5-22

05/21/91 10:04:46
05/22/91 10:04:46 ....
05/22/91 10:04:46 C_LIC_4102

PREV
DISP   B_ROWT1_LEV
ROWT LEVEL IND. TESTING .... -31.15 INCHES PNT
ROWT LEVEL IND. RUNNING ————   ———— 13.32 INCHES 0.0

-39.0

C_CALC_ROWT
B_CALC_ROWT
RO02
30.0
0.0
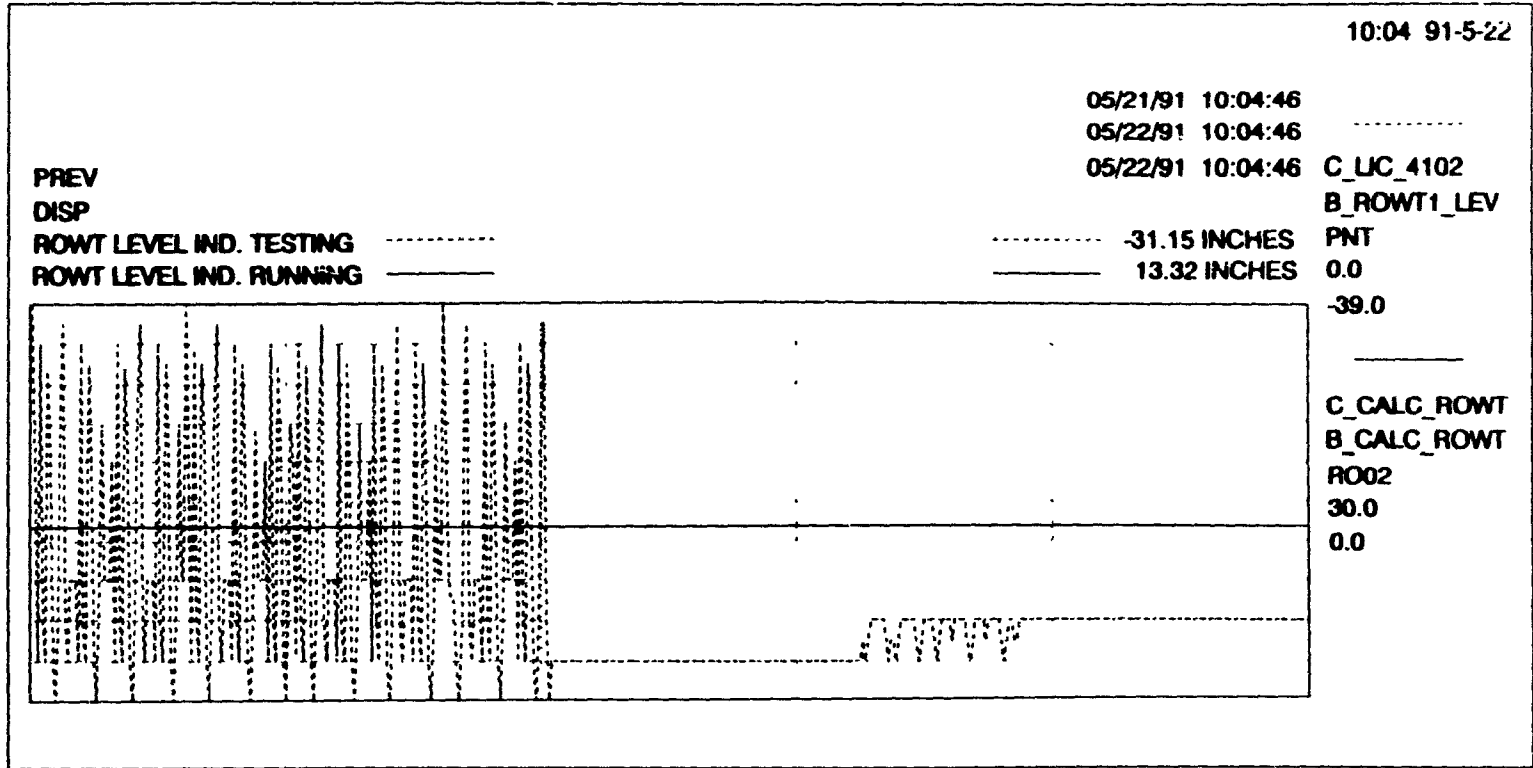
Figure 7.4 Strip chart recorded for two different level detection devices tested in parallel in a 38 m^3 mechanical cell (Strathcona mill, Falconbridge Ltd.) showing the spontaneous appearance of electrical noise in the signal of the conductivity probe (dashed line)

type of cells the conductance measurements and the intensive property to quantify (electrical conductivity), are related by simple mathematical expressions. For any other cell geometry the development of such a relationship involves mathematics that are not elementary. The difficulty arises when the description of the evolution of the potential and current fields is attempted. Because of this, the use of an adaption of one of those three geometries (cells) was preferred in this work.

7.2.1 The conductivity cell formed by grid electrodes

It was shown in Chapter 5 that a conductivity cell formed by two grid electrodes covering the entire cross-sectional area of the column produces conductance measurements from which the effective conductivity of the multiphase system could be estimated by using the equation (Equation (3.8))

$$K - \frac{A}{l} \kappa \tag{3.8}$$

(symbols were introduced before)

Cells that depart from the "ideal" ones tend to underestimate the value of the conductivity, most probably because of the appearance of secondary effects such as polarization and/or poor sampling of the system.

In water-air laboratory columns, it was observed that the equation proposed by Kato et al. (1981) better described conditions where relatively big bubbles (>2 mm) were present (no frother added). This may be due to the resemblance of this condition to that encountered in fluidization systems where relatively big bubbles are common and for which, the relationship of Kato et al. was developed. As soon as frother was added, the bubbles became smaller (and probably of more uniform size) and the models of Maxwell and Bruggeman better fitted the experimental data. No significant difference

between the predictions of the two models exists in the range of gas holdup expected in column flotation (up to ~ 20 %).

7.2.2 The conductivity cell of the level detection probe.

Gas holdup estimation in water-air systems at the industrial scale was also explored. The experiment were conducted off-line. The conductance measurements in the water-air dispersion and in water only were conducted making use of the level detection probe (Figure 4.21). The gas holdup estimates were compared with those obtained from the pressure readings of several pressure sensing devices installed along the vertical axis of the column.

The results showed that fairly good agreement existed between the estimates from conductivity measurements and those from pressure, thus indicating that under the conditions imposed the conductivity cell of the probe is adequate to obtain fairly sound conductance measurements. The analysis of the behaviour of the apparent cell constant of the probe's cell showed, however, that for liquids of high conductivity (> 1-2 mS), the conductivity cell suffers from secondary effects that could hinder its performance. Such effects may well be the appearance of polarization phenomena which are more likely to occur at high conductivities.

The pressure readings collected along the column showed a significant (~ 100%) increase in gas holdup from bottom to top. This increase is partly due to the natural expansion of the bubbles as they rise to locations of diminishing hydrostatic pressure head. This phenomenon certainly poses the question regarding the appropriate location to measure the "local" gas holdup in a flotation column. The phenomenon has not been studied in detail in three-phase system mainly due to the lack of an independent method to compare the estimates, although there exists some evidence that suggests the *density* of the three-phase system remains constant from bottom to top (Huls et al., 1990). In the

absence of actual measurements, if the slurry density is considered constant, a constant zone density translates into a constant gas holdup, which is at odds with the two-phase study. A technique combining conductivity and pressure readings for measuring gas holdup in three phase systems, similar to that used by Begovich and Watson (1978) for fluidized beds, would help elucidate the situation.

7.2.3 Solids holdup estimation from conductivity

In any attempt at measuring gas holdup in flotation columns, the effect of the presence of solids must be taken into account. In this work, it was found that the holdup of non-conductive solids (silica) and conductive solids in flotation pulps (chalcopyrite and pentlandite, for example) could be estimated in the same way as was done for gas bubbles, that is, using Maxwell's (or Bruggeman's) model. The case of silica is not difficult to understand since it falls within the assumptions of the models. The case of the sulphides does not have a straightforward explanation. There is some evidence to indicate that particles of freshly ground sulphides (pyrite), do behave as conductive solids when slurried in water. Thus, it is believed that reactions such as the formation of a xanthate layer, an elemental sulphur layer or an oxide layer on the surface of the solids may render the particles non-conductive. Independent work conducted by Espinosa-Gomez (1990) at Mount-Isa Mines Ltd., Australia, supports these findings. More systematic work to investigate this phenomenon is required.

7.2.4 Gas holdup in three phase systems

The estimation of gas holdup in a three phase system requires knowledge of the effective conductivity of the three phase dispersion and of the effective conductivity of the slurry. Again, Maxwell's (or Bruggeman's) model can be used to estimate the gas holdup.

The possibility of obtaining these two measurements on-line was demonstrated at the laboratory scale using a silica slurry-air system. An independent technique, termed isolating technique, to collect a sample of the three phases system was implemented. The results showed acceptable agreement between the estimates from conductivity and those from direct measurement of the holdup. As a first approximation it can be said that the holdup of the non-conductive phases obtained from conductivity are additive, that is to say, the sum of the gas holdup computed by using κ_{l+g} and $\kappa_{l,s}$ in Maxwell's equation, and the solids holdup computed by using $\kappa_{l,s}$ and κ_l is, approximately, the total holdup obtained by using κ_{l+g} and κ_l.

7.2.5 Gas holdup estimation at the industrial scale

Measurements of the effective conductivity of slurry-air systems in industrial flotation columns can be accomplished by using the level detection probe or a conductivity cell similar to the one used here in laboratory columns (a section of a cylindrical tube 5-10 cm diam. supporting two grid electrodes and having its vertical axis parallel to that of the column). The problem remains in the measurement of the effective conductivity of the slurry (to estimate gas holdup) or the conductivity of the liquid (to estimate the total holdup). It is worth remarking that these conductivities should be measured simultaneously and as close as possible to the position where the conductivity of the three phases is measured. This restriction is posed by the probable existence of a solid percentage profile as well as a profile of liquid conductivity, although the mixing characteristics prevailing in large unbaffled columns (being close to well mixed reactors from mass transport point of view) may lift such a restriction. Nevertheless, the design of the appropriate sensor remains a challenge.

7.3 Bias Rate

As was discussed in this work, with a case study presented, the estimation of bias

rate using conventional methods (e.g. mass balancing) is subject to error. Because of this, intensive properties of the system such as temperature and electrical conductivity have been proposed to measure bias, or a bias-related parameter.

When a difference in temperature between the wash water and flotation slurry exists, temperature profiles around the interface have been demonstrated to give an indication of the bias rate and of the efficiency of the cleaning action of the froth zone. The temperature profiles reflect the relative amount of slurry water, and therefore of fine non-floatable particles, in the froth zone.

7.3.1 Bias rate and conductance profiles

In this work it was shown that, in general, conductance profiles (or conductivity profiles if the appropriate cell is used) also reflect the bias rate, especially under the conditions encountered in industrial operations where the wash water is of lower conductivity than that of the slurry water. This natural difference in conductivity may be enhanced if the wash water is cooler than the flotation slurry (which has passed through a grinding mill, several pumps and perhaps a bank of conventional stirred flotation cells (Moys and Finch, 1988a)).

a).- Water-air systems

From the conventional definition of bias rate, that is, the net flow rate of water across the froth/slurry interface, it is expected that knowledge of the relative proportions of wash water and slurry water around the interface may lead to an identification of the bias. The present work has shown that conductance profiles are a possible indicator.

In general, for the relevant conditions encountered in industrial operation (wash water conductivity smaller than the slurry water), the profiles shift towards larger

conductance values when the bias changes from positive to negative values. The increase in the conductance of the bubbling zone (air-water system) reflects the increased proportion of feed water in the bubbling zone water; because the bias is reduced, the volume of wash water entering this zone is reduced with the consequent increase in the conductance of the bubbling zone. The increase in conductance in the froth zone is similarly related to an increased proportion of feed water in the froth zone water as bias is reduced.

These variations are easy to interpret at the laboratory scale where the effect of the input variables are readily isolated (by maintaining the wash water fixed while varying the gas rate and controlling the level with the feed, for example). However, under industrial conditions the interpretation of the profiles is difficult since conventional control strategies demand simultaneous variations of gas rate and wash water rate. For example, it is common practice that an increase in gas rate (with the aim of improving recovery) is accompanied by an increase in wash water (to compensate for the increase in feed water being driven to the froth zone and, eventually, to the overflow) to maintain a constant bias. (Probably only minor changes will be required in the tailings, or feed, stream so, effectively, a constant bias is achieved).

Now, let us assume that the "constant bias" strategy does achieve a constant bias, which means that the additional feed water driven to the froth is being replaced by the additional wash water added to the column in such a way that the proportions of wash water and feed water around the interface remain the same. Under this condition the conductance profiles should not vary (move) since the bias has remained the same. In reality, the profiles will move because of a change in gas holdup in both zones. In the bubbling zone the profile will shift towards smaller values of conductance because of an increase in gas holdup (due to the increase in gas rate). In the froth zone the profile will shift towards larger conductance values because of an increase in liquid holdup. This situation does not contradict, however, the statement that the profiles shift towards larger

conductance values when the bias is reduced, but requires some intelligence to interpret the variation. Figure 7.5 presents the trends observed in the laboratory (Figure 7.5(a) and (b)), and that proposed for the situation where both the gas rate and wash water rate are varied simultaneously to achieve a constant bias.

b).-   Slurry-air systems

In slurry-air systems, amenability testing performed using a 5.04 cm diam. column showed that the conductance profiles around the interface were related to the bias rate in the way proposed before, that is, the profiles shifted towards larger conductance values when the bias was decreased (from positive to negative values).

Bias experiments performed in a 91 cm diam. industrial column showed, however, an additional complication, which probably arises from the way the bias variation was produced. In these experiments constant gas and tailings rates were used; the bias was varied by varying the wash water rate and the level was controlled with the feed. It was observed that the bias rate varied from positive to negative values as the wash water rate was reduced. According to this, it was expected that the profiles would shift towards larger conductance values. The branch of the profile in the collection zone, in fact, did shift to larger values but that in the froth zone, interestingly, shifted towards smaller values. It is believed, and visual observation tends to corroborate this, that a buildup of solids in the froth zone occurred as the wash water rate was decreased. This buildup of solids translated into an increase in the total non-conductive material (gas and solids) which overwhelmed the presence of increased amounts of slurry water. Such a buildup of solids when the wash water rate is decreased has been documented (Kosick et al., 1991). In water-air systems, however, a decrease of the bulk density (increase in gas holdup) of the froth zone occurs when the wash water is reduced.

Besides this problem, potential complications arise from the fact that the
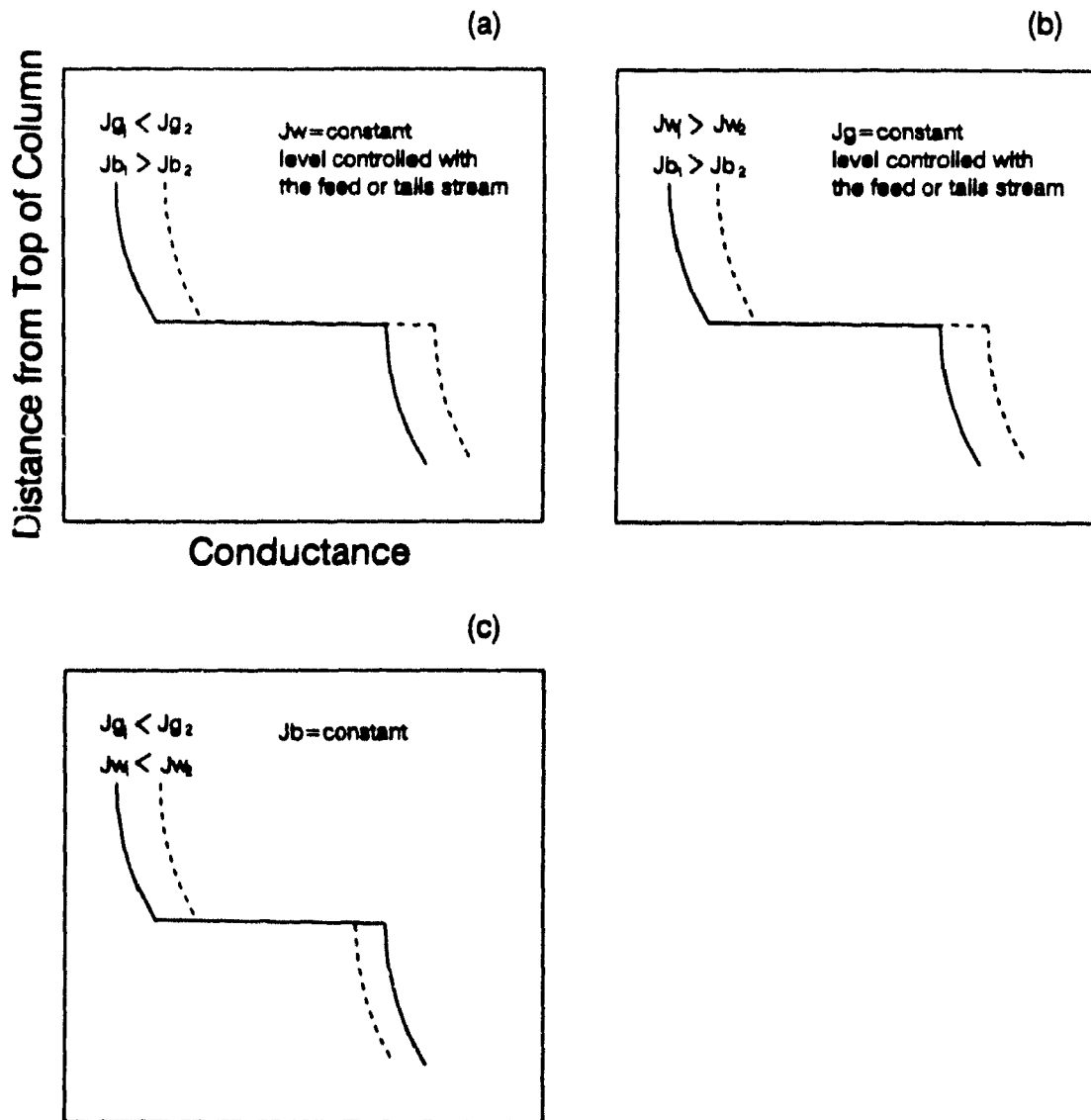
Figure 7.5 Schematic illustration of the effect of input variables wash water and gas rate on the behaviour of conductance profiles in a water-air system: (a) and (b) are trends experimentally observed; (c) is the suggested trend

conductivity of the slurry water is subject to substantial temporary variations, thus producing changes in the conductance profiles which are not related to changes in bias rate. Monitoring the conductivity of the slurry may help to discriminate such variations and to isolate the changes due to bias. Such a normalization requires a sensor (that probably is not commercially available) installed in the feed stream.

Another parameter obtained from the profiles, the *collection to froth zone conductance ratio*, appears to be promising since, in general, the ratio decreases as the bias varies from negative to positive values. However, the complication here is that a family of ratio vs bias curves for different gas rates appears to exist. The consequence is that for a specific bias rate, the value of the ratio depends upon the gas rate, thus making it difficult to relate the conductance ratio with a unique bias rate.

It is evident from the above discussion that the interpretation of the conductance profiles and any additional information extracted from it will require, most probably, the intelligence of an expert system to exploit fully.

7.3.2 Bias rate, feed water entrainment and feed water recovery

While the initial emphasis was to estimate bias, these other measurements were increasingly seen as attractive alternatives. Feed water entrainment was defined here as the volumetric fraction of feed water in the overflow (concentrate), Q_{fc}/Q_c, while the feed water recovery is the volumetric fraction of feed water reporting to the overflow, Q_{fc}/Q_f. Preliminary experiments demonstrated the possibility of making these measurements in industrial scale columns. The results showed that the feed water entrainment and recovery increased as the bias rate was decreased. It was found that the feed water entered the overflow even when bias was positive.

The question regarding which parameter to use has two parts: which is the most

reliable and which is the most indicative of metallurgy.

For the first, the answer is feed water entrainment. It requires only three conductivity measurements, κ_c, κ_w and κ_f, whereas both bias and recovery require in addition two flow measurements. As was shown for estimating bias (Finch and Dobby, 1990a) this leads to a large uncertainty in the calculated value, especially in the industrial situation where the flow measurement requires a combination of slurry mass flow and percent solids. A further attraction of the entrainment parameter is its range, 0-100%, zero indicating no feed water in the overflow (maximum washing efficiency?) and 100% meaning no wash water in the overflow (minimum washing efficiency?). In contrast bias has no limit and, while in theory recovery does (0 to 100%), in reality it is restricted to a range of 0 to an uncertain top value of $\sim 10\%$ or so. In the present case recovery was over the range 0 - 6% which further reduced the ability to detect trends; for example, in Figure 6.13 recovery appears to be independent of wash water rate but this may in part reflect numerical uncertainty.

All three parameters require that the conductivity of the *water* be measured, thus in the industrial case with slurries either the appropriate sensor must be developed or some loss of precision be accepted and use made of slurry conductivity. The use of the latter approach is worth exploring because of the simplification afforded to the sensor design.

The question, which of the three parameters is most indicative of metallurgy, is difficult to address in the present context due to the uncertainty in the slurry-air data. Some comments can be offered, however.

Bias appears to be the least indicative. Previous work showing acceptable grades being maintained into negative bias conditions (e.g. Furey, 1990) is one point. The present observation of the substantial error involved in its measurement is a second point.

A third point is the present observation that bias is not a reliable indicator of the deportment of the feed water, which is ultimately responsible for the deportment of hydrophillic fines.

In principle, feed water recovery is the parameter most directly related to hydrophillic fine particle recovery. Maachar et al.(1990) have shown this relationship is linear for a given particle size, a result similar to that for mechanical cells. Entrainment has been related to metallurgy (Moys and Finch, 1989): perhaps the general question is whether entrainment is related to feed water recovery, which the present study can address.

Figure 6.14 (for the water-air system) and Figure 6.24 (for the slurry-air system) show recovery and entrainment are related but not necessarily linearly; as already mentioned, no example was encountered where the two had opposite trends. This implies that entrainment and hydrophillic fine particle recovery will be related, and hence entrainment should be related to metallurgy.

Combining both factors, reliability of measurement and indication of metallurgy, entrainment seems to hold the most promise as an on-line measurement for diagnostic and control purposes.

While the measurement technique here involved conductivity, use of temperature (in cases where wash water and feed slurry temperature are different) may prove an easier technique since water temperature can be taken as equivalent to the slurry temperature, eliminating the need for any special sensor design.

CHAPTER 8

CONCLUSIONS AND SUGGESTIONS FOR FUTURE WORK

8.1 Conclusions

1.- Conductivity based techniques to estimate interface level, gas holdup and bias rate in flotation columns at the laboratory and industrial scale have been developed and tested.

Interface Level

2.- The interface level in flotation columns is estimated by interpreting a conductance profile collected around the froth/collection zone interface. A sharp change in conductivity on crossing the froth/collection zone interface makes this detection possible. Such a difference in conductivity is primarily due to the difference in gas holdup. The difference in conductivity is enhanced if the water in the froth is of lower conductivity than that in the collection zone. This is normally the case when process water (no flotation reagents added) is used as wash water.

3.- At the laboratory scale sets of facing electrodes installed on the wall of the column and axially separated by equal distances, allowed the collection of conductance profiles around the interface. At the industrial scale, a rod-shape conductivity probe consisting of ring electrodes equally separated by plastic spacers was used.

4.- The interface level is located at the position at which there is a large change in the conductance value. An algorithm (termed "largest slope" algorithm) that searches for this sharp change was used to locate the interface level. The accuracy with which the

level is estimated depends on the axial separation between the electrodes (in both the laboratory and industrial cases). For most of the examples presented in this work the accuracy of detection was ±5 cm.

5.- Owing to the geometry of the conductivity cells in both the laboratory and industrial electrode arrangements and to the nature of the level detection algorithm, the level estimates followed a step shape behaviour, the length of the step being a function of the separation between electrodes. Interpolation of the conductance-position data or filtering of the signal by either electr... ..c or analytical means is recommended to smooth the signal and to make it more amenable for control purposes.

6.- Modelling the response to interface level of complex conductivity cells (those used at the laboratory and industrial scale) in the light of basic principles of electricity is not possible due to the buildup of non-uniform potential and current (i.e. electrical) fields. Thus, more accuracy in the detection of level cannot be gained by attempting the interpretation of the conductance measurements. The response of "ideal" cells (those that provide uniform potential and current fields) are amenable for such an interpretation.

7.- The response of the conductivity cell of the stationary level detection probe (the industrial probe) to interface level position was found to be approximately linear. An empirical interpolation of the conductance-position data based on such a linearity showed that an accuracy of ±1-2 cm in the detection of level was possible.

8.- A time delay in the detection of level exists as a consequence of the period of time needed to collect a conductance profile. Although such a delay does not appear critical, it is possible to reduce it by using a conductivity meter with a shorter time constant.

9.- Conductance profiles collected in mechanical flotation cells with a smaller version

of the stationary probe showed the potential for detecting both the air/froth and froth/slurry interface and, therefore, for estimating the true froth depth.

10.- Long term testing of the stationary probe was performed in a 38 m³ mechanical cell with satisfactory results. No appreciable deterioration of the constructing materials was observed over a four month period, and the buildup of solids on the probe surface was not a critical factor.

Gas Holdup

11.- Gas holdup in water-air and water-silica-air laboratory systems can be estimated making use of conductivity measurements performed with an adaptation of a cell that allows for uniform electrical current field, and classical models such as that due to Maxwell (1892).

12.- The geometry of the conductivity cell was found to be critical in the measurement of the effective conductivity of the two or three phase dispersions. The performance of a particular cell deteriorates as its geometry departs from that allowing for uniform current field. Secondary effects such as polarization of the cell electrodes appeared to be responsible for such a deterioration.

13.- A conductivity cell formed by two grid electrodes covering the entire cross-sectional area of the column appeared to simulate a section of the (ideal) cell consisting of two infinite and parallel plates. The grid electrodes allow the free-flowing of liquid and bubbles through the cell and provide a near uniform potential and current (electrical) fields. This cell appeared to be the most appropriate to perform the measurements of the effective conductivity of two and three phase systems.

14.- Maxwell's model (1892) appeared to predict with satisfactory accuracy gas

holdups within the range expected in colum.. flotation operations: more recent models did not offer substantial advantages (under the experimental conditions explored in this work).

15.- The grid-electrode conductivity cell and Maxwell's model were fully tested in a water-air laboratory column. Variables such as gas rate, liquid conductivity, frother concentration and liquid temperature were explored. The gas holdup estimated from conductivity measurements and Maxwell's model were in good agreement with those obtained from hydrostatic pressure head measurements.

16.- The estimation of holdup of non-conductive solids (silica) and conductive solids (sulphides in flotation pulps) appeared possible making use of the conductivity measurements using the grid-electrode cell and Maxwell's model. Sulphides in flotation pulps appeared to behave as non-conductive solids probably due to a buildup of a non-conductive layer on the particle surface (probably the result of the physical/chemical interaction between the sulphides and components of the flotation liquor).

17.- The estimation of gas holdup in a three phase system was demonstrated in a water-silica-air system using the grid-electrode cell and Maxwell's model. The estimates of holdup were in good agreement with those obtained with an independent technique, termed isolating technique, that allowed the direct measurement of solids and gas holdups.

18.- The holdup of the three phases in the water-silica-air system obtained from conductivity appeared to be additive; that is, the holdup of total non-conductive material (solids plus gas) obtained from conductivity measurements in the three phase system $,\kappa_1,$ $_g,$ and in the liquid alone, $\kappa_1,$ is approximately equal to the summation of the holdup of gas (obtained with κ_{1-g} and $\kappa_1,$), and the holdup of solids (obtained with κ_{1-s} and κ_1). In each case, Maxwell's model was used.

19.-   At the industrial scale, gas holdup estimation was attempted in a water-air system using the conductivity cell of the stationary level detection probe. Under the experimental conditions imposed, good agreement between the gas holdup estimates from conductivity measurements and those obtained from hydrostatic pressure head measurements was observed. The pressure measurements collected along the column revealed the existence of a pronounced gas holdup profile: the gas content increased from bottom to top of the column partly due to the expansion of the gas due to the pressure gradient along the column.

Bias Rate

20.-   The difficulties reported in the estimation of bias by conventional techniques (i.e. mass balancing) were corroborated. Experiments performed in a slurry-air industrial column showed large uncertainties in the bias estimates from mass balancing, most probably caused by problems in the calibration of the instruments and by difficulties in sampling of streams around the column.

21.-   Conductivity techniques which exploit the usual difference in conductivity between the wash water and pulp water in industrial situations appeared suitable for tracing the relative flows of the two waters across the interface and, therefore, for detecting the bias rate.

22.-   Conductance profiles collected in a water-air laboratory column under the conditions relevant to the industrial situation (i.e. wash water of smaller conductivity than the pulp water) appeared to reflect the bias rate. The behaviour of the branches of the profile in the froth and bubbling zone responded to the relative proportions of feed and wash water in both zones: the profiles tended to shift towards larger conductance values as the bias changed from positive to negative values.

23.- The conductivity of the froth zone increased as bias decreased (from positive to negative) due to the increased amount of feed water (of larger conductivity than the wash water) reporting to the concentrate. The conductivity of the bubbling zone increased as bias decreased due to the decreased amount of wash water crossing the interface and diluting the feed water in the collection zone.

24.- When the same source of water is used for wash water and feed water, the behaviour of the conductance profile is primarily dictated by the holdup of gas in both zones and not by the relative flows of the two water across the interface. Under these conditions, the behaviour of the profiles appeared difficult to relate to bias.

25.- Experiments performed in a slurry-air industrial column showed that the behaviour of the branch of the profile in the collection zone was in good agreement with that observed in the water-air laboratory column. The behaviour of the branch in the froth, however, was at odds with that observed in the water-air system. It is believed that a buildup of solids in the froth, that appeared to occur as bias was decreased, caused such a behaviour: as bias was reduced the solids concentration in the froth increased (thus the total holdup of non-conductive material increased) thereby causing the effective conductivity of the froth to decrease.

26.- The interpretation of conductance profiles in terms of bias rate and metallurgy will require, most probably, the intelligence of an expert system to exploit fully.

27.- Experiments performed in a water-air laboratory column under conditions relevant to industrial situations showed that bias rate, and the two alternative parameters feed water entrainment and feed water recovery, can be estimated from conductivity measurements and feed, wash water and tailings rates. Of the three, bias rate appeared the less attractive since its estimation required several conductivity and flowrates measurements and more computation, compared to the situation for the other two

parameters.

28.- Feed water entrainment appeared to offer advantages over feed water recovery, namely: it only requires three conductivity (or temperature) measurements (compared to feed water recovery which in addition requires the measurement of two flows); it appears to be related to metallurgy; and its natural range, 0 - 100%, zero indicating no feed water in the overflow and 100% indicating no wash water in the overflow.

29.- Experiments performed in a slurry-air industrial column showed that feed water entrainment can be estimated from conductivity measurements performed off-line on the feed, wash water and concentrate streams. The development of a conductivity sensor for on-line measurement of the conductivity of the liquid of the streams remains a challenge. The alternative temperature technique, which offers simplifications regarding the sensor design, is a possibility in situations where a substantial difference in temperature between the wash water and feed water exists.

8.2 Claims for Original Research

1.- A conductivity probe for locating the froth/collection zone interface level in flotation columns (and mechanical cells) was conceived, developed and fully tested. The probe has potential to become a commercial interface-level detection device.

2.- A conductivity technique to estimate gas holdup in two and three phase flotation columns was developed. The role played by the geometry and characteristics of the cell used to perform the measurements of conductivity was identified. The appropriate methodology to generate the conductivity data and the appropriate model to process them were determined.

3.- Conductivity based techniques to detect bias rate in flotation columns were

developed. An expression for the alternative parameter Feed Water Recovery was developed.

8.3   Suggestions for Future Work

1.-   Dynamic responses of interface level under conditions encountered in industrial flotation columns is recommended with the aim of determining the degree of accuracy required and the importance of a time delay in the detection of level.

2.-   A dedicated electronic circuit to run the probe needs to be developed in order to make the level detection probe available to potential users.

3.-   Additional work is required regarding the measurement of the "true froth depth" in mechanical flotation cells.

4.-   The reason behind the non-conductive behaviour of sulphides in flotation pulps needs to be determined. The role played by the particle size is worth exploring.

5.-   Gas holdup estimation in slurry-air industrial columns needs to be addressed. The development of an independent technique (similar to that used here at the laboratory scale) to sample the system is encouraged. This is essential for validating the conductivity technique.

6.-   The development of a conductivity sensor suitable for measuring the conductivity of the liquid-solids-gas and liquid-solids systems simultaneously, and at locations not far apart, is required for the estimation of gas holdup in industrial columns.

7.-   The nature of the profile of gas holdup in slurry-air industrial columns is worth examining.

8.- The response of the conductance profiles to bias rate variations at the industrial scale requires more investigation. It is recommended that experiments be performed under a well controlled environment (i.e. accurate measurements of input variables). The use of a conductivity probe consisting of an arrangement of grid electrodes in tandem is also recommended in order to obtain profiles of the effective conductivity of the three-phase system.

9.- It is suggested that a temperature technique (if amenable) be used to explore further the parameter feed water entrainment at the industrial scale and its possible relation to metallurgy. Such a technique offers simplification in terms of sensor design compared with the conductivity technique. Again, it is recommended that the experiments be conducted under well controlled conditions.

REFERENCES

Achwal, S.K., and Stepanek, J.B., 1975. "An Alternative Method of Determining Hold-up in Gas-Liquid Systems," *Chem. Eng. Sci.*, **30**, 1443-1444.

Achwal, S.K., and Stepanek, J.B., 1976. "Holdup Profiles in Packed Beds," *Chem. Eng. Jour.*, **12**, 69-75.

Adamson, A.W., 1979. *A Textbook of Physical Chemistry*, Academic Press, 953 pp.

Agar, G.E., Huls, B.J., and Hyma, D.B., 1991. Editors, Proceedings of *Column '91*, International Conference on Column Flotation. Sudbury, Ont. Canada.

Andrews, D.H., 1970. *Introductory Physical Chemistry*, McGraw Hill Book Co., 689 pp.

Anon., 1978. "Lectralevel, Capacitive Level Detector," Londex Ltd., England.

Anon., 1987. "A Guide to Metritape Gauging," Metritape, Inc. USA.

Anon., 1989. "CannonBear 1001 Microwave Level Transmitter," Texas Nuclear, USA.

Anon., Mineral Control Instrumentation Pty. Ltd., "Pulp Eight-Froth Depth Monitor Operator's Manual," Australia.

Atkins, P.W., 1982. *Physical Chemistry*, W.H. Freeman and Company, 1095 pp.

Barber, S.P., 1990. Warren Spring Laboratory, United Kingdom. Private Communication.

Barrow, G.M., 1973. *Physical Chemistry*, McGraw Hill Book Co., 787 pp.

Begovich, J.M., and Watson, J.S., 1978. "An Electroconductivity Technique for the Measurement of Axial Variation of Holdups in Three-Phase Fluidized Beds," *AIChE*

Jour., **24**, 2, 351-354.

Bergh, L.G., and Yianatos, J.B., 1991. "Advances in Flotation Column Dynamics and Measurements," in *Column '91, Proceedings* of the International Conference on Column Flotation, G.E. Agar, B.J. Huls and D.B. Hyma, Eds., Vol. 2, 409-421.

Binns, K.J., and Lawrenson, P.J., 1963. *Analysis and Computation of Electric and Magnetic Field Problems*, The Macmillan Company, New York.

Boutin, P., and Wheeler, D.A., 1967. "Column Flotation," *Mining World*, **20**, 3, 47-50.

Braunstein, J., and Robbins, G.D., 1971. "Electric Conductance Measurements and Capacitive Balance," *J. Chem. Ed.*, **48**, 1, 52-59.

Bruggeman, D.A.G., 1935. "Berechnung Verschiedener Physicalischer Konstanten von Heterogenen Substanzen," *Annln Phys.*, **24**, 639.

Burgess, J.M., and Calderbank, P.H., 1975. "The Measurement of Bubble Parameters in Two-Phase Dispersions," *Chem. Eng. Sci.*, **30**, 743-750.

Castillejos, A.H., 1986. "A Study of the Fluid-Dynamic Characteristics of Turbulent Gas-Liquid Plumes," Ph.D. Thesis. The University of British Columbia.

Chen, J.J.J., Leung, Y.C., and Spedding, P.L., 1983. "Simple Method of Measuring Voidage in a Bubble Column," *Chem. Eng. Res. Des.*, **61**, 325-328.

Clift, R., Grace, J.R., and Weber, M.E., 1978. *Bubbles, Drops, and Particles*. Academic Press.

Cole. R.H., and Coles, J.S., 1964. *Physical Principles of Chemistry*, W.H. Freeman and Company, 795 pp.

Condon, E.U. (Ed.), 1967. *Handbook of Physics*, Chapter 9, McGraw Hill Book Co., 146-169.

Davies, C.W., 1930. *The Conductivity of Solutions*. Chapman & Hall's. 204 pp.

De la Rue, R.E., and Tobias, C.W., 1959. "On the Conductivity of Dispersions," *Jour. Electrochem. Soc.*, **106**, 827-832.

Dhanuka, V.R., and Stepanek, J.B., 1987. "Gas and Liquid Hold-up and Pressure Drop Measurements in a Three-phase Fluidised Bed," in *Fluidization*, Cambridge University Press, London. 179-183.

Dirsus, D.F., 1988. "Flotation Columns: Level Sensing in Three-Phase Slurries," B.Sc. Thesis, Geo-Engineering, University of Toronto.

Dobby, G.S., Yianatos, J.B., and Finch, J.A., 1988. "Estimation of Bubble Diameter in Flotation Columns from Drift Flux Analysis," *Can. Met. Quart.*, **27**, 2, pp. 85-90.

Espinosa-Gomez, R., Johnson, N.W., Pease, J.D., and Munro, P.D., 1989. "The Commissioning of the First Flotation Columns at Mount Isa Mines Limited," in *Processing of Complex Ores, Proceedings* of the International Symposium, G.S. Dobby and S.R. Rao, Eds., Pergamon Press. 293-309.

Espinosa-Gomez, R., 1990. Mount Isa Mines Ltd., Australia. Private Communication.

Espinosa-Gomez, R., and Johnson, N.W., 1991. "Technical Experience with Conventional Columns at Mount Isa Mines Limited, " in *Column '91, Proceedings* of the International Conference on Column Flotation, G.E. Agar, B.J. Huls and D.B. Hyma, Eds., Vol. 2, 511-523.

Fan, L.-S., 1989. *Gas-Liquid-Solid Fluidization Engineering*. Chapter 2. Butterworth Publishers, 763 pp.

Finch, J.A., and Dobby, G.S., 1990a. *Column Flotation*, Pergamon Press, 180 pp.

Finch, J.A., and Dobby, G.S., 1990b. "Column Flotation: A Selected Review," in *Proceedings of the 2nd Workshop on Flotation of Sulphide Minerals*, Lulea University of Technology, Sweden, 149-160.

Flint, L.R., 1974. "A Mechanical Approach to Flotation Kinetics," *Trans. Inst. Min. Met.*, **83**, C90-C95.

Fuerstenau, M.C., Miller, J D., and Kuhn. M.C., 1985. *Chemistry of Flotation.* Published by SME of AIME. 177 pp.

Fukama, M., Muroyama, K., and Yasunishi, A., 1987. "Properties of Bubble Swarm in a Slurry Bubble Column, " *J. Chem. Engng Japan*, **20**, 1, 28-33.

Furey, J.T., 1990. "Rougher Column Flotation of Gold Tellurides," *Proceedings of the 22nd Annual Meeting of the Canadian Mineral Processors*, Ottawa. p. 242.

Gilmont, R., and Walton, R.F., 1956. "New Design of an Electrolytic Cell for the Study of Electroplating Phenomena," *Jour. Electrochem. Soc.*, **103**, 10, 549-552.

Glasstone, S., 1930. *The Electrochemistry of Solutions.* Methuen & Co. Ltd. 476 pp.

Glasstone, S., 1942. *An Introduction to Electrochemistry.* D.Van Nostrand Company, Inc. 557 pp.

Gomez, C.O., and Finch, J.A., 1989. "Flotation Column Control Using Electrical Conductivity", Progress Report No.6 submitted to Falconbridge Ltd.

Gomez, C.O., Uribe-Salas, A., Finch, J.A., and Huls, B.J., 1990. "A Calibration Probe for Level Detection Systems in Flotation Columns," *CIM Bulletin*, **83**, No. 935, 118-121.

Hashin, Z., 1968. "Assessment of the Self Consistent Scheme Approximation: Conductivity of Particulate Composite," *J. Composite Mater.*, **2**, 284-300.

Hemmings, C.E., 1981. "On the Significance of Flotation Froth Liquid Lamella Thickness," *Trans. Instn. Min. Metall.*, Sec. C, **90**, 96-102.

Himmelblau, D.M., 1970. *Process Analysis by Statistical Methods.* John Wiley & Sons, Inc. 463 pp.

Hine, F., Yoshizawa, S., and Okada, S., 1956. "Effect of the Walls of Electrolytic Cells on Current Distribution," *Jour. Electrochem. Soc.*, **103**, 186-193.

Hoffert, 1987. Presented in *Column Flotation Cell Symposium*, G.Feasby (Ed.), Trail, B.C. Published by CANMET, Ottawa, June 1988.

Huls, B.J., Lachance, C.D., and Dobby, G.S., 1989. "Gas Rate and Froth Depth effects on Performance of a Cu-Ni Separation Flotation Column," in *Processing of Complex Ores, Proceedings* of the International Symposium, G.S. Dobby and S.R. Rao, Eds., Pergamon Press. 311-323.

Huls, B.J., Gomez, C.O., Uribe-Salas, A., and Finch, J.A., 1990. "Level Detection in Flotation Columns at Falconbridge," in *Control '90, Proceedings* of the Min. and Met. Processing Symposium, SME Meeting, Salt Lake City, Utah. 173-177.

Huls, B.J., Lachance, C.D., and Dobby, G.S., 1991. "Bubble Generation Assessment for an Industrial Flotation Column," *Min. Engng*, **4**, 1, 37-42.

Jepsen, J.C., and Ralph, J.L., 1969-70. "Hydrodynamic Study of Two-Phase Upflow in Vertical Pipelines," *Proc. Instn Mech Engrs*, **184**, 3C, 154-165.

Kasper, C., 1940. "The Theory of the Potential and the Technical Practice of Electrodeposition," *Trans. Electrochem. Soc.*, **77**, 353-384; **78**, 131-161

Kato, Y., Uchida, K., Kago, T., and Morooka, S., 1981. "Liquid Holdup and Heat Transfer Coefficient between Bed and Wall in Liquid-Solid and Gas-Liquid Fluidized Beds," *Powder Tech.*, **28**, 173-179

Kelly, E.G., and Spottiswood, D.J., 1982. *Introduction to Mineral Processing*. John Wiley & Sons. 491 pp.

King, L.A., and Duke, F.R., 1964. "Direct Current Measurement of Fused Salt Conductivity: Molten Nitrates," *J. Elechtrochem. Soc.*, 111, 6, 712-719.

Kitzinger, F., Rosenblum, F., and Spira, P., 1979. "Continuous Monitoring and Control of Froth Level and Pulp Density," *Min. Engng.*, 390-394

Klassen, V.I., and Mokrousov, V.A., 1963. *An Introduction to the Theory of Flotation*. Butterworths.

Koivistoinen, P., and Miettunen, J., 1985. "Flotation Control at Pyhäsalmi," in *Flotation of Sulphide Minerals*, K.S.E. Forssberg, Ed., Elsevier. 447-472

Konigsmann, E., 1990. "Column Flotation Experience at Brenda Mines Limited," presented in the *92nd Annual General Meeting of CIM-1990*, Ottawa.

Kosick, G.A., and Dobby, G.S., 1990. "Advanced Control for Column Flotation," *Proceedings* of the Canadian Mineral Processors Annual Meeting, Ottawa.

Kosick, G.A., Dobby, G.S., and Young, P.D., 1991. "Columnex: A Powerful and Affordable Control System for Column Flotation," in *Column '91*, *Proceedings* of the International Conference on Column Flotation, G.E. Agar, B.J. Huls, and D.B. Hyma, Eds., Vol. 2, 359-373

Levine, I.N., 1988. *Physical Chemistry*, McGraw Hill Book Co., 920 pp.

Lin, D., 1988. "Cleaning Action of Water Drained Froths," B.Sc. Thesis. Department of Chem. Eng., University of Toronto.

Lockett, M.J., and Kirkpatrick, R.D., 1975. "Ideal Bubbly Flow and Actual Flow in Bubble Columns," *Trans. Instn. Chem. Engrs*, 53, pp. 267-273.

Lord Rayleigh, 1892. "On the Influence of Obstacles Arranged in Rectangular Order Upon the Properties of a Medium," *Phil. Mag.*, 34, 481-502.

Maachar, A., Lin., D., and Dobby, G.S., 1990. "Measurement of Water Recovery and Entrainment in Flotation Columns," Presented at the 29th Annual CIM Conference of Metallurgists. Hamilton, Canada.

Macnamara, D., 1990. Strathcona mill, Falconbridge Ltd. Private communication.

Maxwell, J.C., 1892. *A Treatise of Electricity and Magnetism*, 3rd Edn., Vol. 1, Part II, Chapter IX, 435-449. Oxford University Press, London.

Meredith, R.E., and Tobias, C.W., 1960. "Resistance to Potential Flow through a Cubical Array of Spheres," *J. Appl. Phys.*, 31, 7, 1270-1273.

Meredith, R.E., and Tobias, C.W., 1961. "Conductivities in Emulsions," *J. Electrochem. Soc.*, **108**, 286-290.

Meredith, R.E., and Tobias, C.W., 1962. "Conduction in Heterogeneous Systems," in *Advances in Electrochemistry and Electrochemical Engineering*, Vol. 2, C.W. Tobias (Ed.), Interscience Publishers, New York, 15-47.

Miettunen, J., 1982. "The Control Strategy of Zinc Flotation at The Pyhasalmi Mine," in *Proceedings* of the 17th International Symposium on Application of Computers and Operations Research in the Mineral Industry, T.O. Johnson and R.J. Barnes, Eds., New York. 657-665.

Moys, M.H., and Finch, J.A., 1988a. "The Measurement and Control of Level in Flotation Columns," in *Column Flotation '88, Proceedings* of the International Symposium on Column Flotation, K.V.S. Sastry, Ed., SME Annual Meeting, Phoenix, Arizona. 103-112.

Moys, M.H., and Finch, J.A., 1988b. "Developments in the Control of Flotation Columns," *Int. J. Mineral Processing*, **23**, 265-278.

Moys, M.H., and Finch, J.A., 1989. "The use of Temperature Measurements in the Analysis and Control of Flotation," *Proceedings of the Symposium Role of the Practical Metallurgist*, Mine Metallurgical Managers Assoc., South Africa, 90-107.

Moys, M.H., 1989. "Further Developments in the Control of Level in Flotation Columns," *Proceedings* of the International Colloquium "Developments in Froth Flotation", Vol.2, Cape Town, South Africa.

Nasr-El-Din, H., Shook, C.A., and Colwell, J., 1987. "A Conductivity Probe for Measuring Local Concentrations in Slurry Systems," *Int. J. Multiphase Flow*, **13**, 3, 365-378.

Nassos, P.G., 1963. "Development of an Electrical Resistivity Probe for Void Fraction Measurements in Air-Water Flow," Argonne National Laboratory, Report ANL-8738.

Neale, G.H., and Nader, W.K., 1973. "Prediction of Transport Processes within Porous

Media: Diffusive Flow Processes within an Homogeneous Swarm of Spherical Particles," *AIChE Jour.*, **19**, 1, 112-119.

Nicol, S.K., Roberts, T., Bensley, C.N., Kidd, G.W., and Lamb, R., 1988. "Column Flotation of Ultrafine Coal: Experience at BHP-Utah Coal Limited's Riverside Mine," in *Column Flotation '88*, Proceedings of the International Symposium, K.V.S. Sastry (Ed.), SME Annual Meeting. Phoenix, Arizona, 7-11.

Nicol, S.K., 1988. BHP Research & New Technology, Australia. Private Communication.

Redfearn, M.A., 1987. Cominco Ltd., Sullivan Concentrator. B.C., Canada. Private Communication.

Richardson, J.F., and Zaki, W.N., 1954. "Sedimentation and Fluidisation: Part I," *Trans. Instn Chem. Engrs*, **32**, 35-53.

Sastry, K.V.S., 1988. Editor, Proceeding of *Column Flotation '88*, SME Meeting. Phoenix, Arizona.

Sawyer, D.T., and Roberts, J.L., 1974. *Experimental Electrochemistry for Chemists*. John Wiley & Sons, Inc. 435 pp.

Sepulveda, C., 1990. Département Mines et Métallurgie, Université Laval. Private Communication.

Serizawa, A., Kataoka, I., and Michiyoshi, I., 1975. "Turbulence Structure of Air-Water Bubbly Flow - II Local Properties," *Int. J. Multiphase Flow*, **2**, 235-246.

Shuey, R.T., 1975. *Semiconducting Ore Minerals*. Elsevier, Amsterdam. 415 pp.

Soto, H.S., 1989. "Column Flotation with Negative Bias," in *Processing of Complex Ores, Proceedings* of the International Symposium. G.S. Dobby and S.R. Rao, Eds., Pergamon Press, 379-385.

Stephanopoulos, G., 1984. *Chemical Process Control, an Introduction to Theory and*

Practice, Prentice-Hall, Inc., N.J., 696 pp.

Stravs A.A., and Von Stockar, U., 1985. "Measurement of Interfacial Areas in Gas-Liquid Dispersions by Ultrasonic Pulse Transmission," *Chem. Engng Sci.*, **40**, 7, pp. 1169-1175.

Tacussel Operating Manual, 1981. Solea Tacussel Electronique, France. 30 pp.

Tsai, T.H., Lane, J.W., and Lin, C.S., 1986. *Modern Control Techniques for the Processing Industries*, Marcel Dekker, Inc., New York.

Turner, J.C.R., 1976. "Two-Phase Conductivity. The Electrical Conductance of Liquid-Fluidized Beds of Spheres," *Chem. Eng. Sci.*, **31**, 487-492.

Uribe-Salas, A., and Finch, J.A., 1990. "Flotation Column Control Using Electrical Conductivity", Progress Report No.8 submitted to Falconbridge Ltd.

Uribe-Salas, A., Gomez, C.O., Finch, J.A., and Huls, B.J., 1991. "Axial Gas Holdup Profiles in Flotation Columns," submitted for publication in *Can. Met. Quart.*

Vince, M.A., Breed, H., Krycuk, G., and Lahey, Jr., R.T., 1982. "Optical Probe for High-Temperature Local Void Fraction Determination," *Applied Optics*, **21**, 5, 886-892.

Wachi, S., Morikawa, H., and Ueyama, K., 1987. "Gas Holdup and Axial Dispersion in Gas-Liquid Concurrent Bubble Column," *J. Chem. Engng Japan*, **20**, 3, 309-316.

Wagner, C., 1962. "The Scope of Electrochemical Engineering," in *Advances in Electrochemistry and Electrochemical Engineering*, Vol. 2, C.W. Tobias (Ed.), Inerscience Publishers, New York, 1-14.

Watson, D., and Grainger-Allen, T.J.N., 1974. "Study of Froth Flotation Using a Steady-state Technique," *Trans. Soc. Mech. Engng AIME*, **256**, 242-247.

Wheeler, D.A., 1966. "Big Flotation Column Mill Tested," *E & MJ*, **167**, 11, 98-99.

William, C.E., 1990. "IR Drop in Electrochemical Corrosion Studies- Part I: Basic

Concepts and Estimates of Possible Measurement Errors", in *The Measurement and Correction of Electrolyte Resistance in Electrochemical Tests*. L.L. Scribner and S.R. Taylor, Eds., ASTM STP 1056. 27-58.

Xu, M., and Finch, J.A., 1990. "Simplification of Bubble Size Estimation in a Bubble Swarm", *J. Colloid and Interface Sci.*, **140**, 1, 298-299.

Yianatos, J.B., Laplante, A.R., and Finch, J.A., 1985. "Estimation of Local Holdup in the Bubbling and Froth Zones of a Gas-Liquid Column," *Chem. Eng. Sci.*, **40**, 1965-1968.

Yianatos, J.B., Finch, J.A., and Laplante, A.R., 1986. "Holdup Profile and Bubble Size Distribution of Flotation Column Froths," *Can. Met. Quart.*, **25**, 1, 23-29.

Yianatos, J.B., Finch, J.A., and Laplante, A.R., 1987. "Cleaning Action in Column Flotation Froths," *Trans. Instn Min. Metall.* (Sec. C), **96**, 199-205

Yianatos, J.B., Finch, J.A., Dobby, G.S., and Manqiu Xu, 1988. "Bubble Size Estimation in a Bubble Swarm," *J. of Colloid and Interface Sci.*, **126**, 1, 37-44.

Yianatos, J.B., and Levy, A.R., 1989. "Estimation of Gas Holdup, Diameter and Apparent Density of Mineralized Bubbles in Industrial Flotation Columns," Presented in the International Colloquium *Developments in Froth Flotation*, Vol. 2, Gordon's Bay, South Africa.

APPENDIX 1

Application of Error Propagation Theory to Bias Determination.

As mentioned in text, bias rate is susceptible to error propagation, which essentially means that errors in measurements can propagate and build up throughout the calculations to produce a number involving a substantial amount of uncertainty.

Considering again the example presented by Finch and Dobby (1990a): A column of 2 m diameter with process flow and density measurements on tailings and feed streams of: $Q_t = 1.90$ m^3/min, $v_{st} = 0.09$, $Q_f = 1.99$ m^3/min, and $v_{sf} = 0.18$. Assuming a relative standard deviation of 3% for each of the process measurements. Then, from the bias rate equation

$$J_B - J_t (1 - v_{st}) - J_f (1 - v_{sf}) \qquad (A.1.1)$$

the expected value (or ensemble mean) of J_B of

$$J_B - \frac{1.9 \times 100}{\pi \times 60} (1 - 0.09) - \frac{1.99 \times 100}{\pi \times 60} (1 - 0.18)$$

$$J_B - 0.052 \frac{cm}{s}$$

From theory of error propagation, after linearizing the J_B function by expanding it in a Taylor series about a mean or reference value of the independent variables, the Variance of J_B is given by

$$Var\{J_s\} = \sum_{i=1}^{n} \left[\frac{\partial J_s(x_1^0,...,x_n^0)}{\partial x_i}\right]^2 Var\{X_i\} \qquad (A.1.2)$$

where x_i stands for Q_f, Q_t, v_{sf}, and v_{st}. In a similar manner x_i^0 stands, for example, for the mean of Q_f, and so on.

It is important to notice that the partial derivatives in Equation (A.1.2) are constants that have been evaluated by introducing the mean values of Q_f, Q_t, v_{sf}, and v_{st}. Applying Equation (A.1.2) to the Equation (A.1.1)

$$S_{J_s}^2 = \left(\frac{\partial J_s}{\partial Q_f}\right)^2 S_{Q_f}^2 + \left(\frac{\partial J_s}{\partial Q_t}\right)^2 S_{Q_t}^2 + \left(\frac{\partial J_s}{\partial v_{sf}}\right)^2 S_{v_{sf}}^2 + \left(\frac{\partial J_s}{\partial v_{st}}\right)^2 S_{v_{st}}^2 \qquad (A.1.3)$$

$$S_{J_s}^2 = (1 - v_{sf})^2 S_{Q_f}^2 + (1 - v_{st})^2 S_{Q_t}^2 + Q_f^2 S_{v_{sf}}^2 + Q_t^2 S_{v_{st}}^2$$

To obtain the variance (or square of the standard deviation) of variables, the definition of *relative standard deviation* (C, or *coefficient of variation*) is used. This is a dimensionless form of the standard deviation which provides information on the relative dispersion of a variable X, such that

$$C_X = \frac{S_X}{\bar{X}} \qquad (A.1.4)$$

where $\bar{X}$ is the ensemble mean of the variable X.

Thus, by using Equation (A.1.4) and the $C=0.03$ (3%) and the mean values for the variables, the standard deviations are obtained as follows

$$S_{Q_f} = C_{Q_f} \times \overline{Q}_f = 0.03 \times \frac{1.99 \times 100}{\pi \times 60} = 0.0317 \; \frac{cm}{s}$$

In a similar way

$$S_{Q_i} = 0.0302 \; \frac{cm}{s}; \quad S_{v_{sf}} = 0.0054; \quad and \quad S_{v_{si}} = 0.0027$$

Thus,

$$S_{J_s}^2 = (1-0.0054)^2 \times 0.0317^2 + (1-0.0027)^2 \times 0.0302^2 + 1.0557^2 \times 0.0054^2 + \ldots$$

$$\ldots + 1.0080^2 \times 0.0027^2$$

$$S_{J_s}^2 = 0.0015 \; \frac{cm^2}{s^2}$$

The relative standard deviation of J_s given by

$$C_{J_s} = \frac{\sqrt{S_{J_s}^2}}{J_s} = \frac{\sqrt{0.0015 \; cm^2/s^2}}{0.052 \; cm/s} = 0.74$$

which translates to a percentage as high as 74%.

The 95% confidence interval given by

$$\overline{J}_s - 2 \, S_{J_s} \leq \mu_{J_s} \leq \overline{J}_s + 2 \, S_{J_s} \qquad\qquad (A.1.5)$$

$$-0.02 \ cm/s \le \mu_{J_a} \le 0.13 \ cm/s$$

Thus, 95% of the occurrences of J_a should lie within -0.02 and 0.13 cm/s.

This analysis gives an idea of the magnitude of the error involved in a parameter which depends both on several measurements and on extensive computation.

APPENDIX 2

A brief introduction to the finite difference numerical method is given here with the aim of providing the basis of a simple approach for modelling potential and current fields in "non-ideal" geometries (Binns and Lawrenson, 1963). The method is shown for the case of a regular distribution of field points, and specifically for a *square array*.

Laplace's equation can be solved numerically by using conventional methods, finite-difference for example, to determine the potential and current field of a system. The method is useful to describe relatively simple geometries. However, complications arise when dealing with complex three-dimensional systems.

To facilitate analysis a *potential function*, ψ, is defined such that the change in this function between any two points is proportional to the *change in potential* between them. Its value at any point, with respect to some origin (of potential), is a direct measure of the value of the potential there and, in addition, a line joining points having the same value of potential function is an equipotential line.

Consider the potential field that builds up in a section of "two infinite parallel

planes" (Figure A.2.1). Let $\psi=0$ represent the value of the potential on one plate and $\psi=1$ that on the other, so that there is unit difference of potential between the plates Equipotential lines can be drawn in the space between the plates, representing $\psi=$constant, for values of ψ between 0 and 1. For example, $\psi=0.1$ represents a line joining points differing in potential from that of the lower potential plate by one tenth of the potential difference between the plates.

In a similar manner a *flux function* ϕ can be defined such that $\phi=$constant defines a flux line; and two lines $\phi=\phi_0$ and $\phi=\phi_0+n$ have n units of flux passing between them (Binns and Lawrenson, 1963).

Then, the Laplace equation of the potential function ψ in Cartesian coordinates and for two-dimensions is written as

$$\nabla^2\psi - \frac{\partial^2\psi}{\partial x^2} + \frac{\partial^2\psi}{\partial y^2} - 0 \qquad (A.2.1)$$

and the current density function as

$$i - -\kappa \nabla\psi - -\kappa \left(\frac{\partial\psi}{\partial x} \vec{i} + \frac{\partial\psi}{\partial y} \vec{j}\right) \qquad (A.2.2)$$

(i and j are unitary vectors).

In replacing the potential field equations by a set of finite difference equations which connect values of the potential function, the first task is the distribution of points. The square mesh and the sector mesh are two of the most popular types. The present analysis will make use of the square mesh distribution.

In Figure A.2.2, point O, *not adjacent to a boundary*, and its closest neighbouring

Figure A.2.1   Definition of potential function, Ψ , and (current) flux function, $\emptyset$ (after Binns and Lawrenson, 1963)

Figure A.2.2   Schematic representation of the elements involved in the finite difference numerical method. Boundary conditions are also presented

points 1, 2, 3 and 4 are shown. The length h, referred to as the mesh length is small compared with the boundary dimensions. The cathode and anode are represented by equipotential surfaces $\psi = 0$ and $\psi = 1$, respectively.

The difference equation is developed by expanding the electric scalar potential ψ at point O in Taylor's series and deriving expressions for $(\partial^2\psi/\partial x^2)_0$ and $(\partial^2\psi/\partial y^2)_0$ which are substituted in Equation (A.2.1).

At any point x, ψ can be expanded in terms of the ψ at point O (e.g., ψ_0) by the use of Taylor's series:

$$\psi = \psi_0 + (\frac{\partial\psi}{\partial x})_0(x-x_0) + \frac{1}{2!}(\frac{\partial^2\psi}{\partial x^2})_0(x-x_0)^2 + \frac{1}{3!}(\frac{\partial^3\psi}{\partial x^3})_0(x-x_0)^3 + ... \quad (A.2.3)$$

substituting for the values $x_1 = x_0 + h$ and $x_3 = x_0 - h$ yields the values of ψ at points 1 and 3 as follows

$$\psi_1 = \psi_0 + h(\frac{\partial\psi}{\partial x})_0 + \frac{1}{2!}h^2(\frac{\partial^2\psi}{\partial x^2})_0 + \frac{1}{3!}h^3(\frac{\partial^3\psi}{\partial x^3})_0 + ... \quad (A.2.4)$$

and

$$\psi_3 = \psi_0 - h(\frac{\partial\psi}{\partial x})_0 + \frac{1}{2!}h^2(\frac{\partial^2\psi}{\partial x^2})_0 - \frac{1}{3!}h^3(\frac{\partial^3\psi}{\partial x^3})_0 + ... \quad (A.2.5)$$

adding Equations (A.2.4) and (A.2.5)

$$\psi_1 + \psi_3 = 2\psi_0 + h^2(\frac{\partial^2\psi}{\partial x^2})_0 + h^4(\frac{\partial^4\psi}{\partial x^4})_0 + ... \quad (A.2.6)$$

ignoring terms containing h to the power four or higher, the expression for $(\partial^2\psi/\partial x^2)_0$ is

$$\left(\frac{\partial^2\psi}{\partial x^2}\right)_0 - \frac{\psi_1 + \psi_3 - 2\psi_0}{h^2} \qquad (A.2.7)$$

In an analogous manner, an expression for $(\partial^2\psi/\partial y^2)_0$ can be obtained, namely

$$\left(\frac{\partial^2\psi}{\partial y^2}\right)_0 - \frac{\psi_2 + \psi_4 - 2\psi_0}{h^2} \qquad (A.2.8)$$

substituting Equations (A.2.7) and (A.2.8) into Equation (A.2.1), Laplace's equation for the point O, *not adjacent to a boundary*, is

$$\psi_0 - \frac{\psi_1 + \psi_2 + \psi_3 + \psi_4}{4} \qquad (A.2.9)$$

The current density vector i at point O is given by

$$i_0 - -\kappa \left[\left(\frac{\psi_1 - \psi_3}{2h}\right) \vec{i} + \left(\frac{\psi_2 - \psi_4}{2h}\right) \vec{j} \right] \qquad (A.2.10)$$

(i and j are unitary vectors)

The magnitude of i and its direction θ is given by

$$|i| - \kappa \sqrt{\left[\left(\frac{\psi_1 - \psi_3}{2h}\right)^2 + \left(\frac{\psi_2 - \psi_4}{2h}\right)^2\right]} \qquad (A.2.11)$$
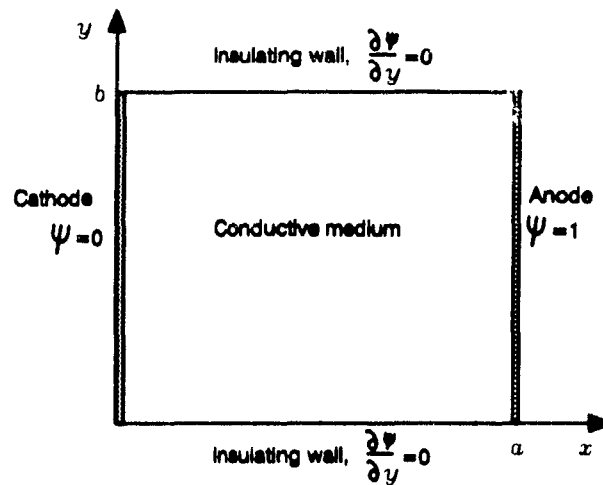
Figure A.2.3   Definition of the boundary conditions in a rectangular cell with two parallel electrodes and two parallel isolating walls

and

$$\theta = tg^{-1}\left(\frac{\psi_2 - \psi_4}{\psi_1 - \psi_3}\right) \qquad\qquad (A.2.12)$$

Boundary Conditions

Thus far, equations that apply for grid points *not adjacent to a boundary* have been presented. Let us consider again the case of flow between two infinite parallel planes, a section of which is depicted in Figure A.2.3.

In Figure A.2.3, the line at $\psi=0$ represents tne grounded or negative electrode (cathode) while that at $\psi=1$ represents the positive electrode (anode). The edges at $y=0$ and $y=b$ are lines impervious to flux which represent insulating walls described by

$$\left(\frac{\partial\psi}{\partial y}\right)_{y=0} = 0 \quad\quad and \quad\quad \left(\frac{\partial\psi}{\partial y}\right)_{y=b} = 0 \qquad\qquad (A.2.13)$$

since no current flow is permitted orthogonal to them (no current crosses such surfaces).

Referring to Figure A.2.2 where an extra layer of grid points adjacent to the boundaries representing insulating walls are shown, let us proceed by putting Equation A.2.13 in a finite difference form for point m lying on the insulating wall

$$\left(\frac{\partial \psi}{\partial y}\right)_m - \frac{(\psi_2 - \psi_4)}{2h} - 0 \,, \quad \text{that is,} \quad \psi_2 - \psi_4 \qquad (A.2.14)$$

This expression is not immediately usable, because the quantity ψ_2 falls outside the domain of computation; however, ψ_2 may be eliminated from the above equation by restating Equation A.2.9 for coordinate point m

$$\psi_m - \frac{(\psi_1 + \psi_2 + \psi_3 + \psi_4)}{4} \qquad (A.2.15)$$

and, substituting the value of ψ_2 ($=\psi_4$), gives

$$\psi_m - \frac{(\psi_1 + \psi_3 + 2\psi_4)}{4} \qquad (A.2.16)$$

which relates the value of ψ_m to points falling inside the dominion of computation. Thus, all the points in the grid are described by a finite difference equation and the computation can be performed.

APPENDIX 3

Computation of Interface Level Using Two Parallel Plates.

In a slurry-air system, the conductance measured with the "level" electrodes, K_l (Figure A.3.1) is given by

$$K_l = K_{lf} + K_{lc} \qquad (A.3.1)$$

where K_{lf} and K_{lc} are the contributions of the froth and slurry zone to the global measurement, given by

$$K_{lf} = \frac{\kappa_f (L-l)\, w}{d} \quad and \quad K_{lc} = \frac{\kappa_s\, l\, w}{d} \qquad (A.3.2)$$

where κ_f and κ_c are the effective conductivities (mS/cm) of the froth and collection zone, respectively; L is the length of the "level" electrode (100 cm); l is the level position within the level electrodes (cm); w is the width of the electrodes (1 cm); and d is distance between electrodes (5 cm).

The conductance measured with the "froth" and "collection" zone electrodes is

$$K_f = \frac{\kappa_f\, l_f\, w}{d} \quad and \quad K_c = \frac{\kappa_c\, l_c\, w}{d} \qquad (A.3.3)$$

where l_f and l_c are the length of the froth and collection zone electrodes (2 cm).

Thus, Equation (A.3.1) becomes
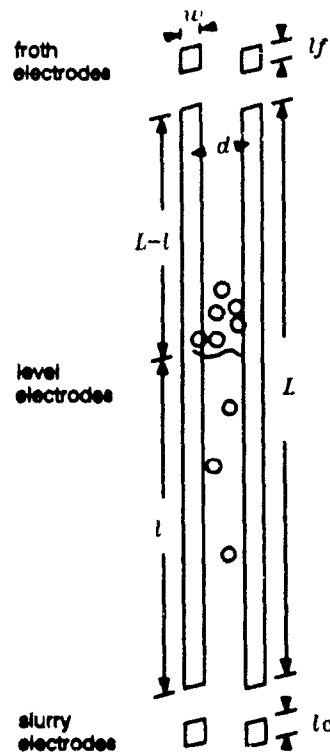
Figure A.3.1   Schematic representation of the experimental arrangement, and notation used in the calculation of level using Equation (4.1)

$$K_l - \frac{K_f}{l_f}(L - l) + \frac{K_c}{l_c} l \qquad (A.3.4)$$

Similar measurements performed in liquid (water) only give:

$$K_{lw} - \frac{\kappa_w L w}{d}, \quad K_{fw} - \frac{\kappa_w l_f w}{d}, \quad and \quad K_{cw} - \frac{\kappa_w l_c w}{d} \quad (A.3.5)$$

where κ_w is the conductivity of the liquid (mS/cm), and K_{lw}, K_{fw}, and K_{cw} are the conductance measured with the level, froth and slurry electrodes (mS), respectively.

This gives

$$l_f - L \frac{K_{fw}}{K_{lw}} \quad and \quad l_c - L \frac{K_{cw}}{K_{lw}} \qquad (A.3.6)$$

and substituting l_f and l_c in Equation (A.3.4), Equation (4.1) is obtained

$$l - L \times \frac{(K_{fw} / K_{lw}) K_l - K_f}{(K_{fw} / K_{cw}) K_c - K_f} \qquad (4.1)$$

APPENDIX 4

Four Electrode Conductivity Cells

In a 4-electrode conductivity cell, two of the electrodes sense the excitation field (potential drop) across the medium. The impedance of the sensor circuit is virtually infinite, and therefore practically no current flows into the sensors. Consequently, no polarization occurs on their surfaces. The other two electrodes are used to create the excitation field and to carry the current. The current required to create the excitation field is sensed and converted to conductivity. This principle is valid because the amount of excitation current required to maintain a constant excitation field in the medium is directly proportional to the conductivity of the medium.

This type of 4-electrode conductivity cell has been described in the literature

(Braunstein and Robbins, 1971), and used to measure conductivity of fused salts (King and Duke, 1964), electrolytes and liquid-solids dispersions (Nasr-El-Din, 1987).

APPENDIX 5

Alternative Definitions of Bias.

The definition of bias used here is the difference in flow (or net flow) of water between tailings and feed. From Figure 6.3, an equivalent definition is the net flow of water across the froth/collection zone interface, or simply the net flow of water through the froth (below the wash water input).

Other definitions are in use, however.

Difference in slurry flow between tailings and feed. This can differ significantly from bias based on water (Finch and Dobby, 1990a).

Bias ratio. In terms of the notation here (Figure 6.3) this is

$$\frac{Q_t}{Q_f} \qquad (A.5.1)$$

giving rise to values such as 1.05 (or 105%), which is a small positive bias.

Bias difference ratio. This is derived from Equation (A.5.1)

$$\frac{(Q_t - Q_f)}{Q_f} \qquad (A.5.2)$$

which, for the same example, would give 5%. Again, these quantities may be calculated based on slurry flow rather than water.

APPENDIX 6

Error Propagation Analysis for Bias Rate, Feed Water Entrainment and Feed Water Recovery from Conductivity Measurements.

The analysis is performed for one set of experimental data in Table 6.2 (option (i)-open circuit), namely $J_g=1.85$ cm/s, $J_l=0.80$ cm/s, $J_w=0.42$ cm/s, $J_c=0.34$ cm/s, $J_f=0.72$ cm/s and $J_B=0.08$ cm/s. A 2% relative standard deviation (e.g. standard deviation of stream i is 2% of Q_i) for the flows is assumed, thus, $S_{Jl}=0.016$ cm/s, $S_{Jw}=0.0084$ cm/s, $S_{Jc}=0.0068$ cm/s, and $S_{Jf}=0.0144$ cm/s. The average of ~25 conductivity values of the stream around the column collected under steady state conditions was $\kappa_l=1.035$ mS/cm, $\kappa_w=0.269$ mS/cm, $\kappa_c=0.308$ mS/cm and $\kappa_f=1.127$ mS/cm. The standard deviation of the conductivity measurements was ~0.0023 mS/cm (approximately constant for all the streams).

From theory of error propagation, the Variance of a function $J_B(X_1,...,X_n)$ is given by (Himmelblau, 1970)

$$Var\{J_B(X_1,...,X_n)\} = \sum_{i=1}^{n} \left[\frac{\partial J_B(x_1^0,...,x_n^0)}{\partial x_i} \right]^2 Var\{X_i\} \qquad (A.6.1)$$

where x_i stands for variables such as Q_f, Q_t, κ_c, κ_w, etc. In a similar manner x_i^0 stands, for example, for the average of Q_f, and so on.

Applying Equation (A.6.1) to the expression to calculate bias from conductivity measurements

$$J_B = \overline{J}_t \frac{\overline{\kappa}_f - \overline{\kappa}_t}{\overline{\kappa}_f - \overline{\kappa}_w} - \overline{J}_c \frac{\overline{\kappa}_c - \overline{\kappa}_w}{\overline{\kappa}_f - \overline{\kappa}_w} = 0.07 \ cm/s \qquad (6.4)$$

the variance of the bias rate, J_B (cm/s), is given by

$$S_{J_B}^2 = \left(\frac{\partial J_B}{\partial J_t}\right)^2 S_{J_t}^2 + \left(\frac{\partial J_B}{\partial J_c}\right)^2 S_{J_c}^2 + \left(\frac{\partial J_B}{\partial \kappa_f}\right)^2 S_{\kappa_f}^2 + \left(\frac{\partial J_B}{\partial \kappa_c}\right)^2 S_{\kappa_c}^2 +$$

$$+ \left(\frac{\partial J_B}{\partial \kappa_w}\right)^2 S_{\kappa_w}^2 + \left(\frac{\partial J_B}{\partial \kappa_t}\right)^2 S_{\kappa_t}^2 \qquad (A.6.2)$$

with

$$\left(\frac{\partial J_B}{\partial J_t}\right)^2 = \left(\frac{\overline{\kappa}_f - \overline{\kappa}_t}{\overline{\kappa}_f - \overline{\kappa}_w}\right)^2 = 0.0115$$

$$\left(\frac{\partial J_B}{\partial J_c}\right)^2 = \left(- \frac{\overline{\kappa}_c - \overline{\kappa}_w}{\overline{\kappa}_f - \overline{\kappa}_w}\right)^2 = 0.0021$$

$$\left(\frac{\partial J_B}{\partial \kappa_f}\right)^2 = \left(\overline{J}_t \frac{\overline{\kappa}_t - \overline{\kappa}_w}{(\overline{\kappa}_f - \overline{\kappa}_w)^2} + \overline{J}_c \frac{\overline{\kappa}_c - \overline{\kappa}_w}{(\overline{\kappa}_f - \overline{\kappa}_w)^2}\right)^2 = 0.7232$$

$$\left(\frac{\partial J_B}{\partial \kappa_c}\right)^2 = \left(-\frac{\overline{J}_c}{\overline{\kappa}_f - \overline{\kappa}_w}\right)^2 = 0.1570$$

$$\left(\frac{\partial J_B}{\partial \kappa_w}\right)^2 = \left(\overline{J}_t \frac{\overline{\kappa}_f - \overline{\kappa}_t}{(\overline{\kappa}_f - \overline{\kappa}_w)^2} + \overline{J}_c \frac{\overline{\kappa}_f - \overline{\kappa}_c}{(\overline{\kappa}_f - \overline{\kappa}_w)^2}\right)^2 = 0.2286$$

and

$$\left(\frac{\partial J_B}{\partial \kappa_t}\right)^2 = \left(-\frac{\overline{J}_t}{\overline{\kappa}_f - \overline{\kappa}_w}\right)^2 = 0.8694$$

which combined with the squared of the standard deviation of the variables give a variance of:

$$S_{J_B}^2 = 1.35 \times 10^{-5} \ \frac{cm^2}{s^2}$$

(or a standard deviation of 0.0037 cm/s)

The 95% confidence interval given by $J_B = 0.07 \pm 0.0074$ cm/s

In a similar manner, the Feed water entrainment, $E(\%)$, expression

$$E = \frac{\bar{\kappa}_c - \bar{\kappa}_w}{\bar{\kappa}_f - \bar{\kappa}_w} \times 100 = 4.55 \ \% \qquad (6.5)$$

gives

$$S_E^2 = \left(\frac{\partial E}{\partial \kappa_c}\right)^2 S_{\kappa_c}^2 + \left(\frac{\partial E}{\partial \kappa_f}\right)^2 S_{\kappa_f}^2 + \left(\frac{\partial E}{\partial \kappa_w}\right)^2 S_{\kappa_w}^2 \qquad (A.6.3)$$

with

$$\left(\frac{\partial E}{\partial \kappa_c}\right)^2 = \left(\frac{100}{\bar{\kappa}_f - \bar{\kappa}_w}\right)^2 = 13583.9$$

$$\left(\frac{\partial E}{\partial \kappa_f}\right)^2 = \left(\frac{\bar{\kappa}_w - \bar{\kappa}_c}{(\bar{\kappa}_f - \bar{\kappa}_w)^2} \times 100\right)^2 = 28.06$$

and

$$\left(\frac{\partial E}{\partial \kappa_w}\right)^2 = \left(\frac{\bar{\kappa}_c - \bar{\kappa}_f}{(\bar{\kappa}_f - \bar{\kappa}_w)^2} \times 100\right)^2 = 12377.09$$

which give a variance of E of 0.137 $\%^2$ (a standard deviation of 0.371 %). The 95% confidence interval being given by $E = 4.55 \pm 0.74 \ \%$.

The feed water recovery R (%), defined by the expression

$$R = \frac{\overline{J_c}}{\overline{J_f}} \frac{\overline{\kappa}_c - \overline{\kappa}_w}{\overline{\kappa}_f - \overline{\kappa}_w} \times 100 = 2.15 \; \% \tag{6.6}$$

has a variance given by

$$S_R^2 = \left(\frac{\partial R}{\partial J_f}\right)^2 S_{J_f}^2 + \left(\frac{\partial R}{\partial J_c}\right)^2 S_{J_c}^2 + \left(\frac{\partial R}{\partial \kappa_c}\right)^2 S_{\kappa_c}^2 + \left(\frac{\partial R}{\partial \kappa_f}\right)^2 S_{\kappa_f}^2 +$$

$$+ \left(\frac{\partial R}{\partial \kappa_w}\right)^2 S_{\kappa_w}^2 \tag{A.6.4}$$

with

$$\left(\frac{\partial R}{\partial J_f}\right)^2 = \left(-\frac{\overline{J_c}}{\overline{J_f}^2} \frac{\overline{\kappa}_c - \overline{\kappa}_w}{\overline{\kappa}_f - \overline{\kappa}_w} \times 100\right)^2 = 8.8876$$

$$\left(\frac{\partial R}{\partial J_c}\right)^2 = \left(\frac{1}{\overline{J_f}} \frac{\overline{\kappa}_c - \overline{\kappa}_w}{\overline{\kappa}_f - \overline{\kappa}_w} \times 100\right)^2 = 39.85$$

$$\left(\frac{\partial R}{\partial \kappa_c}\right)^2 = \left(\frac{\overline{J_c}}{\overline{J_f}} \frac{100}{\overline{\kappa}_f - \overline{\kappa}_w}\right)^2 = 3029.13$$

$$\left(\frac{\partial R}{\partial \kappa_f}\right)^2 = \left(- \frac{\overline{J_c}}{\overline{J_f}} \frac{\overline{\kappa}_c - \overline{\kappa}_w}{(\overline{\kappa}_f - \overline{\kappa}_w)^2} \times 100\right)^2 = 6.2585$$

and

$$\left(\frac{\partial R}{\partial \kappa_w}\right)^2 = \left(- \frac{\overline{J_c}}{\overline{J_f}} \frac{\overline{\kappa}_f - \overline{\kappa}_c}{(\overline{\kappa}_f - \overline{\kappa}_w)^2} \times 100\right)^2 = 2760.02$$

which give a variance for R of 0.0343 %^{2} (a standard deviation of 0.185 %). The 95% confidence interval being given by $R = 2.15 \pm 0.37$ %.

APPENDIX 7

Computer Program Used for Collecting Conductance Profiles.

Computer program written in Basica for collecting conductance profiles. An IBM-compatible PC computer, a 12 bit A/D board (mod. DAS-8PGA), a 12 bit D/A-I/O board (mod. DDA-06), and a Tacussel conductivity meter (mod. CD 810) were used.

```
10 ' This program is intended to collect sets of sixty conductance profiles
20 ' (one every minute) and to save the data in disk as a lotus PRN file.
30 ' A plot "Distance from Top of Column vs Conductance" is displayed on
40 ' the computer monitor. An IBM compatible computer, A Bailey conductivity
50 ' meter (mod. 440 (0-10 Vdc), a 12 bit A/D board (mod. DAS-8PGA), a 24
60 ' channel relay board (mod. ERB-24), and a D/A-I/O board (mod. DDA-06)
70 ' are used. The file DAS8.BIN containing the binary machine language
80 ' must be present in the disk containing this program
90 '
100 ' Initializing parameters for A/D board
```

```
110   CLEAR,20000  :  DEF  SEG = 0  :   SG = 256*PEEK(&H511) + PEEK(&H510)  :
SG = 20000/16 + SG : DEF SEG = SG
120 'Initializing parameters: NF%, profiles counter;TBP, time between points,s;
130 'TBC, time between cycles, s; NS%, number of profiles in a set
140 NF% = 1 · TBP = 4. TBC = 60 : NS% = 60
150 'Dimensioning the array: TIM$, time; YEL, electrode location; COND#,
160 ' conductance value, mS; X, conductance differences
170 DIM TIM$(61),YEL(12), COND#(12,61),X(12): GOTO 250
180 '
190 ' Subroutine to check instructions given to the A/D board
200 IF FL% = 0 THEN RETURN
210 PRINT "ERROR IN DAS8:";MD%;"    ";FL%:END
220 '
230 'Starting the profiling:NC%, profiles counter. The A/D board is initialized
240 'and the first electrode is connected to the conductivity meter
245 TRO# = TIMER
250 NC% = 0 : GOSUB 950 : I = 1 : OUT &H300 + &HC,I
260 ' The screen is plotted and pertinent info is also displayed
270 NC% = NC% + 1 : CLS : GOSUB 670 : TIM$(NC%) = TIME$ : LOCATE 2,60 : PRINT "TIME
- "; TIM$(NC%) : LOCATE 5,64 : PRINT "PROFILE :"; NC%
280 ' The twelve active electrodes are sequentially connected to the
290 ' conductivity meter via the relay board
300 FOR LP% = 1 TO 12 : OUT &H300 + &HC,0 : OUT &H300 + &HE,0 : IF LP% > 8 THEN 320
310 I = 2^(LP%-1) : OUT &H300 + &HC,I : GOTO 350
320 EL = LP%-9 : I = 2^(EL) : OUT &H300 + &HE,I
330 ' A period of time of TBP is allowed to elapse in order to have a stable
340 ' conductance reading
350 TRP# = TRO# + TBC*(NC%-1) + TBP*LP%
360 T2# = TIMER
370 ' when TBP has elapsed, the A/D converted is read, and the value plotted
380 ' on the screen
390 IF (T2#-TRP#) > 0 THEN MD% = 4 : D% = 0 : FL% = 0 : CALL DAS8(MD%,D%,FL%) :
GOSUB 200 : GOTO 410
400 GOTO 360
410 GOSUB 820 : NEXT LP%
420 '
430 ' The largest conductance difference X is computed
440 FOR L = 1 TO 12:X(L) = ABS(COND#(L,NC%)-COND#(L-1,NC%)):NEXT L
450 K = 2:FOR L = K TO 12
460 IF X(K) < X(L) THEN K = L
470 NEXT L
480 ' The value of the estimated interface level is displayed on the screen
490 LOCATE 6,34: PRINT USING "LEVEL (ft): #.##";(YEL(K)-5)/30.5
```

```
500 ' The 4-20 mA signal proportional to level is outputted
510 D = INT(M*(YEL(K)-5)-M*(YEL(1) + 5))
520 XH% = INT(D/256):XL% = D-XH%*256
530 OUT &H300 + 0,XL%
540 OUT &H300 + &H1,XH%
550 '
560 ' The first active electrode is connected to the conductivity meter
570 I = 1: OUT &H300 + &HE,0:OUT &H300 + &HC,I
580 ' Waiting for the 60 sec/scan to elapse and checking if 60 profiles
590 ' have been already collected
600 TRC# = TRO# + TBC*NC%
610 IF NC% > =NS% THEN GOSUB 1200 : NC% = 0 : GOTO 270
620 T3# = TIMER
630 ' when 60 s/scan have elapsed, another profile is began
640 IF (T3#-TRC#) > = 0 THEN GOTO 270
650 GOTO 620
660 '
670 'screen drawing subroutine
680 KEY OFF : CLS : SCREEN 2
690 LINE (230,28)-(630,148),1,B : LINE (466,28)-(630,58),1,B
700 FOR I = 1 TO 7 : LINE (227,20*I + 8)-(230,20*I + 8): NEXT I
710 FOR I = 1 TO 11 : LINE (230,10*I + 28)-(232,10*I + 28): NEXT I
720 LOCATE 4,26 : PRINT "0" : LOCATE 9,26 : PRINT "2" : LOCATE 14,26 : PRINT "4" .
LOCATE 19,26 : PRINT "6"
730 LOCATE 6,14 : PRINT "DISTANCE" : LOCATE 7,14 : PRINT "FROM TOP" : LOCATE 9,16
: PRINT "(ft)"
740 FOR I = 1 TO 9 : LINE (50*I + 180,148)-(50*I + 180,150): NEXT I
750 IF RGE = .1 THEN LOCATE 20,30 : PRINT "0" : LOCATE 20,42 : PRINT "1" · LOCATE
20,54 : PRINT "2" : LOCATE 20,67 : PRINT "3" : LOCATE 20,79 : PRINT "4" : GOTO 780
760 IF RGE = 1 THEN LOCATE 20,30 : PRINT "0" : LOCATE 20,41 : PRINT "10" : LOCATE
20,54 : PRINT "20" : LOCATE 20,66 : PRINT "30" : LOCATE 20,79 : PRINT "40" : GOTO 780
770 LOCATE 20,30 : PRINT "0" : LOCATE 20,41 : PRINT "100" : LOCATE 20,53 : PRINT
"200" : LOCATE 20,66 : PRINT "300" : LOCATE 20,78 : PRINT "400"
780 LOCATE 22,47 : PRINT "CONDUCTANCE (mmhos)"
790 LOCATE 2,34 : PRINT "DATE : ";DATE$
800 RETURN
810 '
820 ' Display of the points of the profile. The digital number D% is converted
830 ' to a conductance value
840 COND#(LP%,NC%) = D%*FACTOR#
850 XX = COND#(LP%.NC%)*KP# + 230 : YY = YEL(LP%)*20/30.48 + 28
860 IF LP% > 1 THEN GOTO 880
870 LINE (XX,YY)-(XX,YY) : GOTO 890
```

```
880 LINE -(XX,YY)
890 LOCATE 6,63 : PRINT "ELECTRODE :"; LP%
900 IF RGE = .1 THEN LOCATE 7,62 : PRINT USING "COND : #.####";COND#(LP%,NC%) :
GOTO 930
910 IF RGE = 1 THEN LOCATE 7,62 : PRINT USING "COND : ##.###";COND#(LP%,NC%) :
GOTO 930
920 LOCATE 7,63 : PRINT USING "COND : ###.##";COND#(LP%,NC%)
930 RETURN
940 '
950 'Loading binary machine language and initializing A/D board
960 BLOAD "DAS8.BIN",0 : DEF SEG =SG : DAS8 =0
970 ' Base address for the A/D board
980 BASADR% =&H310
990 MD% =0 : FL% =0 : CALL DAS8(MD%,BASADR%,FL%) : GOSUB 200
1000 ' Selecting A/D channel "0"
1010 MD% = 1 : LT%(0) =0 : LT%(1) =0 : FL% =0 : CALL DAS8(MD%,LT%(0),FL%): GOSUB
200
1020 ' Selecting 0-10 Vdc range
1030 MD% = 19 : VR% =9 : Fl.% =0 : CALL DAS8(MD%,VR%,FL%) : GOSUB 200
1040 ' Initializing I/O board
1050 OUT &H300 +&HF, &H80
1060 ' Reading the position(respect to top of column) of the active electrodes
1070 FOR I = 1 TO 12 : READ YEL(I) : NEXT I
1080 DATA 25,35,45,55,65,75,85,95,105,115,125,135
1090 ' Obtaining the relationship between 4-20 mA (0-4096) and position
1100 M =4095/(YEL(12)-YEL(1)-10):B =-M*(YEL(1) +5)
1110 ' Selecting the range of the conductivity meter to fit experimental
1120 ' conditions (the conductance vs distance plot is also plotted on the
1130 ' basis of the range of the conductivity meter)
1140 INPUT "ENTER CONDUCTIVITY METER RANGE (0.1, 1, or 10): ", RGE
1150 ' Defining the factor to convert the digital numbers to conductance values
1160 ' and the factor KP# to produce the screen
1170 FACTOR# =RGE/102.4 : KP# = 10/RGE
1180 RETURN
1190 '
1200 ' data saving in disk (up to 99 set of 60 profiles can be saved)
1210 'Every file is identified by the date and the time at which it was stored
1220 IF NF% > 10 THEN 1240
1230 NE$ = "D" +LEFT$(DATE$,2) + MID$(DATE$,4,2) + "-0" + RIGHT$(STR$(NF%),1) + ".PRN"
: GOTO 1250
1240 NE$ = "D" +LEFT$(DATE$,2) + MID$(DATE$,4,2) + "-" + RIGHT$(STR$(NF%),2)) + ".PRN"
1250 OPEN NE$ FOR OUTPUT AS # 1
1260 ' Saving pertinent information of the set of profiles
```

```
1270 PRINT #1, DATE$ : PRINT #1, TIM0# : PRINT #1, RGE : PRINT #1, NC%
1280 ' Saving active electrodes position
1290 FOR I = 1 TO 12 : PRINT #1, YEL(I) : NEXT I
1300 ' Saving the timed-conductance profiles
1310 FOR J = 1 TO NC% : PRINT #1, TIM$(J): FOR I = 1 TO 12 : PRINT #1,USING "###.###";
COND#(I,J);: NEXT I:PRINT #1,: NEXT J
1320 CLOSE : NF% =NF% + 1
1330 RETURN
```

APPENDIX 8

Computer Program Used for the Sedimentation Experiments.

Computer program written in Basica for collecting the data during the sedimentation experiments described in Section 5.1.3. An IBM-compatible PC computer, a 12-bit A/D board (mod. D∴S-8PGA), and a Tacussel conductivity meter (mod. CD 810) were used.


```
10 ' This program is intended to collect timed readings of conductivity
20 ' during the sedimentation experiments described in Section 5.1.3
30 ' The data is saved in a disk file as a PRN Lotus file
40 ' An IBM compatible computer, a Tacussel conductivity meter (mod.
50 ' CD 810), and a 12 bit A/D board (mod. DAS-8PGA) were used.
60 ' (The file DAS8.BIN containing the binary machine language must
70 ' be present in the disk containing this program)
80 '
90 CLS:GOTO 160
100 '
110 ' Subroutine to check well functioning of A/D board
120 IF FL%>0 THEN PRINT "error in das8;";MD%;"   ";FL%:END
130 RETURN
140 '
150 ' Initializing parameters for A/D board
160 CLEAR, 48000!
170 DEF SEG=0
180 SG = 256*PEEK(&H511) + PEEK(&H510)
190 SG = 48000!/16 + SG
200 DEF SEG = SG
```

```
210 ' The File DAS8.BIN is loaded
220 BLOAD "das8.bin",0
230 '
240 'Dimensioning the Conductivity-time array
250 DIM COND#(402),T2#(402)
260 MD% = 0:BASADR% = &H310:FLAG% = 0
270 ' Selecting the base address for the A/D board
280 CALL DAS8(MD%,BASADR%,FLAG%):GOSUB 120
290 ' Selecting the A/D channel (channel 0 in this case)
300 MD% = 1:LT%(0) = 0:LT%(1) = 0:FLAG% = 0:CALL DAS8(MD%,LT%(0),FLAG%):GOSUB
120
310 ' Selecting the range of the A/D channel (0-10 Vdc, in this case)
320 MD% = 19:D%(0) = 9:FLAG% = 0:CALL  DAS8(MD%,D%(0),FLAG%):GOSUB 120
330 ' Entering parameters of the experiment
340 PRINT:INPUT "range. 0.5, 5, 50 or 500 mS:";R
350 PRINT:INPUT "number of points (<400):";N
360 PRINT:INPUT "kcell (in the conductivity meter):";KCELL
370 PRINT:INPUT "Time between readings, sec:";T
380 ' Initiating the collection of data
390 J = 1
400 ' Time counter
410 T1# = TIMER
420 T2# = TIMER
430 IF ABS(T2#-T1#-T)< .1 THEN GOTO 460
440 GOTO 420
450 ' Performing an A/D conversion and time-tagging the reading
460 MD% = 4:D% = 0:FLAG% = 0
470 T2#(J) = T2#:CALL DAS8(MD%,D%,FLAG%)
480 ' Transforming the digital number to conductance (mS)
490 COND#(J) = D%*10/4096
500 ' Displaying (on the monitor screen) the time, conductance data
510 PRINT USING "######.###"; J,COND#(J),T2#(J)
520 ' Checking if the number of desired data have been completed; if
530 ' this is the case the data will be saved to disk
540 IF J>N THEN 570
550 J = J+1:GOTO 410
560 '
570 ' Data saving subroutine
580 ' Entering file name
590 INPUT "lotus file name";F$: F$ = F$+".prn"
600 OPEN F$ FOR OUTPUT AS#1
610 ' Saving pertinent parameters of the experiment
620 PRINT #1, USING "###.###";R,KCELL
```

```
630 ' Saving the time-conductance data
640 FOR J = 1 TO N:PRINT #1, USING "###.####", T2#(J);COND#(J)
650 NEXT J
660 CLOSE #1: END
```